

THESE

dans le cadre d'une procédure de co-tutelle
présentée devant la Pontificia Universidad Catolica de Chile

en vue de l'obtention du **Doctorat de l'Université de Toulouse**
délivré par l'**Université Toulouse III – Paul Sabatier** et du **Doctorat**
de la Pontificia Universidad Catolica de Chile

Ecole Doctorale : Sciences de la Matière

Soutenue le 29 Novembre 2007

par

Christopher ADAMS

Synthèse, caractérisation et étude de l'activité catalytique de complexes organométalliques du rhodium dans la réaction de silylation déshydrogénante des oléfines

Directeurs de thèse: **Mme. A. Castel**, Chargée de Recherche au CNRS, Toulouse
M. M. J. Manriquez et **Mme I. Chavez**, Professeurs à la Pontificia
Universidad Catolica de Chile, Santiago

JURY

M. J. Costamagna	Professeur à l'Universidad de Santiago de Chile	Président
M. M. Dahrouch	Professeur à l'Universidad de Concepcion	Rapporteur
M. H. Klahn	Professeur à la Pontificia Universidad Catolica de Valparaiso	Rapporteur
M. P. Rivière	Professeur à l'Université Paul Sabatier, Toulouse	Examineur
M. R. Contreras	Professeur à la Pontificia Universidad Catolica de Chile	Examineur
M. H. Gornitzka	Professeur à l'Université Paul Sabatier, Toulouse	Examineur

Laboratoire d'Hétérochimie Fondamentale et Appliquée UMR-CNRS 5069
Université Paul Sabatier, Bat 2R1 - 118 route de Narbonne - 31062 Toulouse cédex 9
Departamento de Inorganica, Facultad de Quimica
Pontificia Universidad Catolica de Chile - Casilla 306 - Santiago

To my son, Alexander

Acknowledgments:

This thesis was supported by the French Embassy as well as the ECOS-CONICYT (C04E05 and C01E06) agreement of France and Chile, between the L'Université Paul Sabatier, Toulouse, France and the Pontificia Universidad Católica de Chile, Santiago, Chile, (Projects FONDECYT 1060588 (I.Ch.) and 1040455 (J.M.M.))during the years 2003 and 2007. Also, this project was supported by scholarships DIPUC, MECESUP, CONICYT (Término de Tesis) throughout the whole process.

First and foremost, I owe my deepest gratitude to the “Facultad de Química Inorgánica II, Facultad de Ciencias Químicas” and to the “Laboratoire d'Hétérochimie Fondamentale et Appliquée” (LHFA), for welcoming me in their premises, allowing me to become a better skilled worker in the areas of Chemistry of Materials, becoming acquainted and learning from several tools and techniques which were, at first, unknown to me.

From the LHFA my heart-felt thanks go to Ms. Annie Castel for her council and remarkable patience. A special vote of thanks also goes to M. Antoine Barceiredo, M. Guy Bertrand, M. Pierre Rivière, Ms. Monique Rivière-Baudet, M. Fabien Delpéch, M. Heinz Gornitzka, M. Henri Ranaivonjatovo, M. Jean Escudie, together with Ms. Maryse Béziat, Ms. Marie José Pedussault, M. Pierre Hernandez and M. Olivier Volpato, whom not only guided me throughout the whole cooperation process during my stays in Toulouse teaching me how to handle different equipment and how to interpret the obtained results, but also had the patience to guide me into learning as much of the French language as possible.

I must profoundly thank Mr. Juan Manual Manriquez and Ms. Ivonne Chavez, who welcomed and encouraged me into learning a very challenging division of Chemistry, and also motivated me to apply for the France-Chile cooperation program in order to further increase my skills and prove myself capable of becoming the best chemist I could be. Also, I must thank M. Deodato Radic, M. Ricardo Tapia, M. Raul Contreras, M. Mauricio Valderrama, Ms. Barbara Loeb, Ms. Veronica Arancibia, M. Jose Santos, M. Mohammed Dahrouch, M. Hugo Klahn, M. Rodrigo del Río, M. Juan Costamagna, M. Nelly Faundez, M. Sergio Alegria, M. Helmuth Scholz, M. Humberto Fuentes, M. Juan “Gato” Latorre, M. Iván Tapia, and very especially, Carlos Cayuta for their support.

Many more took part of my process in completing this Ph.D., not only professionally, but also morally. Amongst those whom made my stay in Toulouse much more pleasant are: Raluca Şeptolean, Aldelkrim Elkadib, Richard Menye-Biyogo, Nadia Katir, Lucian Pop, Dumitru Ghereg, Raluca Pop, Nancy Hawi, Omar Mouhtady, Ali Mcheik, Roxana Pop, Sonia García Alonso and Rami El Ayoubi. To my labmates in Chile, for their priceless support: Silvana Salinas, César Morales, Desmond MacLeod-Carey, Álvaro Muñoz, Juan Araneda, Edgardo Esponda, Jose María Ureta, Juan Pablo Melo, Verónica Morales, Francisco Gajardo, Mauricio Arias, Victor Molina, Felipe Angel, Fernanda Duarte, Francisco Barraza, Luciano Oehninger and last but not least, the Diana Abril.

An unconditional pillar of support during the whole process was and still is my family. My parents, John Anthony Adams and Carmen Wrighton together with my brother and sister-in-law, Anthony E. Adams and Lorena Leigh ought to be commended for putting up with my terrible temper, as well as helping me on the completion of this thesis.

The most recent addition to my life; my wife Ana Villalobos, is deeply thanked for not only being my driving force to always move forward, but for also rewarding me with the most beautiful creation I've ever taken part of: my son, Alexander Damien Adams Villalobos.

The help and kindness of many friends will never go unremembered. These include: Miguel Jara, Valeria Burboa, Eric Parra, Marcela Parra, Carlos Caro, Mónica Mendoza, Carolina Carrasco, Francisco Rodríguez, Olga Cifuentes, Margarita Aliaga, Ignacio Silva, Víctor Pérez, Valeska Carillo, Luis Cortez, Karina Romero, Mariela Aranda and finally, Rosario Valenzuela.

Table of Contents:

Introduction Générale:.....	1
General Data and Instrumentation:.....	6
Abbreviations & Symbols:.....	7
Chapter 1	9
Introduction	9
1.1 Importance of catalysis.....	11
1.1.1 Homogenous and Heterogeneous Catalysts	13
1.1.2 Homogenous Catalysis and its Development	15
1.2 Designing Catalysts	19
1.2.1 Metals, Ligands and Spacer Ligands in Homogenous Catalysis.....	19
1.2.2 New Silicon Products, Hydrosilylation and Dehydrogenative Silylation.	23
1.3 Objectives	25
References	27
Chapter 2	33
Synthesis and Spectroscopic Studies of Polyalkylated 1,5-dihydro- <i>s</i> -Indacene Ligands	33
2 Introduction	35
2.1 Preparation of 2,4,6,8-Substituted 1,5-dihydro- <i>s</i> -indacenes:	36
2.2 Preparation of 2,3,4,6,7,8-Substituted 1,5-dihydro- <i>s</i> -indacenes:	41
2.3 Preparation of 3-chloro-2,6-diethyl-4,7,8-trimethyl-1,5-dihydro- <i>s</i> -indacene ligand:	42
2.4 Physical Characteristics of <i>s</i> -indacene ligands:.....	43
2.5 Spectroscopic Characteristics of <i>s</i> -indacene ligands:.....	43
2.5.1 NMR Properties.....	44
2.5.1.1 ¹ H- NMR:	44
2.5.1.2 ¹³ C- NMR:	45
2.5.2 ESR Study:	46
2.6 Conclusions:	57
2.7 Experimental Section.....	58
2.7.1 Experimental Procedure for 2,6-diethyl-4,8-dimethyl-1,5-dihydro- <i>s</i> -indacene 8b:.....	58
2.7.1.1 Synthesis of 1,4-bis(bromomethyl)-2,5-dimethylbenzene 1 :	58
2.7.1.2 Synthesis of α,α'-bis(ethoxycarbonyl)-α,α'-diethyl-2,5-dimethyl-diethyl ester-1,4-Benzenedipropionic acid 3b :	59

2.7.1.3 Synthesis of α,α' -dicarboxy- α,α' -diethyl-2,5-dimethyl-1,4-Benzenedipropanoic acid 4b :	60
2.7.1.4 Synthesis of α,α' -diethyl-2,5-dimethyl-1,4-Benzenedipropanoic acid 5b :	61
2.7.1.5 Synthesis of 2,6-diethyl-2,3,6,7-tetrahydro-4,8-dimethyl- <i>s</i> -indacene-1,5-dione 6b :	62
2.7.1.6 Synthesis of 1,2,3,5,6,7-hexahydro-2,6-diethyl-4,8-dimethyl- <i>s</i> -indacene-1,5-diol 7b :	63
2.7.1.7 Synthesis of 2,6-diethyl-1,5-dihydro-4,8-dimethyl- <i>s</i> -Indacene 8b :	63
2.7.2 Experimental Procedure for 2,6-di- <i>n</i> -butyl-4,8-dimethyl-1,5-dihydro- <i>s</i> -indacene 8c :	65
2.7.2.1 Synthesis of diethyl <i>n</i> -butylmalonate 2c :	65
2.7.2.2 Synthesis of α,α' -bis(ethoxycarbonyl)- α,α' -dibutyl-2,5-dimethyl-diethyl ester-1,4-Benzenedipropanoic acid 3c :	66
2.7.2.3 Synthesis of α,α' -dicarboxy- α,α' -dibutyl-2,5-dimethyl-1,4-Benzenedipropanoic acid 4c :	67
2.7.2.4 α,α' -dibutyl-2,5-dimethyl-1,4-Benzenedipropanoic acid 5c :	68
2.7.2.5 Synthesis of 2,6-dibutyl-4,8-dimethyl-2,3,6,7-tetrahydro- <i>s</i> -indacene-1,5-dione 6c :	69
2.7.2.6 Synthesis of 2,6-dibutyl-4,8-dimethyl-1,2,3,5,6,7-hexahydro- <i>s</i> -indacene-1,5-diol 7c :	70
2.7.2.7 Synthesis of 2,6-dibutyl-1,5-dihydro-4,8-dimethyl- <i>s</i> -Indacene 8c :	70
2.7.3 Experimental Procedure for 3-chloro-2,6-diethyl-4,7,8-trimethyl-1,5-dihydro- <i>s</i> -indacene:	71
2.7.3.1 Synthesis of 5,5-dichloro-2,6-diethyl-4,8-dimethyl-2,3,6,7-tetrahydro- <i>s</i> -indacen-1(5H)-one 11 :	71
2.7.3.2 Synthesis of 3-chloro-2,6-diethyl-4,7,8-trimethyl-1,5-dihydro- <i>s</i> -indacene 13 :	72
2.7.4 Preparation of dilithiated derivatives of <i>s</i> -indacene:	74
2.7.5 Preparation of ESR Experiments:	74
References	75
Chapter 3	77
Synthesis and Spectroscopic Study of Organometallic complexes	77
3 Introduction	79
3.1 Preparation of starting metallic materials	80
3.1.1 Preparation of metallic (acac) compounds	80
3.1.2 Preparation of Cp*M (M: Fe, Co, Ru) building blocks	81
3.1.2.1 Preparation of Cp*M(acac), (M: Fe, Co):	81

3.1.2.2 Preparation of [Cp* <i>RuCl</i>] ₄ :	82
3.1.3 Preparation of Rhodium Starting compounds	83
3.2 Preparation of Mononuclear complexes	83
3.2.1 Preparation of Rhodium Complexes bearing 1,2,3,4,5-pentamethyl- cyclopentadiene and Indene ligands	84
3.2.2 Preparation of Mononuclear Complexes Bearing 1,5-dihydro-2,6-diethyl-4,8- dimethyl- <i>s</i> -indacene.	85
3.3 Preparation of Dinuclear compounds	88
Scheme 2: Formation of <i>anti</i> - and <i>syn</i> - isomers of <i>s</i> -indacene binuclear complexes.	89
3.3.1 Preparation of Homobinuclear complexes	90
3.3.2 Preparation of Heterobinuclear complexes.....	91
3.4 Reactivity test with CO	93
3.4.1 (1,2,3,4,5-Pentamethylcyclopentadienide)-Rhodium-diene	93
3.4.2 Indenyl-Rhodium-diene.....	94
3.5 Physical Characteristics of <i>s</i> -indacene Metallic Complexes	95
3.6 Physical-Chemical Characteristics of <i>s</i> -indacene metallic complexes.....	95
3.6.1 NMR Properties.....	96
3.6.1.1 ¹ H-NMR:	96
3.6.1.2 ¹³ C{ ¹ H}-NMR.....	99
3.6.1.3 ¹⁰³ Rh-NMR:	102
3.6.2 Electrochemical Properties.....	103
3.6.2.1 Cyclic voltammograms of mononuclear complexes	105
3.6.2.2 Cyclic voltammograms of binuclear complexes	109
3.6.3 ESR Properties.....	115
3.6.4 X-Ray Diffraction Structures.....	117
3.6.4.1 X-ray Structure of Complex 21a :	117
3.6.4.2 X-ray Structure of Complex 22b :	119
3.6.4.3 X-ray Structure of Complex 24a :	120
3.7 Conclusions	123
3.8 Experimental Section:	124
3.8.1 Synthesis of Iron(II) Bis(Acetylacetonate) 14a	124
3.8.2 Synthesis of Cobalt(II) Bis(Acetylacetonate) 14b.....	125
3.8.3 Synthesis of 1,2,3,4,5-Pentamethylcyclopentadienide-M-(acetyl-acetonato) (M: Fe ^{II} : 15a, Co ^{II} : 15b).....	125

3.8.4 Synthesis of bis-[1,2,3,4,5-Pentamethylcyclopentadienide-Ruthenium ^{III} - μ - (bis-chloro)] 16.....	126
3.8.5 Synthesis of tetrakis-[1,2,3,4,5-Pentamethylcyclopentadienide-Ruthenium ^{II} - μ_3 -(chloro)] 17.....	126
3.8.6 Synthesis of [Rh- μ -Cl-(η^4 -1,5-cyclooctadiene)] ₂ 18a.....	127
3.8.7 Synthesis of [Rh- μ -Cl-(η^4 -bicyclo[2.2.1]hepta-2,5-diene)] ₂ 18b.....	128
3.8.8 Synthesis of 1,2,3,4,5-Pentamethylcyclopentadienide-Rh(η^4 -1,5- cyclooctadiene) 19a.....	128
3.8.9 Synthesis of 1,2,3,4,5-Pentamethylcyclopentadienide-Rhodium- (bicyclo[2.2.1]hepta-2,5-diene) 19b.....	129
3.8.10 Synthesis of Indenyl-Rh(η^4 -1,5-cyclooctadiene) 20a.....	130
3.8.11 Synthesis of Indenyl-Rhodium(bicyclo[2.2.1]hepta-2,5-diene) 20b.....	131
3.8.12 Synthesis of Indenyl-Rhodium-(biscarbonyl) 20c.....	132
3.8.13 Synthesis of 1,2,3,4,5-Pentamethylcyclopentadienide-Iron(II)- η^5 -(2,6- diethyl-4,8-dimethyl- <i>s</i> -indacene) 21a:.....	133
3.8.14 Synthesis of 1,2,3,4,5-Pentamethylcyclopentadienide-Ruthenium(II)- η^5 -(2,6- diethyl-4,8-dimethyl- <i>s</i> -indacene) 21b:.....	134
3.8.15 Synthesis of 1,2,3,4,5-Pentamethylcyclopentadienide-Cobalt(II)-(2,6-diethyl- 4,8-dimethyl- <i>s</i> -indacene) 21c.....	136
3.8.16 Synthesis of 2,6-diethyl-4,8-dimethyl- <i>s</i> -indacene-Rhodium(I)-(η^4 -1,5- cyclooctadiene) 21d.....	137
3.8.17 Synthesis of 1,2,3,4,5-Pentamethylcyclopentadienide-Cobalt(III)-(2,6- diethyl-4,8-dimethyl- <i>s</i> -indacene) tetrafluoroborate [21c] ⁺ [BF ₄ ⁻].....	138
3.8.18 Bis-(1,2,3,4,5-pentamethylcyclopentadienyl-ruthenium(II))- μ - <i>s</i> - indacenediide 22a:.....	140
3.8.19 [(2,6-diethyl-4,8-dimethyl- <i>s</i> -indacenediide)-bis-(Rhodium(I)(1,5- cyclooctadiene))] 22b and 22c.....	141
3.8.19.1 Step by Step.....	141
3.8.19.2 Direct Synthesis.....	141
3.8.20 <i>anti</i> -(1,2,3,4,5-Pentamethylcyclopentadienide)-Iron(II)-2,6-diethyl-4,8- dimethyl- <i>s</i> -indacenediide-Rhodium(I)-(1,5-cyclooctadiene) 23a:.....	143
3.8.21 <i>anti</i> -(1,2,3,4,5-Pentamethylcyclopentadienide)-Ruthenium(II)-2,6-diethyl- 4,8-dimethyl- <i>s</i> -indacenediide-Rhodium(I)-(η^4 -1,5-cyclooctadiene) 23b.....	145
3.8.22 <i>anti</i> -(1,2,3,4,5-Pentamethylcyclopentadienide)-Cobalt(II)-2,6-diethyl-4,8- dimethyl- <i>s</i> -indacenediide-Rhodium(I)-(1,5-cyclooctadiene) 23c:.....	146
3.8.23 <i>syn</i> -(1,2,3,4,5-Pentamethylcyclopentadienide)-Ruthenium(II)-2,6-diethyl- 4,8-dimethyl- <i>s</i> -indacenediide-Rhodium(I)-(η^4 -1,5-cyclooctadiene) 24a:.....	146

3.8.24 anti-(1,2,3,4,5-Pentamethylcyclopentadienide)-Cobalt(III)-2,6-diethyl-4,8-dimethyl-s-indacendiide-Rhodium(I)-(η ⁴ -1,5-cyclooctadiene) Tetrafluoroborate [23c] ⁺ [BF ₄ ⁻]:	148
References	149
Chapter 4	155
Catalytic Study of Rhodium Organometallic Complexes in Dehydrogenative Silylation of Olefins	155
4 Introduction	157
4.1 Solvent and Temperature Effect	159
4.2 Effect of Chemical Substrates	162
4.2.1 Effect of Substrate Ratio.....	162
4.2.2 Olefin Effect	164
4.2.3 Silane Effect	169
4.3 Effect of Ligands	173
4.3.1 Influence of Main Ligand.....	173
4.3.2 Influence on Ancillary Ligand.....	176
4.4 Conclusions	178
4.5 Experimental Section.....	179
4.5.1 Characterization silicon products from 2,4,6-trimethylstyrene:.....	180
References	182
Conclusions	185
Compound Number Summary:.....	189

Introduction Générale:

Durant la seconde partie du vingtième siècle, de grands progrès ont été réalisés en science et en technologie en particulier en électronique, physique nucléaire, biologie et médecine. Un tel développement a été permis en particulier par l'utilisation de ressources naturelles comme le pétrole. Des produits qu'il était impossible de trouver il y a 40 ans sont maintenant commerciaux comme par exemple : le fuel, les fibres synthétiques, les matières plastiques, les détergents, les lubrifiants, les produits chimiques etc... incluant les produits alimentaires et les médicaments, tout cela grâce à l'utilisation, dans la plupart des cas, de catalyseurs.

Ces nouveaux dérivés ont permis de diminuer le coût de différents processus industriels, de préparer des produits avec de très bons rendements, une meilleure pureté et dans certains cas d'accéder à des composés impossible à préparer par des voies usuelles.

La première définition d'un catalyseur a été donnée par Berzelius en 1836 : il l'a qualifié de "catalytic force". Actuellement, un catalyseur est une substance qui augmente la vitesse d'une réaction chimique en introduisant de nouveaux chemins de réaction (mécanisme) et en abaissant son énergie d'activation. Il participe à la réaction mais il ne fait partie ni des produits, ni des réactifs et est régénéré à la fin.

Il existe trois grands types de catalyse :

- homogène : le catalyseur ne forme qu'une seule phase avec les réactifs
- hétérogène : le catalyseur est généralement à l'état solide alors que la phase réactive est soit une solution, soit un gaz
- par transfert de phase : le catalyseur sert à transférer une espèce chimique d'une phase à l'autre

Alors que les catalyseurs hétérogènes (nickel ou platine finement divisés) sont très largement utilisés dans l'industrie mais nécessitent des conditions de température et de pression élevées, la catalyse homogène présente d'autres avantages comme la possibilité d'étudier les mécanismes de ces réactions en jouant soit sur le métal utilisé soit sur les ligands entourant le métal. Dans ce travail, nous nous sommes intéressés essentiellement à la catalyse homogène.

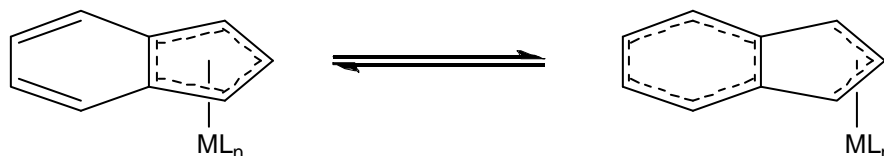
Introduction

L'un des catalyseurs les plus connus dans cette catégorie est le catalyseur de Wilkinson ($\text{RhCl}(\text{PPh}_3)_3$) utilisé, par exemple, pour l'hydrogénation des oléfines, l'hydroboration des alcènes, la réduction 1,4 de composés carbonylés insaturés par les silanes.

L'importance de ce catalyseur réside dans la possibilité de présenter plusieurs configurations électroniques (14, 16 ou 18 électrons) durant le cycle catalytique. Un subtil équilibre entre stabilité et instabilité de ces différentes configurations est nécessaire pour obtenir une espèce catalytiquement active. De nombreux autres métaux offrent également cette possibilité comme le Ni^{2+} , Pd^{2+} , Rh^+ .

Dans ce type de catalyse homogène, les complexes comprennent différents ligands qui non seulement peuvent les stabiliser mais également les rendre plus solubles. L'utilisation de ligands présente de plus l'avantage de pouvoir modifier la densité électronique des métaux et donc leurs propriétés catalytiques.

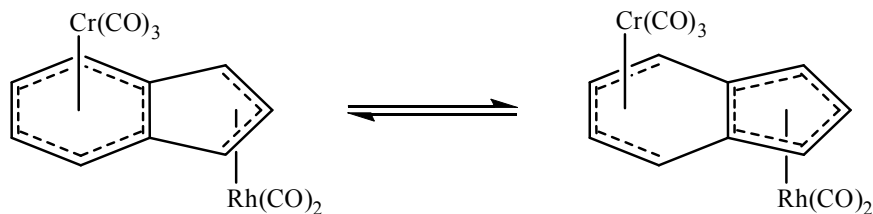
C'est cette dernière particularité qui a été très développée dans les ligands organométalliques où l'on parle d'effet haptotropique ou "indenyl effect". Il s'agit d'un équilibre entre différents modes de coordination dépendant à la fois de la nature du ligand et de la configuration électronique du métal. Cet effet a été fréquemment mis en évidence dans des complexes possédant des ligands de la famille des cyclopentadiényles (cyclopentadiényles substitués, indényle, fluorényle...) et il se révèle d'autant plus important que le système π conjugué est étendu. Il est également susceptible de jouer un rôle prépondérant dans les processus catalytiques puisqu'il libère sur le métal, un ou plusieurs sites de coordination qui pourront être utilisés pour complexer des réactifs.



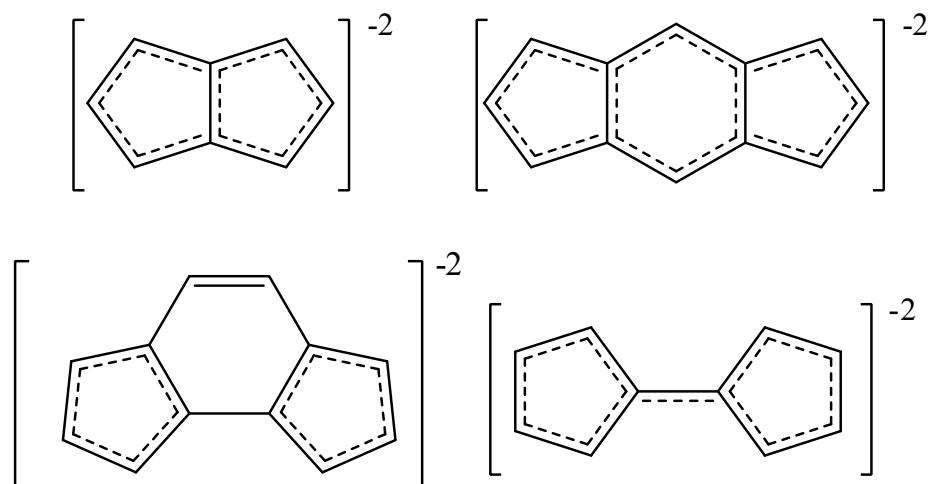
Par ailleurs, la complexation d'un second centre métallique susceptible de se comporter comme source d'électrons (ou de pompe d'électrons) pourraient permettre d'ajuster au mieux les besoins en électrons du second centre métallique catalytiquement actif. Récemment, Ceccon et al. ont décrit l'effet de complexes bimétalliques de l'indényle

Introduction

sur la cyclotrimérisation d'alcynes. La présence du fragment $(\text{CO})_3\text{Cr}$ modifie le pouvoir catalytique du rhodium et augmente la vitesse de réaction dans un rapport de 1000.



En général, les complexes bimétalliques présentant une bonne délocalisation électronique constitueront de bons candidats pour ce type d'effet. Parmi eux, on peut citer des ligands de type pentalène, s- et as-indacène, indényle...



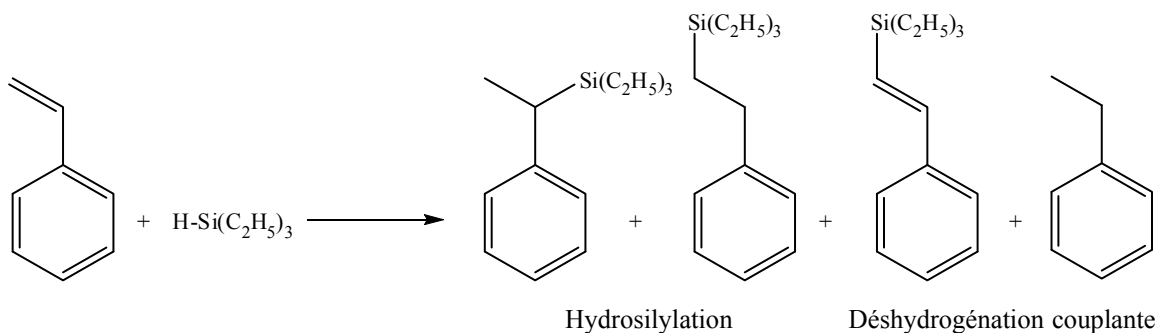
Ces phénomènes de communication entre centres métalliques ont été mis en évidence par électrochimie (écart $\Delta E_{1/2}$ des potentiels rédox des deux métaux) et par « NIR » (bande de transfert dans le proche infrarouge). D'autres techniques plus spécifiques devraient permettre d'étudier leurs interactions électronique (RPE) et nucléaire (spectroscopie Mössbauer) alors que la RMN multinucléaire et la diffraction par rayons X devraient donner plus d'information sur leurs structures en solution et à l'état solide.

Comme test catalytique nous avons choisi la silylation d'oléfines et en particulier la réaction de déshydrogénation couplante.

Les réactions d'hydrosilylation sont connues depuis très longtemps et constituent une des voies d'accès très utilisées pour la formation de liaison silicium-carbone. Elles nécessitent l'emploi de catalyseurs (Pt, Ir) et leur mécanisme a été décrit par Chalk et Harrod.

Introduction

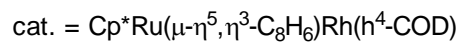
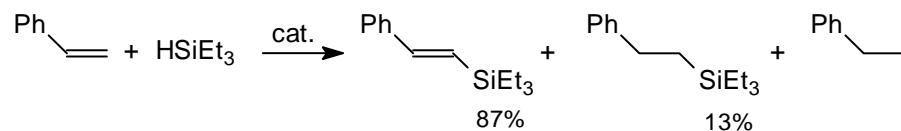
L'utilisation croissante de produits siliciés comme matériaux résistants à la chaleur (couches, peintures), céramiques, moulages, polymères (implants, circuits électronique...) a fortement développé l'étude ces réactions d'hydrosilylation. Plus récemment, il a été montré la formation de produits secondaires identifiés à des vinylsilanes à côté des produits d'hydrosilylation classique.



Suivant la nature du catalyseur utilisé, on peut favoriser l'une ou l'autre de ces réactions. Par exemple, les complexes du platine donnent quasi exclusivement les réactions d'hydrosilylation alors que les complexes du Fe, Ru, Rh, Co conduisent préférentiellement aux réactions de silylation déshydrogénante. Ces dernières réactions sont de loin les plus intéressantes car elles permettent de conserver la fonction éthylénique qui présente un très grand intérêt non seulement sur le plan fondamental (grand potentiel de fonctionalisation) mais également sur le plan industriel (accès direct aux allyl- et vinyl-silanes). Cependant, ces réactions ne sont pas sélectives et s'accompagnent de la formation de produits secondaires (oléfines hydrogénées, dimères)

Il existe à ce jour quelques catalyseurs spécifiques qui permettent la formation majoritaire de vinylsilanes mais le champ d'investigation reste grand ouvert en particulier sur le plan mécanistique. Pour notre part, nous avons obtenu une très bonne sélectivité dans la réaction de silylation du styrène par le triéthylsilane en présence d'un nouveau complexe hétérobimétallique du rhodium et du ruthénium ayant le groupe pentalène comme espaceur pontant.

Introduction



Cependant, le pentalène est un composé instable et la synthèse est assez longue et difficile. Dans ce travail, nous avons projeté d'étudier de nouveaux motifs de structure voisine les s-indacènes diversement substitués, la synthèse et la caractérisation des complexes mono- et bimétalliques correspondants ainsi que leurs applications en catalyse.

General Data and Instrumentation:

All reactions were performed under nitrogen using standard Schlenk tube techniques and dry solvents.

NMR spectra were recorded on Bruker AC 80 (^1H , 80 MHz), ARX400 (^1H , 400.13 MHz); AC 200 (^{13}C , 50.32 MHz), ARX 400 (^{13}C , 100.62 MHz) spectrometers.

The $\delta(^{103}\text{Rh})$ values were calculated by determining the absolute frequency of the cross peak (HMBC experiments) relating it to the reference frequency of 12.64 MHz ($\bar{\nu} = 3.16$ MHz at 100 MHz).

Gas chromatography (GC) was done on a Hewlett Packard HP 6890 instrument using a 5%-Diphenyl-siloxane-95%-Dimethyl-siloxane column of 30 m of length and 0.2 mm diameter. Product Abundancy was determined with the integrated area below each chosen peak and divided by the addition of the integrated areas of all relevant peaks. Mass and gas chromatography (GC/mass) and mass spectra were recorded with a Hewlett Packard HP5989 in electron impact mode (Ei, 70 Ev), or a Rybermag R10-10 spectrometer operating in Ei mode, or by chemical desorption (DCi/ CH_4 or NH_3).

Infrared spectra were recorded on a Perkin Elmer 1600FT spectrometer. ESR spectra were recorded on a Bruker ER200 instrument with frequency meter EIP, in toluene / THF solutions at 243°K.

All cyclic voltammetry experiments were performed in an airtight three-electrode cell connected to an argon line. The reference electrode was a SCE. The counter electrode was a platinum wire, and the working electrode was a Pt disc of ca. 3 mm in diameter. The currents and potentials were recorded on a Pentium II 350 MHz processor, with a BAS CV-50 Voltammetric Analyzer Potentiometer. Supporting Electrolyte $[\text{NBu}_4]\text{BF}_4$ was commercially acquired from Aldrich, and dried prior use.

ESR spectra were recorded on a Bruker ER200 instrument with frequency meter EIP, in toluene / THF solutions at 243°K.

Abbreviations

Abbreviations & Symbols:

<i>t</i> -Bu	<i>tert</i> -butyl
acacH	Acetylacetate
acac	Acetylacetonate
Cp	Cyclopentadienyl
Cp*	Pentamethylcyclopentadienyl
COD	1,5-cyclooctadiene
NLO	Non-Linear Optics
NBD	Norbornadiene (bicyclo[2.2.1]hepta-2,5-diene)
DMSO	Dimethylsulfoxyde
PPA	Polyphosphoric Acid
Et	Ethyl
Cp ₂ Fe	Ferrocene
[Cp ₂ Fe] ⁺ [BF ₄] ⁻	Ferrocenium tetrafluoroborate
<i>p</i> -CH ₃ C ₆ H ₄ SO ₃ H	<i>para</i> -Toluenesulphonic acid
Me	Methyl
Ind	Indenyl
Ic	<i>s</i> -Indacene
Pn	pentalene
<i>i</i> -Pr	<i>iso</i> -Propyle
Ph	Phenyl
THF	Tetrahydrofurane
DEPT	Distortionless Enhancement by Polarization Transfer
EPR	Electron paramagnetic resonance
ESR	Electron spin resonance
NMR	Nuclear Magnetic Resonance
HMBC	Heteronuclear Multiple Bond Connectivity
HSQC	Heteronuclear Single Quantum Coherence

Chapter 1

Introduction

1.1 Importance of catalysis

During the second half of the twentieth century, considerable progress has taken place in science and technology, especially, in the fields of electronics, nuclear physics, biology, and medicine, amongst others.

Nevertheless, the largest field which has allowed such development has been the non-renewable and basic natural resources such as oil. Several new products which 40 years ago were almost impossible to acquire are now commercially available, thanks to the industry of oil products and its respective subproducts. Some of these are: fuels, synthetic fibers, lubricants, detergents, plastics, chemical reagents, etc., including food and drug production. The tremendous variety of oil products and its respective derivatives they nowadays provide is in most cases thanks to the use of catalysts.

These new substances have allowed different industrial processes to become cheaper, allowing the formation of products with greater yields, or in a greater purity, and in some cases, to permit the formation of products that otherwise were impossible to synthesize by common means^[1].

The definition of a catalyst, or how a substance acts as a catalyst, is extremely variable, though it is widely accepted that a catalyst provides an alternative route of reaction where the activation energy is lower than the original chemical reaction, never modifying the free energy difference associated to the reaction, which is always favorable ($\Delta G < 0$). Generally, “good” catalysts participate in reactions but are neither reactants nor products of the reaction they catalyze. An exception is the process of autocatalysis where the product of a reaction helps to accelerate the reaction itself. They work by providing an alternative pathway for the reaction to occur, thus reducing the activation energy and increasing the reaction rate. More generally, one may at times call anything that accelerates a reaction, without itself being consumed or changed, a "catalyst".

Chapter 1: Introduction

In the middle ages, some chemical transformations were considered “magical” processes, due the presence of some certain unidentified materials which once combined with common substances would form products useful to man.

The results of different experiments at the time about unexplainable transformations, led Berzelius in 1835 to propose: “It has been proved that some simple or complex substances have the property of exerting over other substances an effect which is very different to that of common chemical affinity. By means of this effect, they may produce the decomposition of the elements within these substances, and promote different recombinations. This new unknown force is common to both organic and inorganic fields. I do not believe this is an independent force from electrostatic interactions, on the contrary; it is a new manifestation of this affinity. Nonetheless, as we are unable to determine its connection and mutual dependence, it seems more appropriate to provide this force with a separate name. I shall name it *catalytic force*, and name the decomposition of substances *catalysis*, in a similar way how the decomposition of substances by affinity is named *analysis*.”^[2]

Some other important phenomena concerning catalytic processes may be listed in order of their appearance:

- 1812: Thenard observed the spontaneous decomposition of hydrogen peroxide by addition of metallic powders.
- 1817: Sir Humphrey Davy reported a platinum wire in contact with ethanol would irradiate heat, together with the formation of acetic acid.
- 1825: Fumiseri suggested there should be a connection between adsorption and chemical reactivity, thus increasing the importance of the heterogeneity of different surfaces.
- 1831: The first patent for the oxidation of sulphur dioxide by means of a platinum sponge appears.
- 1834: Faraday mentions the phenomenon of metal poisoning due to certain impurities.
- 1836: Berzelius collected the above-listed processes to describe what he would name “catalytic force”.

Chapter 1: Introduction

- 1915: The synthesis of ammonia is now carried out in industrial processes, by the Haber process, which uses iron as a catalyst.
- 1920: The first book on catalysis was published by Paul Sabatier, providing valuable details about catalytic processes and their importance in future applications, such as the formation of methane using carbon dioxide and hydrogen catalyzed by finely divided metallic nickel, known today as the Sabatier Reaction, for which he shared the 1912 Nobel Prize in Chemistry^[3].

By the late 1930's, there was a massive exploitation of oil resources, and different catalysts were developed to allow the *cracking* of heavy oil molecules into lighter ones, mainly for the purpose of fuelling petrol-motorized vehicles. With time, catalysts were highly improved their efficiency, and nowadays many companies devote their time and resources to purifying and refining oil products. By the end of the 20th century, most of the processes involving oil and its refinement were catalytic, and their development has gone forward even faster than the understanding of how these processes function. Because of this, *catalysis* was considered to be a technological or empirical discipline, closer to a *test-and-try* method, instead of a theoretically-related field.

From 1970 and onwards, the development of the study of catalytic processes has grown very strongly; up to the point that nowadays, many research centers have departments specifically meant to further explore these areas, together with numerous journals exclusively dedicated to reporting studies of this nature^[4,5,6,7,8].

1.1.1 Homogenous and Heterogeneous Catalysts

Homogeneous catalysis is the chemical term which describes catalysis when catalyst, reagents, and products are in the same phase (ie. solid, liquid and/or gas). In heterogeneous catalysis, the catalyst is in a different phase from one of the reactants. Each sub-field has its advantages as well as its drawbacks. By the end of the 20th century most industrial processes used only heterogeneous catalysts, such as finely divided nickel

or platinum, and very few used homogenous catalysts, possibly due to their inability to compete with the high reaction rates heterogeneous catalysts usually have.

In order to understand better the differences and benefits of each type of catalyst, Table 1 summarizes the details.

Table 1: Comparison of Homogeneous and Heterogeneous Catalysis

Catalytic Feature	Homogeneous	Heterogeneous
Reaction Conditions	Mild	Harsh
Product Isolation	Difficult	Simple
Catalyst Recovery	Expensive	Unnecessary
Thermal Stability of the Catalyst	Low	High
Activity	Variable	High
Selectivity	High	Variable
Sensitivity to Catalyst Poisoning	High	Intermediate-Low
Determination of the steric and electronic effects of the catalyst	Viable	Very Difficult
Determination of the Mechanism	Frequent	Very Difficult
Diffusion	Low	Important

In general, homogenous catalysis allows a greater insight to the catalytic cycle, as in most cases, heterogeneous catalysts tend to require very elevated temperatures and/or high pressures, making the working conditions difficult to reproduce in a research laboratory, and increasing the uncertainty of how a catalytic center behaves once the reaction has initiated. Because of this, homogeneous catalysts have several advantages related to the feasibility of making catalysts with suitable molecular fragments and/or a suitable metallic fragment, thereby making it possible to alter reactivity by changing the nature of an atom or one ligand for another.

A new notion of catalysis is the combination of the advantages both catalytic areas present, this being the supporting of the homogenous catalyst in a heterogeneous

phase, such as poly-(4-ethylene-pyridine), silica gel, etc. This alternative provides a solution for the easy removal of the catalyst from the formed products, also allowing the possibility of studying the catalyst in milder conditions than those normally used in heterogeneous systems.

1.1.2 Homogenous Catalysis and its Development

The most popular homogeneous catalyst, is the Wilkinson's Catalyst ($\text{RhCl}(\text{PPh}_3)_3$)^[9], which is nowadays still used for the hydrogenation of olefins^[10], the hydroboration of alkenes^[11], the 1,4-reduction of unsaturated carbonyl compounds with trialkylsilanes^[12], amongst other uses. The compound receives its name from the 1973 Nobel Prize winner Sir Geoffrey Wilkinson who discovered its use.

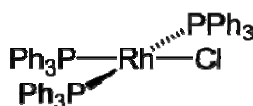


Figure 1: The square-planar geometry of Wilkinson's Catalyst

This rhodium-based catalyst is used in many research groups as a “standard” catalyst in order to compare the performance of other catalysts with this remarkable molecule. Despite the fact that many newer catalysts have higher activities than Wilkinson's Catalyst, this molecule is exceptional in terms of its mechanism because it displays within catalytic cycles of olefins the addition of simple molecules such as H_2 , $\text{HSi}(\text{C}_2\text{H}_5)_3$ or CH_3I , forming Rh^{III} species, in a reaction better known as an oxidative addition. Figure 2 shows how this catalyst proceeds in a simple olefin hydrogenation.

This catalyst is especially important in revealing the electron count throughout the catalytic cycle. As viewed, Wilkinson's Catalyst has a 16-electron configuration, and within the cycle this configuration changes repeatedly, where one of the reactions inducing this change is the oxidative addition of a hydrogen molecule in a cis fashion. This latter and other changes depending on the substrate concentration, as well as on the

nature of the reactants themselves. Thus, the performance of a catalyst is also connected to the electronic configuration that the metallic center has. In a very stable complex such as ferrocene, having a Noble gas 18-electron configuration is completely inert as a catalyst (as far as is known nowadays). This fact clearly indicates that a subtle equilibrium between stability and instability is required to produce catalytically active complexes^[13].

Most metals that naturally provide this subtle equilibrium are those that present a d^8 electronic configuration, such as Ni^{2+} , Pd^{2+} , Au^{3+} , Rh^+ , etc. Complexes with a square planar geometry are normally connected to a 16 electron configuration, reacting in similar ways as the figure shown below.

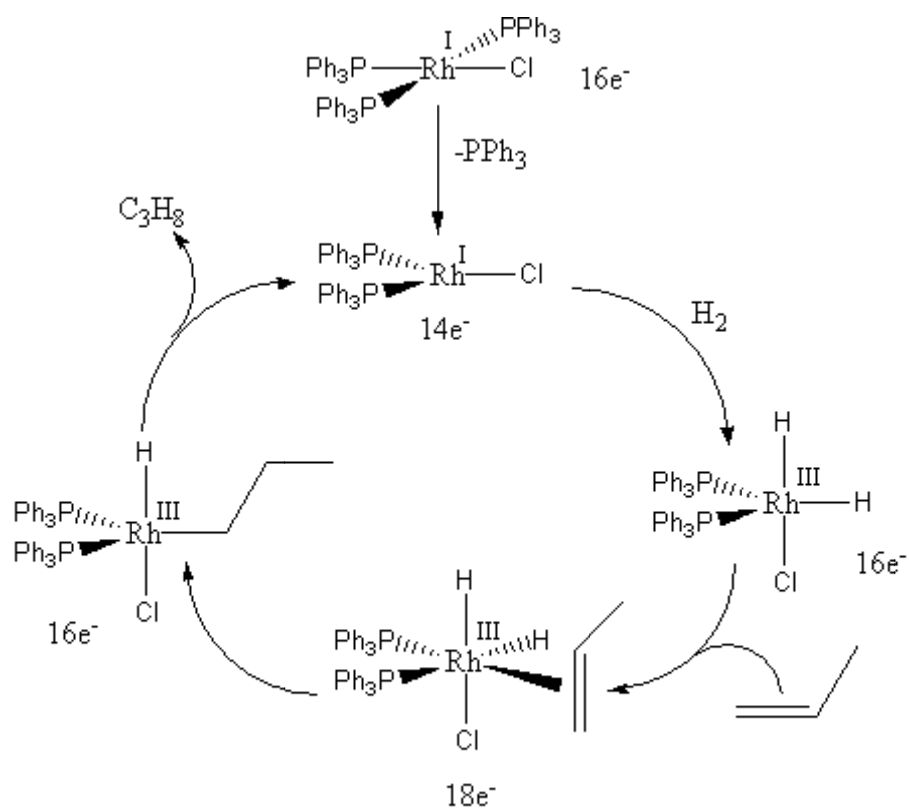


Figure 2: The Catalytic Hydrogenation of Propene

In metal-assisted homogeneous catalysis, a metal ion is usually coordinated to different ligands which allow the metal to remain stable under certain conditions, as well

as granting the whole complex an important degree of interaction with the solvent, allowing it to remain soluble. Ligands also have the advantage of modifying the electron density at a metallic center, depending on the chosen ligands. The formal electron count may remain the same, although the reactivity of the metal may (or may not) be dramatically modified, allowing a “fine tuning” of the behavior of a complex with catalytic properties^[12b].

This tuning of the reactivity may arise not only from ligands or the metal itself, but also from working temperatures, solvents, pressure, and even co-catalytic factors, as those in the Wacker process^[14] (Figure 3) or in Ziegler-Natta olefin polymerizations^[15] (Figure 4). The first consists of the oxidation of ethylene to form acetaldehyde using a copper complex to regenerate the initial palladium catalyst, while the second uses a trialkylaluminium compound to form highly acidic 14 electron species, which will readily undergo the entry of an olefin, subsequently inserting the olefin in the Metal-Alkyl bond. This process takes place several times, also known as the chain growth.

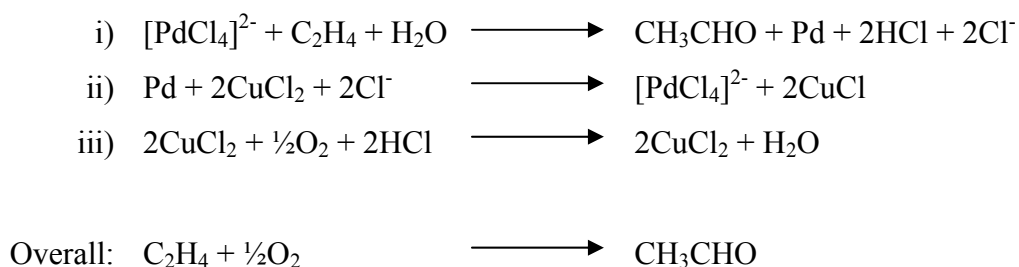


Figure 3: The stepwise formation of acetaldehyde in the Wacker Process

Fine tuning is not only crucial for the sake of high reaction rates, but also to achieve high selectivities in industrial processes, because in most cases more than one product may be formed and usually one of the products portrays a much larger theoretical (and financial) value than any other. Many new substances have been synthesized by

means of homogeneous catalysts, and finding the ideal working parameters is directly related to the correct and systematic study of these complexes. In the case of commonly known reaction systems, e.g. Wacker Process, Ziegler-Natta Polymerizations, Monsanto Process, Hydrogenation or Hydroboration of olefins, amongst others, years (if not decades) of study have taken place to characterize each process, hence the need to determine as much as possible how a catalyst functions in each step.

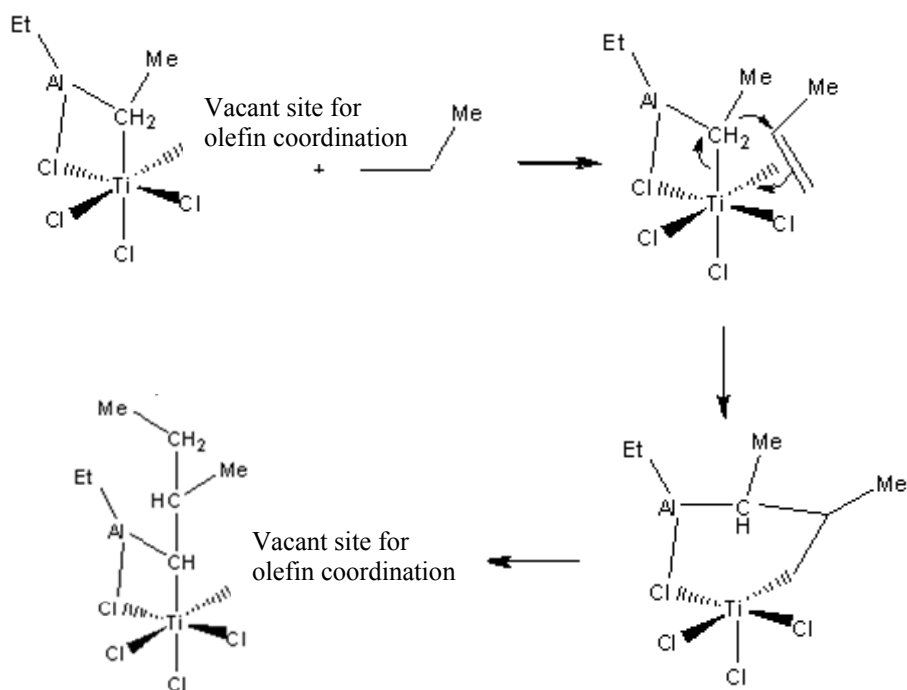


Figure 4: The mechanism of chain growth in the Ziegler Natta reaction assisted by a trialkylaluminium compound.

1.2 Designing Catalysts

1.2.1 Metals, Ligands and Spacer Ligands in Homogenous Catalysis

In order to achieve a highly-desired tuning in transition metal catalysts, ligands have a direct role in modifying the electronic density at the metallic site. It is precisely in this role that organic ligands become important with delocalized π electrons have undergone an important development due to haptotropic effect, better known as the indenyl effect^[16].

The indenyl effect is well known for allowing an equilibrium between the different bonding modes a ligand may have, obviously depending on the nature of the ligand itself, and the electronic demands the metal may require under different conditions. The indenyl effect could be the way to make finely tuned catalysts, as this equilibrium, in most cases, might take place even at very low temperatures, indicative of the low energy demands a ligand shift or change might have (Figure 5).

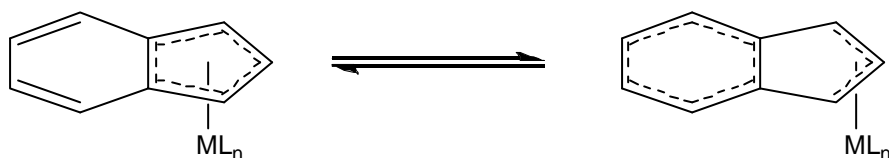


Figure 5: An illustrated example of how an arbitrary metal may shift from a pentahapto bonding mode (left) to a trihapto (right)

As seen, this equilibrium is somewhat more energy-demanding for other ligands, such as Cp (cyclopentadienyl) and Cp* (pentamethylcyclopentadienyl), due to the fact that the aromatic ring stabilizes the localized pair of electrons a metal would release to change to a lower hapticity mode (see Figure 6). Regardless of this, lower coordination modes from Cp-like rings is not unheard of, and many examples are described in the literature^[17]. The most popular and well-studied cases on how ligands do have interesting

effects on their catalytic behavior are the group 4 catalysts in Ziegler-Natta polymerizations^[18].

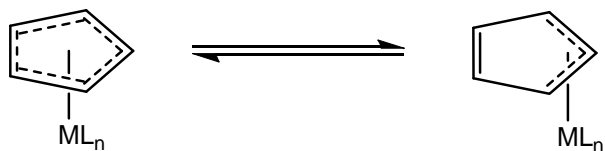


Figure 6: A bonding equilibrium which strongly (or completely) favours the pentahapto bonding mode.

Another more recent case is that reported by Ceccon *et.al.*, describing the effect some indenyl binuclear complexes have in cyclotrimerization of alkynes^[19]. A secondary metallic fragment such as $(\text{CO})_3\text{Cr}$ - modified the catalytic behavior a Rh center has on the interaction with catalytic substrates increasing the reaction rate by 1000 times, as well as modifying the performance of the complex in other simpler reactions such as kinetics of ligand exchange. This was explained as a cooperative effect both metals have on one another, due to an equilibrium between the two different bonding modes each metallic center presents. As visualized in Figure 7, a subtle balance between ${}^6\eta:3\eta$ and ${}^4\eta:5\eta$ arrays, increases the reactivity of the Rh center, making it more susceptible to nucleophilic attacks. This was named by its author, a “super indenyl” effect, because of the enhancement in reactivity a secondary metallic fragment would grant another metallic center by means of a spacer ligand^[20].

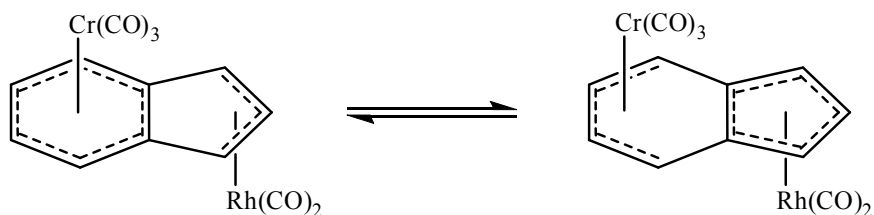


Figure 7: An equilibrium in heterobinuclear complex $(\text{CO})_3\text{Cr}$ -Ind-Rh $(\text{CO})_2$.

The cooperative effect has been defined and re-defined in many articles. This effect has been mostly understood and defined as the energetic-wise assistance one

groups or atom of a certain molecule may assist another, depending on the needs of this secondary group or atom. In bimetallic complexes, this has also been described in terms of “mixed valence” complexes, which have an increased stability of a mono-oxidized species, due to an electronic transfer which may make the energy changes for each metallic centers more discrete^[21] or even make the mono-oxidation process take place centered on the spacer ligand rather than on the metals^[22], thus increasing the stability of binuclear complexes.

A particularly significant example has been the Creutz-Taube ion complex^[23], as shown in Figure 8, consisting of two pentammine ruthenium units linked to the nitrogen atoms by a bridging pyrazine ligand which completes the octahedral coordination sphere of each metal. A most unusual feature of this compound is that the two metals apparently have fractional oxidation states, $\text{Ru}^{+2.5}$. As most ions have integral oxidation states, the fact that the oxidation states are half-integral indicates that the two $\text{Ru}(\text{NH}_3)_5$ centers are equivalent in terms of the number of electrons. Crystallographic and theoretical studies are consistent with this description, i.e. the two metals are equivalent.

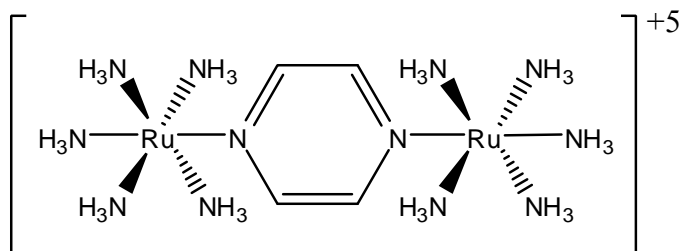


Figure 8: The Creutz-Taube ion

Characteristic of a mixed valence complex, this ion strongly absorbs light in the near-Infra-red part of the electromagnetic spectrum. In the case of the Creutz-Taube ion, the absorption maximum occurs at 1570 nm. This absorption is described as an intervalence charge-transfer band^[24].

In general, binuclear complexes with spacer ligands having a large degree of electronic delocalization (Figure 9) tend to be very good candidates for producing mixed valence species, such as pentalene, *s*- and *as*-indacene, indenyl, amongst many others.

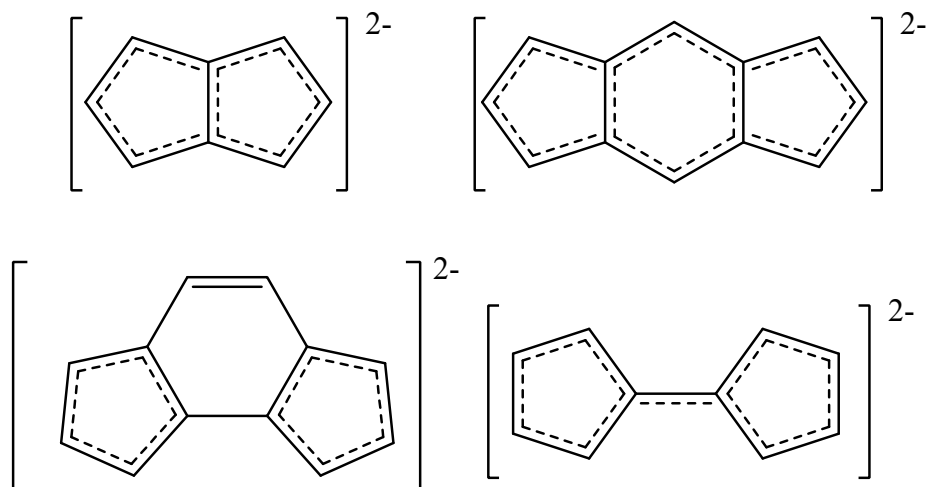


Figure 9: Diagrams of the dianionic species of pentalene, *s*-indacene, *as*-indacene, and fulvalene.

Many of the techniques employed to study the different phenomena associated with the communication between the metal centers are applied to mixed-valence species. Among the physical properties which afford information on these properties, two of these, the $\Delta E_{1/2}$ values relative to the redox potential of the two metal centers^[25], and the optical intervalence transfer band in the near-infrared (NIR) are widely used to classify the extent of interaction between the metals^[26,27]. Other specific techniques are suitable to study the electronic (ESR spectroscopy) and nuclear interaction (⁵⁷Fe-Mössbauer spectroscopy)^[28,29] between metal centers, whilst NMR spectroscopy and X-ray crystallography give useful structural information in solution and solid state^[30,31,32].

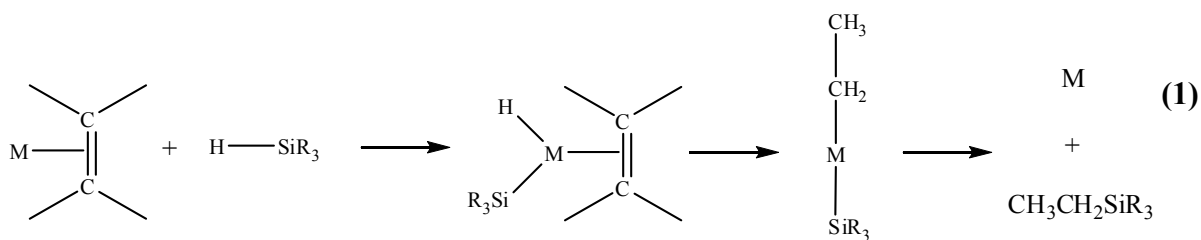
As described in both cases above, the cooperative effect has been defined in different ways in different articles. In some cases, authors have used many spectroscopic methods to determine the degree of communication between metallic fragments, mostly

focusing on the oxidation state of the resulting mono-oxidized product^[12,13], while other authors attribute the cooperative effect to an electronic rearrangement a secondary metallic may induce on the primary fragment, similar to a plain haptotropic effect^[10,33].

It appears that no single definition of a cooperative effect exists, although the cooperative effect between two metallic centers can be described as an electronic and/or structural rearrangement that would not occur without the secondary metallic fragment, in which its effectiveness depends on the nature of the bridging ligand, the metals, and the ancillary ligands each fragment may have.

1.2.2 New Silicon Products, Hydrosilylation and Dehydrogenative Silylation.

The first report describing the formation of new silicon-carbon atoms assisted by transition metal catalysts, was performed by Chalk and Harrod^[34], detailing the hydrosilylation of olefins. In this article, transition metals such as Ir and Pt were used. These metals would react with trialkylsilanes with various olefins forming a new open alkyl chain with a trialkylsilyl group, as seen in Reaction 1.



Further research proved the existence of a trace amount of a secondary product considered as an “unidentified impurity”, later properly identified as an unsaturated organosilicon compound, or vinylsilane^[35]. The initial Chalk-Harrod mechanism was incapable of describing its formation, hence a Modified Chalk-Harrod mechanism^[36] was proposed, Figure 10.

Silicon products have an increasing popularity, as these are the building blocks for different and useful substances, such as heat-resistant materials (coatings, paints or preregs), ceramics, NLO devices, new silicon polymers (used in medical implants or coatings for delicate electronic circuitry), amongst other uses^[37].

Despite the great importance of these new materials, little is known about the factors involved, such as the effect of ligands, rate-determining steps, and experimental evidence of intermediate species, specially with late transition metals^[38]. Some attempts have been made, such as the isolation of Rh(V) species after undergoing a double oxidative addition by a trialkylsilane^[39], the use of deuterated substrates^[40], time-resolved spectroscopy in the case of catalysts with carbonyl ligands in photocatalysis^[41], showing the existence and reversibility of the oxidative addition of the silane to the metallic center, as well as the formation of a metal-carbon and a metal-silicon bond supporting the currently accepted Chalk-Harrod mechanism (Figure 10).

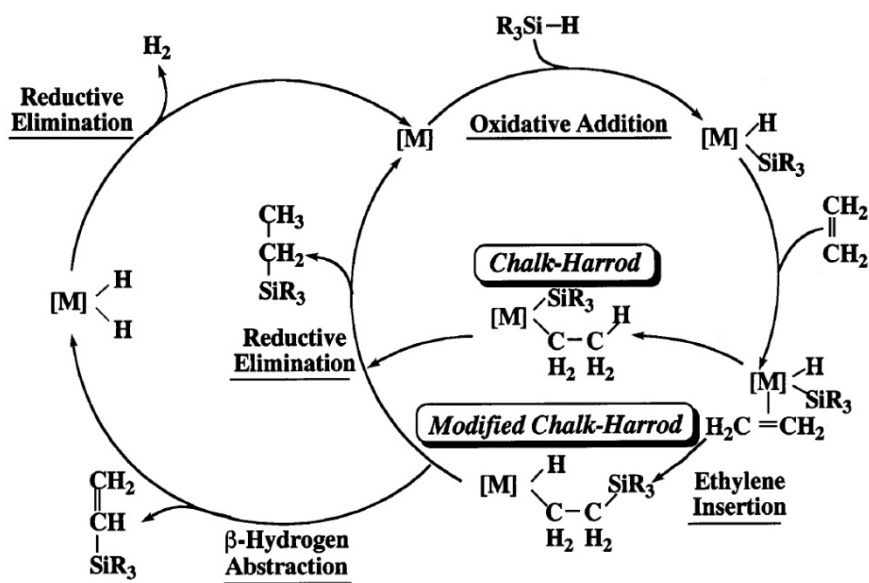
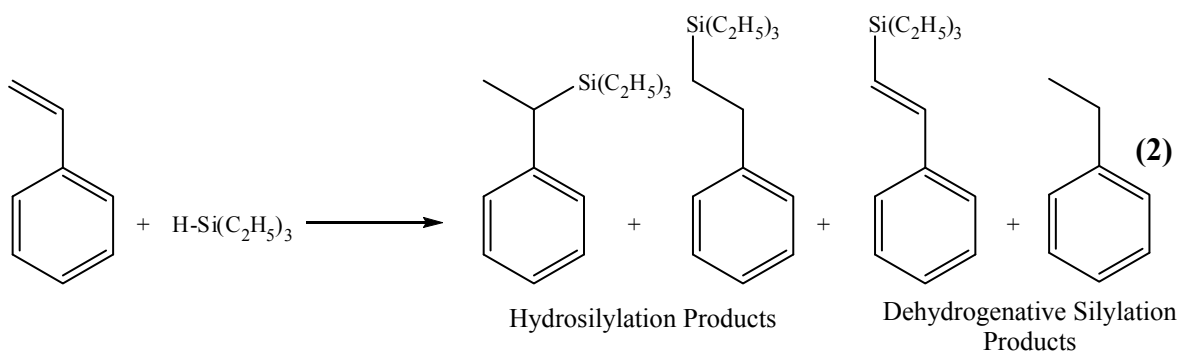


Figure 10: Chalk-Harrod and Modified Chalk-Harrod Mechanisms involving Transition Metals.

We have been motivated by the serious lack of precise information about the most relevant steps in the catalytic cycle to study some of the factors involved.

So far, there are only two known articles which describe the most feasible pathways to yield these interesting products with transition metals by means of theoretical calculations^[42,43], but using only extremely simplified ligand systems, or reaction pathways which do not always agree with the results of other catalytic systems. Hence, the need for further understanding the mechanistic cycle involved in the formation of the products exemplified below in equation 2.



The formation of vinylsilanes and hydrosilylated products is competitive, and dependent on countless factors, which would be difficult to summarize. Some aspects have been clarified, such as Pt catalysts seem to favor the insertion of the olefin in the M-H bond, thus becoming a potent hydrosilylation catalyst^[44]. On the other hand, rhodium presents a high oxidation number during the cycle (Rh^{I} to Rh^{III}), which would make the β -abstraction of an hydrogen atom a faster step, forming vinylsilanes^[26].

Recent advances are now taking place in such a manner as to stimulate new synthetic and mechanistic work aimed at the selective control of these reactions, hoping to further clarify this catalytic cycle.

1.3 Objectives

Previously, our research group published the results obtained for the heterobinuclear complex $\text{Cp}^*\text{Ru-Pentalene-Rh}(\text{COD})$, in which an X-ray structure

determination shows a bonding mode for rhodium similar to that in $(\text{CO})_3\text{Cr-Indenyl-Rh}(\text{CO})_2$, bringing it closer to an allylic array. Analogous to the Cr-Rh complex, allylic bonding produced an enhanced reactivity at Rh in two cases, these being the exchange of COD for carbon monoxide, and also in the dehydrogenative silylation of styrene^[45]. This exchange has motivated us to work on the design of catalysts using bridging ligands and varying the secondary metallic fragment, in addition to an ancillary on the Rh center.

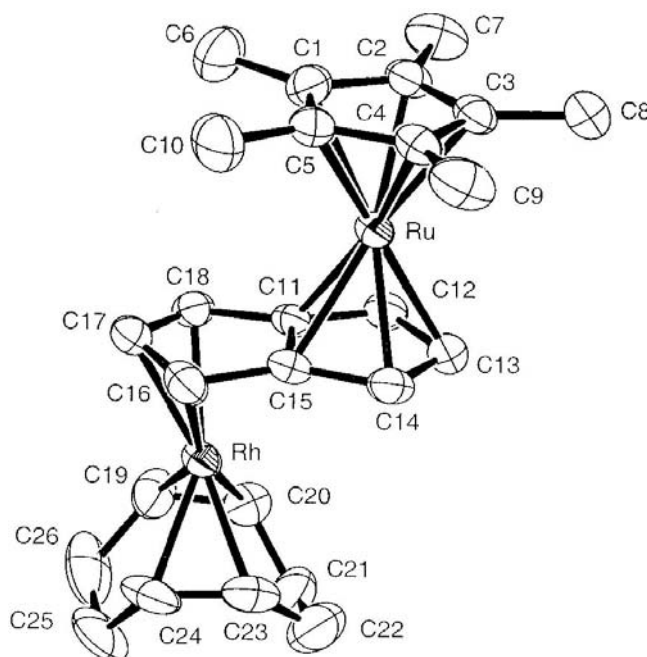


Figure 11: X-ray structure of Cp*Ru-Pn-Rh(COD).

Pentalene is a very unstable compound, and its synthesis is long and expensive^[46]. *s*-Indacene is a better alternative because its effectiveness as a spacer ligand has been well documented^[12,13].

The main goal of this project is to attempt to determine what effect a secondary metallic fragment has on the catalytically active metal, together with shedding some light on how the Chalk-Harrod and Modified Chalk-Harrod mechanisms are affected by modifying the nature of the ligands, and by comparing the effect on different substrates, such as olefins and silanes.

This thesis is divided into three sections: (i) The synthesis and characterization of s-indacene ligands, (ii) the synthesis of the homo- and hetero-binuclear rhodium complexes; and (iii) the catalytic study of each synthesized catalyst in different conditions.

References

¹ (a) G. Castellan, *Fisicoquímica*, Second Edition in Spanish, Addison-Wesley Iberoamericana S.A., **1987**, 877. (b) P. Atkins, *Fisicoquímica*, Third Edition in Spanish, Addison-Wesley Iberoamericana S.A., **1986**, 845.

² *New Encyclopaedia Britannica*, **1987**, 15th edition, Vol 2, 164.

³ Nobel Prize Database Website:

http://nobelprize.org/nobel_prizes/chemistry/laureates/1912/sabatier-bio.html

⁴ (a) T. Steinke, C. Gemel, M. Cokoja, M. Winter, R. Fischer, *Dalton. Trans.*, **2005**, 55. (b) J. Cunningham, S. Duckett, *Dalton. Trans.*, **2005**, 744. (c) H. Alt, A. Koppl, *Chem. Rev.*, **2000**, *100*, 1205. (d) F. Tanaka, *Chem. Rev.*, **2002**, *102*, 4885. (e) J. Melero, R. Van Grieken, G. Morales, *Chem. Rev.*, **2006**, *106*, 3790. (f) F. Kuhn, A. Santos, M. Abrantes, *Chem. Rev.*, **2006**, *106*, 2455. (g) C. Hartmuth, T. Kolb, K. Van Nieuwenhze, B. Sharpless *Chem. Rev.* **1994**, *94*, 2483.

⁵ A. Magistrato, T. Woo, A. Togni, U. Rothlisberger, *Organometallics* **2004**, *23*, 3218.

⁶ D. Carmona, M. Lamata, L. Oro, *Coord. Chem. Rev.*, **2000**, *200*, 717.

⁷ J. Martinho, J. Beauchamp, *Chem. Rev.*, **1990**, *90*, 629.

⁸ Y. Wang, S. Ou, P. Liu, F. Xue, S. Tang, *Journal of Molecular Catalysis A.*, **2006**, *252*, 107.

- ⁹ J. Osborn, F. Jardine, J. Young, G. Wilkinson, *J. Chem. Soc. A*, **1966**, 1711.
- ¹⁰ (a) A. J. Birch, D. H. Williamson, *Org. React.* **1976**, *24*, 155. (b) B.R. James, *Homogeneous Hydrogenation*. John Wiley & Sons, New York, **1973**.
- ¹¹ D. Evans, G. Fu, A. Hoveyda. *J. Am. Chem. Soc.*, **1988**, *110*, 6917.
- ¹² I. Ojima, T. Kogure, Y. Nagai, *Tetrahedron Lett.* **1972**, 5035.
- ¹³ (a) F. Cotton, G. Wilkinson, C. Murillo, M. Bochman, *Advanced Inorganic Chemistry*, Sixth Edition, John Wiley & Sons, Inc., **1999**, 661. (b) C. Masters, *Homogeneous Transition-metal Catalysis-A Gentle Art*, University Press, **1981**, 1.
- ¹⁴ (a) F.C. Phillips, *J. Am. Chem.*, **1894**, *16*, 255. (b) F.C. Phillips, *Z. Anorg. Chem.*, **1894**, *6*, 213. (c) J. Smidt, W. Hafner, R. Jira, J. Sedlmeier, R. Sieber, R. Rüttinger, H. Kojer, *Angew. Chem.*, **1959**, *71*, 176. (d) W. Hafner, R. Jira, J. Sedlmeier, J. Smidt, *Chem. Ber.*, **1962**, *95*, 1575. (e) J. Smidt, W. Hafner, R. Jira, R. Sieber, J. Sedlmeier, A. Sabel, *Angew. Chem., Int. Ed. Engl.*, **1962**, *1*, 80.
- ¹⁵ T. Takahashi, "Titanium(IV) Chloride-Triethylaluminum": *Encyclopedia of Reagents for Organic Synthesis*. John Wiley & Sons, Ltd, **2001**, 156.
- ¹⁶ M. Stradiotto, M. McGlinchey, *Coord. Chem. Rev.*, **2001**, *311*, 219.
- ¹⁷ M. J. Calhorda, C. Romão, L. Veiros, *Chem. Eur. J.*, **2002**, *8*, 868.
- ¹⁸ M. Bochman, *J. Chem. Soc., Dalton Trans.*, **1996**, 255.

¹⁹ L. Mantovani, A. Ceccon, A. Gambaro, S. Santi, P. Ganis, A. Venzo, *Organometallics* **1997**, *16*, 2682.

²⁰ C. Bonifaci, G. Carta, A. Ceccon, A. Gambaro, S. Santi, A. Venzo, *Organometallics* **1996**, *15*, 1630.

²¹ J. Manriquez, M. Ward, W. Reiff, J. Calabrese, N. Jones, P. Carroll, E. Bunel, J. Miller, *J. Am. Chem. Soc.* **1995**, *117*, 6182.

²² P. Roussel, D. Cary, S. Barlow, J. C. Green, F. Varret, D. O'Hare, *Organometallics* **2000**, *19*, 1071.

²³ (a) C. Creutz, H. Taube, *J. Am. Chem. Soc.*, **1969**, *91*, 3988. (b) C. Creutz, H. Taube, *J. Am. Chem. Soc.*, **1973**, *95*, 1086.

²⁴ U. Fürholz, S. Joss, H. Bürgi, A. Ludi, *Inorg. Chem.*, **1985**, *24*, 943.

²⁵ W. Nevin, M. Hempstead, W. Liu, C. Leznoff, A. Lever, *Inorg. Chem.*, **1987**, *26*, 570.

²⁶ K. Demadis, C. Hartshorn, J. Meyer, *Chem. Rev.*, **2001**, *101*, 2655.

²⁷ M. DeRosa, C. White, C. Evans, R. Crutchley, *J. Am. Chem. Soc.*, **2001**, *123*, 1396.

²⁸ G. Long, J. Wroblewski, R. Thundathil, D. Sparlin, E. Schlemper, *J. Am. Chem. Soc.*, **1982**, *104*, 1156.

²⁹ S. Taylor, J. Cashion, L. Brown, C. Hawkins, G. Hanson, *Inorg. Chem.*, **1995**, *34*, 1487.

³⁰ (a) M.D. Ward, *Chem. Soc. Rev.* **1995**, *24*, 121, (b) F. Paul, C. Lapinte, *Coord. Chem. Rev.* **1998**, *431*, 178.

³¹ D. Yokogawa, H. Sato, Y. Nakao, S. Sakaki, *Inorg. Chem.*, **2007**, *47*, 173.

³² S. Barlow, D. O'Hare, *Chem. Rev.* **1997**, *97*, 637.

³³ A. Cecon, A. Bisello, L. Crociani, A. Gambaro, P. Ganis, F. Manoli, S. Santi, A. Venzo, *J. Organomet. Chem.*, **2000**, *600*, 94.

³⁴ J. Chalk, J. Harrod, *J. Am. Chem. Soc.*, **1965**, *87*, 16.

³⁵ J. Speier, J. Webster, G. Barnes, *J. Am. Chem. Soc.*, **1956**, *79*, 974.

³⁶ M. Schroeder, M. Wrighton, *J. Organomet. Chem.*, **1977**, *128*, 345.

³⁷ (a) P. Pawluc, B. Marciniak, I. Kownacki, H. Maciejewski, *Appl. Organometal. Chem.* **2005**, *19*, 49. (b) N. Sabourault, G. Mignani, A. Wagner, C. Mioskowski, *Org. Lett.*, **2002**, *4*, 2117.

³⁸ B. Marciniak, *Coord. Chem. Rev.*, **2005**, *249*, 2374.

³⁹ J. Ruiz, P. Bentz, B. Mann, C. Spencer, B. Taylor, P. Maitlis, *J. Chem. Soc. Dalton Trans.*, **1987**, 2709.

⁴⁰ S. Bergens, P. Noheda, J. Whelan, B. Bosnich, *J. Am. Chem. Soc.*, **1992**, *114*, 2128.

⁴¹ C. Randolph, M. Wrighton, *J. Am. Chem. Soc.*, **1986**, *108*, 3366.

⁴² S. Sakaki, N. Mizoe, M. Sugimoto, *Organometallics*, **1998**, *17*, 2510

⁴³ S. Sakaki, M. Sumimoto, M. Fukuhara, M. Sugimoto, H. Fujimoto, S. Matsuzaki, *Organometallics*, **2002**, *21*, 3788.

⁴⁴ N. Sabourault, G. Mignani, A. Wagner, C. Mioskowski, *Org. Lett.*, **2002**, *4*, 2117.

⁴⁵ F. Burgos, I. Chavez, J. M. Manriquez, M. Valderrama, E. Lago, E. Molins, F. Delpech, A. Castel, P. Rivière, *Organometallics*, **2001**, *20*, 1287.

⁴⁶ A. Griesbeck, *Synthesis* **1990**, 144.

Chapter 2

Synthesis and Spectroscopic Studies of Polyalkylated 1,5-dihydro-s-Indacene Ligands

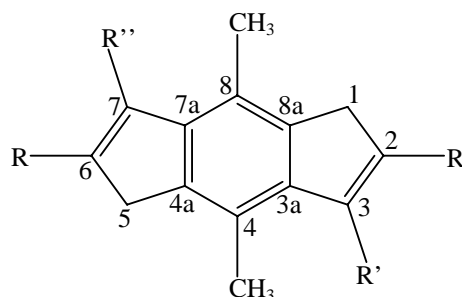
Chapter 2: Synthesis and Spectroscopic Study of Polyalkylated 1,5-dihydro-s-Indacene Ligands

Introduction

Un des objectifs de ce travail est d'étudier comment les groupements *s*-indacènes substitués se comportent en tant que ligands pontants et en particulier leur capacité d'établir une communication électronique, processus fondamental dans les réactions chimiques qui permet de modifier totalement la réactivité de tels systèmes. Les systèmes de type *s*-indacène comprenant trois cycles accolés (un phényle entouré de deux groupements cyclopentadiényles) ont été beaucoup moins étudiés que d'autres ligands comme les fulvalènes ou les groupements indényles. Notre groupe s'est focalisé sur l'étude des motifs *s*-indacènes polysubstitués dans le but de définir:

- l'effet de la nature des substituants sur le ligand
- l'effet du nombre de substituants
- l'effet sur la communication électronique en utilisant des substituants différents.

Pour cela, nous avons synthétisé une série de 2,4,6,8- et 2,3,4,6,7,8-alkyl 1,5-dihydro-*s*-indacènes diversement substitués :



- R = Me, R' = R'' = H
- R = Et, R' = R'' = H
- R = n-Bu, R' = R'' = H
- R = R' = R'' = Me
- R = Et, R' = R'' = Me
- R = Et, R' = Cl, R'' = Me

Nous avons tout d'abord mis au point un procédé général de synthèse en sept étapes qui nous a permis de les préparer en grande quantité.

Après une réaction de bromation du *p*-xylène, l'action d'un sel (Na) d'alkyldiéthylmalonate conduit au tétraester qui est transformé en acide par hydrolyse, s'ensuit une réaction de décarbonylation conduisant au diacide. Il est impératif que ces diacides soient parfaitement purs pour que l'étape suivante de cyclisation par l'acide polyphosphorique se fasse avec de bons rendements. De plus, la présence de substituants sur le cycle à 6 chaînons est indispensable pour que cette réaction de cyclisation soit

régiosélective et donne exclusivement la forme *s*-indacène de la dicétone en évitant toute formation secondaire de la forme *as*-indacène. Ensuite, cette dicétone est transformé en diol soit par réduction par LiAlH_4 ou par action d'un magnésien. La dernière étape de déshydratation est réalisée en présence d'acide para toluène sulfonique.

La plupart de ces 1,5-dihydro-*s*-indacènes ont été purifiés par sublimation. Ils se présentent sous forme de poudres dont la couleur varie du jaune au marron. Ils sont stables à l'air indéfiniment et aisément manipulables.

Nous avons ensuite réalisé une étude physicochimique approfondie de tous ces nouveaux dérivés (RMN du ^1H , ^{13}C , spectrométrie de masse, IR).

L'effet (nature et nombre) des substituants portés par le groupement *s*-indacène joue un rôle très important non seulement au niveau de la stabilité et de la solubilité propre des ligands mais également pour les complexes métalliques dont ils sont les précurseurs. En particulier, leur présence peut faciliter la formation d'intermédiaires réactionnels (mono ou dilithiés) à l'origine de la sélectivité des complexes hétérobimétalliques comme nous le verrons dans le prochain chapitre.

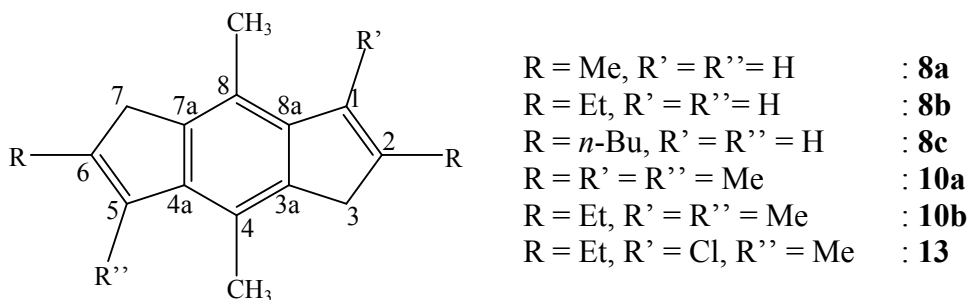
Dans la dernière partie de ce chapitre, l'étude par RPE des radicaux anions générés par oxydation des dérivés dilithiés correspondant a permis de mettre en évidence une bonne délocalisation de l'électron célibataire sur ces systèmes tricycliques quels que soient les substituants R en position 2 et 6.

2 Introduction

This part of the thesis is to understand how effective substituted *s*-indacenes act as spacer ligands, possibly generating internal electronic communication, a fundamental process in chemical reactions, which might modify the reactivity of certain simple molecular systems into higher and more complex systems. To the best of our knowledge, fused ring systems have not been as thoroughly characterized as other systems, such as fulvalene, indene, substituted indenenes, and 1,3,5,7-tetra-(*t*-butyl)-1,5-dihydro-*s*-indacene^[1] and its metallic complexes^[2]. Our group has centered its work on *s*-indacenes, towards elucidating:

- The effect and nature of the substituent, as this has proven to have an effect on the stability of the resulting spacer ligand^[3].
- The effect of the number of substituents.
- The effect on electronic communication using asymmetric ligands.

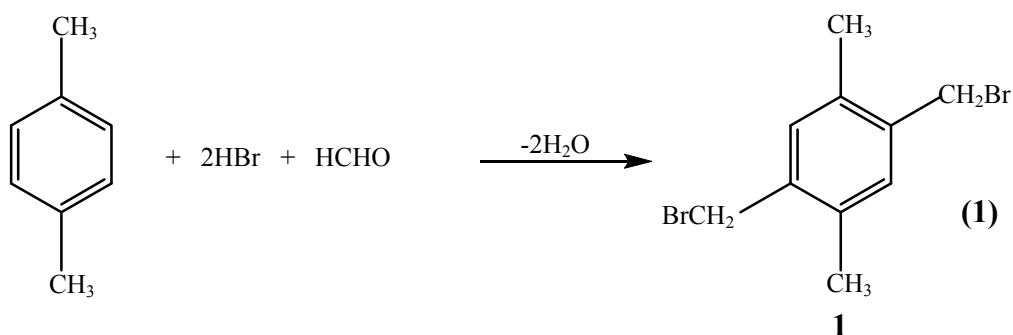
Therefore, a certain number of different 2,4,6,8- and 2,3,4,6,7,8-substituted 1,5-dihydro-*s*-indacene ligands have been prepared by our research group^[4].



2.1 Preparation of 2,4,6,8-Substituted 1,5-dihydro-*s*-indacenes:

The synthetic route to substituted *s*-indacenes, consists of seven reactions which form substituted 1,5-dihydro-*s*-indacenes, as seen in the above diagram. This route has high overall yields, making it suitable for these fused ring systems.

The first step of this process is the bromomethylation of *p*-xylene, yielding an almost quantitative yield of the 2,5-bis(bromomethyl)-1,4-dimethylbenzene, a well known and simple reaction which uses a mixture of formaldehyde and hydrobromic acid, and is feasible to carry out on a large scale (over 200 g of product). The reason why this reaction has such a remarkable yield is due to the initial methyl groups in the xylene starting reagent, which prevents other unwanted secondary reactions, unlike those reported in the past.^[5,6,7,8,9,10,11]

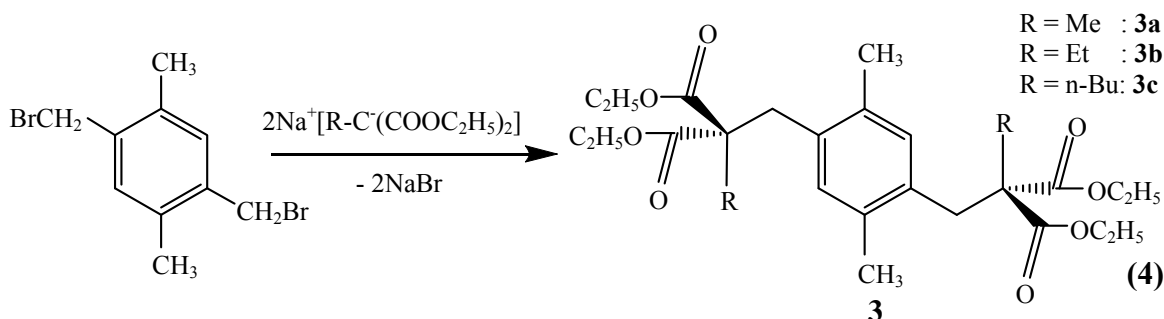


The second step employs an alkylated diethyl malonate reagent, which will determine the desired alkyl group to be placed in positions 2 and 6 in the final product. In this step only primary alkyl substituted malonates may be used, because in the case of *iso*-propyl- or *tert*-butyl diethyl malonates, only trace amounts of the respective tetraester are formed, due to the fact the steric hinderance of these branched alkyl chains restricts the reaction from taking place properly.

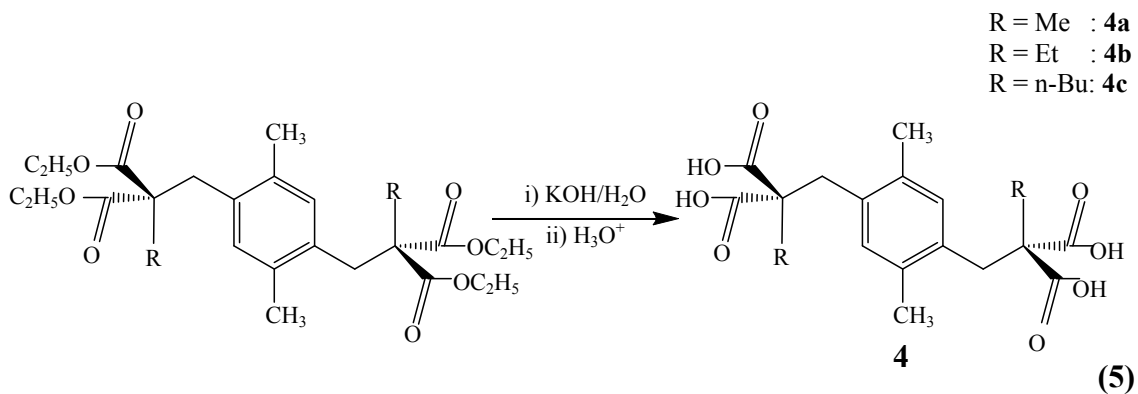
The suitable alkyl diethyl malonate is deprotonated using *in-situ* formed ethoxide for base (Reactions 2, 3 and 4). The tetraester product **3** is easily formed by a nucleophilic substitution over the brominated carbon of product **1**. In this case, the

Chapter 2: Synthesis and Spectroscopic Study of Polyalkylated 1,5-dihydro-*s*-Indacene Ligands

importance of an inert atmosphere and anhydrous solvent throughout the whole process in order to have large yields is critical.

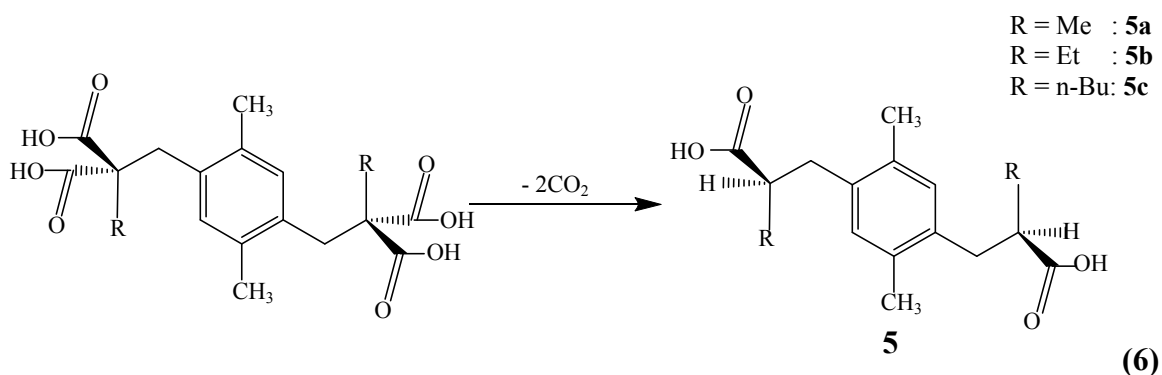


Reaction 5 is a simple ester hydrolysis in aqueous potassium hydroxide, followed by the addition of aqueous hydrochloric acid. This reaction is complete within 48 hours of solvent reflux, even if the tetraester has dissolved before this time. This is done to ensure that all four ester groups have reacted; otherwise, after adding concentrated HCl, a mixture of semi-hydrolyzed and fully hydrolyzed products forms a paste, rather than a pure white solid (product **4**).

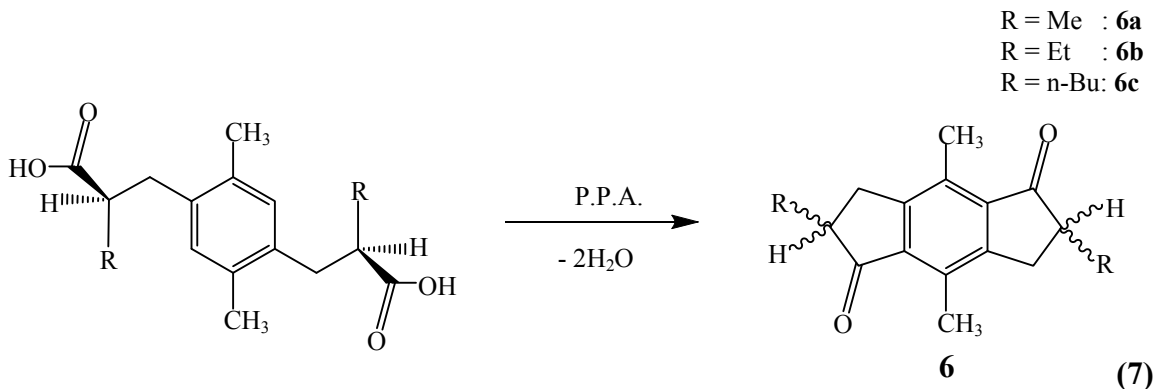


Chapter 2: Synthesis and Spectroscopic Study of Polyalkylated 1,5-dihydro-*s*-Indacene Ligands

Following the hydrolysis, a decarboxylation is done (Reaction 6) in a strict inert atmosphere to prevent air from oxidizing the mixture. The starting solid is heated to 190°C when a strong evolution of carbon dioxide occurs easily together with the formation of a brownish liquid corresponding to the respective diacid. Product **5** dissolves readily in ethyl ether to form a yellow solution. At this point an overall yield of 40% is normally reached.



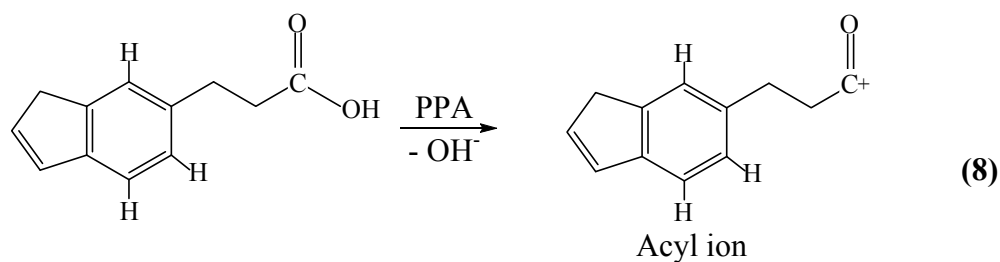
Compounds **1** to **5** are indefinitely stable in air, and completely insoluble in water. Since product **7** is sensitive to impurities, it is imperative to have product **5** completely pure. Trace amounts of water plus small amounts of the precursors decrease the yield of compound **6** drastically. Dissolving the diacid in concentrated KOH followed by an ethyl ether extraction and a reprecipitation with HCl yields pure **5**.



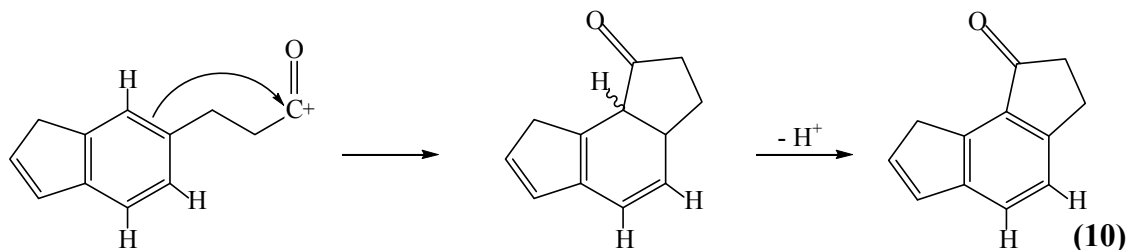
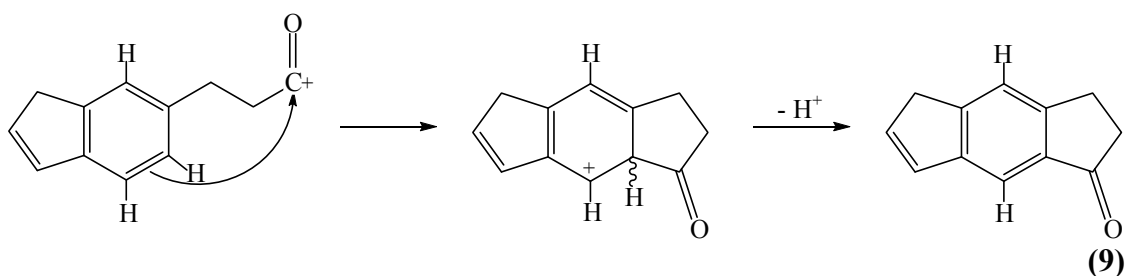
The formation of the diketone **6** is achieved when very dry **5** and polyphosphoric acid (PPA) undergo regioselective symmetrical cyclization to give the corresponding

Chapter 2: Synthesis and Spectroscopic Study of Polyalkylated 1,5-dihydro-*s*-Indacene Ligands

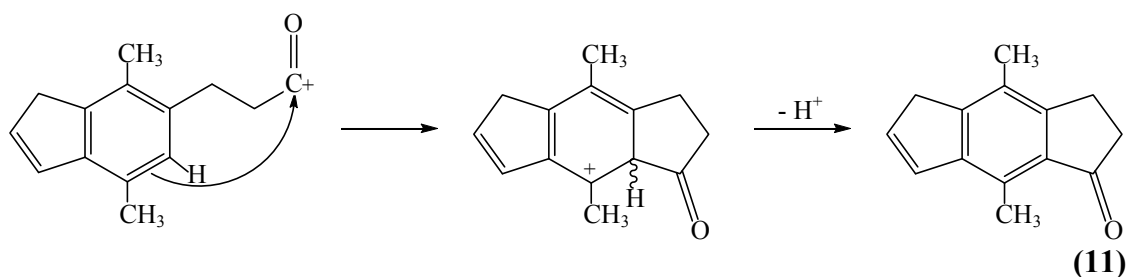
diketone by means of an acyl intermediate (see reaction 9), common in many processes involving PPA^[12], shown in Reaction 8.



The high specificity of these reactions is due to the presence of the methyl groups which prevents any other cyclations. Lacking these methyl groups, an isomer mixture would be produced (see reactions 9 and 10).

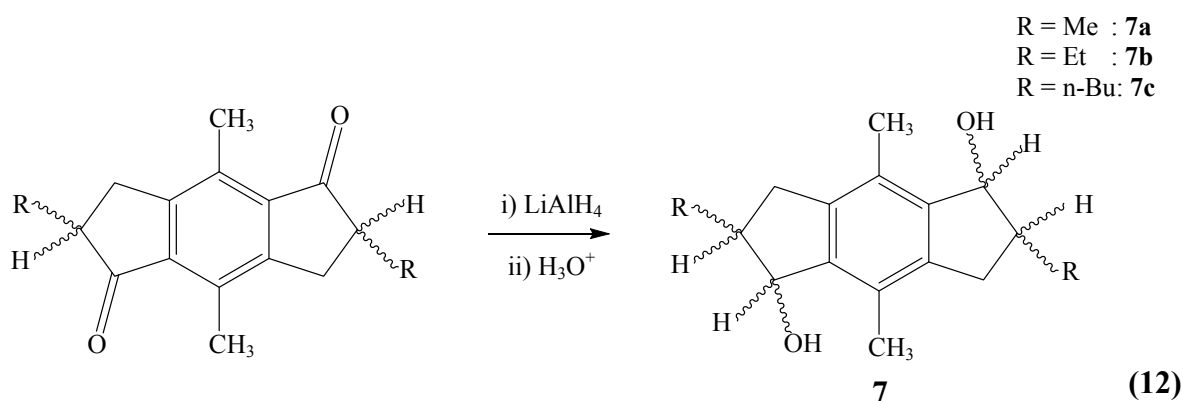


The methyl groups of *p*-xylene make Reaction 11 impossible and force the reaction to yield a linear molecule Reaction 12. For this reason the yield of the entire reaction is high.

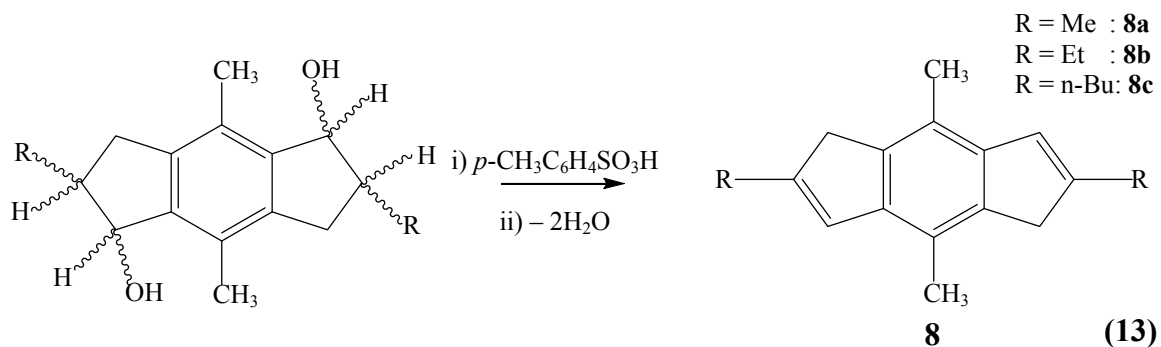


Chapter 2: Synthesis and Spectroscopic Study of Polyalkylated 1,5-dihydro-*s*-Indacene Ligands

The remaining steps include the formation of 3,7-diols, **7**, together with the acidic intramolecular dehydration of these diols, which must at all times be degassed and handled with dried solvents in an inert atmosphere. The reduction of the keto groups into alcohols by LiAlH₄ (Reaction 12) proceeds smoothly and with good yields, forming a total of four chiral carbon atoms which leads to several diastereoisomers, making the characterization by means of any spectroscopic method extremely difficult, if not impossible.

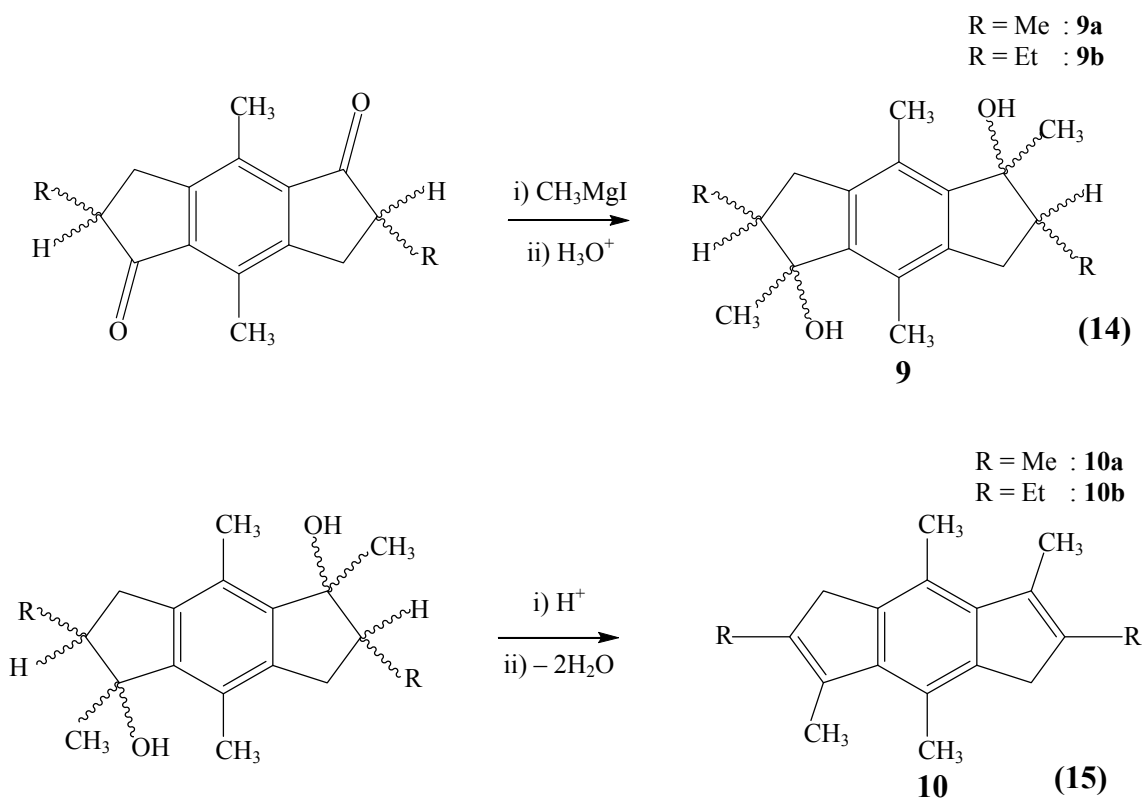


The intramolecular dehydration of the diols (Reaction 14) proceeds in benzene or toluene with no difference in yields or reaction times. The *para*-toluenesulphonic acid must be completely dry to increase reaction rates.

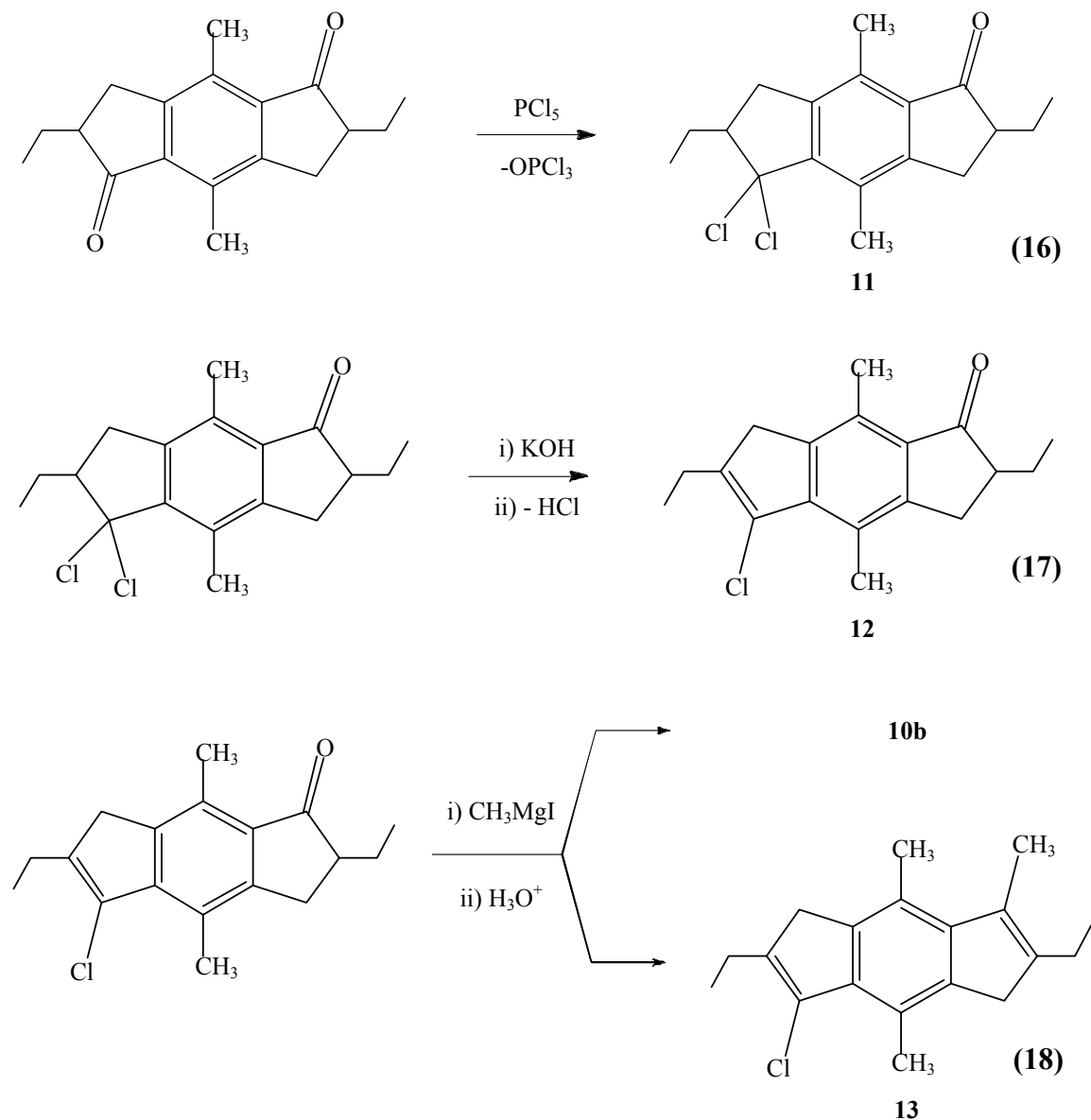


2.2 Preparation of 2,3,4,6,7,8-Substituted 1,5-dihydro-*s*-indacenes:

Using a similar procedure as described above, our group has also worked on the formation of hexasubstituted 1,5-dihydro-*s*-indacenes **10**, achieved using Grignard reagents combined with compounds **6a** or **6b** instead of LiAlH_4 ; more specifically using CH_3MgI in each case, carrying out a simple nucleophilic attack on the carbonyl group, thus, the simple formation of 2,6-dialkyl-3,4,7,8-tetramethyl-1,5-dihydro-*s*-indacene occurs. The syntheses and characterizations of these products are not given in this project, but they are fully detailed in reference 4. Reactions 14 and 15 show how these *s*-indacenes are formed.



2.3 Preparation of 3-chloro-2,6-diethyl-4,7,8-trimethyl-1,5-dihydro-*s*-indacene ligand:



The preparation of the first chloro-*s*-indacene, compound **13**, is very interesting because not only are there no previous reports of halo-indacenes, but also because it is an attractive option to asymmetrically substituted 1,5-dihydro-*s*-indacenes.

The first step is to cause one of the ketone groups of compound **6b** to react with phosphorous pentachloride in order to produce the *gem*-dichloro compound **11**. This

reaction yields a mixture of the original diketone and compound **11**, and surprisingly **12**, explained by spontaneous elimination of HCl. As these compounds could not be easily separated by conventional means, the mixture was made to react with an aqueous solution of KOH to convert all remaining **11** into **12**, followed by reaction with CH₃MgI and then the addition of water. This procedure once again yielded a mixture of products, these being **10b**, and the desired **13** in a 4:1 ratio. These two compounds were separated by preparative HPLC and isolated as pure products after crystallization.

2.4 Physical Characteristics of *s*-indacene ligands:

All 1,5-dihydro-*s*-indacene ligands (**8a-c**) are yellow to brownish powders. After purification by sublimation, they become white to pale yellow crystals, and are indefinitely stable in air at room temperature, allowing their easy manipulation. They are readily soluble in solvents such as benzene, toluene, but poorly in hexane, chloroform, THF and dichloromethane, and completely insoluble in polar solvents such as methanol, ethanol and water. Only in hot hexane, do these compounds have intermediate solubility, allowing their use in crystallization of the *s*-indacene derivatives before final purification by sublimation.

In general, *s*-indacenes with ethyl or butyl groups have radical changes in their solubility, making them easier to dissolve in any solvent than their methylated analogues.

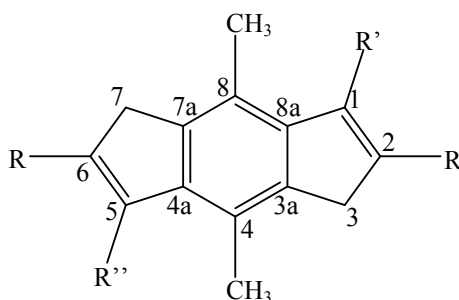
2.5 Spectroscopic Characteristics of *s*-indacene ligands:

All compounds described in this thesis have been thoroughly characterized by means of ¹H, ¹³C NMR, FT-IR, Mass Spectrometry and Elemental Analysis. Some of these compounds have already been reported^[4], but some corrections are described here, together with the characterization of the unreported products.

2.5.1 NMR Properties

All comparable NMR chemical shifts are fairly similar, as the differences between one ligand and the others are small, based on the effect of the substituent. Further details on the multiplicity of the each NMR signal, together with their coupling constant (when applicable) can be found in the experimental section of this chapter, and in the case of the hexasubstituted 1,5-dihydro-*s*-indacenes, refer to reference 4.

The following atomic label was followed in order to identify each nucleus active in NMR Spectroscopy.



2.5.1.1 ¹H- NMR:

The characteristic proton peaks for the groups (Table 2) of the *s*-indacene compounds are those of the two methyl groups in the center ring of the *s*-indacene appearing at 2.2 to 2.5 ppm, together with those in positions 3 and 7 (3.1 to 3.3 ppm), which are the acidic protons readily removed by KH, *t*-BuLi or *n*-BuLi, forming the respective anion or dianion, depending on the number of substituents and the kind of base used^[13].

In the case of 2,4,6,8-tetrasubstituted-*s*-indacenes, the typical chemical shifts ranging from 6.4 to 6.7 indicate the presence of an olefinic proton, absent in hexasubstituted analogues.

Table 1: Proton NMR chemical shifts for *s*-indacene ligands **8b**, **8c** and **13**.

	8b (R = C ₂ H ₅ ; R'=R''=H)	8c (R = <i>n</i> -C ₄ H ₉ ; R'=R''=H)	13 (R = C ₂ H ₅ ; R'=Cl; R''=CH ₃)
R group	1.24 (CH ₂ CH ₃) 2.64 (CH ₂ CH ₃)	0.99 (CH ₂ CH ₂ CH ₂ CH ₃) 1.66 (CH ₂ CH ₂ CH ₂ CH ₃) 2.55 (CH ₂ CH ₂ CH ₂ CH ₃)	1.15 (C ₍₆₎ -CH ₂ CH ₃) 1.18 (C ₍₂₎ -CH ₂ CH ₃) 2.48 (C ₍₆₎ -CH ₂ CH ₃) 2.57 (C ₍₂₎ -CH ₂ CH ₃)
R' group	6.62	6.66	2.26 (CH ₃ -C ₍₅₎)
R'' group			
CH ₃ -C _{4,8}	2.36	2.40	2.51 (CH ₃ -C ₈) 2.65 (CH ₃ -C ₄)
C _(3,7) H ₂	3.24	3.26	3.19 (C ₍₃₎ H ₂) 3.22 (C ₍₇₎ H ₂)

2.5.1.2 ¹³C- NMR:

The assignment of certain Carbon-13 NMR chemical shifts (Table 3) was no easy task; hence the need for other NMR methods, such as DEPT 135, plus 2D experiments HSQC and HMBC. Because certain carbon atoms are very similar it was impossible to properly distinguish one from the other. Usually, this would be the case with the aromatic carbon atoms in the central benzene ring of each *s*-indacene ligand.

Carbon-13 NMR signals can therefore be divided into two groups. First, those which ranged within 10.0 to 41.0 ppm belong to an alkyl group whether a methyl, ethyl, butyl, or the cyclic CH₂ group bonded to the central phenyl ring. Secondly, the signals between 120.0 and 150.0 ppm belong to olefinic carbon atoms, or to quaternary carbon atoms.

In the case of compound **13**, the complexity of the spectrum increases, because its asymmetry leads to a greater number of carbon atom signals.

Table 2: Carbon-13 NMR chemical shifts for *s*-indacene ligands **8b**, **8c** and **13**.

	8b (R = C ₂ H ₅ ; R'=R''=H)	8c (R = <i>n</i> -C ₄ H ₉ ; R'=R''=H)	13 (R = C ₂ H ₅ ; R'=Cl; R''=CH ₃)
R group	13.6 (CH ₂ CH ₃) 24.7 (CH ₂ CH ₃)	13.9 (CH ₂ CH ₂ CH ₂ CH ₃) 21.5 (CH ₂ CH ₂ CH ₂ CH ₃) 22.5 (CH ₂ CH ₂ CH ₂ CH ₃) 31.3 (CH ₂ CH ₂ CH ₂ CH ₃)	13.2 (C ₍₂₎ -CH ₂ CH ₃) 14.3 (C ₍₆₎ -CH ₂ CH ₃) 21.6 (C _(2,6) -CH ₂ CH ₃)
C _{3,7}	40.0	40.0	37.5 (C ₃) 38.8 (C ₇)
CH ₃ -C _{4,8}	14.0	15.0	14.5 (CH ₃ -C ₄) 14.9 (CH ₃ -C ₈)
C _{1,5}	123.7	124.7	126.7 (C ₁) 133.2 (C ₅)
C _{2,6}	150.2	148.7	142.6 (C ₂) 144.1 (C ₆)
C _{4,8}	121.9	121.9	122.9, 123.0 (C _{4,8})
C _{3a,4a,7a,8a}	140.5, 140.6	140.57, 140.67	135.1 (C _{3a}) 139.6 (C _{8a}) 141.5 (C _{7a}) 142.0 (C _{4a})

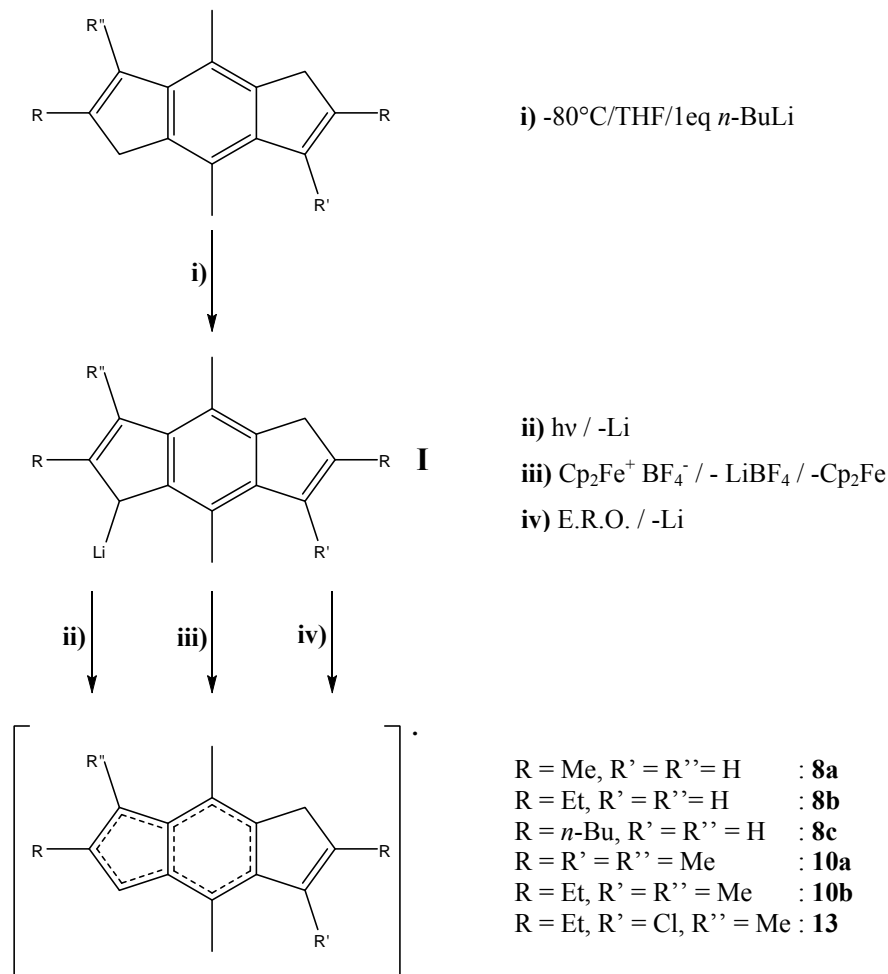
2.5.2 ESR Study:

The products obtained are suitable for ESR study once a free radical is generated, whether neutral or negatively charged. Such studies could shed some light on how the π electrons behave, showing if there is facile communication from one extreme of the ligand to the other, possibly allowing transition metals to form an electronic communication.

Chapter 2: Synthesis and Spectroscopic Study of Polyalkylated 1,5-dihydro-*s*-Indacene Ligands

The first method of preparation, (Schemes 1 and 2, *ii*), has often been reported in the literature^[14,15,16,17,18]. The second method, (Schemes 1 and 2, *iii*), occurs by a chemical oxidation of the mono- or dilithiated respective ligand using $\text{Cp}_2\text{Fe}^+ \text{BF}_4^-$. The third method, (Schemes 1 and 2, *iv*), proceeds by a SET / retro - SET process between the mono- or dilithium derivative **II** and an electron rich olefin (ERO, Scheme 2).

Scheme 1:

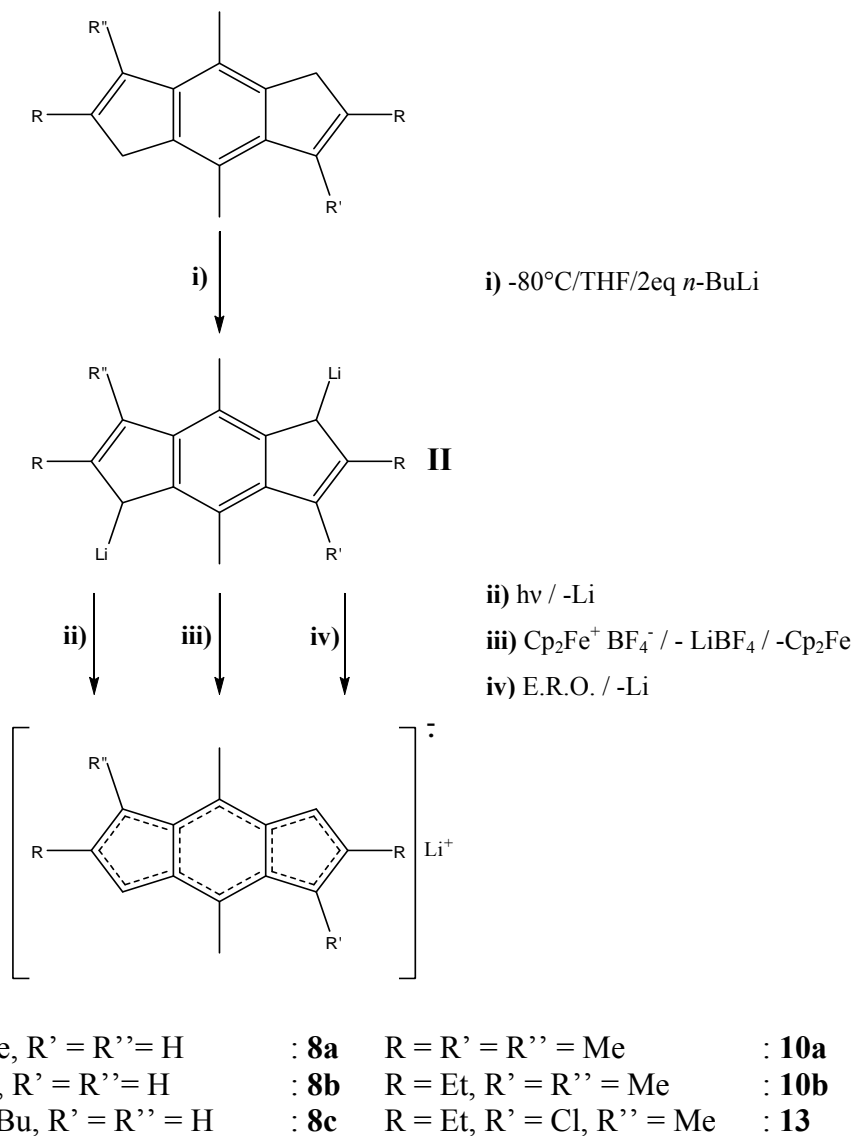


All radical anions which gave ESR spectra were exclusively prepared from the corresponding dilithium derivatives of various polyalkyl-*s*-indacenes (Scheme 2 and 3), as those experiments attempting to form free radicals starting from the monolithiated indacenes in Scheme 1 yielded a minimal concentration of free radicals that were detected only in a single experiment done with ligand **8a**, shown later in Figure 9. The

Chapter 2: Synthesis and Spectroscopic Study of Polyalkylated 1,5-dihydro-*s*-Indacene Ligands

instability can be explained by the fact that the neutrally charged radical formed from the monolithiated ligand **I** has only two rings instead of three which can stabilize the resonating single electron, as in the case of the anion radicals formed in Scheme 2.

Scheme 2:

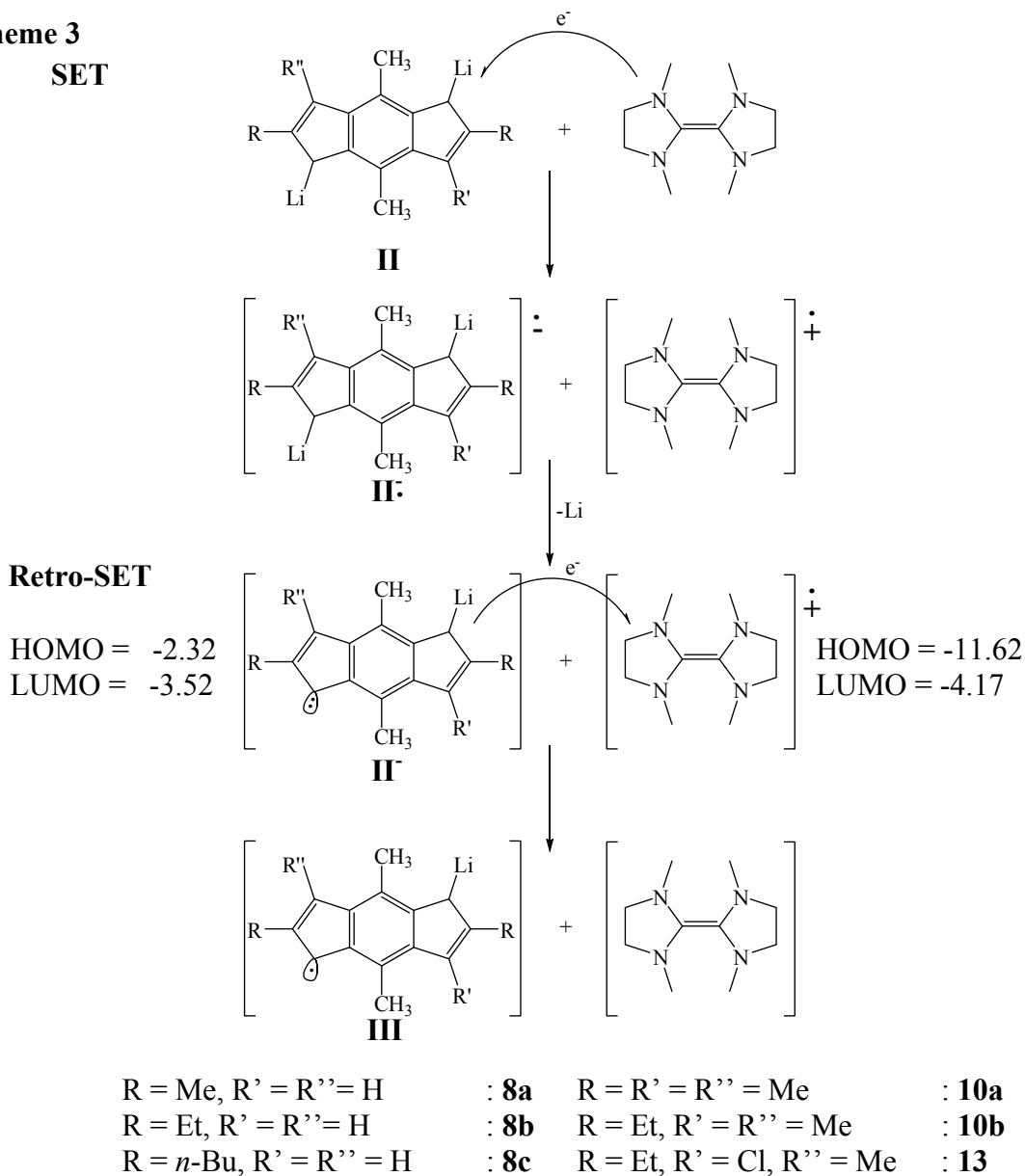


The ERO has been used before to produce metal-centred radicals, by chlorine abstraction from $\text{MCl}^{[19]}$ and organic anion radicals^[20]. The initial SET processes were also established in the case of various electron acceptors^[21]. In our case (Scheme 3), the retro - SET reaction between anion $\text{II}^{(-)}$ and the ERO radical cation is favoured by the

Chapter 2: Synthesis and Spectroscopic Study of Polyalkylated 1,5-dihydro-*s*-Indacene Ligands

difference in the energy levels of the LUMO in $\text{II}^{(-)}$ and the LUMO in ERO $(^{+})$. This retro-SET process is supported by the fact that a 100% excess of **II** leaves the ERO almost unchanged as followed by ESR and GC.

Scheme 3
SET



ESR spectra were studied by means of theoretical simulation taking one ligand in particular for stepwise analysis. It is well known that a single electron can couple with its neighbours differently, depending on proximity, and on the nuclei which can couple with this electron.

Chapter 2: Synthesis and Spectroscopic Study of Polyalkylated 1,5-dihydro-s-Indacene Ligands

The characteristics of the ESR signals of the radical anions **8a**, **8b**, **8c**, **10a**, **10b** and **13** were examined by theoretical simulation (Figures 2 - 7). Molecular calculations (Hyperchem at the AM1 level) of the density of spin localization, show in each case that in a 1/1 toluene/THF solution, ESR spectra of dilithiated **8a**, **8b**, **8c**, **10a** and **10b** (Figures 1-5) are more consistent with the structure of a radical anion. All of them have a very symmetrical distribution of spin (Figure 1 for **8b**), and also show that localisation of the odd electron does not go farther than the methylene group of the R side chain in positions 2 and 6, as observed experimentally (Figures 3, 4 and 6).

In Scheme 4 theoretical spectra were constructed, and the representation of the coupling constants of each specific interaction with each hydrogen atom is clearly evident.

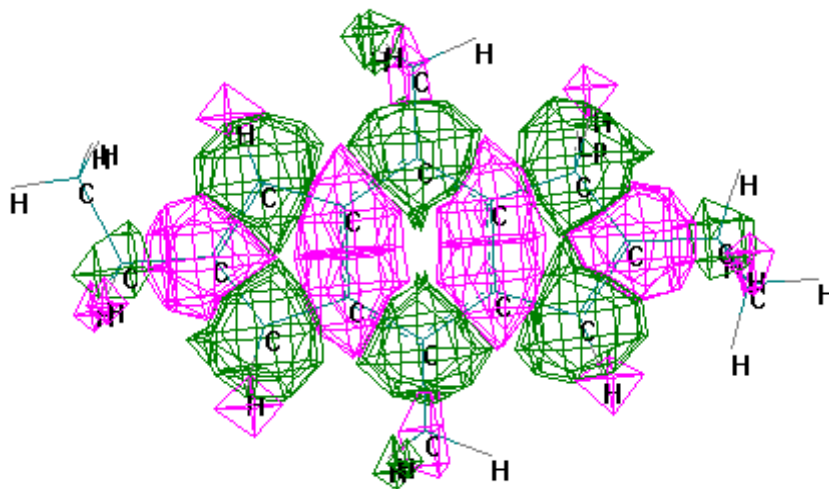
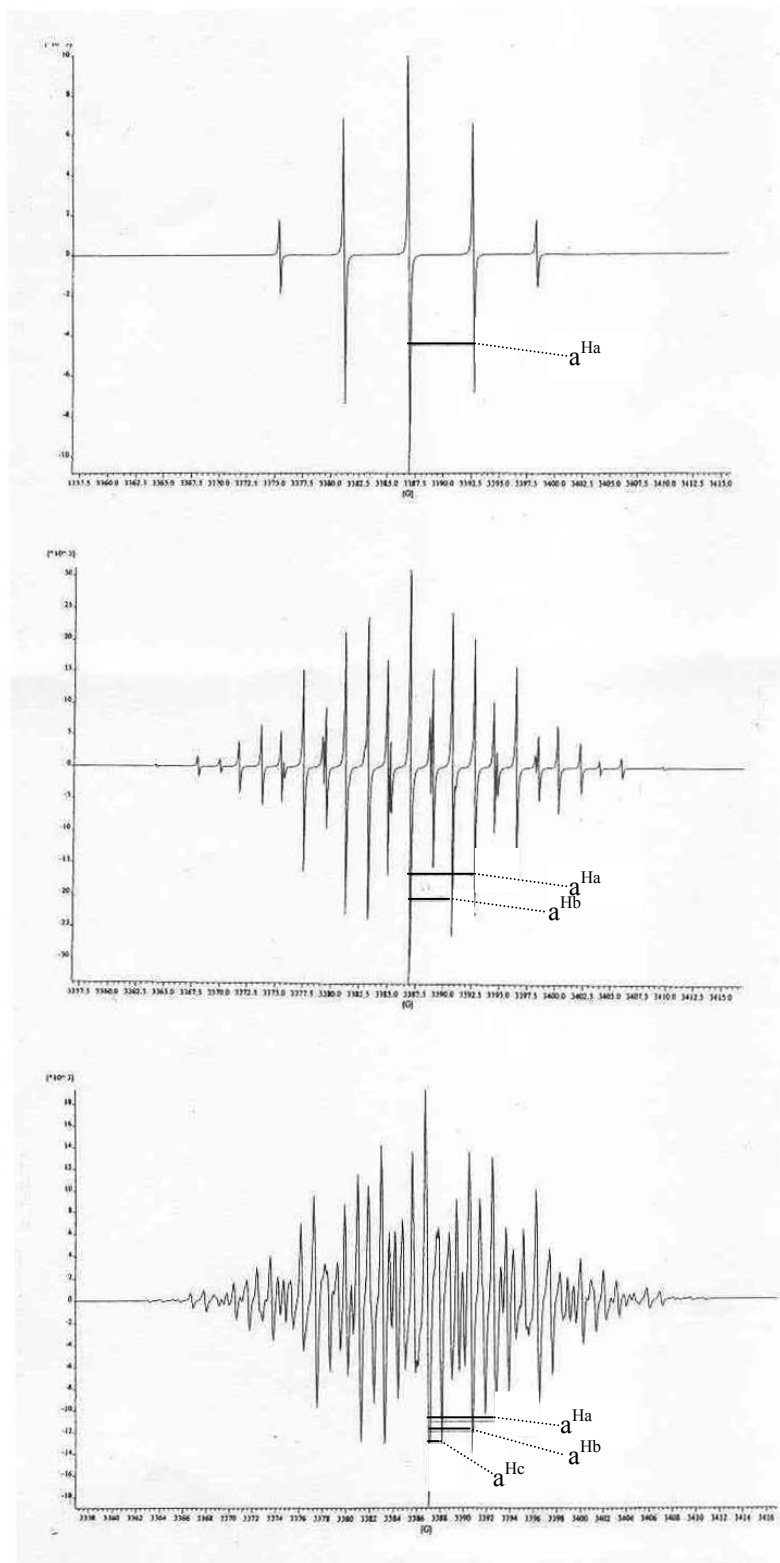


Figure 1: Density of spin localization for **8b**.

Chapter 2: Synthesis and Spectroscopic Study of Polyalkylated 1,5-dihydro-*s*-Indacene Ligands



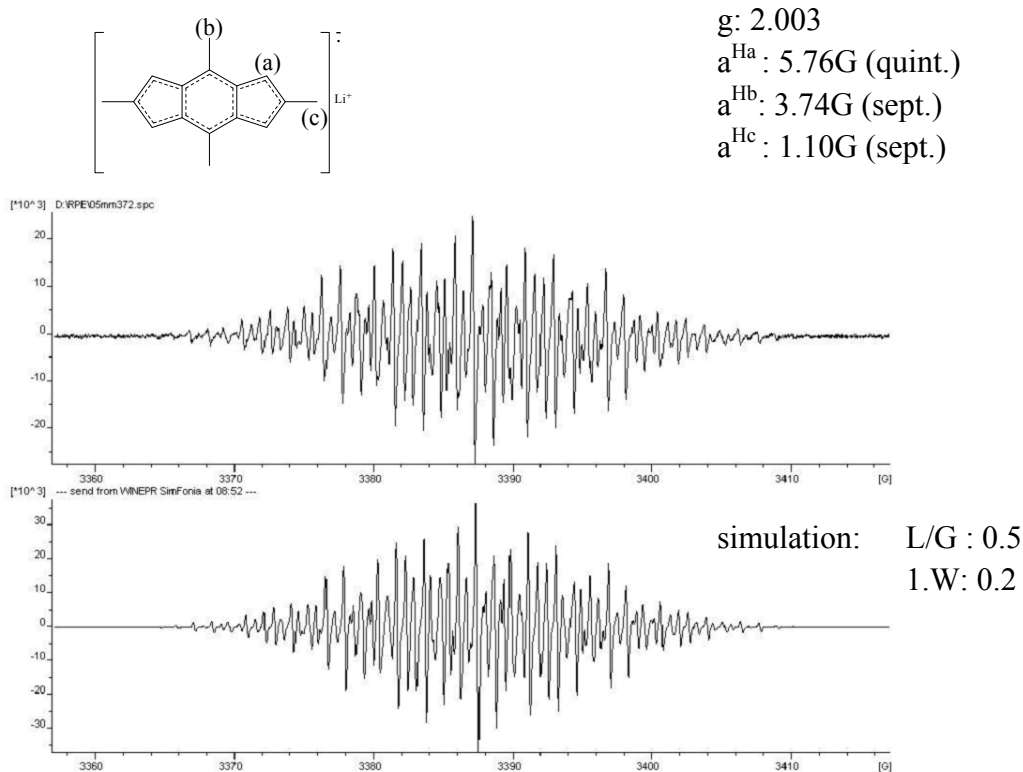
Scheme 4: Construction of a theoretical EPR spectrum for anionic radical of ligand **8b**.

Chapter 2: Synthesis and Spectroscopic Study of Polyalkylated 1,5-dihydro-*s*-Indacene Ligands

The coupling constant a^{Ha} represents the interaction of the lone electron with four nuclei producing a large value of 5.76G, thus forming a quintuplet. Each signal forms a septuplet (with a value of a^{Hb} of 3.74G), and finally, each of these signals forms another quintuplet (a^{Hc} equaling 1.10G). This reveals the major interactions which take place on the four hydrogens of the Cp-like rings of the *s*-indacene ligand, to later interact with the six hydrogen atoms of the two methyl groups in the middle ring, and finally have a weaker coupling with the CH₂ groups of the ethyl group.

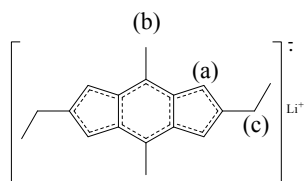
If the final spectrum is compared to the experimental spectrum of **8b**, the similarities are noteworthy. Both are almost identical, supporting the suggested theoretical coupling sequence. All other experimental spectra were very similar, if not identical, to corresponding theoretical simulations.

Figure 2: ESR Spectra and simulation for **8a**.



Chapter 2: Synthesis and Spectroscopic Study of Polyalkylated 1,5-dihydro-*s*-Indacene Ligands

Figure 3: ESR Spectra and simulation for **8b**.



g: 2.003
 a^{Ha} : 5.76G (quint.)
 a^{Hb} : 3.74G (sept.)
 a^{Hc} : 1.10G (quint.)

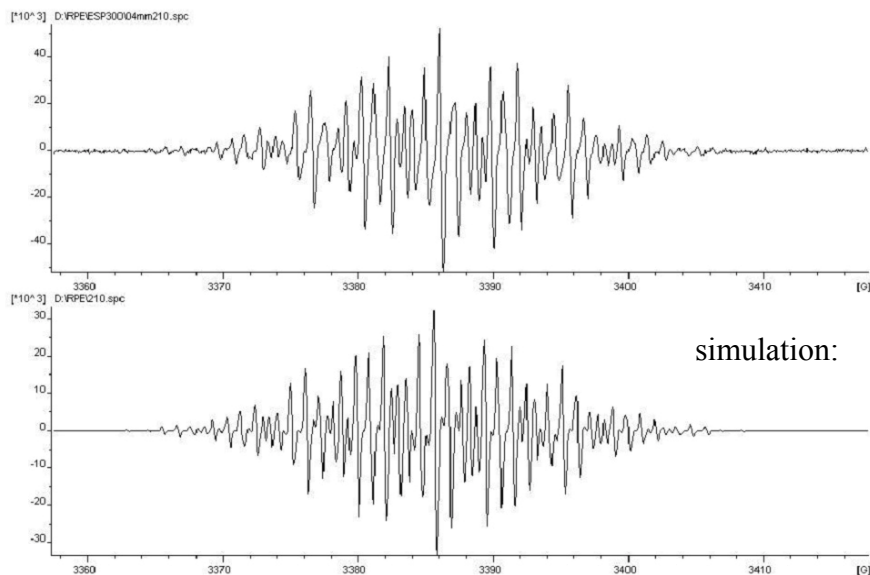
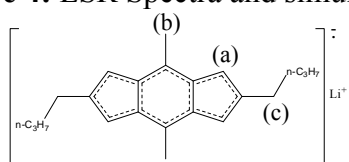


Figure 4: ESR Spectra and simulation for **8c**.



g: 2.003
 a^{Ha} : 5.78G (quint.)
 a^{Hb} : 3.70G (sept.)
 a^{Hc} : 0.95G (quint.)

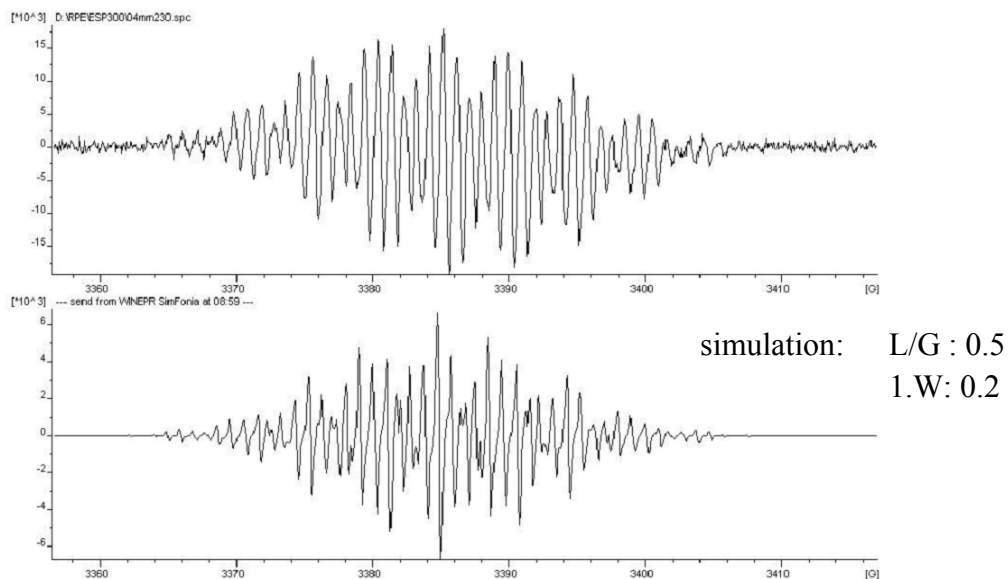


Figure 5: ESR Spectra and simulation for 10a.

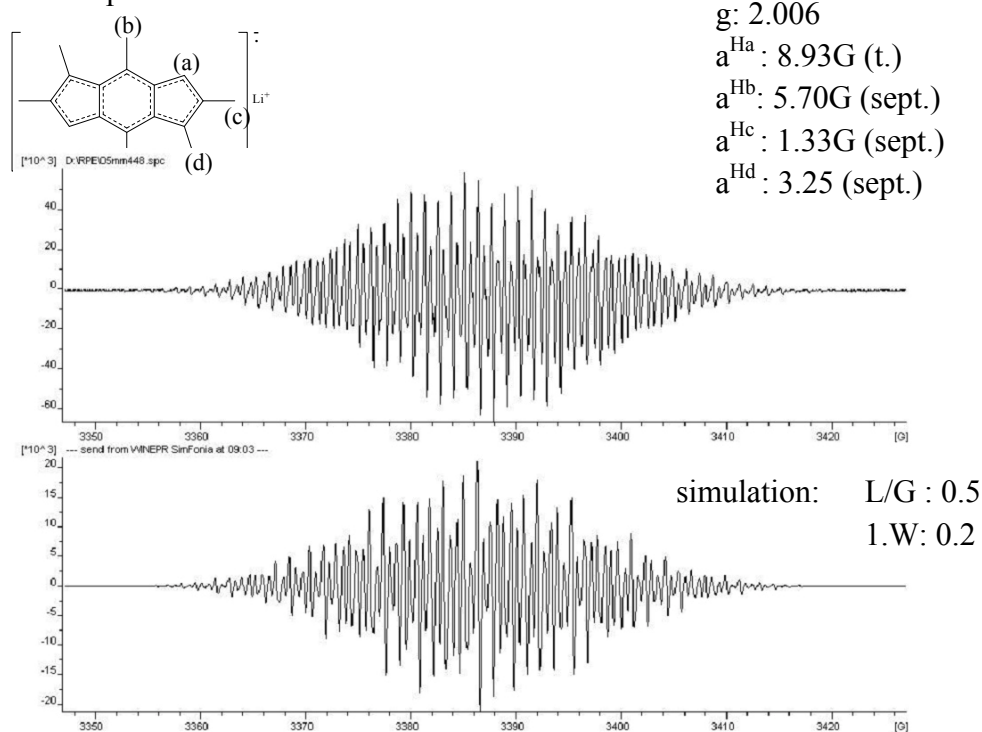


Figure 6: ESR Spectra and simulation for 10b.

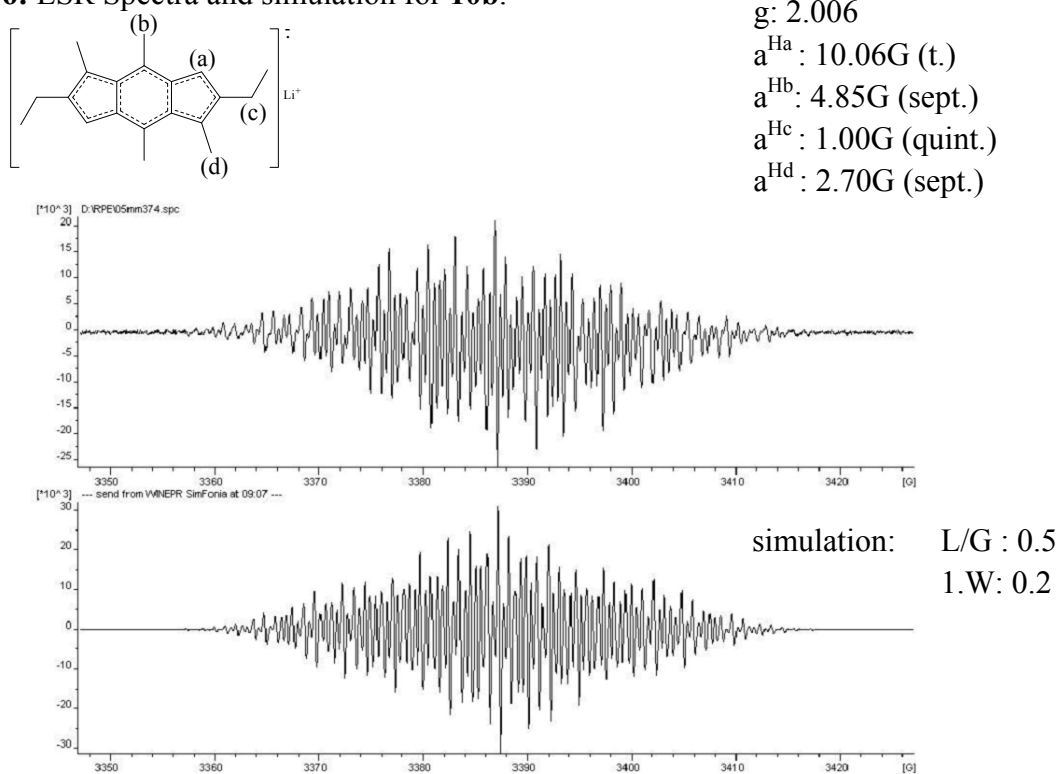
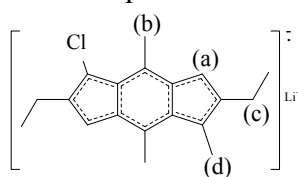
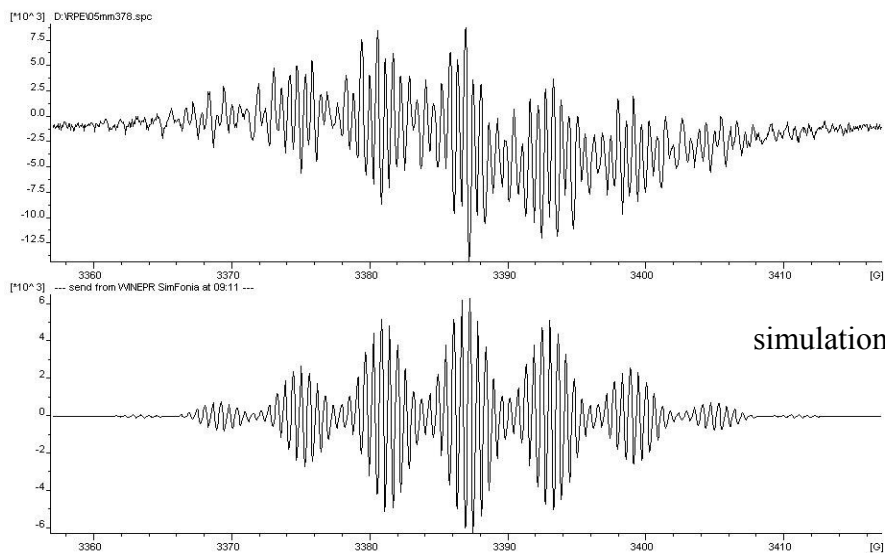


Figure 7: ESR Spectra and simulation for **13**.



$g: 2.006$
 $a^{\text{Ha}}: 6.35\text{G (t.)}$
 $a^{\text{Hb}}: 5.83\text{G (sept.)}$
 $a^{\text{Hc}}: 1.17\text{G (quint.)}$
 $a^{\text{Hd}}: 0.56\text{G (q.)}$



simulation: $L/G : 0.5$
 $1.W : 0.2$

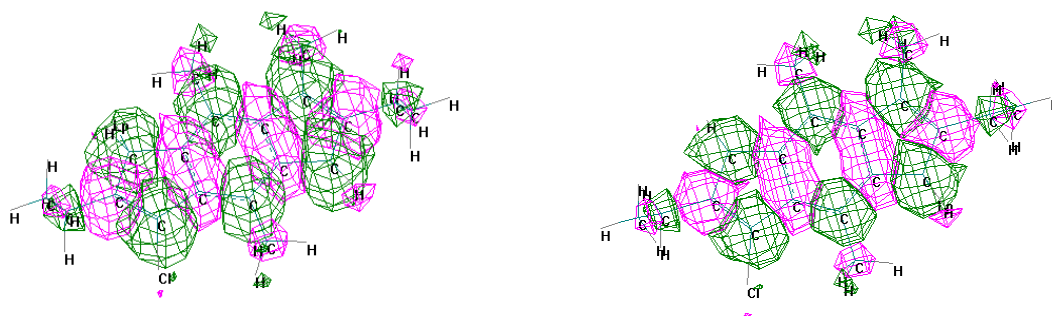
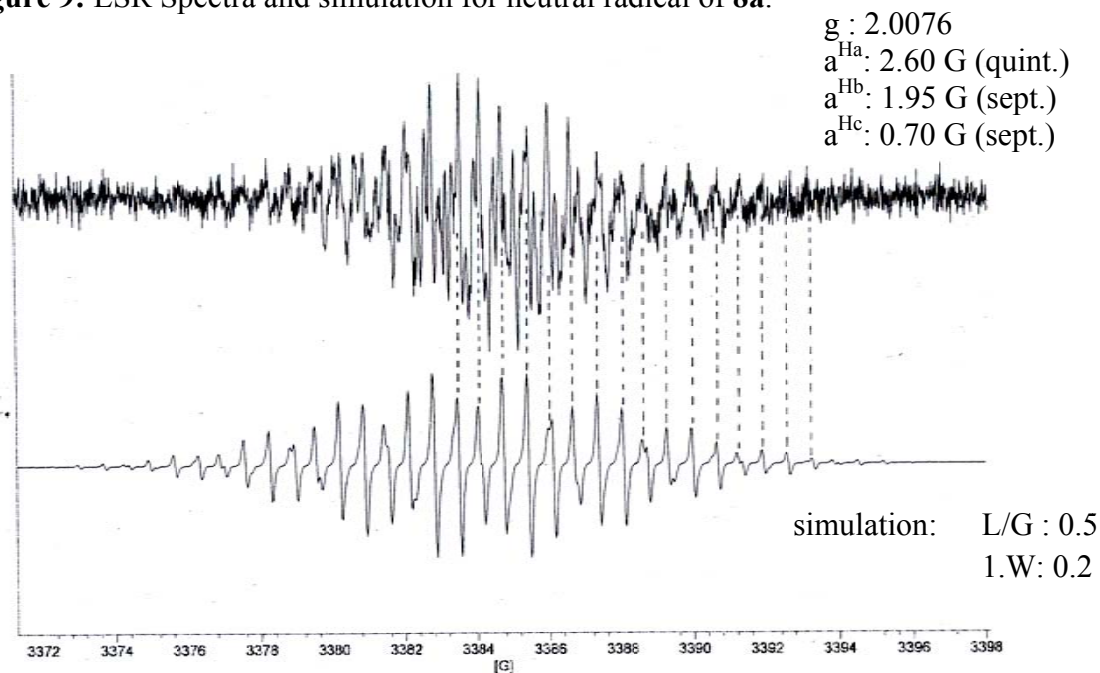


Figure 8: Density of spin localization for **13** in the two limit forms of same energy.

Figure 8 shows how the spin density is located throughout the three fused rings of the chlorinated *s*-indacene. Two limit forms, one where the unpaired electron is located in the chlorinated ring (left) or in the methylated five-membered ring (right) show identical spin distributions in the resulting calculation procedure, indicating there is no difference between one form or the other, as the difference in energy is minimal.

Figure 9: ESR Spectra and simulation for neutral radical of **8a**.



From the reaction of 2,4,6,8-tetramethyl-1,5-dihydro-*s*-indacenyllithium with ERO (Scheme 1), we observed the formation of the corresponding neutral radical. This radical had, under the experimental conditions previously used (243 K), a lower stability compared to the anion-radicals of dilithiated *s*-indacenes, as evident from the lower intensity of each signal, most likely due to a lower concentration of the radical in solution. Despite this, the localization of spin density appears almost symmetrical. This unexpected symmetry takes place even in the presence of a saturated moiety such as a methylene group (CH₂), though it is consistent with the observed hyperfine coupling in Figure 9, as well as the spin localization, as seen in Figure 10.

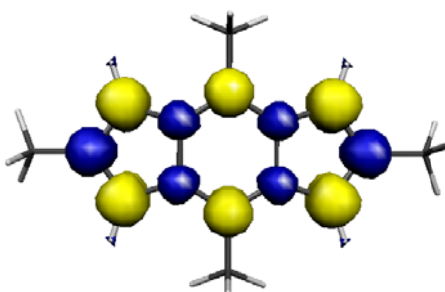


Figure 10: Density of spin localization for radical **8a**.

2.6 Conclusions:

Previously reported *s*-indacenes and a new dibutylated derivative plus a chloro-*s*-indacene have been successfully synthesized and characterized by means of previously described methods, such as RMN (^1H , ^{13}C), IR Spectroscopy, Mass Spectrometry and EPR Spectroscopy.

The newly reported ligands may be very important in providing a different reactivity in the case of metallic complexes of asymmetric halo-substituted *s*-indacenes; they may not necessarily affect the reactivity of mono- or binuclear metallic complexes, possibly due to the high symmetry observed in the chlorinated anion radical. In this particular case, there seems to be simply an increase and/or modification of the solubility not only of the ligand itself, but also of their respective metallic complexes.

Concerning the ESR measurements, these have been evidenced that simple theoretical calculations indeed reproduce those same results obtained by experimental measurements, which combined they further characterized the nature of these spacer ligands, showing that the electronic communication from one ring to the other is highly effective. The lack of importance (other than solubility) of alkyl groups in positions 2 and 6 beyond the first methylene group was also confirmed.

2.7 Experimental Section

2.7.1 Experimental Procedure for 2,6-diethyl-4,8-dimethyl-1,5-dihydro-*s*-indacene 8b:

2.7.1.1 Synthesis of 1,4-bis(bromomethyl)-2,5-dimethylbenzene 1:

Paraformaldehyde (80.5 g, 2.63 mole) and *p*-xylene (160.0 mL, 1.26 mole) are added to a solution of 48% HBr (1000 mL, 6.0 mole) in a 2L round-bottomed flask fitted with a reflux condenser. After 48 h of stirring at reflux temperature, an off-white precipitate is clearly visible. This solid is filtered, and recrystallized in CCl₄ giving pure **1** as white crystals. Yield: 214.8 g (97%).

Melting Point:	126-127°C
¹H-NMR (CDCl ₃ , δ ppm):	2.37 (s, 6H, CH ₃) 4.47 (s, 4H, CH ₂) 7.14 (s, 2H, C ₆ H ₂)
¹³C-NMR (CDCl ₃ , δ ppm):	18.2 (CH ₃) 31.7 (CH ₂) 132.4 (CH) 135.2 and 136.4 (C ₆ H ₂)
Mass Spectrum (EI, 70eV) m/z:	[M] ⁺ = 292 (10%) [M] ⁺ - Br = 211 (55%) [M] ⁺ - 2Br = 132 (100%)
FT-IR (KBr):	526 cm ⁻¹ (ν C-Br)
Analysis Calculated:	C ₁₀ H ₁₂ Br ₂ : C, 41.38; H, 4.14. Found: C, 41.50; H, 4.08.

Chapter 2: Synthesis and Spectroscopic Study of Polyalkylated 1,5-dihydro-*s*-Indacene Ligands

2.7.1.2 Synthesis of α,α' -bis(ethoxycarbonyl)- α,α' -diethyl-2,5-dimethyl-diethyl ester-1,4-Benzenedipropanoic acid **3b**:

In a two-necked 2L round flask fitted with a reflux condenser and a nitrogen inlet and a rubber septum, Na pieces (22.6 g, 0.98 mole) are added to 800 mL of ethanol with intense stirring at room temperature. After all Na pieces are consumed, **2b** (185 mL, 0.51 mole) is slowly added. After 30 min of stirring at room temperature, **1** (150 g, 0.51 mole) is added and the solution heated at reflux for 3 h. The excess ethanol is later distilled, and to the residue, an ice-cold water and diethyl ether mixture (2:1) is added. After stirring and decantation, the two phases are separated. The solvent of the organic phase is removed under vacuum, affording a white powder which is subsequently recrystallized from ethanol. Yield: 158.7 g (61%).

Melting Point:	51.4-52.7°C
¹H-NMR (CDCl ₃ , δ ppm):	0.88 (t, 6H, CH ₂ CH ₃ , ³ J _{H-H} = 7.4 Hz) 1.21 (t, 12H, OCH ₂ CH ₃ , ³ J _{H-H} = 7.1 Hz) 1.86 (q, 4H, CH ₂ CH ₃ , ³ J _{H-H} = 7.4 Hz) 2.17 (s, 6H, CH ₃ -Ph) 3.18 (s, 4H, CH ₂ -Ph) 4.05-4.19 (m, 8H, OCH ₂ CH ₃) 6.79 (s, 2H, C ₆ H ₂)
¹³C-NMR (CDCl ₃ , δ ppm):	9.0 (CH ₂ CH ₃) 14.0 (OCH ₂ CH ₃) 19.5 (CH ₃ -Ph) 25.6 (CH ₂ CH ₃) 33.8 (CH ₂ -Ph) 59.2 (C _{IV} -CH ₂ CH ₃) 61.0 (OCH ₂ CH ₃) 132.2 (CH _{AR}) 133.2, 134.2 (C _{IV AR}) 171.6 (C=O)
Mass Spectrum (EI, 70eV) m/z:	[M] ⁺ = 506 (21%)

Chapter 2: Synthesis and Spectroscopic Study of Polyalkylated 1,5-dihydro-*s*-Indacene Ligands

$[M]^+ - (OCH_2CH_3) = 461$ (9%)

$[M]^+ - EtC(OCH_2CH_3)_2 = 319$ (100%)

FT-IR (KBr):

1731 cm^{-1} (ν C=O)

Analysis Calculated:

$C_{28}H_{42}O_8$: C, 77.53; H, 9.56.

Found: C, 78.22; H, 8.98

2.7.1.3 Synthesis of α,α' -dicarboxy- α,α' -diethyl-2,5-dimethyl-1,4-Benzenedipropanoic acid **4b**:

In a 1L round-bottomed flask with a reflux condenser, compound **3b** (100 g, 0.20 mole) is added to a solution of KOH (135.4 g, 2.41 mole) in 100 mL of H_2O . The mixture is heated to reflux for 48 hours. The resulting solution was poured into a mixture of water and ice, and in order to prevent excessive heating, HCl (37%) is dropwise added till no further precipitation occurs. The white precipitate is filtered, and later washed with water, and dried at 100°C for 12 h. Yield: 66.9 (86%).

Melting Point:

196-198°C (sealed capillary)

1H -NMR (DMSO, δ ppm):

0.92 (t, 6H, CH_2CH_3 , $^3J_{H-H} = 7.4$ Hz)

1.74 (q, 4H, CH_2CH_3 , $^3J_{H-H} = 7.4$ Hz)

2.23 (s, 6H, CH_3 -Ph)

3.11 (s, 4H, CH_2 -Ph)

6.93 (s, 2H, C_6H_2)

12.41 (s, 4H, COOH)

^{13}C -NMR (DMSO, δ ppm):

8.8 (CH_2CH_3)

19.2 (CH_3 -Ph)

24.3 (CH_2CH_3)

32.8 (CH_2 -Ph)

57.9 (C_{IV} - CH_2CH_3)

131.6 (CH_{AR})

133.0, 133.6 ($C_{IV AR}$)

172.9 (COOH)

Chapter 2: Synthesis and Spectroscopic Study of Polyalkylated 1,5-dihydro-*s*-Indacene Ligands

Mass Spectrum (EI, 70eV) m/z: Thermal Decomposition of **4b** into **5b**

FT-IR (KBr): 1712 cm⁻¹ (ν C=O)

3314 cm⁻¹ (ν OH)

Analysis Calculated: C₂₀H₂₆O₈: C, 60.91; H, 6.60.

Found: C, 60.57; H, 6.43.

2.7.1.4 Synthesis of α,α'-diethyl-2,5-dimethyl-1,4-Benzenedipropanoic acid **5b**:

In a two necked 1L round flask fitted with a nitrogen inlet, **4b** (50 g, 0.13 mole) is placed and heated until the evolution of CO₂ ends. The liquid residue is cooled, becoming a very hard brownish solid. This is dissolved in large amounts of ethyl ether, to later transfer into a more suitable flask and dried under vacuum, affording a white grainy solid. Yield: 36.1g (93%).

Melting Point: 193-194°C

¹H-NMR (CDCl₃, δ ppm): 0.95 (t, 6H, CH₂CH₃, ³J_{H-H} = 7.4 Hz)

1.60 (m, 4H, CH₂CH₃, ³J_{H-H} = 7.4 Hz)

2.26 (s, 6H, CH₃-Ph)

2.40-2.90 (m, 6H, CH₂-Ph and CH₂CH₃-CH)

6.94 (s, 2H, C₆H₂)

12.19 (s, 2H, COOH)

¹³C-NMR (CDCl₃, δ ppm): 11.8 (CH₂CH₃)

18.9 (CH₃-Ph)

25.0 (CH₂CH₃)

34.7 (CH₂-Ph)

47.8 (CH₂CH₃-CH)

131.1 (CH_{AR})

133.7, 135.4 (C_{IV AR})

176.3 (COOH)

Mass Spectrum (EI, 70eV) m/z: [M]⁺ = 306 (34%)

Chapter 2: Synthesis and Spectroscopic Study of Polyalkylated 1,5-dihydro-*s*-Indacene Ligands

	$[M]^+ - H_2O = 288$ (100%)
	$[M]^+ - HCOOH = 260$ (12%)
FT-IR (KBr):	1702 cm^{-1} (ν C=O)
	3001 cm^{-1} (ν OH)
Analysis Calculated:	$C_{18}H_{26}O_4$: C, 70.59; H, 8.49.
	Found: C, 70.78; H, 8.78.

2.7.1.5 Synthesis of 2,6-diethyl-2,3,6,7-tetrahydro-4,8-dimethyl-*s*-indacene-1,5-dione **6b**:

In a round three necked 2L round flask, provided with a nitrogen inlet, a septum and a mechanical stirrer, polyphosphoric acid (1 Kg) is placed, and heated at 90°C for 30 minutes, to later add **5b** (32 g, 0.1 mole) and heat at the same temperature for another 4 hours. This being completed, to the resulting dark brown mixture, a large amount of ice-cold water is slowly poured till no more precipitate is formed. The resulting yellow product is filtered, washed with water, and dried at 60°C, for 20h. Yield: 25.4 g (90%)

Melting Point:	148-150°C
1H-NMR ($CDCl_3$, δ ppm):	1.03 (t, 6H, CH_2CH_3 , $^3J_{H-H} = 7.4$ Hz)
	1.51 (m, 4H, 50% of CH_2CH_3)
	1.96 (m, 4H, 50% of CH_2CH_3)
	2.60 (m, 50% of 4H, CH_2 -Ph)
	2.61 (s, 6H, CH_3 -Ph)
	2.66 (m, 2H, CH_2CH_3 -CH)
	3.19 (d.d., 2H, 50% of 4H, CH_2 -Ph, $^2J_{gem} = 17.5$ Hz, $^3J_{trans} = 8.5$ Hz)
^{13}C-NMR ($CDCl_3$, δ ppm):	11.6 (CH_2CH_3)
	13.0 (CH_3 -Ph)
	24.7 (CH_2CH_3)
	30.1 (CH_2 -Ph)
	43.8 (CH_2CH_3 -CH)

Chapter 2: Synthesis and Spectroscopic Study of Polyalkylated 1,5-dihydro-*s*-Indacene Ligands

132.8, 137.4, 152.6 (C_{IV AR})

210.6 (C=O)

Mass Spectrum (EI, 70eV) m/z: [M]⁺ = 270 (88%)
[M]⁺ - C₂H₄ = 242 (98%)
[M]⁺ - 2C₂H₄ = 214 (100%)

FT-IR (KBr): 1697 cm⁻¹ (ν C=O)

Analysis Calculated: C₁₈H₂₀O₂: C, 80.00; H, 8.15.
Found: C, 79.80; H, 8.01.

2.7.1.6 Synthesis of 1,2,3,5,6,7-hexahydro-2,6-diethyl-4,8-dimethyl-*s*-indacene-1,5-diol **7b**:

In a 1L round flask fitted with a reflux condenser and a nitrogen inlet, LiAlH₄ (7.2 g, 0.19 mole) is added in 250 mL of ethyl ether. Later, **6b** (20 g, 74 mmole) is quickly added and the mixture is refluxed for 6 hours. After this, the solution is cooled at 0°C, to gently add a 1:1 mixture of HCl:water, avoiding excessive warming. In this stage, the product appears as a precipitate and is vacuum filtered, and dried at 70°C for 6 hours. The product is a mixture of several diastereoisomers of the diol and *s*-indacene ligand, so no further characterization was performed other than FT-IR spectrum. Yield: 19.4 g

FT-IR (KBr): 3540 cm⁻¹ (ν OH)

2.7.1.7 Synthesis of 2,6-diethyl-1,5-dihydro-4,8-dimethyl-*s*-Indacene **8b**:

In a 250 mL two necked round flask provided with a reflux condenser and a nitrogen inlet, p-toluenesulphonic acid (0.47 g, 21.96 mmole) is added to 120 mL of benzene. This solution is stirred for 30 mins., to then add the previously obtained mixture of **7b** and **8b** (10.0 g) and heat to 60°C for two hours. After this, the resulting mixture is cooled and washed with 2 portions of a saturated NaHCO₃ solution (100 mL each), and the organic phase is separated and dried with MgSO₄ for 24 hrs. The benzene solution is dried using a rotary evaporation system, to yield a yellow-orange solid, this

Chapter 2: Synthesis and Spectroscopic Study of Polyalkylated 1,5-dihydro-*s*-Indacene Ligands

being crude 2,6-diethyl-1,5-dihydro-4,8-dimethyl-*s*-Indacene. This solid is recrystallized in hexane and later sublimed, affording a white solid. Yield 6.8 g (78%)

Melting Point:	148-171°C
¹H-NMR (CDCl ₃ , δ ppm):	1.24 (t, 6H, CH ₂ CH ₃ , ³ J _{H-H} = 7.4 Hz) 2.36 (s, 6H, CH ₃ -Ph) 2.64 (qd, 4H, CH ₂ CH ₃ , ³ J _{H-H} = 7.4 Hz, ⁴ J _{H-H} = 3.0 Hz) 3.24 (s, 4H, CH ₂ -Ph) 6.62 (t, 2H, C=CH, ⁴ J _{H-H} = 3.0 Hz)
¹³C-NMR (CDCl ₃ , δ ppm):	13.6 (R = CH ₂ CH ₃) 14.0 (CH ₃ -Ph) 24.7 (CH ₂ CH ₃) 40.0 (CH ₂ -Ph) 123.7 (C=CH) 121.9 (C=C-CH ₂ CH ₃) 140.5, 140.6, 150.2 (C _{IV AR})
Mass Spectrum (EI, 70eV) m/z:	[M] ⁺ = 238 (100%) [M] ⁺ - CH ₃ = 223 (69%) [M] ⁺ - 2CH ₃ = 208 (20%)
FT-IR (KBr):	1597 cm ⁻¹ (ν C=C)
Analysis Calculated:	C ₁₈ H ₂₂ : C, 90.75; H, 9.25. Found: C, 90.06; H, 9.95.

2.7.2 Experimental Procedure for 2,6-di-*n*-butyl-4,8-dimethyl-1,5-dihydro-*s*-indacene 8c:

2.7.2.1 Synthesis of diethyl *n*-butylmalonate 2c:

To 100 mL of ethanol in a 300 mL round-bottomed flask fitted with a reflux condenser, Na pieces (3.91 g, 0.17 mole) are added with stirring at room temperature. When all Na is consumed, diethylmalonate (28.0 mL, 0.175 mole) is added slowly. After 30 min stirring at room temperature, 1-bromo-*n*-butane (23.96 g, 0.175 mole) is added and the solution heated at reflux for 3h. The excess of ethanol is later distilled. To the cooled residue (0°C), water and diethyl ether are added. After stirring and decantation, the two phases are separated. The solvent of the organic phase is removed on a rotary evaporator affording a liquid which can be purified by distillation in vacuum. Yield: 31g (82%).

Boiling Point:	67°C (0.8 mm Hg)
¹H-NMR (CDCl ₃ , δ ppm):	0.83 (t, 3H, CH ₂ CH ₂ CH ₂ CH ₃ , ³ J _{H-H} = 7.1 Hz) 1.01 – 1.30 (m, 10H, CH ₂ CH ₂ CH ₂ CH ₃ and OCH ₂ CH ₃) 1.81 (m, 2H, CH ₂ CH ₂ CH ₂ CH ₃) 3.24 (t, 1H, <i>n</i> -Bu-CH, ³ J _{H-H} = 7.6 Hz) 4.12 (q, 4H, OCH ₂ CH ₃ , ³ J _{H-H} = 7.1 Hz)
¹³C-NMR (CDCl ₃ , δ ppm):	13.4 (CH ₂ CH ₂ CH ₂ CH ₃) 13.8, 13.9 (CH ₂ CH ₂ CH ₂ CH ₃) 28.2 (CH ₂ CH ₂ CH ₂ CH ₃) 29.26 (OCH ₂ CH ₃) 51.81 (<i>n</i> -Bu-CH) 60.94 (OCH ₂ CH ₃) 169.3 (C=O).
Mass Spectrum (EI, 70eV) m/z:	[M] ⁺ = 216 (100%) [M] ⁺ - OCH ₂ CH ₃ = 171 (84%)

Chapter 2: Synthesis and Spectroscopic Study of Polyalkylated 1,5-dihydro-*s*-Indacene Ligands

$$[M]^+ - \text{CH}_2\text{CH}_2\text{CH}_2\text{CH}_3 = 159 \text{ (15\%)}$$

Analysis Calculated:

$$\text{C}_{11}\text{H}_{20}\text{O}_4: \text{C}, 61.09; \text{H}, 9.32.$$

$$\text{Found: C}, 61.28; \text{H}, 9.28.$$

2.7.2.2 Synthesis of α, α' -bis(ethoxycarbonyl)- α, α' -dibutyl-2,5-dimethyl-diethyl ester-1,4-Benzenedipropanoic acid **3c**:

Following the same procedure as for **3b**, but using ethanol (100 mL), Na(3.17 g, 0.138 mole), **2c** (30 g, 0.139 mole) and **1** (20.22 g, 0.069 mole), **3c** of were obtained. Yield: 35.8 g (92%).

Melting Point:

69°C

¹H-NMR (CDCl₃, δ ppm):

0.86 (t, 6H, CH₂CH₂CH₂CH₃, ³J_{H-H} = 7.1 Hz)

1.10 – 1.25 (m, 8H, CH₂CH₂CH₂CH₃)

1.18 (t, 12H, OCH₂CH₃, ³J_{H-H} = 7.0 Hz)

1.77 (m, 4H, CH₂CH₂CH₂CH₃)

2.14 (s, 6H, CH₃-Ph)

3.17 (s, 4H, CH₂-Ph)

3.98-4.19 (m, 8H, OCH₂CH₃)

6.78 (s, 2H, CH_{AR})

¹³C-NMR (CDCl₃, δ ppm):

13.7 (CH₂CH₂CH₂CH₃)

13.9 (OCH₂CH₃)

19.2 (CH₃-Ph)

22.8, 26.4 (CH₂CH₂CH₂CH₃)

32.3 (CH₂CH₂CH₂CH₃)

34.0 (CH₂-Ph)

58.6 (C_{IV}-*n*-Bu)

60.9 (OCH₂CH₃)

132.1 (CH_{AR})

133.1-134.0 (C_{IV}AR)

171.6 (C=O).

Mass Spectrum (EI, 70eV) m/z:

$$[M]^+ = 562 \text{ (12\%)}$$

Chapter 2: Synthesis and Spectroscopic Study of Polyalkylated 1,5-dihydro-*s*-Indacene Ligands

$$[M]^+ - (n\text{-Bu-C(OCH}_2\text{CH}_3)_2 = 347 \text{ (100\%)}$$

Analysis Calculated:

C₃₂H₅₀O₈: C, 68.30; H, 8.96.

Found: C, 68.10; H, 8.79

2.7.2.3 Synthesis of α,α' -dicarboxy- α,α' -dibutyl-2,5-dimethyl-1,4-Benzenedipropionic acid **4c**:

In a 1L round-bottomed flask with a reflux condenser, compound **3c** (100 g, 0.20 mole) is added to a solution of KOH (135.4 g, 2.41 mole) in 100 mL of a 1:1 mixture of H₂O/Ethanol. The mixture is heated to reflux for 24 hours. The resulting solution was poured into a mixture of water and ice, and then in order to prevent excessive heating, HCl (37%) is dropwise added till no further precipitation occurs. The white precipitate is filtered, and later washed with water, and dried at 70°C for 12 h. Yield: 29.41 g (68%).

Melting Point:

188°C

¹H-NMR (DMSO, δ ppm):

0.92 (t, 6H, CH₂CH₂CH₂CH₃, ³J_{H-H} = 6.8 Hz)

1.23 (m, 8H, CH₂CH₂CH₂CH₃)

1.62 (br.s, 4H, CH₂CH₂CH₂CH₃)

2.14 (s, 6H, CH₃-Ph)

3.02 (s, 4H, CH₂-Ph)

6.84 (s, 2H, CH_{AR})

12.86 (s, 4H, COOH)

¹³C-NMR (DMSO, δ ppm):

14.6 (CH₂CH₂CH₂CH₃)

19.7 (CH₃-Ph)

22.6, 23.0 (CH₂CH₂CH₂CH₃)

32.1 (CH₂CH₂CH₂CH₃)

34.5 (CH₂-Ph)

57.7 (C_{IV}-*n*-Bu)

132.1 (CH_{AR})

132.9, 134.3 (C_{IV} AR)

177.0 (COOH)

Chapter 2: Synthesis and Spectroscopic Study of Polyalkylated 1,5-dihydro-*s*-Indacene Ligands

Mass Spectrum (EI, 70eV) m/z: Thermal Decomposition of **4c** into **5c**

FT-IR (KBr): 1707 cm⁻¹ (ν C=O)

3304 cm⁻¹ (ν OH)

Analysis Calculated: C₂₄H₃₄O₈ C, 63.98; H, 7.61.

Found: C, 63.89; H, 7.53.

2.7.2.4 α,α'-dibutyl-2,5-dimethyl-1,4-Benzenedipropanoic acid **5c**:

Following the same procedure as for **5b**, **4c** (27.08g, 0.060 mole) is placed in a round bottomed flask (500mL) fitted with a nitrogen inlet and heated (190-200°C) until the evolution of CO₂ ended. Yield: 21.18g (97%).

Melting Point: 131°C

¹H-NMR (DMSO, δ ppm): 0.79 (t, 6H, CH₂CH₂CH₂CH₃, ³J_{H-H} = 7.0Hz)

1.20 (m, 8H, CH₂CH₂CH₂CH₃)

1.43 (br.s, 4H, CH₂CH₂CH₂CH₃)

2.13 (s, 6H, CH₃-Ph)

2.41 (s, 4H, CH₂-Ph)

2.68-2.73 (m, 2H, *n*-Bu-CH)

6.82 (s, 2H, CH_{AR})

11.70 (s, 2H, COOH)

¹³C-NMR (DMSO, δ ppm): 13.8 (CH₂CH₂CH₂CH₃)

18.6 (CH₃-Ph)

22.1, 29.1 (CH₂CH₂CH₂CH₃)

31.6 (CH₂CH₂CH₂CH₃)

34.8 (CH₂-Ph)

45.7 (*n*-Bu-CH)

131.1 (CH_{AR})

132.7, 135.5 (C_{IV AR})

Chapter 2: Synthesis and Spectroscopic Study of Polyalkylated 1,5-dihydro-*s*-Indacene Ligands

	176.6 (COOH)
Mass Spectrum (EI, 70eV) m/z:	$[M]^+ = 362$ (21%) $[M]^+ - H_2O = 344$ (100%) $[M]^+ - HCOOH = 316$ (22%)
FT-IR (KBr):	1698 cm^{-1} (ν C=O) 3011 cm^{-1} (ν OH)
Analysis Calculated:	C ₂₂ H ₃₄ O ₄ : C, 72.89; H, 9.45. Found: C, 73.20; H, 9.51.

2.7.2.5 Synthesis of 2,6-dibutyl-4,8-dimethyl-2,3,6,7-tetrahydro-*s*-indacene-1,5-dione **6c**:

Following the same procedure described for **6b**, polyphosphoric acid (500 g, a large excess) and **5c** (19.17 g, 0.053 mole) are placed in a round bottomed flask (1L) fitted with a mechanical stirrer and a nitrogen inlet. The mixture is stirred vigorously under nitrogen at 90°C for 6h. It is later poured into a solution of 500g of ice in 2L of H₂O. The resulting bright yellow precipitate is filtered, washed with water, dried and recrystallized in hexane. Yield: 14.4 g (83%).

Melting Point:	112-113°C
¹H-NMR (CDCl ₃ , δ ppm):	0.92 (t, 6H, CH ₂ CH ₂ CH ₂ CH ₃ , ³ J _{H-H} = 7.1 Hz) 1.38-1.50 (m, 12H, CH ₂ CH ₂ CH ₂ CH ₃) 1.94 (d.d, 50% of 4H, CH ₂ -Ph) 2.59 (s, 6H, CH ₃ -Ph) 2.64 (m, 2H, <i>n</i> -Bu-CH) 3.19 (d.d., 2H, 50% of 4H, CH ₂ -Ph, ² J _{gem} = 17.6 Hz, ³ J _{trans} = 8.6 Hz)
¹³C-NMR (CDCl ₃ , δ ppm):	12.8 (CH ₃ -Ph) 13.9 (CH ₂ CH ₂ CH ₂ CH ₃) 22.7, 29.5 (CH ₂ CH ₂ CH ₂ CH ₃) 31.3 (CH ₂ CH ₂ CH ₂ CH ₃)

Chapter 2: Synthesis and Spectroscopic Study of Polyalkylated 1,5-dihydro-*s*-Indacene Ligands

	30.6 (CH_2 -Ph)
	48.4 (<i>n</i> -Bu-CH)
	132.7, 137.2, 152.5 ($C_{IV\ AR}$)
	210.5 (C=O)
Mass Spectrum (EI, 70eV) m/z:	$[M]^+ = 326$ (56%)
	$[M]^+ - n\text{-Bu} = 269$ (98%)
	$[M]H^+ - 2(n\text{-Bu}) = 213$ (100%)
FT-IR (KBr):	1707 cm^{-1} , (ν C=O)
Analysis Calculated:	$C_{22}H_{30}O_2$: C, 80.94; H, 9.26.
	Found: C, 80.88; H, 9.15.

2.7.2.6 Synthesis of 2,6-dibutyl-4,8-dimethyl-1,2,3,5,6,7-hexahydro-*s*-indacene-1,5-diol **7c**:

Following the same procedure described for **7b**, LiAlH₄ (0.71 g, 18.7 mmole), 25 mL of ethyl ether and, **6c** (3.72 g, 11.4 mmole) are mixed. Yield: 3.52 g

Melting Point:	143-150°C
FT-IR (KBr):	3270 and 3175 cm^{-1} (ν OH)

2.7.2.7 Synthesis of 2,6-dibutyl-1,5-dihydro-4,8-dimethyl-*s*-Indacene **8c**:

Following the procedure for **8b**, combining *p*-Toluenesulphonic acid (0.25 g, 1.5 mmole), 100 mL of benzene, and **7c** (3.53 g, 10.68 mmole). Yield: 2.46 g (78%)

Melting Point:	132-138°C
¹H-NMR (CDCl ₃ , δ ppm):	0.99 (t, 6H, $CH_2CH_2CH_2CH_3$, $^3J_{H-H} = 7.4$ Hz)
	1.44 (qt, 4H, $CH_2CH_2CH_2CH_3$, $^3J_{H-H} = 7.4$ Hz, $^3J_{H-H} = 7.6$ Hz)
	1.66 (quint., 4H, R = $CH_2CH_2CH_2CH_3$, $^3J_{H-H} = 7.6$ Hz)

Chapter 2: Synthesis and Spectroscopic Study of Polyalkylated 1,5-dihydro-*s*-Indacene Ligands

	2.40 (s, 6H, CH_3 -Ph)
	2.55 (t, 4H, $CH_2CH_2CH_2CH_3$, $^3J_{H-H} = 7.4$ Hz)
	3.26 (s, 4H, CH_2 -Ph)
	6.66 (t, 2H, C= CH , $^4J_{H-H} = 3.0$ Hz)
^{13}C -NMR ($CDCl_3$, δ ppm):	13.9 ($CH_2CH_2CH_2CH_3$)
	15.0 (CH_3 -Ph)
	21.5 ($CH_2CH_2CH_2CH_3$)
	22.5 ($CH_2CH_2CH_2CH_3$)
	31.3 ($CH_2CH_2CH_2CH_3$)
	40.0 (CH_2 -Ph)
	121.9 ($C_{4,8}$)
	124.7 (C= CH)
	148.7 (C=C-R)
	140.57, 140.67 ($C_{IV AR}$)
Mass Spectrum (EI, 70eV) m/z:	$[M]^+ = 294$ (84%)
	$[M]^+ - Pr = 251$ (100%)
	$[M]^+ - 2Pr = 208$ (6%)
	$[M]^+ - (2Pr + 2 Me) = 178$ (3%)
FT-IR (KBr):	1601 cm^{-1} (ν C=C)
Analysis Calculated:	$C_{22}H_{30}$: C, 89.73; H, 10.27.
	Found: C, 89.59; H, 10.42.

2.7.3 Experimental Procedure for 3-chloro-2,6-diethyl-4,7,8-trimethyl-1,5-dihydro-*s*-indacene:

2.7.3.1 Synthesis of 5,5-dichloro-2,6-diethyl-4,8-dimethyl-2,3,6,7-tetrahydro-*s*-indacene-1(5H)-one **11**:

To a solution of **6b** (4.03g, 14.93 mmole) in 100 mL of CH_2Cl_2 in a round bottomed flask (500mL) fitted with a nitrogen inlet and a reflux condenser is added at room temperature and with stirring PCl_5 (4.16g, 20 mmole) in suspension in 80 mL of

Chapter 2: Synthesis and Spectroscopic Study of Polyalkylated 1,5-dihydro-s-Indacene Ligands

CH₂Cl₂. The mixture is stirred at reflux for 48h and then cooled to 0°C and water (100mL) later added. After 2 extractions with 30mL of CH₂Cl₂ and 30mL of ether, the organic phase is treated with 50 mL of an aqueous solution of Na₂CO₃ (10%) and then separated and dried over MgSO₄ for 12 hours prior to removal of solvent on a rotary evaporator. A sticky residue (3.57g) was analyzed by IR and GC/mass(EI), and identified as a mixture of initial diketone **6b**, intermediate compound **11** and mainly compound **12**.

FT-IR (KBr):

Diketone **6b**: 1697 cm⁻¹ (ν C=O)

Mass Spectrum (EI, 70eV) m/z:

Diketone **6b**: [M]⁺ = 270 (85%)
[M]⁺ - C₂H₄ = 242 (100%)
11: [M]⁺ = 324 (100%)
[M]⁺ - Cl = 289 (63%)
12: [M]⁺ = 288 (100%)
[M]⁺ - C₂H₄ = 260 (83%)

2.7.3.2 Synthesis of 3-chloro-2,6-diethyl-4,7,8-trimethyl-1,5-dihydro-s-indacene **13**:

The above resulting mixture is dissolved in 50 mL of ether and treated with 10 mL of an aqueous solution of KOH (1%) to convert **11** to **12**. The organic phase was dried over MgSO₄ for 48h and then treated with an excess of methylmagnesium iodide (52.5 mmole), as 35mL of 1.5M CH₃MgI in ether). The mixture was stirred and heated for 6 h at reflux, then cooled and hydrolyzed with HCl (37%) and extracted with 50 mL of diethylether. The organic phase was dried over MgSO₄ 12 hours prior to the removal of solvent on a rotary evaporator. The residue was dissolved in 25mL of hexane and stored in a deep freezer. After a few days, large yellow brown needles (0.73g) were isolated by filtration. Yield 17%. Mp: 176-179 °C. A GC/mass analysis of a benzene solution of these needles shows that they are formed from a cocrystallization of two compounds: about 80% of the dissymmetric **13**, GC/mass, Ei, m/z %: [M]⁺ = 286

Chapter 2: Synthesis and Spectroscopic Study of Polyalkylated 1,5-dihydro-*s*-Indacene Ligands

(100%); $[M]^+$ - Cl = 251 (77%) and 20% of **10b**, GC/mass, Ei, m/z %: $[M]^+$ = 266. These two compounds were separated by preparative HPLC on a column of silicagel microspheres 12 μ m (20g, Merck), pressure 10 bar, eluent: 90% petroleum ether and 10% of (CH₂Cl₂: 75%, ethylacetate: 25%). Each compound was crystallized in CH₂Cl₂ and identified. The predominant one was identified as **10b**, with the same properties as described in the literature^[14].

13:

Melting Point: 176-178°C

¹ H-NMR (CDCl ₃ , δ ppm):	1.15 (t, 3H, C ₍₆₎ -CH ₂ CH ₃ , ³ J _{H-H} = 7.6 Hz)
	1.18 (t, 3H, C ₍₂₎ -CH ₂ CH ₃ , ³ J _{H-H} = 7.6 Hz)
	2.26 (s, 3H, CH ₃ -C ₍₅₎)
	2.48 (q, 2H, C ₍₆₎ -CH ₂ CH ₃ , ³ J _{H-H} = 7.6 Hz)
	2.51 (s, 3H, CH ₃ -C ₍₄₎)
	2.57 (q, 2H, C ₍₂₎ -CH ₂ CH ₃ , ³ J _{H-H} = 7.6 Hz)
	2.65 (s, 3H, CH ₃ -C ₍₈₎)
	3.19 (s, 2H, C ₍₃₎)
	3.22 (s, 2H, C ₍₇₎)
¹³ C-NMR (CDCl ₃ , δ ppm):	13.2 (C ₍₂₎ -CH ₂ CH ₃)
	14.2 (CH ₃ -C ₍₅₎)
	14.3 (C ₍₆₎ -CH ₂ CH ₃)
	14.5 (CH ₃ -C ₍₈₎)
	14.9 (CH ₃ -C ₍₄₎)
	21.6 (C _(2,6) -CH ₂ CH ₃)
	37.5 (C ₃)
	38.8 (C ₇)
	122.9, 123.0 (C _{4,8})
	126.7 (C ₁)
	133.2 (C ₅)
	135.1 (C _{3a})
	139.6 (C _{8a})
	141.5 (C _{7a})

Chapter 2: Synthesis and Spectroscopic Study of Polyalkylated 1,5-dihydro-*s*-Indacene Ligands

142.0 (C_{4a})

142.6 (C₂)

144.1 (C₆)

Mass Spectrum (EI, 70eV) m/z: [M]⁺ = 286 (100%)
[M]⁺ - CH₃ = 271 (83%)
[M]⁺ - Cl = 251 (77%)
[M]⁺ - (Cl + C₂H₅) = 222 (31%)

FT-IR (CDCl₃): 1605, 1622 cm⁻¹ (ν C=C)

Analysis Calculated: C₁₉H₂₃Cl: C, 79.56; H, 8.08; Cl, 12.36.
Found: C, 79.37; H, 8.17, Cl, 12.24.

2.7.4 Preparation of dilithiated derivatives of *s*-indacene:

The dilithium derivatives of **8a**, **8b**, **8c**, **10a**, **10b** and **13**, are prepared according to the general procedure described in reference 4. These compounds are dissolved in THF, to later add 2 molar equivalents of *n*-BuLi (1.6 M in hexane) at -80°C with stirring. The solution is later warmed to room temperature.

2.7.5 Preparation of ESR Experiments:

Each THF/pentane solution of dilithium derivatives **8a**, **8b**, **8c**, **10a**, **10b** and **13** in approximately 0.04M concentration was divided into three ESR quartz tubes ii), iii) and iv). To ii) was added one volume of toluene and the sample was irradiated at 254 nm at 243°K in the ESR cavity.

To iii) frozen in liquid nitrogen was added a solution of Cp₂Fe⁺ BF₄⁻ in dichloromethane and the ESR spectrum was recorded at 243°K. To iv) frozen in liquid nitrogen was added a solution of the ERO in toluene and ESR spectra were recorded at 243°K.

References

-
- ¹ K. Hafner, B. Stowasser, H. P. Krimmer, S. Fischer, M. C. Bohm, H. J. Lindner, *Angew. Chem., Int. Ed. Engl.* **1986**, *25*, 630.
- ² P. Roussel, D. Cary, S. Barlow, J. C. Green, F. Varret, D. O'Hare, *Organometallics* **2000**, *19*, 1071.
- ³ C. Gellini, C. Cardini, P. Salvi, G. Marconi, K. Hafner, *J. Phys. Chem.* **1993**, *97*, 1286.
- ⁴ M. R. Dahrouch, P. Jara, L. Mendez, Y. Portilla, D. Abril, G. Alfonso, I. Chavez, J. M. Manriquez, M. Rivière-Baudet, P. Rivière, A. Castel, J. Rouzaud, H. Gornitzka, *Organometallics* **2001**, *20*, 5591.
- ⁵ K. Hafner, K. Häfner, C. König, M. Kreuder, G. Ploss, G. Schulz, E. Sturm, K. Vöpel, *Angew. Chem., Int. Ed. Engl.* **1963**, *2*, 123.
- ⁶ L. Trogen, U. Edlung, *Acta Chem. Scand. B* **1979**, *33*, 109.
- ⁷ K. Hafner, B. Stowasser, H. Krimmer, S. Fischer, M. Bohm, H. Lindner, *Angew. Chem., Int. Ed. Engl.* **1986**, *25*, 630.
- ⁸ W. Bell, C. Curtis, C. Eigenbrot, C. Pierpont, J. Robbins, J. Smart, *Organometallics* **1987**, *6*, 266.
- ⁹ S. Barlow, D. O'Hare, *Organometallics* **1996**, *15*, 3483.
- ¹⁰ S. Barlow, D. O'Hare, *Chem. Rev.* **1997**, *97*, 637.
- ¹¹ S. Barlow, D. Cary, M. Drewit, D. O'Hare, *J. Chem. Soc., Dalton Trans.* **1997**, 3867.

- ¹² Y. Asscher, I. Agranat, *J. Org. Chem.* **1980**, *45*, 3364.
- ¹³ A. Bisello, A. Ceccon, A. Gambaro, P. Ganis, F. Manoli, S. Santi, A. Venzo, *J. Organomet. Chem.* **2000**, *593*, 315.
- ¹⁴ A. Davies, J. Lusztki, *J. Chem. Soc. Perkin II*, **1981**, 692.
- ¹⁵ D. Wilhelm, J. Courtneidge, T. Clark, A. Davies, *J. Chem. Soc. Chem. Commun.* **1984**, 810.
- ¹⁶ C. Chatgililoglu, *Organosilanes In Radical Chemistry: Principles, Methods and Applications*; Wiley: Chichester, U.K., **2004**.
- ¹⁷ S. Patai, Z. Rappoport, Y. Apeloig, *The Chemistry of Organogermanium, Tin and Lead Compounds*, Eds., Wiley, Chichester, UK, **2002**, *Vol. 2*, 653.
- ¹⁸ P. Rivière, M. Rivière-Baudet, J. Satgé, *Comprehensive Organometallic Chemistry I*; Pergamon Press: A.G. Davies, University College London, UK., **1982**, *Vol. 2*, 399.
- ¹⁹ P. Rivière, M. Rivière-Baudet, J. Satgé, *Comprehensive Organometallic Chemistry II*; Pergamon Press: A.G. Davies, University College London, UK., **1995**, *Vol. 2*, 137.
- ²⁰ M. Gynane, M. Lappert, P. Riley, P. Rivière, M. Rivière-Baudet, *J. Organomet. Chem.* **1980**, *202*, 5.
- ²¹ A. Feddoui, A. El Kadib, P. Rivière, F. Delpech, M. Rivière-Baudet, A. Castel, J. Manriquez, I. Chavez, Y. Ait Ito, M. Ahbala, *Appl. Organomet. Chem.*, **2004**, *18*, 233.

Chapter 3

Synthesis and Spectroscopic Study of Organometallic complexes

Introduction

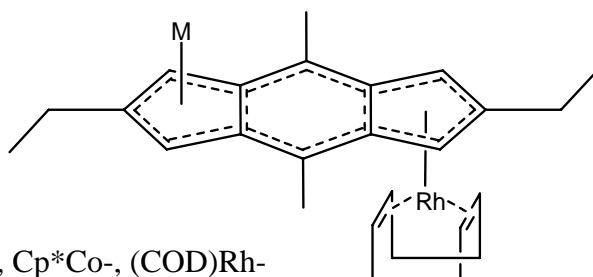
Ce chapitre concerne la synthèse et la caractérisation physicochimique de complexes homo- et hétéro-bimétalliques.

Comme nous l'avons vu dans le chapitre précédent au cours de l'étude par RPE des ligands *s*-indacènes, l'électron célibataire présente une forte interaction avec les trois cycles accolés, ce qui laisse présager une bonne communication électronique entre les deux métaux qui seront greffés sur les cyclopentadiényles.

Par ailleurs, il a déjà été montré dans la littérature qu'un certain degré de communication existe entre deux centres métalliques avec des ligands comme le pentalène ou le *s*-indacène non-substitué c'est ce que l'on appelle l'effet coopératif. Cet effet peut induire une réactivité très spécifique que l'on ne peut pas observer avec des espèces mononucléaires.

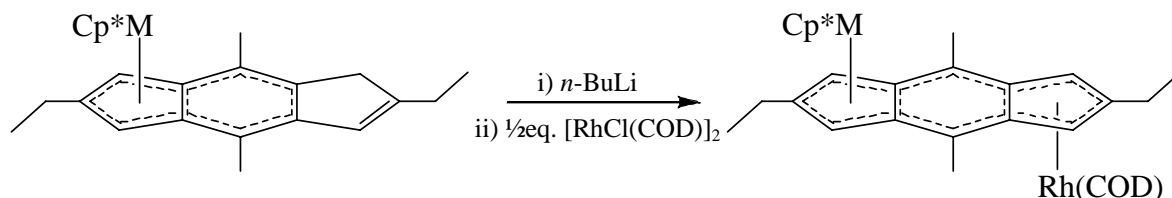
La plupart des articles portent sur l'influence du ligand (labilité, substitution...) pour démontrer l'existence de cet effet, mais jusqu'à présent il y a peu d'information sur l'effet d'un fragment métallique sur le deuxième métal qui est en général le site catalytiquement actif. Le but de ces travaux est donc de synthétiser des complexes organométalliques du rhodium puis de déterminer l'effet de l'introduction d'un fragment organométallique (électron attracteur ou électron donneur) comme Cp**Ru*-, Cp**Fe*-, Cp**Co*- et (COD)*Rh*- sur le rhodium qui est le site actif en catalyse.

Dans une première partie, nous avons préparé une série de complexes monométalliques et homo- et hétéro-bimétalliques du rhodium, fer, ruthénium et cobalt :

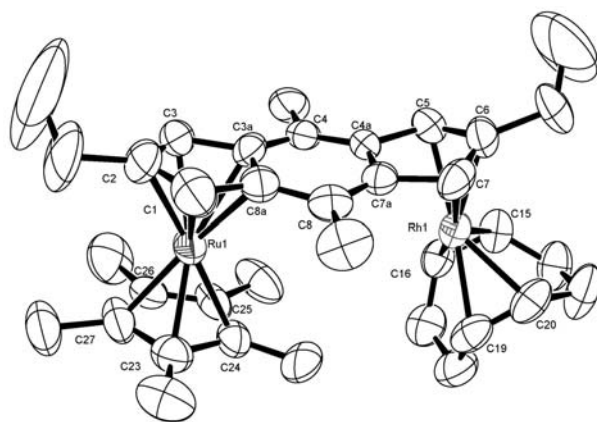


Un des intérêts de ces ligands *s*-indacènes polysubstitués est de permettre la formation mais surtout la stabilisation des composés mono-lithiés correspondants ce qui permet un greffage en deux étapes des motifs métalliques et donc facilite l'accès aux complexes

hétérobinucléaires. Ces complexes peuvent se présenter sous les deux formes isomères : *syn* et *anti*. Le pourcentage *syn/anti* dépend essentiellement du complexe mononucléaire intermédiaire, par exemple, à partir de complexes mononucléaires comportant des groupements stériquement encombrant comme le pentaméthylcyclopentadiényle (Cp*), seule la formation du complexe *anti* est observée.



Nous avons ensuite réalisé une étude physicochimique approfondie (RMN du ^1H , ^{13}C , ^{103}Rh) de tous ces complexes. La RMN du rhodium est une technique particulièrement adaptée pour évaluer le degré de coordination de ce métal ce qui est très important pour les applications en catalyse. Dans notre cas, les déplacements chimiques observés pour les complexes hétérobimétalliques indiquent une hapticité intermédiaire entre η^3 et η^5 c'est-à-dire ($\eta^2 + \eta^3$). Ces résultats sont en accord avec les structures de complexes déterminées par diffraction des rayons X.



Nous avons réalisé également des études par RPE et électrochimie qui sont des techniques complémentaires dans la mesure où elles permettent l'observation des formes oxydées et d'en déduire la localisation de l'électron célibataire.

L'ensemble de ces résultats montre que l'effet coopératif et la communication entre les centres métalliques dépend non seulement du ligand mais également du fragment métallique utilisé.

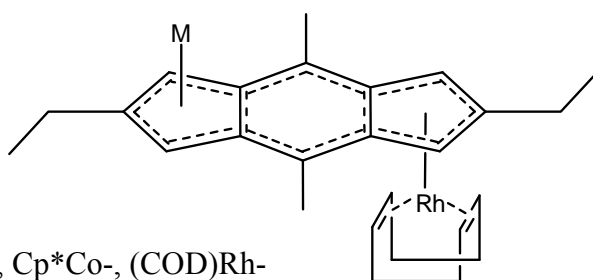
3 Introduction

This chapter refers to the synthesis of metallic complexes, and their characterization by means of different techniques. As discussed in the previous chapter, the sole electron of the radicals formed by the dilithiated *s*-indacenes, have a strong interaction with the organic framework of the three fused rings, a promising result which could allow communication between two metals bonded to each five membered ring of this ligand.

Previous results revealed a high degree of communication between two metallic centers within ligands such as pentalene and non-substituted *s*-indacene^[1], a process which has been named “cooperative effect”. This effect may lead to new and/or enhanced reactivity impossible with mononuclear species.

In the literature, most articles have focused their attention mainly on ligand lability or substitution susceptibility in order to prove this cooperative effect, and mostly on ligands such as fulvalene and their analogues, but little about the effect a secondary metallic fragment may have on a catalytically active metal, much less on poly-fused ring ligands^[2].

Figure 1: Binuclear *s*-indacene complexes

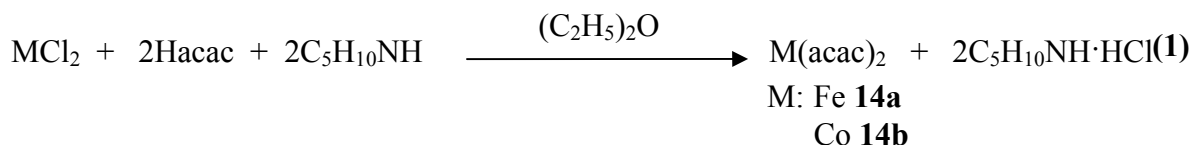


M: Cp*Ru-, Cp*Fe-, Cp*Co-, (COD)Rh-

The main focus of this chapter is to synthesize complexes (Figure 1), and then determine, to what extent electron withdrawing or electron donating fragments such as Cp*Ru-, Cp*Fe-, Cp*Co- and (COD)Rh- may affect a catalytically active metal.

3.1 Preparation of starting metallic materials

3.1.1 Preparation of metallic (acac) compounds



Metal-bis(acac) compounds provide excellent alternative starting compounds, because they are readily soluble in most common organic solvents, and acac anion is a weak coordinating ligand leading to the facile removal of this oxygenated ligand^[3].

Bis(2,4-pentanedionato)iron(II) is a polymeric crystalline material. It is brownish-orange when finely divided but darkens to almost black in larger clusters. Its X-ray structure shows it to be a tetramer with six-coordinate iron(II) as a result of two oxygen bridges and weak Fe-C bonds. It is paramagnetic and very air-sensitive, but there is a only a slight change in color after oxidation. It sublimes without appreciable decomposition. It is slightly soluble in aromatic solvents and aliphatic hydrocarbons; it dissolves easily in coordinating solvents like THF with the formation of monomeric adducts^[22].

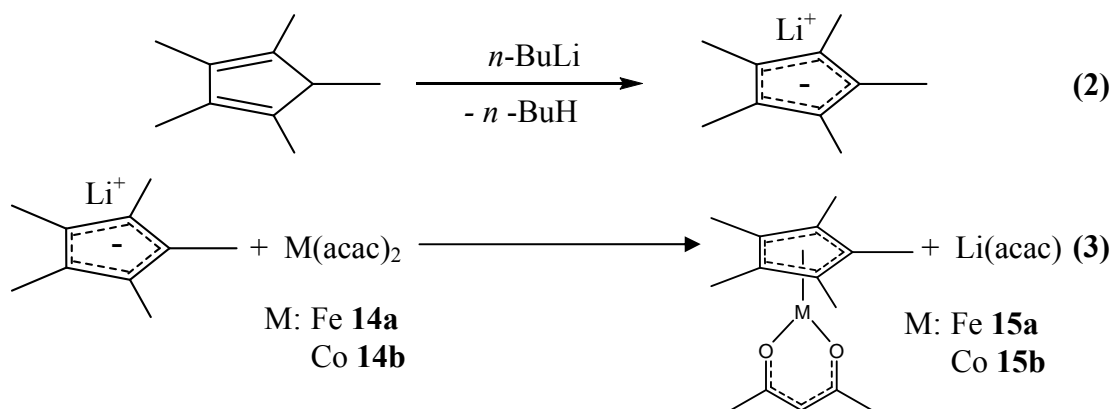
If either **14a** or **14b** are exposed to air, the diaquo-metal-bis(acac) complexes form, dramatically decreasing the yield when reacting with other substances, especially lithiated organic ligands such as Cp*Li. Therefore these products must be manipulated in a strictly inert atmosphere, either under nitrogen or argon.

3.1.2 Preparation of Cp*M (M: Fe, Co, Ru) building blocks

These semi-sandwich compounds are ideal building blocks for the construction of new and more complex molecules, being widely used in organometallic chemistry in addition reactions to metallic clusters^[4], as well as in the design of catalysts for oxidative additions to olefins^[5] and alkyne cyclotrimerizations^[6], amongst other uses.

Given the fact that these compounds are all sensitive to air, they must be manipulated under an inert atmosphere at all times.

3.1.2.1 Preparation of Cp*M(acac), (M: Fe, Co):

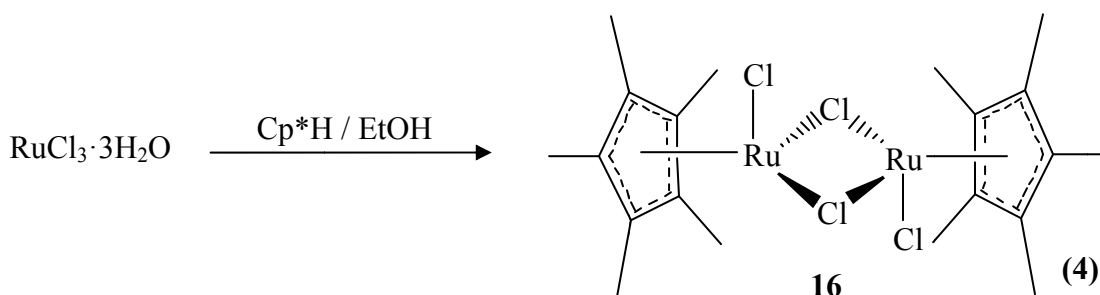


Compounds **15a** and **15b** were prepared by using **14a** and **14b** as starting agents, in addition to 1,2,3,4,5-pentamethylcyclopentadiene (Cp*H) previously synthesized by literature methods^[7].

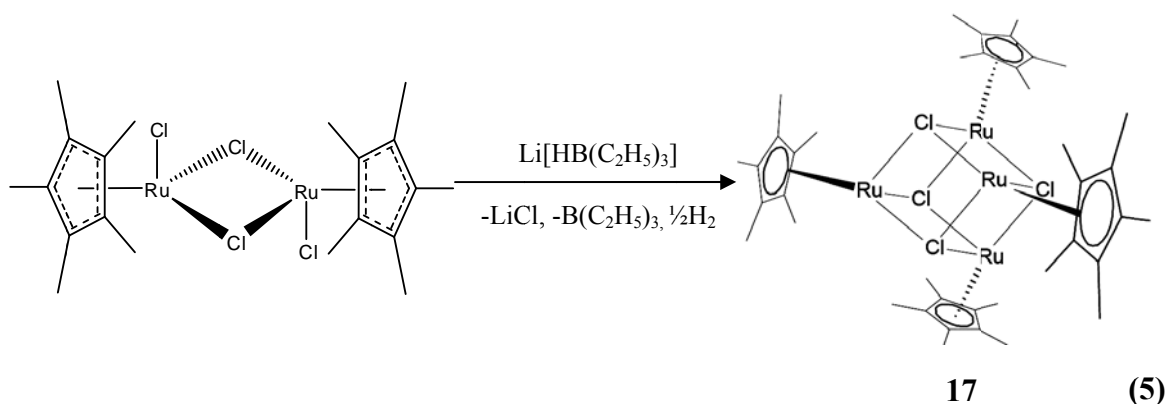
Once Cp*H was combined with *n*-BuLi, the corresponding lithiated salt was formed, a very slow dropwise addition of the Cp*Li solution in THF was imperative to avoid decamethyl sandwich derivatives of each metal^[24]. The resulting complexes have 16 and 17 electrons, at Fe (**15a**) and Co (**15b**), respectively.

3.1.2.2 Preparation of $[\text{Cp}^*\text{RuCl}]_4$:

The preparation of this ruthenium tetramer consists of two simple steps. First, the formation of a chloro-bridged dimer **16**, and secondly the reduction of the metallic center using a mild reducing agent, such as super hydride (lithium triethylhydroborate) to form the poorly soluble product **17**. Compound **16** is easy to prepare because it can be manipulated in air (Reaction 4), though it is recommended to store it under an inert atmosphere for extended periods of time^[29,30].

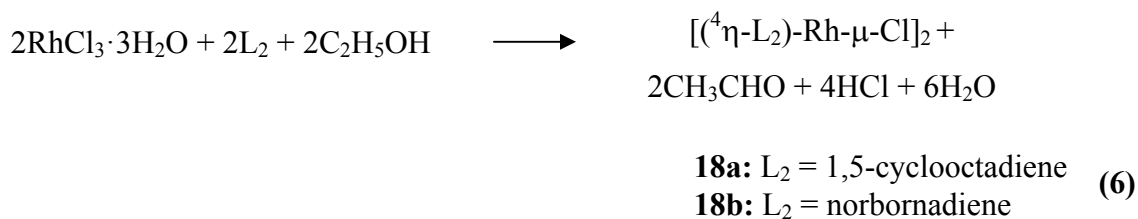


Fagan *et al*^[30] describe the use of these ruthenium compounds as building blocks for large oligomers, and in the use of different phosphines and simple dienes to form discrete monomeric molecules. The formation of halo-bridges occurs in order to increase the number of electrons per metallic center, achieving an 18-electron configuration and stabilizing the final product.



3.1.3 Preparation of Rhodium Starting compounds

The starting Rh reagents **18a** and **18b** are usually electrophilic species which subsequently react with a nucleophile, such as lithiated ligands. In this thesis, those made with dienes such as 1,5-cyclooctadiene and norbornadiene form halo-bridged dimers, (Reaction 6)^[31].



Normally, these complexes always tend to form dimers in order to complete a 16-electron configuration with a square planar geometry, increasing the stability of the final product. This could explain their stability regarding air and water, thus allowing their easy manipulation.

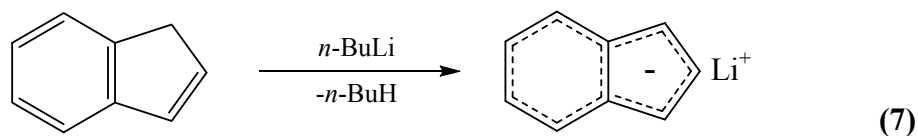
3.2 Preparation of Mononuclear complexes

This section deals with the synthesis of numerous organorhodium complexes, having primary organic ligands, such as 1,2,3,4,5-pentamethylcyclopentadiene, indene and 1,5-dihydro-2,6-diethyl-4,8-dimethyl-*s*-indacene, and having CO, 1,5-cyclooctadiene and norbornadiene as ancillary ligands.

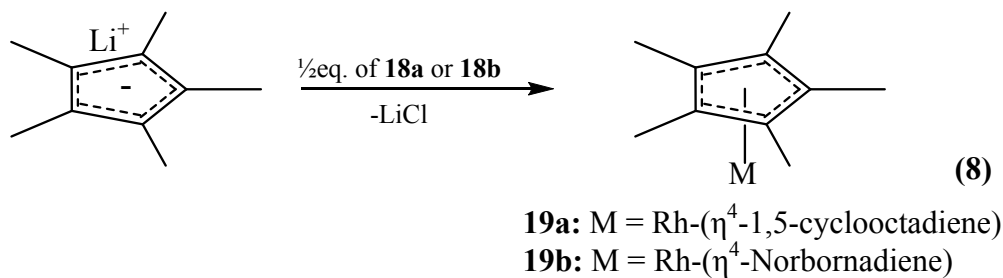
3.2.1 Preparation of Rhodium Complexes bearing 1,2,3,4,5-pentamethyl-cyclopentadiene and Indene ligands.

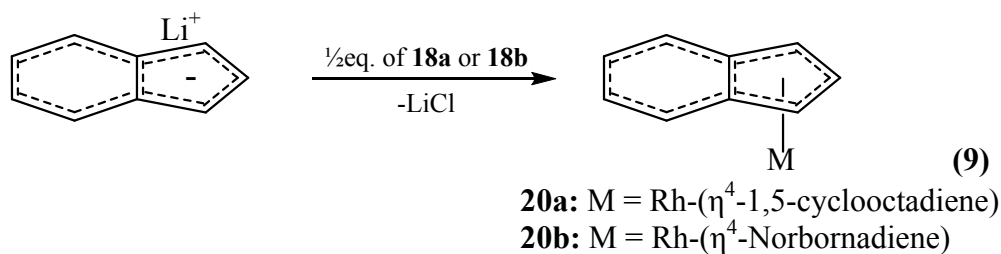
Complexes with simple ligands, such as 1,2,3,4,5-pentamethyl-cyclopentadiene (Cp*) and indene were synthesized according the methods detailed in the literature^[32,33,34,35], in order to establish comparisons with the new rhodium complexes which will be described in section 3.3. This was done because Cp* bonds to different metals in a perfect (or quasi perfect) η^5 array, while indenyl ligands are known to have an equilibrium between η^5 and η^3 , shifted to one configuration or the other depending on factors such as the final electronic configuration of the metallic fragment involved, solvent effect, and the concentration of other ligands^[8].

These complexes are easily prepared by methods described in the literature. Grignard reagents^[9,10], or simple bases such as sodium carbonate are used to remove the proton which would form the 6- or 10-electron aromatic intermediate, as shown previously in Reaction 2 and below in Reaction 7.

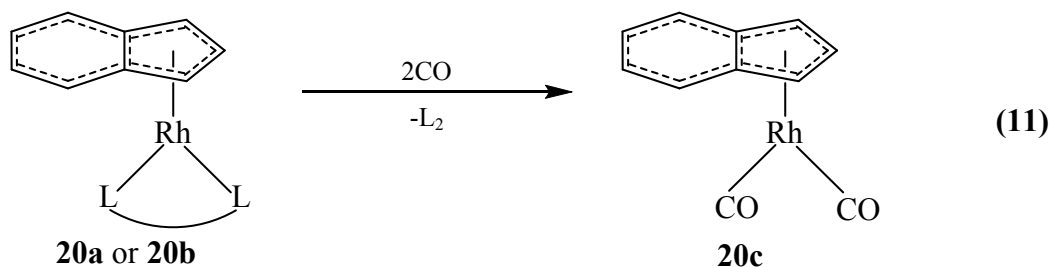
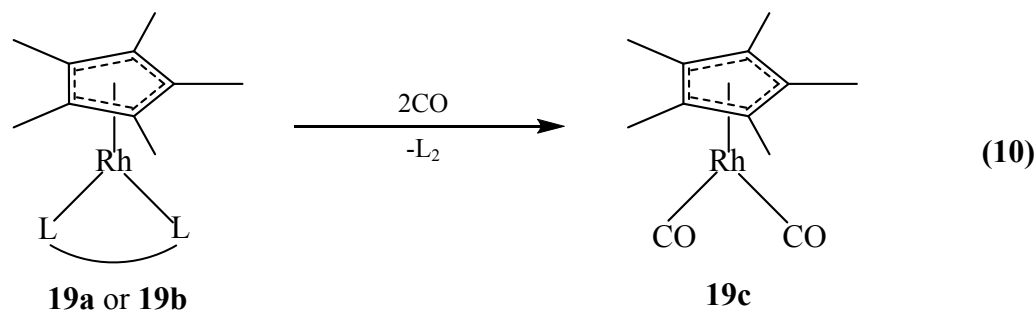


Once the lithiated ligand is formed, a suitable rhodium complex yields the desired product, whether forming Cp* or indenyl complexes:





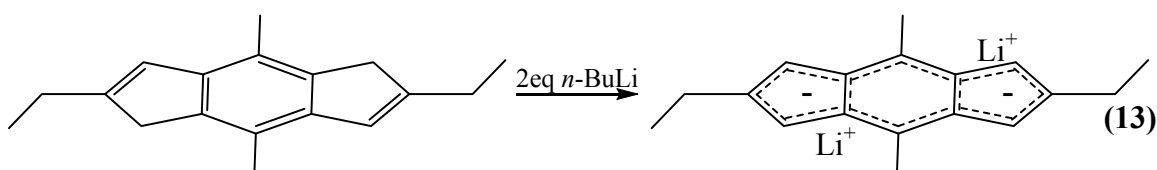
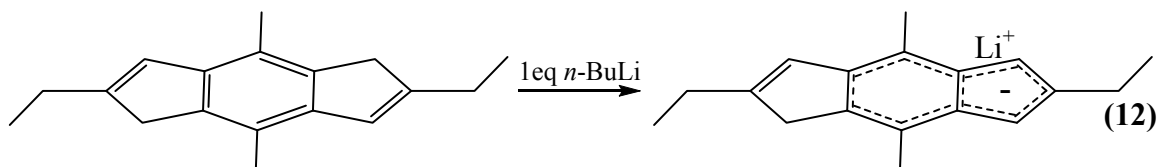
The reactivity for compounds **19a**, **19b**, **20a** and **20b** was also examined, by bubbling CO into each solution. This was done not only to determine how labile the ancillary diene ligands were, but also to isolate carbonylated rhodium complexes and determine their effectiveness as catalysts (Reactions 10 and 11) similar to reference methods^[11]. The catalytic behavior of the complexes will be described in Chapter 4.



3.2.2 Preparation of Mononuclear Complexes Bearing 1,5-dihydro-2,6-diethyl-4,8-dimethyl-*s*-indacene.

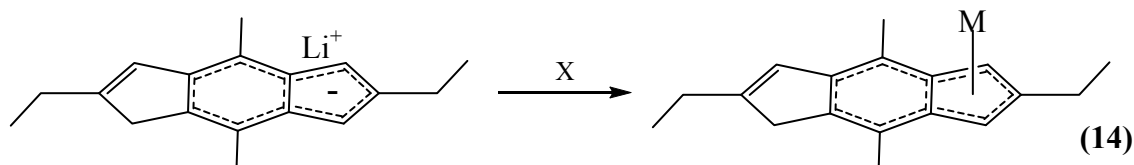
The steps to follow in the preparation of mononuclear complexes with 1,5-dihydro-2,6-diethyl-4,8-dimethyl-*s*-indacene **8b** are also simple^[12]. First, the ligand must

be dissolved in THF. Although the solubility of ligand **8b** is low in THF, so it may be more suitable to refer to this as a suspension of the spacer molecule in THF, the suspension quickly produces the soluble lithiated species upon the addition of one equivalent of *n*-BuLi, yielding a completely transparent orange solution.



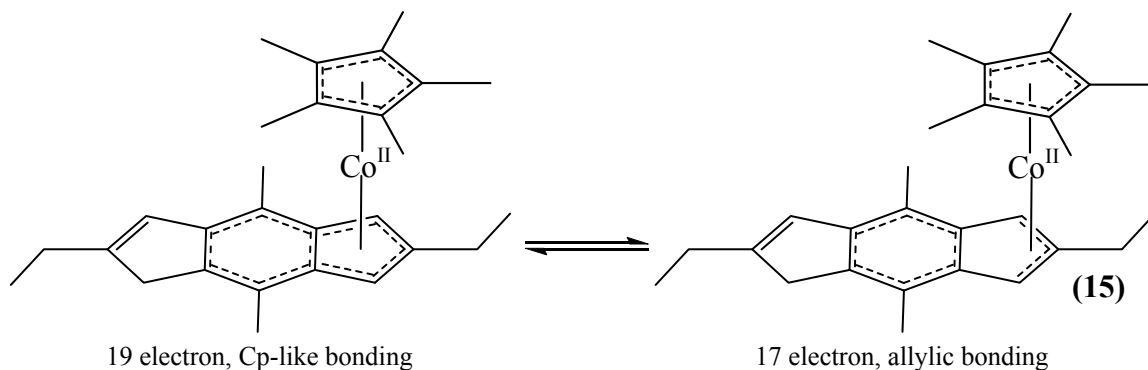
The amount of added *n*-BuLi must be very accurately calculated for 1:1 stoichiometry (Reaction 12), as a smaller amount yields a final mixture of free ligand plus the desired complex, whereas a minimal excess yields a mixture of the mononuclear complex and the dinuclear species (see Reaction 13). In either case, the yields decrease dramatically, because several recrystallizations are needed to purify the desired product.

Secondly, once the ligand has been properly monolithiated, a solution of the desired metallic fragment in THF is added to form the respective mononuclear complex. The nature of these complexes depends on the metal bonded to *s*-indacene. In the case of the diamagnetic complexes **21a** and **21b**, both are well known to have an η^5 array with Cp-like rings of ligands such as indene, together with *s*-indacene as well^[13].

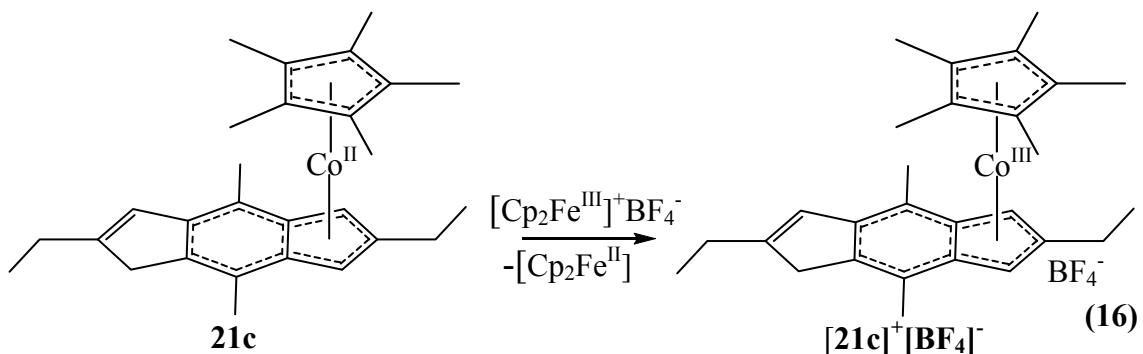


- 21a:** X = 1eq. **15a**, M = Cp*Fe-
21b: X = ¼eq. **17**, M = Cp*Ru-
21c: X = 1eq. **15b**, M = Cp*Co-
21d: X = ½eq. **18a**, M = (COD)Rh-

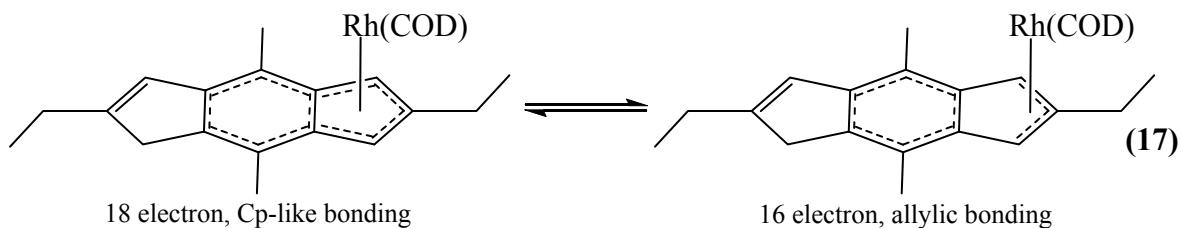
Complex **21c** is a special case, with an additional electron when compared to complex **21a**. A paramagnetic final product is formed, which may possibly induce the metallic center to have a η^5 to η^3 equilibrium towards indacene, similar to what has been previously reported with indenyl ligands^[14], resulting in electronic configurations of 19- and 17-electrons, none of which is a noble gas configuration.



Because compound **21c** is paramagnetic, NMR spectra are unsuitable for its characterization; therefore, a diamagnetic species must be prepared. Ferrocenium tetrafluoroborate is a one electron mild oxidant which may remove the one-electron from the cobalt moiety (Reaction 16) to form complex $[\mathbf{21c}]^+[\mathbf{BF}_4]^-$, which is stable in air, and readily soluble in organic polar solvents, such as acetone, acetonitrile, and THF. This complex will be used to characterize indirectly complex **21c**.



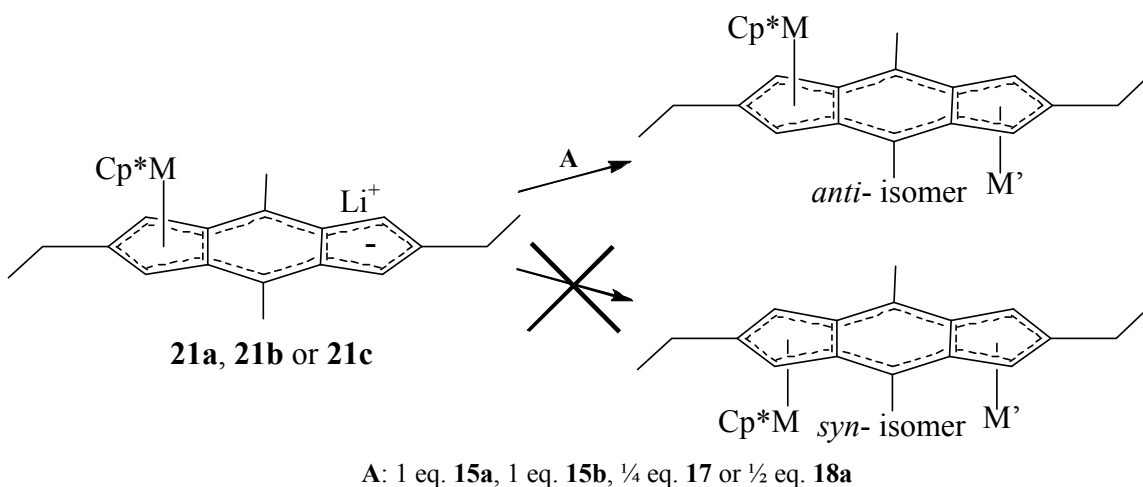
Complex **21d**, has an intermediate configuration, surely due to an equilibrium between the 18-electron noble gas configuration and the equally stable 16-electron pseudo-square planar geometry, characteristic of the $4d^8$ configuration of rhodium(I) (Reaction 17). In the case of **21d**, a ^{103}Rh -NMR analysis confirms this statement, which will be evident in the spectroscopic characterization section.



3.3 Preparation of Dinuclear compounds

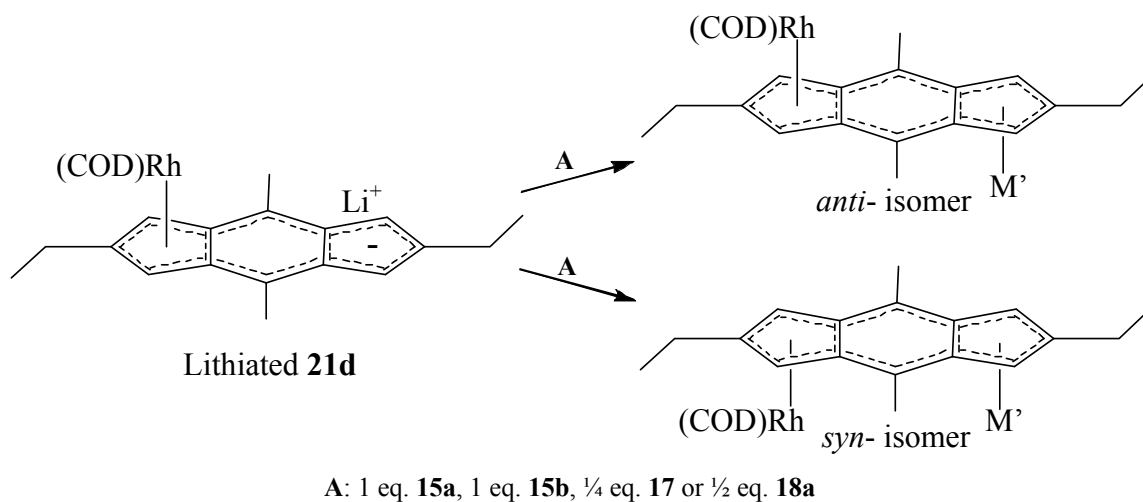
Dinuclear complexes can be divided into two basic subcategories: homobinuclear and heterobinuclear. These complexes are prepared with the intention of determining the degree of communication between both metallic centers even if these are not identical, more specifically with fragments such as $\text{Cp}^*\text{Ru}^{\text{II}}$ -, $\text{Cp}^*\text{Fe}^{\text{II}}$ -, $\text{Cp}^*\text{Co}^{\text{II}}$ -, and $(\text{COD})\text{Rh}^{\text{I}}$.

When starting with a mononuclear *s*-indacene complex with large bulky groups, such as those with a Cp^* ligand, the formation of a *syn*- isomer is not detected. This is the synthetic route that allows us to generate the *anti*- isomer stereospecifically.



Scheme 1: Formation of the *anti*- isomer in hetero- and homobinuclear complexes.

On the other hand, if the rhodium mononuclear complex is used as a starting material to yield a binuclear complex, two isomers may form, the *anti*- and *syn*-binuclear complexes, shown in the following scheme:



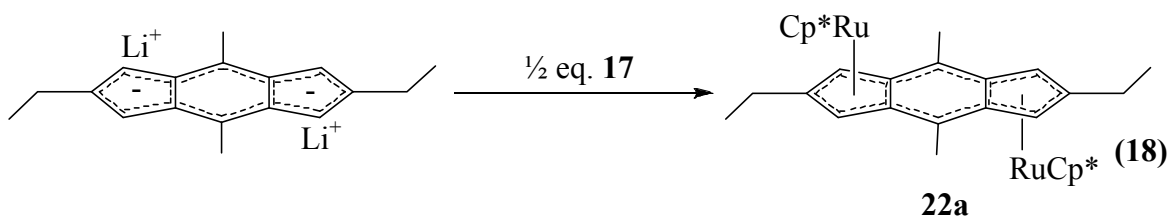
Scheme 2: Formation of *anti*- and *syn*- isomers of s-indacene binuclear complexes.

The reason why the stereoselectivity of both synthetic routes are different is due to the greater flexibility that a (COD)Rh- fragment has over a bulky and more rigid Cp*M- (M: Fe, Ru, Co) group, thus allowing the entry of a secondary group with greater ease.

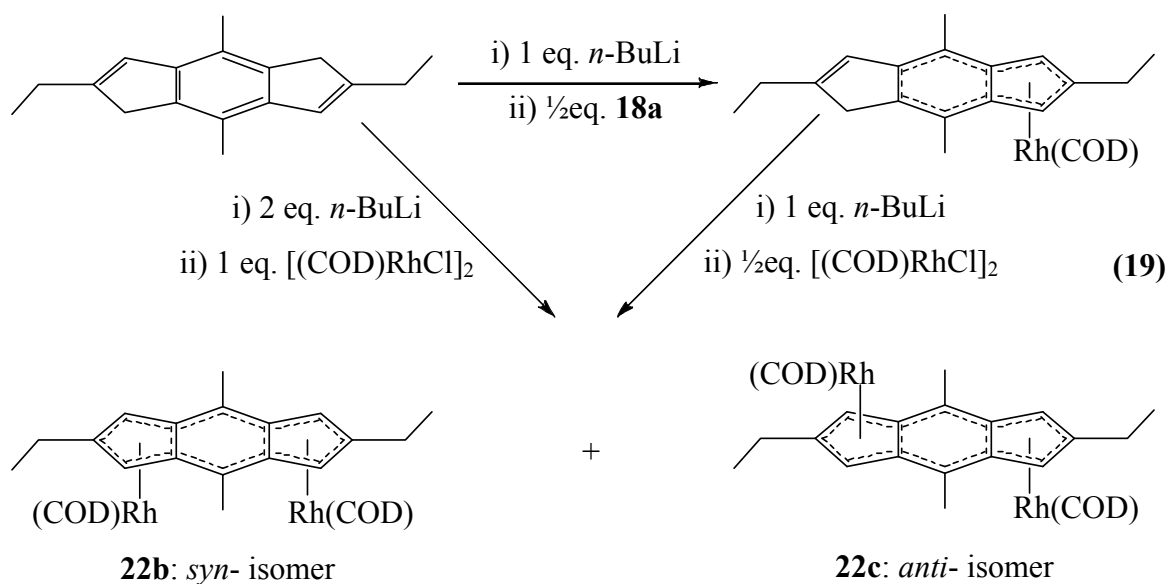
The *anti:syn* ratio is mainly dependent on the metallic fragments used, as described in the following subsections concerning the preparation of homobinuclear and heterobinuclear complexes.

3.3.1 Preparation of Homobinuclear complexes

In this thesis, only three homobinuclear complexes are reported, whether synthesized by a step-by-step lithiation of the *s*-indacene ligand, or by a direct double lithiation. In the synthesis of the bi-ruthenium complex, regardless of stepwise or direct dilithiation, only an *anti*- isomer is obtained due to the reasons discussed earlier.



In the case of the homobirhodium complexes, both stepwise and direct lithiation (see Reaction 19), form an *anti/syn* mixture in a 2:1 ratio.

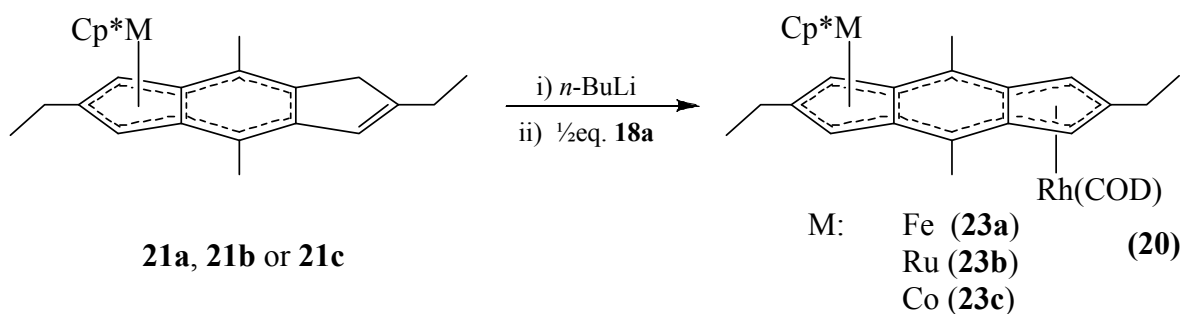


Several hypotheses have been already proposed to explain different *syn/anti* ratio in related homo- and heterobinuclear complexes^[11,15,36b,36c]. Amongst them: structures and relative stabilities of both lithiated intermediates and metal dimers, steric hindrance, solvent effect (THF), influence of the ancillary ligand of rhodium (COD vs. CO). Ceccon *et al*^[11], who studied these aspects in greater detail, concluded that the role of a ligand seems preponderant, there being a large preference for the *syn* isomer with COD or NBD as ancillary ligands, whereas the *anti* form was preferred with CO. In our case, where two different pathways were used, implying various reaction intermediates but the same deprotonation/metallation procedures, it seems reasonable to envisage that the same hypothesis (dominant influence of the COD ligand) can explain the identical ratio obtained for the two paths.

3.3.2 Preparation of Heterobinuclear complexes

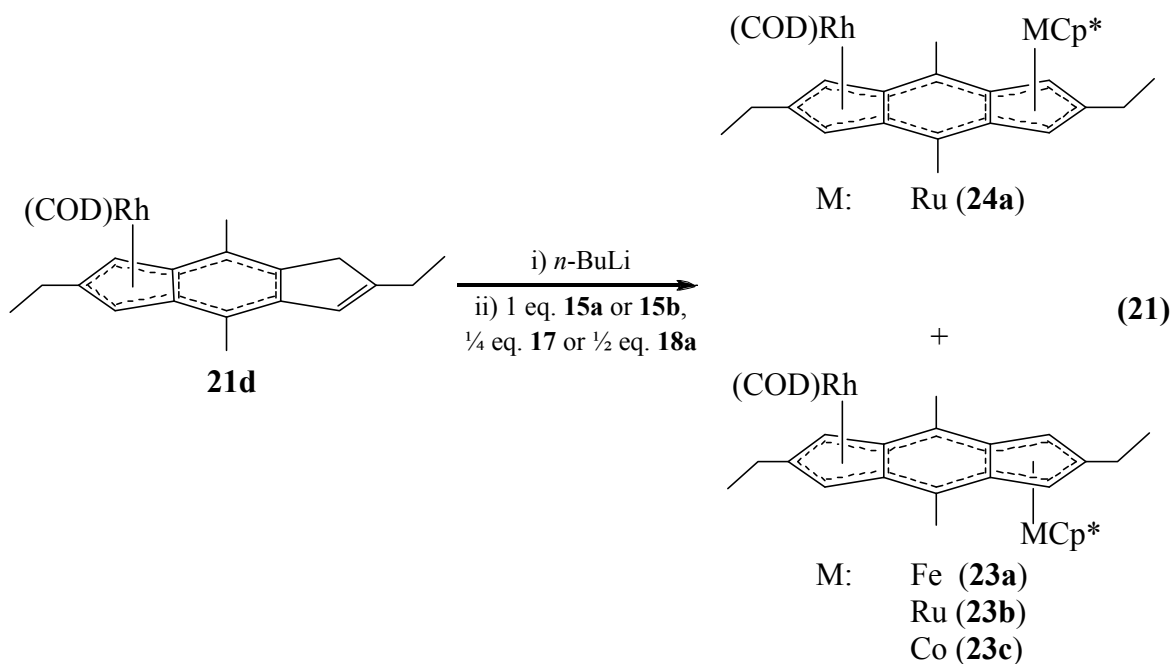
Heterobinuclear complexes enclosing one Rh center are also included in this thesis. Such complexes are usually obtained in yields of over 80% in all cases. The removal of the acidic proton from a mononuclear complex is a slower process, surely due to the negatively charged spacer molecule which will undergo a reaction to provoke the

ligand to be doubly negatively charged. Nevertheless, the yields indicate that the proton is effectively removed, but only at a slower pace.



Reaction 20 shows that the *anti*-isomers are formed by starting from any of the complexes having the bulky Cp* ligand, yielding the most stable isomer stereospecifically.

Contrary to an article reported by Ceccon *et. al.*^[15], claiming that bulky Cp* groups strictly induce *anti*-isomers when using *s*-indacene ligands, the formation of *syn*-isomers is feasible. Similar to the case of the homobinuclear complexes, if the starting material is a mononuclear rhodium *s*-indacene complex, to our surprise and despite the fact that the entry of an extremely bulky group such as Cp* could impede the formation of a *syn*-isomer, an *anti:syn* mixture was obtained (Reaction 21).

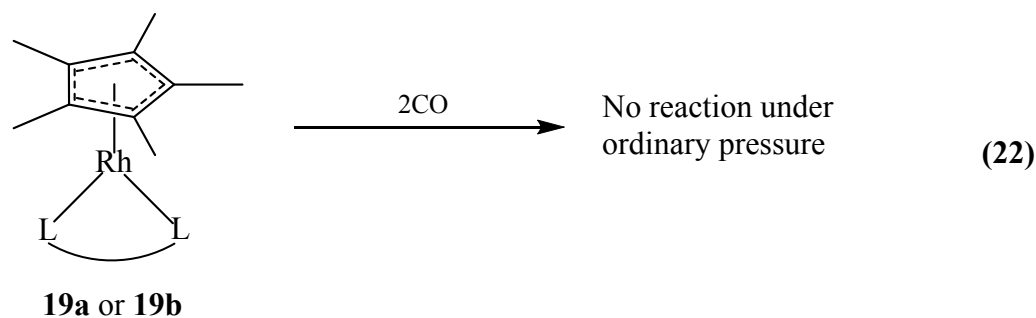


3.4 Reactivity test with CO

Reactivity tests were carried out with simple rhodium complexes by bubbling CO into an NMR tube containing a saturated solution of each complex in deuterated chloroform. Normally, the bubbling time would never be continued for extended periods of time due to the high volatility of this solvent; but in order to keep the initial concentration in equivalents of rhodium constant, some additional CDCl_3 was added at the end of each experiment.

3.4.1 (1,2,3,4,5-Pentamethylcyclopentadienide)-Rhodium-diene

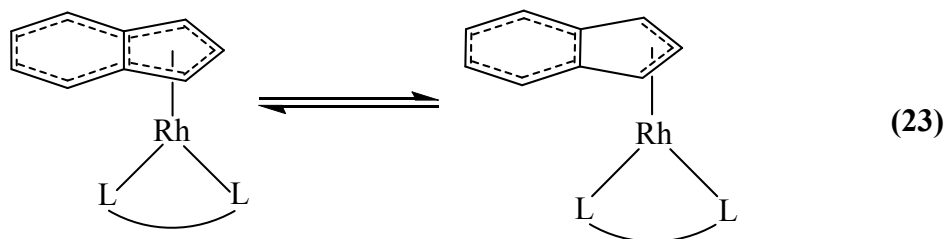
Complexes **19a** and **19b** were completely inert to CO in the above tests. This lack of reactivity may be explained by the 18-electron (noble gas) configuration which does not allow the formation of the carbonylated derivative. According methods described in literature^[16], the carbonylated derivative can only be obtained under high pressures of CO close to 10 atmospheres.



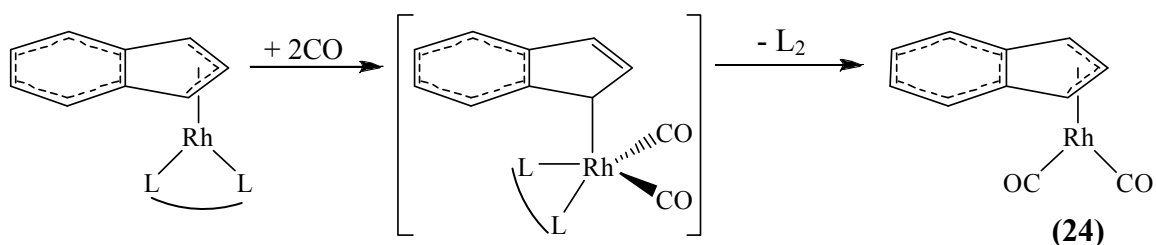
3.4.2 Indenyl-Rhodium-diene^[17]

Indenyl complexes **20a** and **20b**, on the other hand, are astonishingly reactive with CO. Within 30 seconds of bubbling this gas in the tube, a color change had occurred and NMR measurements confirmed a quantitative change from the diene form of the rhodium complex to a bis-carbonylated complex.

This reactivity can be attributed to an equilibrium of different bonding modes occurring even at room temperature, an effect that does not happen with Cp* ligands. This 18- to 16-electron equilibrium may allow the entry of a CO molecule in order to displace the respective diene. Such an associative reaction is common in square planar complexes^[18], so we may assume CO reacts with the complex in a tri-hapto configuration, as shown on the right side of reaction 23.



The haptotropic effect of the indenyl ligand might also include monohapto intermediates, providing a plausible mechanism that might include a pentacoordinate rhodium center (η^1 species), as shown below:



3.5 Physical Characteristics of *s*-indacene Metallic Complexes

Most rhodium complexes such as Wilkinson's Catalyst, $\text{Rh}(\text{NH}_3)_6^{+3}$ and $\text{Rh}_4(\text{CO})_{12}$ amongst many other, regularly form yellow to red solids. Those reported here and synthesized, are all yellow or orange crystalline substances, with the exception of those heterobinuclear rhodium complexes.

All heterobinuclear rhodium complexes are dark brown or black (**23a**, **23b** and **23c**), with the exception of the ruthenium-rhodium complex, which is intensely orange. Homobinuclear rhodium complexes (**22b** and **22c**) are both orange, while the homobinuclear ruthenium **22a** is dark purple.

In general, all mononuclear complexes reported here, are readily soluble in organic solvents such as toluene, benzene, pentane, THF, dichloromethane and chloroform, amongst others. All binuclear complexes are almost insoluble in pentane and THF, and only mildly in hexane and dichloromethane. These compounds have a fairly good solubility in toluene, especially if warmed.

3.6 Physical-Chemical Characteristics of *s*-indacene metallic complexes

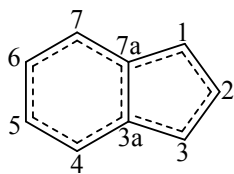
The ideal method for characterizing these compounds is NMR spectroscopy due to the fact that most of them are diamagnetic, with only few exceptions, and there are several nuclei which can be thoroughly analyzed by this means. These include the

classical ^1H , ^{13}C and ^{103}Rh , all of which have a nuclear spin number $+1/2$, but because the sensitivity of ^{13}C and ^{103}Rh is extremely low, highly concentrated samples and long measurement times are required.

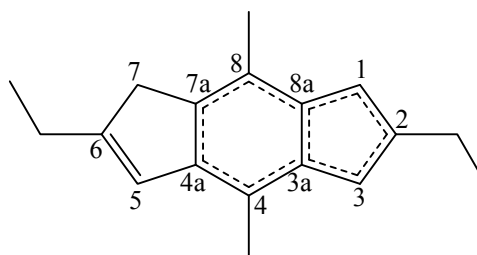
Also, ESR and FT-IR spectroscopies were carried out, as well as elemental analysis, cyclic voltammetry and X-ray diffraction studies for complexes **21a**, **22b**, and **24a**.

3.6.1 NMR Properties

The NMR assignments for the organometallic complexes were carried out with the following schemes:



Indenyl atom label



s-Indacene atom label

3.6.1.1 ^1H -NMR:

Table 1: Proton chemical shifts of Indenyl complexes (in ppm, in CDCl_3).

Proton:	20a	20b	20c
1, 3	4.90	4.95	5.81
2	5.92	6.02	6.10
4,7	7.07	7.02	7.15
5,6	7.13	7.15	7.30

Table 2: Proton chemical shifts of the mononuclear *s*-indacene complexes (in ppm, in CDCl₃ with the exception of [21c]⁺[BF₄⁻] which is in CD₃CN).

Proton:	21a	21b	[21c] ⁺ BF ₄ ⁻	21d
1,3	4.02	4.67	5.46	4.98, 5.00
5	6.60	6.24	6.74	6.67
7	3.04	3.04	3.40	2.99
CH ₃ (C ₄)	2.32	2.27	2.39	2.34
CH ₃ (C ₈)	2.19	2.14	2.34	2.21
CH ₂ (C ₂)	2.22	2.37	2.28	2.28
CH ₂ (C ₆)	2.27	2.41	2.52	2.59
CH ₃ (C ₂)	1.08	1.11	1.15	1.08
CH ₃ (C ₆)	1.10	1.18	1.26	1.38

Table 3: Proton chemical shifts of the homobinuclear *s*-indacene complexes (in ppm, in CDCl₃).

Proton:	22a	22b	22c
1,3,5,7	4.20	4.93	5.00
CH ₃ (C _{4,8})	2.38	2.20	2.29
CH ₂ (C _{2,6})	2.25	2.56	2.52
CH ₃ (C _{2,6})	1.03	1.31	1.31

Table 4: Proton chemical shifts of the heterobinuclear *s*-indacene complexes (in ppm, in CDCl₃ with the exception of [23c]⁺[BF₄⁻] which is in CD₃CN).

Proton:	23a	23b	[23c] ⁺ BF ₄ ⁻	24a
1,3	4.20	4.74	5.38	4.61
5,7	5.04	5.00	5.53	4.90
CH ₃ (C _{4,8})	2.38	2.27	2.32	2.06
CH ₂ (C ₂)	2.25	2.21	2.52	2.19
CH ₂ (C ₆)	2.53	2.53	2.69	2.52
CH ₃ (C ₂)	1.03	1.11	1.18	1.13
CH ₃ (C ₆)	1.32	1.30	1.39	1.22

The chemical shift values for each complex are comparable and similar to those other complexes listed in each respective table. The differences from one complex to the other are explained to the effect the metal has on the closest protons. For instance, protons 1 and 3 for mononuclear complexes in tables 2 and 4 have largely different values directly related to the effect on the electropositivity (or electronegativity) of each metal. As complex **[21c]⁺BF₄⁻** has a metallic fragment with a Co^{III} center, this strongly deshields protons 1 and 3 to a value of 5.46 ppm, while a less electronegative metal, as Fe^{II} (Cp*Fe- fragment in complex **21a**) shifts these same protons to 4.02 ppm.

Complex **21d** does has comparable chemical shifts when compared to those in the literature for a similar complex used by Ceccon, with 2,6-dimethyl-*s*-Indacene^[19], despite the fact these latter were determined in deuterated dichloromethane, rather than C₆D₆. In spite of this, the chemical shifts never differ in values larger than 0.5 ppm, and both spectra are surely very similar, excluding the unexistent methyl groups in position 4 and 8, and the singlets for the methyl groups in positions 2 and 6 for Ceccon's mononuclear rhodium complex. In the case of homobinuclear rhodium complexes, Ceccon and co-workers have also reported similar *anti*- and *syn*-binuclear compounds using 2,6-dimethyl-*s*-Indacene^[11]. Complexes **22b** and **22c** have also strong similarities regardless of the different solvent choice; only in this case the analogue and comparable protons differ with values from 0.6 ppm only.

The most important differences worth mentioning are the differences between the *anti* and *syn* isomers. Complexes **23b** and **24a**, as well as **22b** and **22c** have fairly discrete chemical shift value differences, although the structural differences between one isomer with the other are large. In each entry for these complexes, the differences are never larger than 0.2 ppm for protons 1 and 3, together with 5 and 7. As *syn*- isomers tend to force the spacer ligand to have a small torsion angle (planarity loss) that the respective *anti*- isomer possibly does not have, this effect may influence each respective five-membered ring for each metal bonded to *s*-indacene. For further information on the torsion angles, refer to Crystallography section (3.6.4).

3.6.1.2 $^{13}\text{C}\{^1\text{H}\}$ -NMR:

^{13}C -NMR chemical shifts not only provide information that allows us to further characterize the molecules, but also the coupling constants with rhodium reveal information about the hapticity of the organic ligand.

In the following tables, not only are ^{13}C chemical shifts listed, but also the value for each respective coupling constant of those carbon atoms bonded to rhodium. All coupling constants are small, ranging from 1.2 to 6.0 Hz, and as listed in each table, the closer the carbon atom is to rhodium, the larger the value.

The apical carbon atom (carbon atom number 2 for indenyls, carbon atoms number 2 and/or 6 for *s*-indacene complexes) has in all cases the largest value. Since rhodium in each case is bonded closer to a tri-hapto array, the coupling constants are smaller the longer (thus, weaker) the carbon-rhodium bonds are.

Some carbon atoms could not be distinguished from each other because they are too similar. In those cases, the entries are given only for the possible values they may have. Normally, the carbon atoms that are far too complex to identify are those in positions 1 and 3, together with 3a and 8a in mononuclear *s*-indacene complexes.

In the case of the oxidized derivative of complex **23c**, coupling constants of carbon atoms 5, 7, 4a and 7a could not be determined. Apparently, its solubility in CD_3CN is so low that determination of the coupling constants with rhodium was prevented, and only broad small singlets were observed.

Concerning similar complexes reported in the literature^[11,19], the coupling constants with rhodium are almost identical, differing by 0.1 Hz at the most. This can be easily understood due to the fact that only the substituents on positions 2, 4, 6 and 8 are the sole difference, though these effects combined with the different solvent used (CD_2Cl_2 was used in the literature) do have a marked difference with the chemical shift

values, reaching these 5 to 12 ppm. Regardless, this analogy makes it clear the assignation has been correctly carried out.

Table 5: Carbon chemical shifts and coupling constants with rhodium of Indenyl complexes (in ppm, in CDCl₃).

Carbon:	20a	20b	20c
1, 3	76.3 ¹ J _{C-Rh} = 4.4 Hz	74.4 ¹ J _{C-Rh} = 5.5 Hz	75.4 ¹ J _{C-Rh} = 3.5 Hz
2	92.4 ¹ J _{C-Rh} = 5.2 Hz	91.6 ¹ J _{C-Rh} = 6.0 Hz	97.7 ¹ J _{C-Rh} = 6.1 Hz
3a, 7a	113.2 ¹ J _{C-Rh} = 2.1 Hz	110.0 ¹ J _{C-Rh} = 1.4 Hz	117.6 ¹ J _{C-Rh} = 1.6 Hz
4,7	122.7	121.6	125.1
5,6	119.4	120.1	118.8

Table 6: Carbon chemical shifts of the mononuclear *s*-indacene complexes (in ppm, in CDCl₃ with the exception of [21c]⁺[BF₄]⁻ which is in CD₃CN).

Carbon:	21a	21b	[21c] ⁺ BF ₄ ⁻	21d
C ₁	66.59	62.90	75.11	75.33 or 75.62 ¹ J _{C-Rh} = 4.3 Hz
C ₂	96.00	92.70	106.2	114.93 ¹ J _{C-Rh} = 5.0 Hz
C ₃	66.91	62.90	75.20	75.33 or 75.62 ¹ J _{C-Rh} = 4.3 Hz
C _{3a}	95.06	90.48	124.14	110.86 or 113.10 ¹ J _{C-Rh} = 2.5 Hz
C ₄	119.78	119.60	117.45	139.57
CH ₃ (C ₄)	15.34	15.43	15.08	15.32
C _{4a}	138.27	139.36	148.54	115.37
C ₅	124.38	124.19	145.38	39.61

C ₆	148.82	135.20	157.90	149.12
C ₇	39.09	38.84	40.09	124.84
C _{7a}	134.13	125.39	144.62	119.56
C ₈	123.52	143.52	148.39	136.23
CH ₃ (C ₈)	14.94	15.68	15.31	15.51
C _{8a}	93.47	88.40	123.95	110.86 or 113.10 ¹ J _{C-Rh} = 2.5 Hz
CH ₂ (C ₂)	25.14	22.03	20.43	23.09
CH ₃ (C ₂)	13.13	16.46	15.69	16.00
CH ₂ (C ₆)	22.59	24.81	25.36	25.00
CH ₃ (C ₆)	15.18	12.70	12.70	13.92

Table 7: Carbon chemical shifts of the homobinuclear *s*-indacene complexes (in ppm, in CDCl₃).

Carbon:	22a	22b	22c
C _{1,3,5,7}	68.59	73.69 ¹ J _{C-Rh} = 5.0 Hz	73.75 ¹ J _{C-Rh} = 5.0 Hz
C _{2,6}	101.26	117.18 ¹ J _{C-Rh} = 6.0 Hz	117.50 ¹ J _{C-Rh} = 6.0 Hz
C _{3a,4a,7a,8a}	99.09	115.92 ¹ J _{C-Rh} = 1.2 Hz	114.28 ¹ J _{C-Rh} = 1.6 Hz
C _{4,8}	116.79	112.13	110.94
CH ₃ -(C _{4,8})	15.97	15.08	15.59
CH ₂ (C _{2,6})	17.32	23.78	23.55
CH ₃ (C _{2,6})	15.99	15.22	15.21

Table 8: Carbon chemical shifts of the heterobinuclear *s*-indacene complexes (in ppm, in CDCl₃ with the exception of [23c]⁺[BF₄]⁻ which is in CD₃CN).

Carbon:	23a	23b	[23c] ⁺ BF ₄ ⁻	24a
C _{1,3}	61.54	65.69	75.02	65.97
C ₂	92.34	95.78	106.00	95.83
C _{3a,8a}	117.62	96.62	121.54	97.28
C _{4,8}	92.98	96.59	112.95	95.71
CH ₃ -(C _{4,8})	16.24	15.29	14.81	14.73
C _{4a,7a}	117.84 ¹ J _{C-Rh} = 1.3 Hz	116.00 ¹ J _{C-Rh} = 1.4 Hz	99.75	116.48 ¹ J _{C-Rh} = 1.1 Hz
C _{5,7}	71.81 ¹ J _{C-Rh} = 4.9 Hz	71.73 ¹ J _{C-Rh} = 4.5 Hz	69.68	72.71 ¹ J _{C-Rh} = 5.1 Hz
C ₆	121.03 ¹ J _{C-Rh} = 6.7 Hz	120.55 ¹ J _{C-Rh} = 6.5 Hz	126.77 ¹ J _{C-Rh} = 5.0 Hz	120.41 ¹ J _{C-Rh} = 7.8 Hz
CH ₂ (C ₂)	22.55	22.74	19.97	22.76
CH ₃ (C ₂)	16.55	15.20	14.13	15.35
CH ₂ (C ₆)	24.05	25.25	20.17	24.00
CH ₃ (C ₆)	14.85	15.10	14.28	14.97

3.6.1.3 ¹⁰³Rh-NMR:

The chemical shift values for ¹⁰³Rh were calculated by determining the absolute frequency of the cross-peak (HMBC experiments) relating it to the reference frequency of 12.64 MHz (N = 3.16 MHz at 100 MHz). These experiments are very time-consuming, due to the low sensitivity this nucleus has, which is indicative of the need of a highly concentrated solution of the analyzed complex.

Although measurements of ¹⁰³Rh-NMR chemical shifts in rhodium complexes are fairly uncommon, they can be used as good indicators of the degree to which Rh centers undergo slippage. In fact, the chemical shifts are highly dependent on the hapticity of organic ligands. For example, Cp-Rh(COD) has a ¹⁰³Rh chemical shift of -777 ppm, while Indenyl-Rh(COD) has a value of -487 ppm, and trihapto-cycloheptenyl-Rh(COD) has a value of only -7 ppm, directly related to the lower number of hapticity modes^[15].

In Table 9 are listed the different chemical shifts for each complex with Rh(I). $\delta(^{103}\text{Rh})$ of *syn* complex **22b** is shifted about 70 ppm downfield compared to that of *anti* analogue **22c**. This difference may reflect a slightly more pronounced η^3 -character in the *syn* complex, presumably to possible higher steric repulsion of Rh(COD) fragments in **22c** which, then, slips away.

All other *s*-indacene complexes have similar chemical shifts, ranging from -486 to -261 ppm, very much in the range of indenyl and substituted indenyl rhodium complexes. If complex **21d** is excluded, we can see that all other Rh complexes have chemical shifts ranging from -334 to -261 ppm, characteristic of a tri-hapto configuration, or possibly an intermediate between η^3 - and η^5 -coordination (i.e., $\eta^2 + \eta^3$).

Table 9: Rhodium chemical shifts of the binuclear *s*-indacene complexes.

Complex:	19a	19b	20a	20b	20c	21d	22b	22c	23a	23b	[23c] ⁺ BF ₄ ⁻	24a
Chemical shift (ppm):	-789	-786	-486	-521	-1038	-486	-261	-334	-275	-281	-271	-245

3.6.2 Electrochemical Properties

It is widely known that cyclic voltammetry is a very powerful tool that can provide information concerning the degree of communication between two metallic centers bridged by a ligand favoring a “cooperative effect”^[20]. This method is used only on *s*-indacene complexes in this thesis.

If a strong cooperative effect exists between two metallic centers, the first one-electron oxidation occurs easily, and the second oxidation is extremely difficult, due to the fact that a highly delocalized molecule compensates for the electronic deficiency, thanks to a large electronic delocalization throughout the whole molecule. Therefore, the larger the difference between the first and second oxidation peaks, the greater the stability and the greater the communication these molecules portray^[21].

In most cases, all peaks correspond to one-electron oxidations, based on the peak difference between each respective couple.

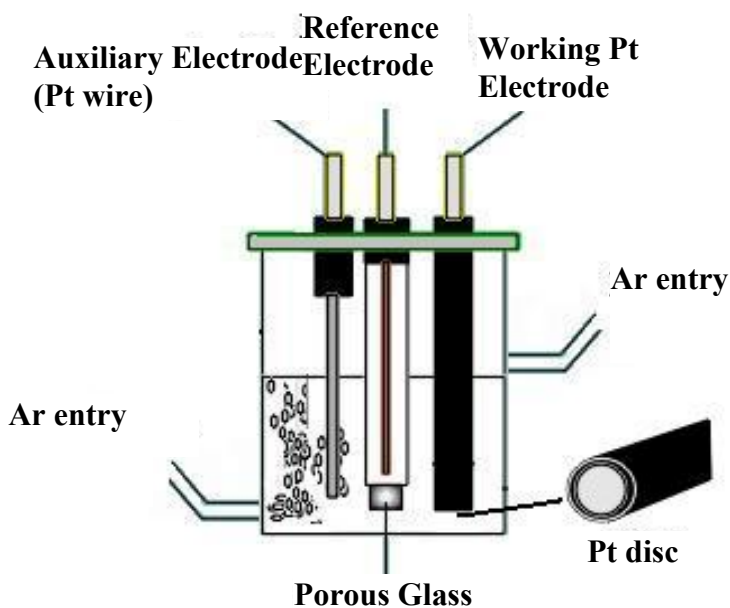


Figure 2: Drawing of the electrochemical cell used for each voltammetry experiment.

In a typical electrochemical experiment dichloromethane freshly distilled over phosphorous pentoxide is used, together with a 0.1M tetrabutylammonium tetrafluoroborate as the supporting electrolyte, in addition to $5 \cdot 10^{-4}M$ of the complex. Usually a 30-second period of bubbling argon in the solution assures a complete removal of any traces of oxygen which may not only oxidize the air-sensitive complex, but also show a large oxygen reduction peak near -850 mV in this particular solvent.

The electrodes used were a platinumium disc for the working electrode, and a platinumium wire as the auxiliary electrode, all in a saturated calomel electrode (SCE) for reference purposes.

3.6.2.1 Cyclic voltammograms of mononuclear complexes

The cyclic voltammograms are displayed in Figures 3 to 6. They were carried out to compare the effects of changing one metal to the other, and also to compare with binuclear analogues. A shift of any redox couple may certainly take place when going from a mononuclear complex to a binuclear complex, due to two main factors: i) the possible communication between a second metallic center, and ii) the fact that the *s*-indacene ligand is now doubly deprotonated (or doubly negatively charged). Either way, the former has a dramatic difference in terms of shifting, while the latter has only discrete effects.

As viewed in each voltammogram, each molecule is active electrochemically. Since these molecules are rich in electrons, they have important activities as one-electron reducing agents. In some cases, there is more than one redox couple which strongly depends on the nature of the metal, and therefore, its reactivity.

Complexes **21a** and **21b** are both complexes from group 8 metals, similar to a ferrocene or ruthenocene, respectively. Complex **21a** does not differ greatly from ferrocene, nor does **21b** from ruthenocene, other than a minor potential shift due to substituent effects, together with the additional aromatic ring the *s*-indacene encloses, and the lack of reversibility, becoming quasi-reversible.

In the case of **21a**, iron oxidizes into Fe⁺³ at 72 mV, while other irreversible oxidation peaks occurring at potential values over +1000 mV are probably related to oxidation of the organic framework of the complex, in a coupled chemical reaction. This same complex has a decreased reversibility (75 mV of peak difference) when compared to ferrocene, which is well known to have a completely reversible one-electron redox couple. Complex **21a** has a Cp* ligand, which is a much stronger electron-donor ligand when compared to Cp. This may explain the large difference of 430 mV between **21a** and

ferrocene (in the same conditions), this latter presenting a completely reversible redox couple at +502 mV^[22].

Complex **21b** shows two redox couples, corresponding to the oxidation of Ru⁺² to Ru⁺³ at 523 mV, plus a second at 1089 mV. The electrochemical behavior of ruthenocene-like molecules is not as clear as that of ferrocene in which a number of earlier studies found that the oxidation of ruthenocene results in products that vary with the nature of the medium, yielding a possible one- or two-electron oxidation, possibly due to the highly electron-donor Cp*ligand. A second one-electron oxidation is feasible^[23].

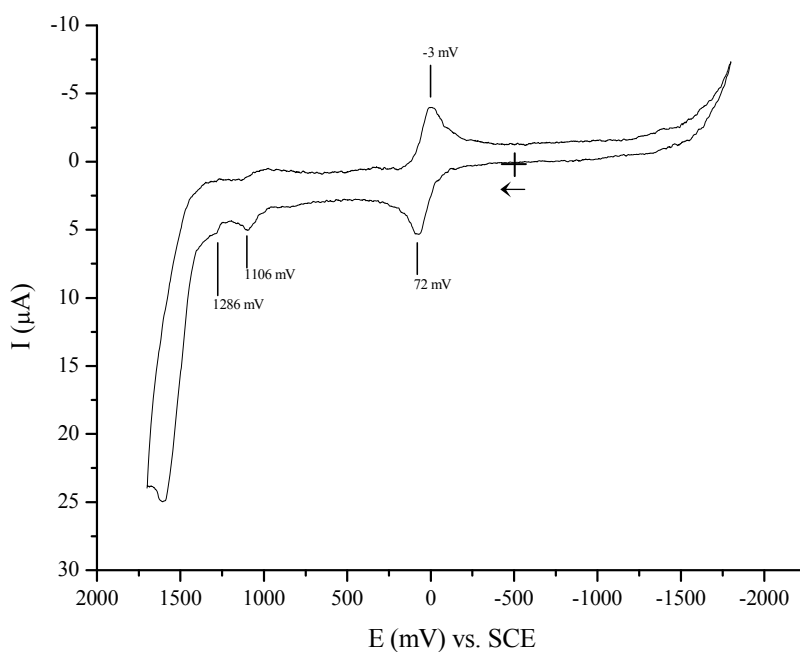


Figure 3: Cyclic Voltammogram of complex **21a**.

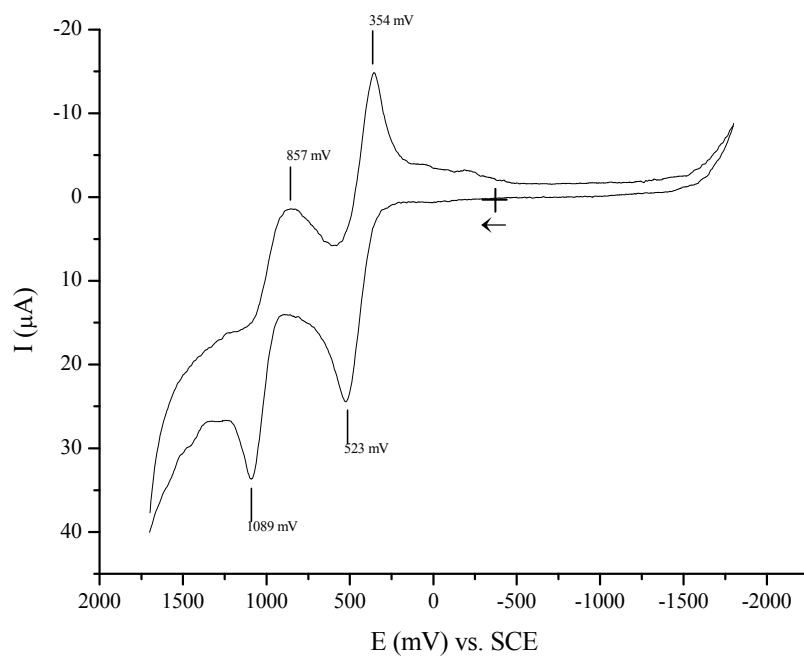


Figure 4: Cyclic Voltammogram of complex **21b**.

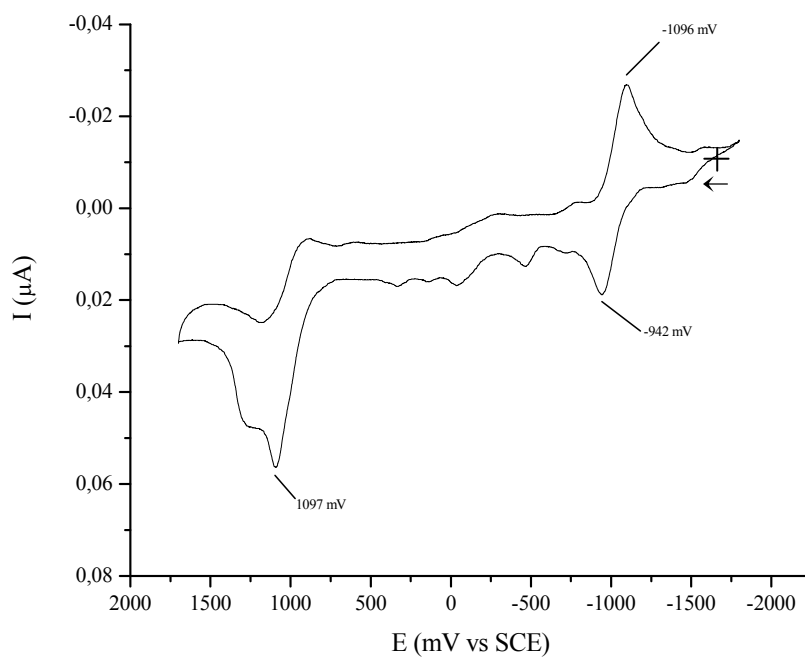


Figure 5: Cyclic Voltammogram of complex **21c**.

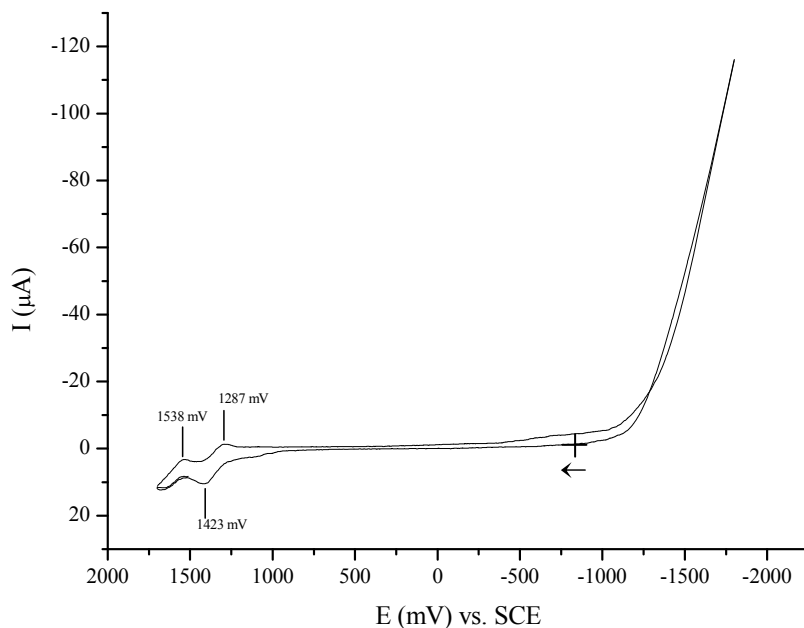


Figure 6: Cyclic Voltammogram of complex **21d**.

Complex **21c** is a cobaltocene-like molecule, and because it has a single electron in a non-bonding orbital, it behaves as a strong reducing agent. This complex releases its lone electron to become an 18-electron species at a much lower potential (-942 mV) when compared to **21a** and **21b**. The secondary process at 1097 mV is most likely related to an irreversible oxidation of the s-indacene ligand.

The rhodium complex **21d** has a very high oxidation peak, which has been reported in several articles to be strongly dependent on such factors as solvent and supporting electrolyte^[24]. It undergoes one-electron transfers together with chemical reactions in addition to the initial electrochemical process. This complex is thermodynamically very difficult to oxidize as evident from its potential value of +1423 mV, probably due to a high instability of the resulting 15-electron rhodium complex.

3.6.2.2 Cyclic voltammograms of binuclear complexes

In binuclear complexes the second oxidation peak, corresponding to the oxidation of a second metallic center in homo- and heterobinuclear complexes was not possible to observe, most likely due to its shift out of the working potential range of the solvent used. Since complex **21d** already showed processes near the positive working limit of dichloromethane, and if a binuclear complex with rhodium has a high cooperative effect, the outcome may turn out to be a highly reducing process (greatly shifted to less positive values), together with a difficult second electronic transfer which may not be evident within the potential working range.

Cyclic voltammograms for all binuclear complexes are given in Figures 7 to 13. Complex **22a** shows two clearly defined quasi-reversible processes with a large difference (781 mV) between both oxidation peaks, thus indicating a great stability of the monooxidized species.

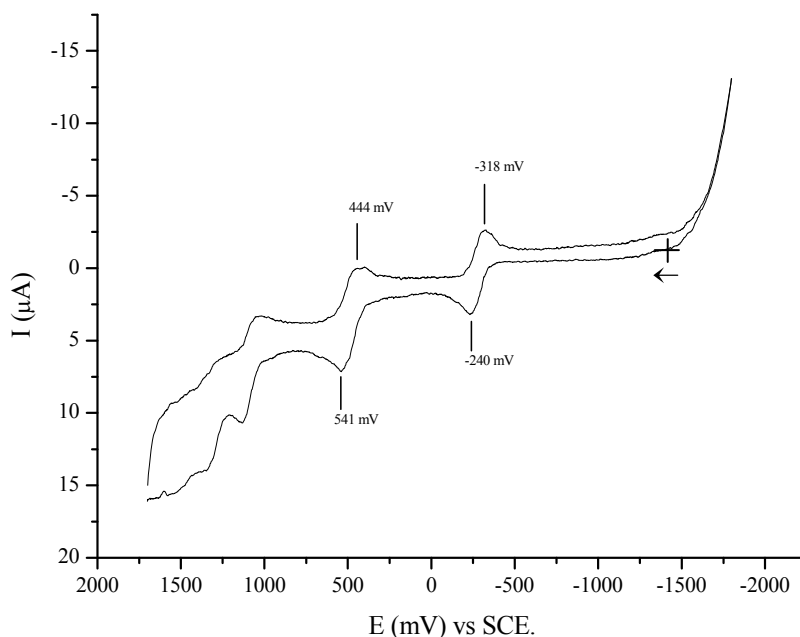


Figure 7: Cyclic Voltammogram of complex **22a**.

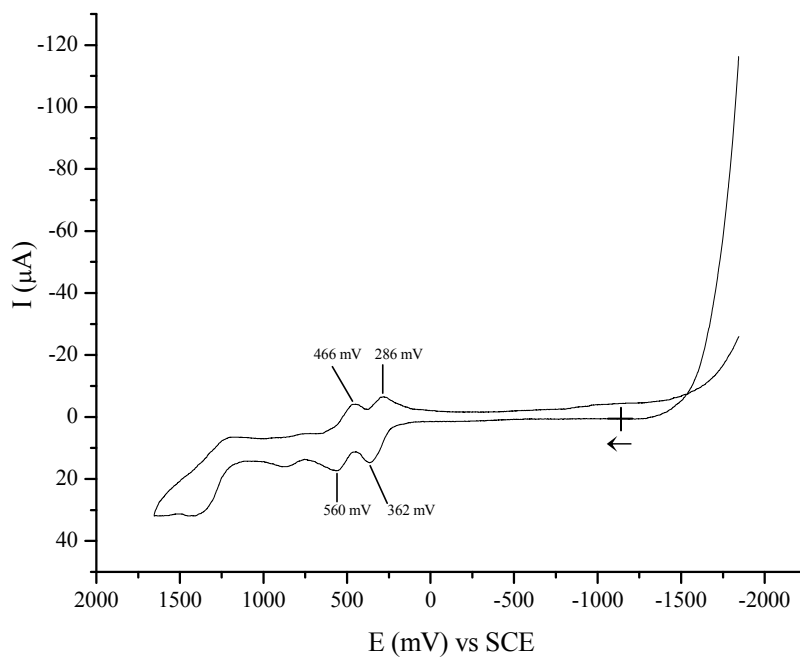


Figure 8: Cyclic Voltammogram of complex **22b**.

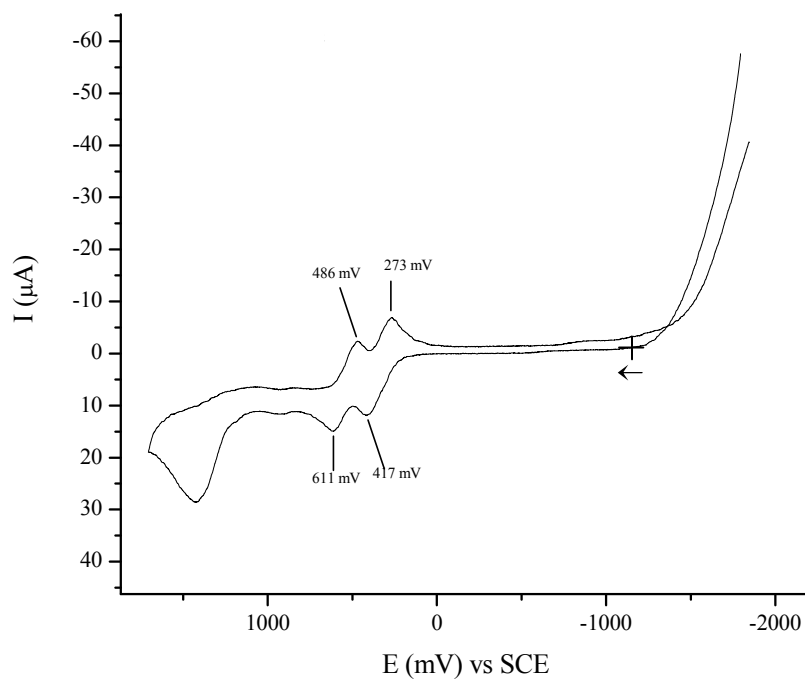


Figure 9: Cyclic Voltammogram of complex **22c**.

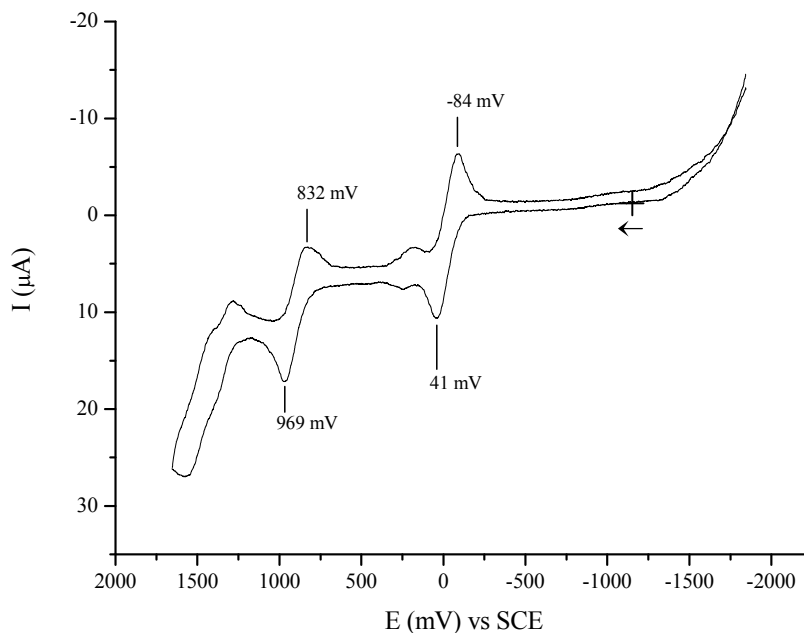


Figure 10: Cyclic Voltammogram of complex **23a**.

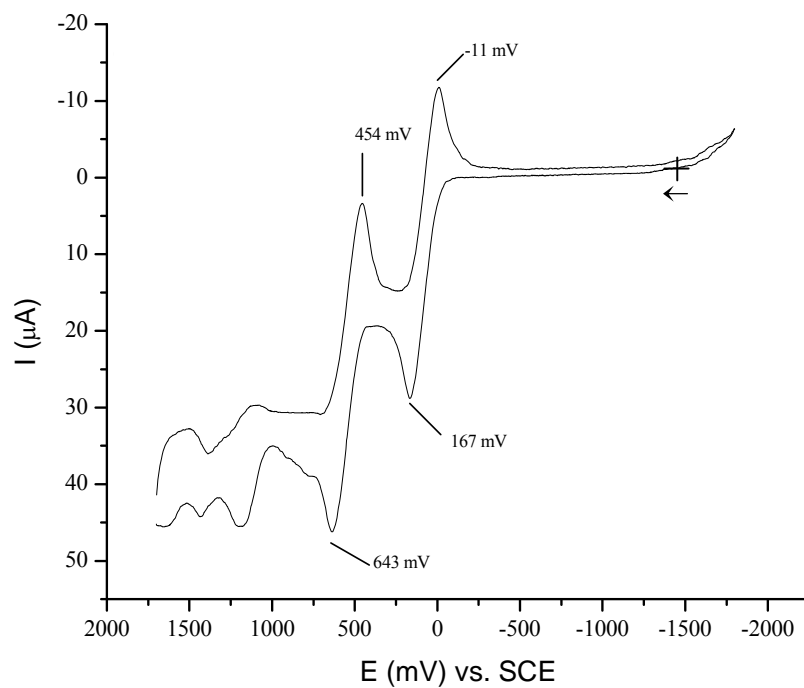


Figure 11: Cyclic Voltammogram of complex **23b**.

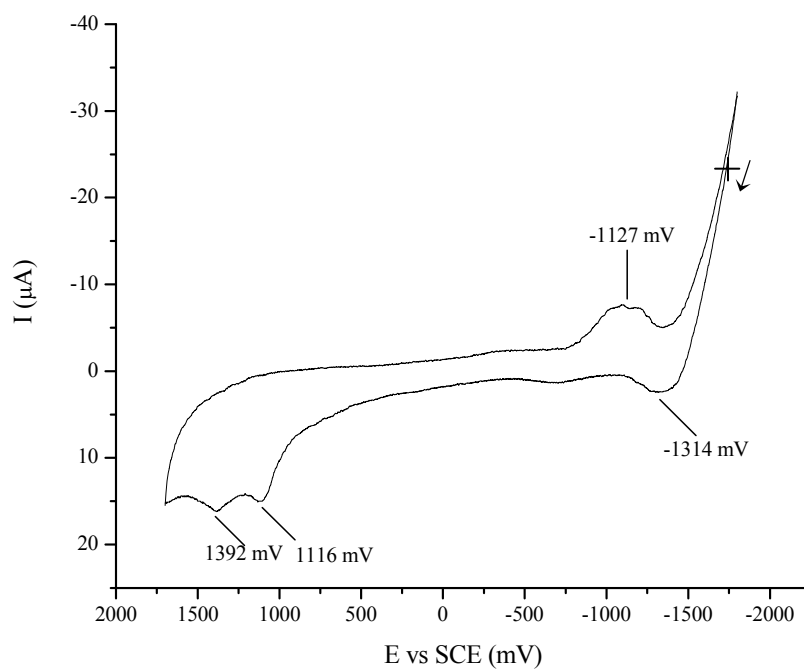


Figure 12: Cyclic Voltammogram of complex **23c**.

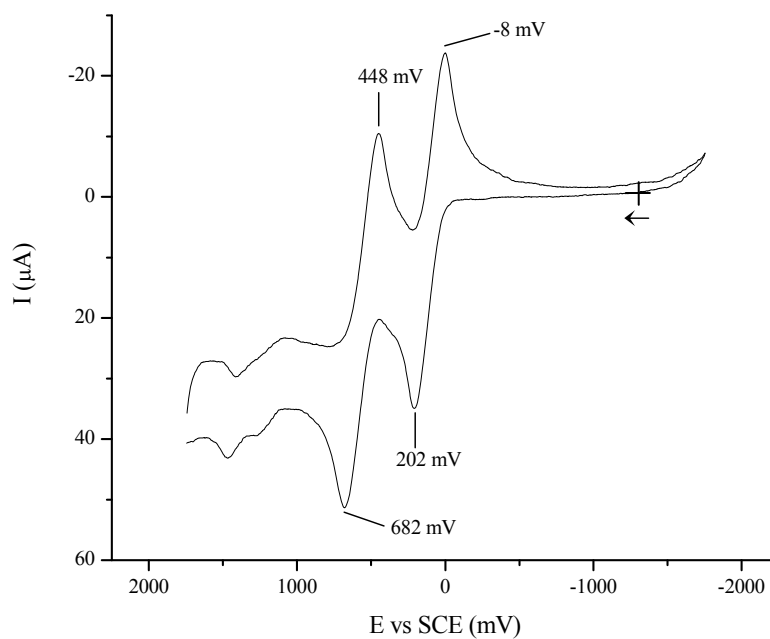


Figure 13: Cyclic Voltammogram of complex **24a**.

Table 10: Summary of Cyclic Voltammetry Results.

Complex	E_{p1}^a	ΔE_{p1}^b	I_c / I_a	ΔE_p^c
21a	72	75	1.0	-
21b	523	169	1.0	-
21c	-942	154	1.0	-
21d	1423	136	1.6	-
22a	-240	78	1.0	763 (21b)
22b	417	76	1.8	1006 (21d)
22c	362	144	1.0	1061 (21d)
23a	41	125	1.0	31 (21a)
23b	167	178	1.0	356 (21b)
23c	-1314	^d	^d	372 (21c)
24a	202	210	1.0	321 (21b)

All potential values listed in millivolts.

^aPotential value for the first anodic peak.

^bDifference between respective cathodic peak.

^cDifference between reference analogue mononuclear complex and listed compound of the first oxidation peak.

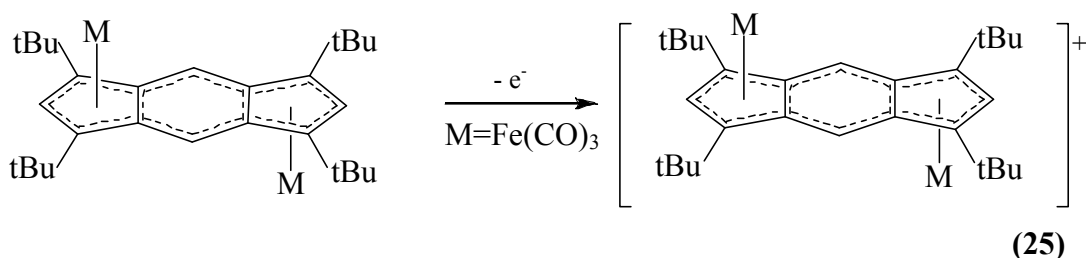
^dUnable to determine properly.

With the sole exception of complex **22a**, the determination of the difference in energy (in mV) from one oxidation state to the other is difficult due to fact that in most cases the second oxidation peak is outside the limits allowed by the solvent, or fact that the second oxidation process is of unknown origin and may be related to the oxidation of an organic moiety, or possibly to the second metallic center.

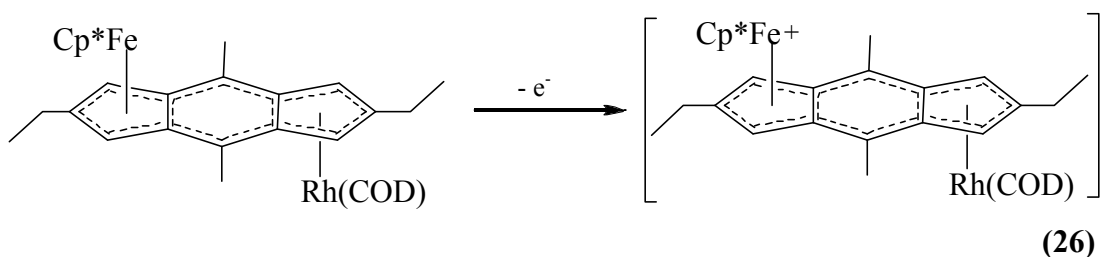
However, another parameter listed in the fourth column of Table 10 may allow us to elucidate the degree of influence a secondary metallic fragment might have. The difference between the reference analogue mononuclear complex and the listed compound of the first oxidation peak is an indication of the potential shift due to the doubly negatively charged spacer ligand together with the second metallic center. The highest values belong to the homobinuclear complexes, which certainly happens because of the same energy level each metallic fragment has in the resulting complex and its

monooxidized derivative. On the other hand, in the case of each heterobinuclear complex there is a lower stability due to the higher electropositivity of one of the metals in each listed complex (**23a**, **23b**, **23c** and **24a**).

For example, in a recent published article by O'Hare *et al.*,^[1b] a thorough theoretical analysis of the homobinuclear complex [1,3,5,7-tetra-terbutyl-*s*-indacene][Fe(CO)₃]₂ was made, in which the one-electron oxidation by chemical and electrochemical means is ligand centered, yielding a completely delocalized species in which the unpaired electron is localized on an organic orbital, as shown in Reaction 25. A similar situation happens with all homobinuclear complexes which have shift values over 700 mV, and in the case of **22b** and **22c**, over 1000 mV. These huge values may indicate that the molecular orbital diagram in the article by O'Hare *et al* may also apply here, implying a high cooperative effect.



The unpaired electron resulting from the one-electron oxidation in the case of heterobinuclear complexes may be more localized in certain moieties of the molecule, if not directly localized on the most electropositive metal. In the case of complex **23a**, the potential difference is only 31 mV, indicating that the charge of the oxidized species in the iron-rhodium complex is most likely centered on the ferrocene moiety (note the position of the positive charge in Reaction 26).

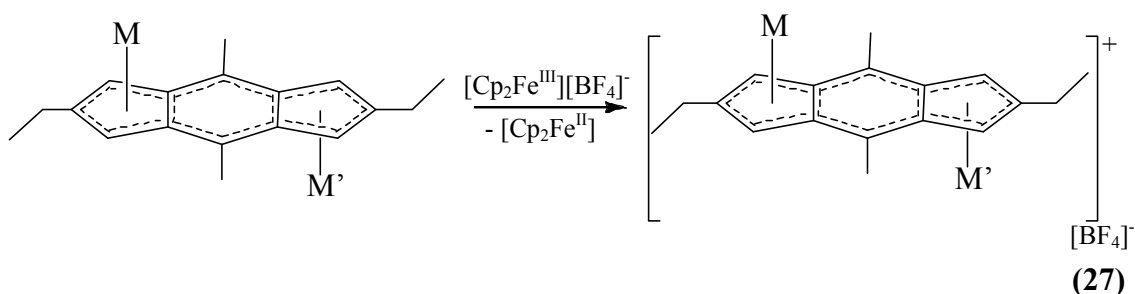


Finally, the cyclic voltammograms also disclose details about the differences between *anti* and *syn* isomers. In the case of **23b** and **24a**, the differences are minimal, being only 35 mV, with no difference whatsoever in the charge transfer process or in the reversibility of the first redox couple.

An interesting difference is evident in the case of complexes **21d**, **22b** and **22c**. The values of I_c/I_a listed in Table 10 are higher than unity for complexes **21d** and **22b**, suggesting the presence of a coupled irreversible chemical reaction while **22c** has quasi-reversible electrochemistry. This might indicate a cooperative effect between both metallic centers, absent in isomer **22b**, and possibly related to a spatial interaction between both Rh centers, yielding a decomposition of the oxidized species, consistent with its electrochemical irreversibility.

3.6.3 ESR Properties

ESR measurements were made on some of the more stable binuclear complexes by generating a radical through an *in situ* chemical oxidation with a ferrocenium salt inside the ESR tube. The following reaction shows what reaction took place inside the tube (Reaction 27).



The positively charged radical has an unpaired electron which should couple with those nuclei having a non-zero nuclear moment different from zero, thus revealing how effective electronic resonance is. Coupling of the lone electron with all protons near the aromatic rings of the spacer ligand, would have indicated a high degree of communication between both metallic fragments.

Unfortunately, the heavy metals in complexes **22a**, **22b**, **22c**, **23a** and **23b** made it impossible to observe hyperfine couplings, due to distortions the heavy elements produce. O'Hare *et al*^[1b] published a few years ago an article where they correlated the values of *g* in ESR spectra with the nature of the radical formed. The higher the value, the closer the electron is to the moiety of a metallic center; the lower the value, the closer the electron is to an organic orbital. The values of *g* for each complex are listed in Table 11.

Table 11: Values of *g* and details on the ESR spectra for the binuclear complexes.

Complex Oxidized	Value of <i>g</i>	Details of the Spectrum	Interpretation
22a	2.0870	Fairly narrow and intense signal	Unpaired electron is mostly located in the organic system
22b	2.0470	Narrow and small signal	Unpaired electron is mostly located in the organic system
22c	2.0365	Narrow and small signal	Unpaired electron is mostly located in the organic system
23a	2.1489	Wide and intense signal	Strong electronic localization in the iron moiety
23b	2.1073	Narrow and small signal	Unpaired electron strongly localized in the ruthenocene moiety

The results indicate that delocalization of the unpaired electron is not only dependent on the spacer molecule, but also on the nature of the metallic fragment. In the case of the Fe-Rh complex (molecule **23a**), the high electropositivity of the iron atom certainly makes the lone electron reside on the iron moiety rather than on the rest of the molecule.

Exactly the opposite happens with homobinuclear complexes. As both metals are identical their energy levels are identical; therefore, the unpaired electron may resonate from one side of the molecule to the other with no major energy barriers to overcome,

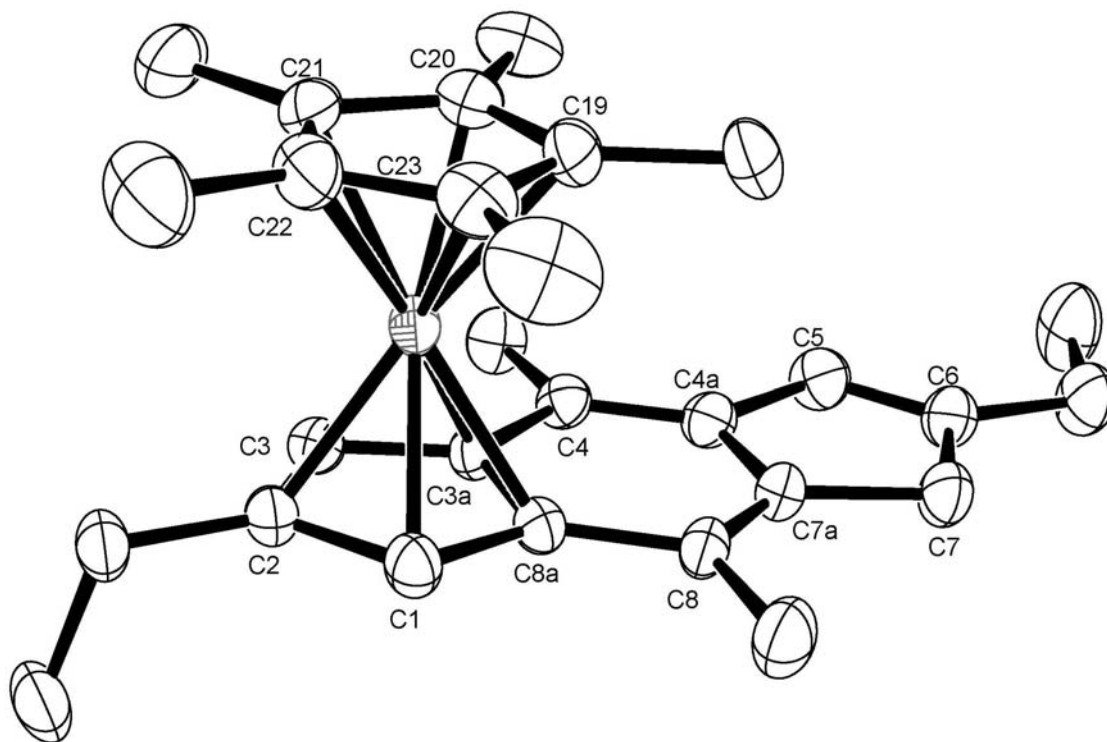
staying in the organic framework. The low values of g for homobinuclear complexes when compared to the heterobinuclear molecules indicates that the delocalization is dependent on the nature of every fragment that composes the complex, not just the ligand. This is supported by the electrochemical behaviour of each respective complex, as previously discussed.

3.6.4 X-Ray Diffraction Structures

X-Ray structures are shown in Figures 14 to 16. In Tables 12 to 14 only selected bond distances are highlighted. These tables not only include the most relevant bond lengths and torsion angles, but also a parameter $\Delta M-C^{[25]}$, which is defined by the equation shown. This parameter is the difference between two averaged bond distances, the values of which will indicate the ring slippage of each metallic center from the Cp-like centroid of *s*-indacene. If this value is zero, the metal is in a perfect η^5 configuration; if larger, the greater the ring slippage.

3.6.4.1 X-ray Structure of Complex **21a**:

As expected, $CpFe^{II}$ and their analogues usually form penta-hapto coordination in order to achieve an 18-electron configuration and have minimal ring slippage, usually staying in the center of another Cp-like ring. When $\Delta M-C$ is 0.046, the presence of a quasi-perfect η^5 system with *s*-indacene is indicated.

Image 1: The X-ray structure of complex **21a**.Table 12: Selected Bond Distances (Å) for Complex **21a**:**Indacene**

Fe-C1	2.041(2)	C3a-C4	1.440(3)
Fe-C2	2.046(2)	C4-C4a	1.377(4)
Fe-C3	2.050(2)	C4a-C5	1.466(4)
Fe-C3a	2.095(2)	C5-C6	1.347(4)
Fe-C8a	2.092(3)	C6-C7	1.500(4)
C3a-C8a	1.439(4)	C7-C7a	1.513(4)
C1-C8a	1.432(3)	C7a-C8	1.353(4)
C1-C2	1.420(4)	C8-C8a	1.443(4)
C2-C3	1.426(4)	C7a-C4a	1.441(4)
C3-C3a	1.431(3)		

Centroids

Fe-C _{g(Cp*)}	1.645	Fe-C _{g(Ic)}	1.669
ΔFe-C	0.046		

$$\Delta M-C = \frac{\{(Fe-C_{8a}) + (Fe-C_{3a})\}}{2} - \frac{\{(Fe-C_1) + (Fe-C_3)\}}{2}$$

3.6.4.2 X-ray Structure of Complex **22b**:

The homobinuclear complex **22b**, presented an apparent symmetrical structure, slightly curved on the tips, with a molecular angle distortion of 6.89° . Consequently, the *s*-indacenediide loses its aromaticity as evidenced by the noticeable deviation from planarity of the five membered rings.

The COD ligands assume the usual conformation: the two olefin double bonds of each COD lie in a plane almost parallel to the indacenediide ligand and are oriented in a direction almost perpendicular to the ring junction bonds (C4a–C7a and C3a–C8a). This orientation allows the absence of short intramolecular distances between COD (shortest non-bonded C...C: 3.94\AA). In contrast, in the related *syn*-[(2,7-dimethyl-*as*-indacenediide){Rh(COD)}₂], the proximity of the olefinic ligand (C...C: 3.47\AA) results in the change of conformation of one COD and in the emergence of intramolecular p-hydrogen bonds between indacenediide and COD ligand^[10].

Image 2: The X-ray structure of complex **22b**.

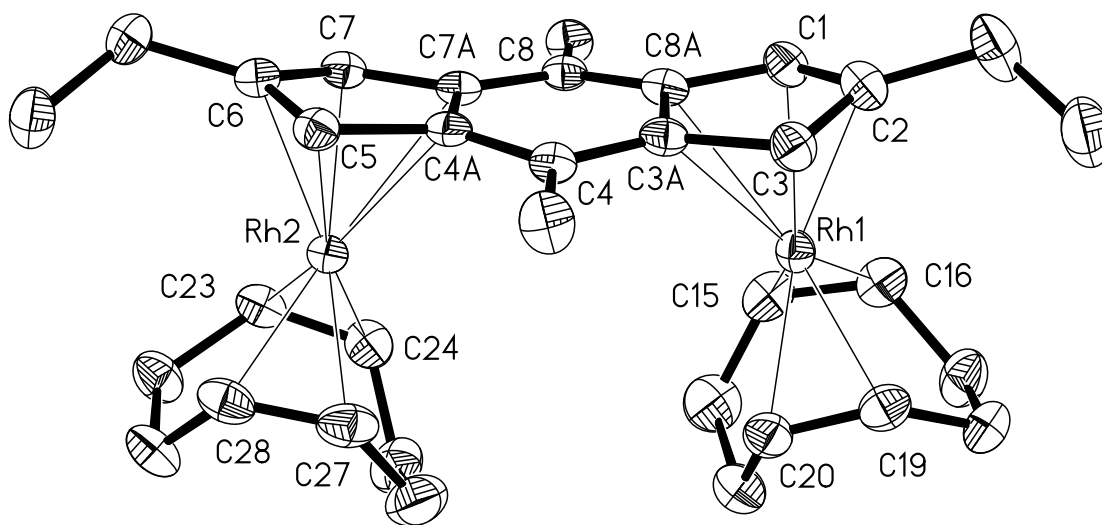


Table 13: Selected distances for compound **22b**:

Rh(1)-C(8a)	2.419(3)	Rh(1)-C(3a)	2.479(3)
Rh(1)-C(3)	2.226(3)	Rh(1)-C(2)	2.218(3)
Rh(1)-C(1)	2.169(3)	Rh(2)-C(4a)	2.407(3)
Rh(2)-C(7a)	2.441(3)	Rh(2)-C(7)	2.202(3)
Rh(2)-C(6)	2.223(3)	Rh(2)-C(5)	2.178(3)
C(3a)-C(8a)	1.448(3)	C(4a)-C(7a)	1.448(3)
C(1)-C(8a)	1.463(4)	C(3)-C(3a)	1.448(3)
C(1)-C(2)	1.426(4)	C(2)-C(3)	1.420(4)
C(4a)-C(5)	1.468(4)	C(5)-C(6)	1.427(4)
C(6)-C(7)	1.423(4)	C(7)-C(7a)	1.448(4)
Rh(1)-C(15)	2.150(3)	Rh(1)-C(16)	2.122(3)
Rh(1)-C(19)	2.114(3)	Rh(1)-C(20)	2.123(3)
Rh(2)-C(23)	2.217(3)	Rh(2)-C(24)	2.130(3)
Rh(2)-C(27)	2.110(3)	Rh(2)-C(28)	2.133(3)
C(15)-C(16)	1.404(4)	C(19)-C(20)	1.407(4)
C(23)-C(24)	1.388(5)	C(27)-C(28)	1.393(4)
$\Delta\text{Rh}_1\text{-C=}$	0.25	$\Delta\text{Rh}_2\text{-C=}$	0.23

$$\Delta\text{Rh}_1\text{-C=} = \frac{\{(Rh-C_{8a})+(Rh-C_{3a})\}}{2} - \frac{\{(Rh-C_1)+(Rh-C_3)\}}{2}$$

$$\Delta\text{Rh}_2\text{-C=} = \frac{\{(Rh-C_{7a})+(Rh-C_{4a})\}}{2} - \frac{\{(Rh-C_5)+(Rh-C_7)\}}{2}$$

3.6.4.3 X-ray Structure of Complex **24a**:

The X-ray structure of this unprecedented heterobinuclear complex clearly shows a different bonding arrangement of both metallic atoms towards *s*-indacene, the values of $\Delta\text{M-C}$ being 0.07 for ruthenium and 0.42 for rhodium.

The ligand loses its aromaticity as evident by a deviation from planarity of the five-membered rings, and also due to a localization of the double bonds. Bonds C4-C4a and C8-C7a are within the range of a localized double bond^[26], much shorter than bonds C4a-C5, C7a-C7, C3a-C4 and C8a-C8. This may prove a lower degree of communication between both metals due to the difference in nature these fragments present, translated on how these bond to the spacer ligand.

The *anti*- isomer may present a similar bonding mode, due to the fact that the chemical shifts for Rh (see Table 9) are very similar, differing only in 36 ppm. This difference could be explained by a bulky moiety such as Cp**Ru* exerts over Rh(COD) when both fragments are bonded to the same side of the spacer ligand.

Image 3: The X-ray structure of complex **24a**.

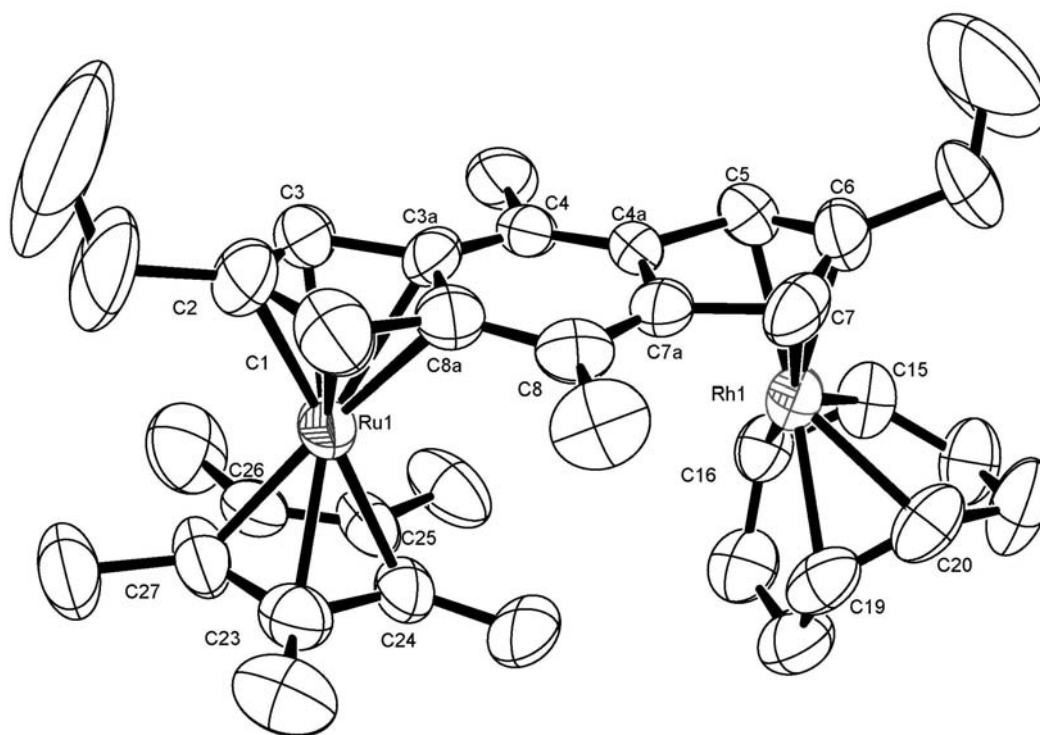


Table 14: Selected distances for compound **24a**:

Indacene

Rh-C8a	2.595(11)	Ru-C4a	2.245(12)
Rh-C3	2.170(12)	Ru-C5	2.189(13)
Rh-C1	2.195(12)	Ru-C6	2.166(12)
Rh-C3a	2.597(11)	Ru-C7	2.167(13)
Rh-C2	2.153(10)	Ru-C7a	2.260(12)
C3a-C8a	1.416(14)	C4a-C7a	1.433(16)
C1-C8a	1.494(14)	C3-C3a	1.485(15)
C1-C2	1.424(17)	C2-C3	1.404(17)
C4a-C5	1.403(16)	C5-C6	1.43(17)
C6-C7	1.396(19)	C7-C7a	1.463(16)
C4-C4a	1.348(19)	C7a-C8	1.347(17)
C3a-C4	1.405(16)	C8-C8a	1.455(15)
Ic Torsion Angle (C2-C8a-C7a-C6)	14.0°		

Ic Torsion Angle 7.5°
(C_{g1}-C_{g3}-C_{g2})

Ciclooctadiene

Rh-C15	2.150(11)	Rh-C16	2.189(11)
Rh-C19	2.151(11)	Rh-C20	2.127(11)
C15-C16	1.387(16)	C19-C20	1.380(17)

Cp*

Ru-C23	2.172(13)	Ru-C24	2.161(12)
Ru-C25	2.136(12)	Ru-C26	2.122(13)
Ru-C27	2.142(11)	Ru-C _{g(Cp*)}	1.775

Others

Rh-C _{g1(Ic)}	2.006	Ru-C _{g2(Ic)}	1.843
ΔRu-C	0.07	ΔRh-C	0.42
Ru-Rh	5.461		

$$\Delta\text{Ru-C} = \frac{\{(Ru-C_{8a}) + (Ru-C_{3a})\}}{2} - \frac{\{(Ru-C_1) + (Ru-C_3)\}}{2}$$

$$\Delta\text{Rh-C} = \frac{\{(Rh-C_{7a}) + (Rh-C_{4a})\}}{2} - \frac{\{(Rh-C_5) + (Rh-C_7)\}}{2}$$

C_{g1}=Centroid at Cp rhodium; C_{g2}= Centroid at Cp ruthenium; C_{g3}= Centroid at benzene ring

3.7 Conclusions

Several mono-, homo- and heterobinuclear complexes have been synthesized and fully characterized with the purpose of assessing their effectiveness in catalytic systems, more particularly, in dehydrogenative silylation of olefins (Chapter 4), as well in determining the degree of their “cooperative effect”, which should be reflected in their reactivity and spectroscopic properties when compared to mononuclear analogues.

ESR and voltammetric studies are complimentary in terms of determining how these molecular systems respond to simple electronic transfers, whether in chemical or electrochemical reactions. These tests provided valuable information indicating that the “cooperative effect” and communication between metallic centers is strongly dependent not only on the ligand, but also on the metallic fragments present.

Comparing X-ray structures of complexes **22b** and **24a**, it becomes evident how -Rh(COD) does have a change in its bonding mode towards *s*-indacene, depending on the secondary metallic fragment. While **22b** is closer to a $\eta^3 + \eta^2$ mode, **24a** is much closer to η^3 . As commented before, a rhodium center bonded to an organic spacer closer to an allylic bond could decrease the degree of delocalization both metallic centers may have, thus a lower communication between the two fragments. Cyclic voltammetry studies support this, as heterobinuclear complexes have lower shifts in their oxidation peaks, indicative of a lower effect a heterofragment may produce.

3.8 Experimental Section:

3.8.1 Synthesis of Iron(II) Bis(Acetylacetonate) 14a^[27]

Iron (II) bis(acetylacetonate) is prepared using iron(II) chloride (20.0 g, 0.156 mol) in 900 mL of ethyl ether with 2,4-pentanedione (32.4 mL, 0.312 mol) in the presence of piperidine (30.1 mL, 0.316 mol). A one liter, two-necked, round-bottomed flask is fitted with a reflux condenser with a nitrogen inlet, a rubber septum, and an efficient stirring bar. The flask is evacuated and filled with nitrogen three times. Ferrous chloride is added and dissolved in diethyl ether, to later add 2,4-Pentanedione and the piperidine to the flask. At this point, the temperature of the reaction must be kept below its boiling point. After completion of the addition, a fine precipitate appears and the mixture has a rusty color. The mixture is stirred for 2 h at room temperature. The mixture is filtered to remove the piperidine hydrochloride, the solid is washed twice with 50 mL portions of diethyl ether and the filtrate, which is dark brownish red, is evaporated to dryness under vacuum to get a dark red solid. Then 60 mL of petroleum ether (40-60°C) is added. The mixture is filtered and washed twice with 15-mL portions of petroleum ether to remove traces of tris(2,4-pentanedionato)iron(III). The brownish-red solid is dried under vacuum to yield approximately 26-28 g of the crude product. It is sublimed at 140°C (10⁻⁴ torr) to yield the product as a brownish-orange crystalline powder. Yield: 23.3 g (58%).

Melting Point (sealed capillary): 169 – 171°C

Mass Spectrum (EI, 70eV) m/z: [M]⁺ = 254 (100%)
[M]⁺ - (acac) = 155 (26%)

FT-IR (Nujol): 1570, 1152 cm⁻¹ (ν C=O)

Analysis Calculated: C₁₀H₁₄FeO₄: C, 47.27; H, 5.55
Found: C, 47.69; H, 5.18

3.8.2 Synthesis of Cobalt(II) Bis(Acetylacetonate) 14b

Analogue to the procedure for **14a**, using 20.1 g (0.156 mol) of anhydrous CoCl_2 , with in 800 mL of ethyl ether with 2,4-pentanedione (32.4 mL, 0.312 mol) in the presence of piperidine (30.1 mL, 0.316 mol). Yield: 24.2 g (61%)

Melting Point (sealed capillary):	170°C(dec)
Mass Spectrum (EI, 70eV) m/z:	$[\text{M}]^+ = 257$ (100%) $[\text{M}]^+ - (\text{acac}) = 158$ (54%)
FT-IR (Nujol):	1598, 1202 cm^{-1} (ν C=O)
Analysis Calculated:	$\text{C}_{10}\text{H}_{14}\text{CoO}_4$: C, 46.71; H, 5.49 Found: C, 47.59; H, 6.03

3.8.3 Synthesis of 1,2,3,4,5-Pentamethylcyclopentadienide-M-(acetyl-acetonato) (M: Fe^{II}: 15a, Co^{II}: 15b)

A solution of Cp^*H (0.37 ml, 2.3 mmol) in 20 mL of THF is cooled to -80°C , and afterwards is added an *n*-BuLi solution (1,6 M in hexanes, 1,48 mL, 2,4 mmol). This mixture is vigorously stirred for one hour and allowed to reach room temperature. The resulting solution is cooled to -80°C once again, and a solution of $\text{Fe}(\text{acac})_2$ (0,603 g, 2,4 mmol) in 20 ml of THF is added, and stirred for two hours at room temperature. The product, $\text{Cp}^*\text{M}(\text{acac})$ (whether M: Fe or Co) is a red-brown paramagnetic solid, highly unstable in air and water.

If $\text{Cp}^*\text{Co}(\text{acac})$ is the desired product, $\text{Co}(\text{acac})_2$ (0.61 g, 2.4 mmol) is used instead of the above mentioned iron compound. $\text{Cp}^*\text{Co}(\text{acac})$ can be isolated and purified by means of sublimation and kept under an inert atmosphere, where it can last indefinitely, whereas $\text{Cp}^*\text{Fe}(\text{acac})$ must be used right after preparation, assuming a quantitative yield. Yield for $\text{Cp}^*\text{Co}(\text{acac})$): 0.9 g (81%)

These two complexes were not further characterized other than mass spectrometry due to the fact these products are not only paramagnetic, but are highly unstable in air and it is

recommended to use them as soon as possible. The procedure in literature methods uses secondary reactions in order to verify the product is truly the desired one^[28].

For **15a**:

Mass Spectrum (EI, 70eV) m/z: $[M]^+ = 290$ (100%)
 $[M]^+ - (\text{acac}) = 191$ (42%)

For **15b**:

Mass Spectrum (EI, 70eV) m/z: $[M]^+ = 293$ (100%)
 $[M]^+ - (\text{acac}) = 194$ (72%)

3.8.4 Synthesis of bis-[1,2,3,4,5-Pentamethylcyclopentadienide-Ruthenium^{III}- μ -(bis-chloro)] **16**

In a two-necked 50 mL round flask fitted with a reflux condenser and a nitrogen inlet and a rubber septum, 5 g (19.11 mmol) of $\text{RuCl}_3 \cdot 3\text{H}_2\text{O}$ is added in 200 mL of absolute methanol, together with 7 mL (6.09 g 44.8 mmol) of Cp^*H . This solution is refluxed for three hours under an inert atmosphere. This solution is later evaporated to 150 mL approximately, forming a black-brownish crystalline solid. This solid is filtered, and washed with methanol, *n*-hexane and ethyl ether. Further characterization of this product may be found in literature methods^[29]. Yield: 4.12g (71%).

Melting Point (sealed capillary): 168-171°C

Mass Spectrum (EI, 70eV) m/z: $[M]^+$ (dimer) = 614 (24%)
 $[M]^+$ (monomer) = 307 (100%)
 $[M]^+$ (monomer) - Cl = 272 (21%)

3.8.5 Synthesis of tetrakis-[1,2,3,4,5-Pentamethylcyclopentadienide-Ruthenium^{II}- μ_3 -(chloro)] **17**^[30,31]

Following literature methods, a $\text{Li}^+[\text{HB}(\text{C}_2\text{H}_5)_3]^-$ solution (1.0M in THF) (26.4 mL, 26.40 mmol) is dropwise added to a 50 mL two necked flask with nitrogen inlet and a septum, containing 4.12 g (13.40 mmol) of $(\text{Cp}^*\text{RuCl}_2)_2$ in 25 ml of dry THF in a strict inert atmosphere. Once the super hydride is injected, the mixture is stirred at room

temperature for 90 minutes. After this, an orange-brownish crystalline solid is formed which is isolated by filtration and washed twice with small amounts of cold THF (5 mL each time). The isolated solid is dried under vacuum. Yield: 2.83 g (81%). This product must be stored under an inert atmosphere at all times, due to its reactivity to air.

Melting Point (sealed capillary):	121°C(dec)
¹H-NMR (C ₆ D ₆ , δ ppm):	1.67 (s, 60H, CH ₃ , Cp)
¹³C-NMR (C ₆ D ₆ , δ ppm):	11.0 (CH ₃ -Cq) 84.6 (CH ₃ -Cq)
Analysis Calculated:	C ₄₀ H ₆₀ Ru ₄ Cl ₄ : C, 44.20; H, 5.56.
	Found: C, 45.91; H, 5.89

3.8.6 Synthesis of [Rh-μ-Cl-(η⁴-1,5-cyclooctadiene)]₂ 18a^[32]

In a two-necked 100 mL round flask fitted with a reflux condenser and a nitrogen inlet and a rubber septum, previously deperoxidized* COD (6.4 mL, 67.2 mmol) is added to a water/ethanol solvent mixture (1:5, 45 mL). Then, 4.0 g (15.2 mmol) of RhCl₃·3H₂O are added. The mixture is refluxed for 8 hours under an inert atmosphere, and the initial red solution slowly gives way to an orange-yellowish precipitate. The resulting mixture is allowed to cool down, and the precipitate filtered. This solid is washed with three portions of 5 mL of a water/ethanol (1:5) solvent mixture and with two portions of 5 mL each of cold hexane, and finally dried under vacuo. This product is stable in air, and readily soluble in dichloromethane, chloroform and acetone, mildly soluble in ethyl ether and benzene and poorly soluble in methanol, ethanol and hexane. It is insoluble in water. Yield: 3.44 g (92%)

*: Removal of possible peroxides in COD is achieved by a simple filtration of COD on neutral alumina. The collected liquid may be stored indefinitely under an inert atmosphere.

Melting Point:	158-162°C
¹H-NMR (C ₆ D ₆ , δ ppm):	1.26-2.10 (m, 8H, CH ₂ , COD) 4.30 (br. s, 4H, CH, COD)
¹³C-NMR (C ₆ D ₆ , δ ppm):	30.91 (CH ₂ , COD)

78.51 (d, $^1J_{C-Rh} = 14.0\text{Hz}$, C=C, COD)

Analysis Calculated:

$C_{16}H_{24}Rh_2Cl_4$: C, 38.97; H, 4.91.

Found: C, 37.94; H, 5.21

3.8.7 Synthesis of $[Rh-\mu-Cl-(\eta^4\text{-bicyclo}[2.2.1]\text{hepta-2,5-diene})]_2$ 18b

Analogue as the previously described method, only that 4.0 g (15.2 mmol) of $RhCl_3 \cdot 3H_2O$ are used, together with 5 mL (49.16 mmol) of NBD.

Melting Point:

142-147°C

1H -NMR (C_6D_6 , δ ppm):

0.62 (t, 2H, CH_2 , $^3J_{H-H} = 1.6\text{Hz}$)

3.14 (br. s, 2H, CH)

3.76 (m, 4H, C=CH)

^{13}C -NMR (C_6D_6 , δ ppm):

49.71 (d, CH, $^1J_{C-Rh} = 7.2\text{Hz}$)

50.27 (d, C=CH, $^1J_{C-Rh} = 11.0\text{Hz}$)

59.93 (d, CH_2 , $^1J_{C-Rh} = 3.0\text{Hz}$)

Analysis Calculated:

$C_{14}H_{16}Rh_2Cl_2$: C, 36.48; H, 3.50.

Found: C, 37.08; H, 4.01

Synthesis of mononuclear complexes

3.8.8 Synthesis of 1,2,3,4,5-Pentamethylcyclopentadienide-Rh(η^4 -1,5-cyclooctadiene) 19a^[33]

In a 100 mL Schlenk tube, **18a** (0.5 g, 1.0 mmol) is added in 30 mL of methanol, together with Cp^*H (0.5 mL, 1.86 mmol) and anhydrous Na_2CO_3 (0.528 mg, 4 mmol). This mixture is refluxed under an inert atmosphere for 2 hours. After 30 mins., the color of the reaction notably changes from orange to light yellow. Later, the mixture is allowed to cool in an ice-bath, where yellow microcrystals of the desired product are formed. A second recrystallization allows the formation of a second batch of $Cp^*Rh(COD)$. Yield: 0.64 g (91%).

Melting Point:

162-163°C

¹H-NMR (CDCl ₃ , δ ppm):	1.78 (s, 15H, CH ₃) 1.89 - 2.15 (m, 8H, CH ₂) 2.92 (bs, 4H, C=CH)
¹³C-NMR (CDCl ₃ , δ ppm):	9.5 (CH ₃ -Cq) 32.7 (CH ₂) 70.2 (d, C=CH, ¹ J _{C-Rh} = 14.2 Hz) 96.2 (d, CH ₃ -Cq, ¹ J _{C-Rh} = 4.2 Hz)
¹⁰³Rh-NMR (CDCl ₃ , δ ppm):	-789
Mass Spectrum (EI, 70eV) m/z:	[M] ⁺ = 346 (100%) [M] ⁺ - COD = 238 (63%) [Cp*] ⁺ = 135 (12%)
Analysis Calculated:	C ₁₈ H ₂₇ Rh: C, 62.43; H, 7.86. Found: C, 63.02; H, 7.96

3.8.9 Synthesis of 1,2,3,4,5-Pentamethylcyclopentadienide-Rhodium-(bicyclo[2.2.1]hepta-2,5-diene) **19b** ^[34]

In a 100 mL Schlenk tube under inert atmosphere conditions, Cp*H (0.5 mL, 1.86 mmol) is added in 20 mL of THF, followed by a dropwise addition of *n*-BuLi (1.2 mL, 1.9 mmol, 1.6M in hexanes) at -80°C. The mixture is allowed to reach room temperature and later vigorously stirred for one hour. The solution is cooled once again to -80°C and **18b** (0.43 g, 0.93 mmol) is added and allowed to reach room temperature and stirred for one hour. After this, all solvent is removed under vacuum and 20 mL of pentane is added, and the mixture is filtered to remove the insoluble LiCl, and all pentane is removed under vacuum. The remaining yellow-orange powder is completely stable in air and moisture. Yield: 0.59 g (96%).

Melting Point:	120-128°C (dec.)
¹H-NMR (CDCl ₃ , δ ppm):	0.84 (t, 2H, CH ₂ , ³ J _{H-H} = 1.6 Hz) 1.89 (s, 15H, CH ₃) 2.41 (d.d, 4H, C=CH, ³ J _{H-H} = 2.2 Hz, ² J _{H-Rh} = 2.6 Hz) 3.31 (m, 2H, CH)

$^{13}\text{C-NMR}$ (CDCl_3 , δ ppm):	10.34 ($\text{CH}_3\text{-Cq}$) 32.96 (d, $\text{C}=\text{CH}$, $^1\text{J}_{\text{C-Rh}} = 10.4$ Hz) 47.01 (d, CH , $^1\text{J}_{\text{C-Rh}} = 2.6$ Hz) 55.41 (d, CH_2 , $^1\text{J}_{\text{C-Rh}} = 6.7$ Hz) 94.96 (d, $\text{CH}_3\text{-Cq}$, $^1\text{J}_{\text{C-Rh}} = 4.9$ Hz)
$^{103}\text{Rh-NMR}$ (CDCl_3 , δ ppm):	-786
Mass Spectrum (EI, 70eV) m/z:	$[\text{M}]^+ = 330$ (100%) $[\text{M}]^+ - \text{NBD} = 238$ (52%) $[\text{Cp}^*]^+ = 135$ (8%)
Analysis Calculated:	$\text{C}_{17}\text{H}_{23}\text{Rh}$: C, 61.82; H, 7.02. Found: C, 62.38; H, 6.89

3.8.10 Synthesis of Indenyl-Rh(η^4 -1,5-cyclooctadiene) **20a** ^[35]

In a 100 mL round flask provided with a nitrogen inlet, indene (0.35 mL, 3.0 mmol) is added in 20 mL of THF. Later, the solution is cooled to -80°C , and *n*-BuLi is added (1.9 mL, 1.6M in hexane, 3.0 mmol), and the whole mixture is allowed to reach room temperature. After one hour at room temperature, the solution is once again cooled to -80°C and **18a** is added (0.75 g, 1.5 mmol). Then, the solution is allowed to reach room temperature, and the solvent is removed by vacuum, and the remaining solid is washed with pentane to filter the insoluble LiCl, thus forming the desired product. Yield: 0.92g (94%)

Melting Point:	142-144 $^\circ\text{C}$
$^1\text{H-NMR}$ (CDCl_3 , δ ppm):	1.65-1.88 (m, 8H, CH_2) 3.99 (bs, 4H, $\text{C}=\text{CH}$) 4.90 (d, 2H ($\text{H}_{1,3}$), $^3\text{J}_{\text{H-H}} = 2.8$ Hz) 5.92 (d.t, 1H (H_2), $^3\text{J}_{\text{H-H}} = 2.8$ Hz, $^2\text{J}_{\text{H-Rh}} = 2.0$ Hz) 7.07 (m, 2H ($\text{H}_{4,7}$)) 7.13 (m, 2H ($\text{H}_{5,6}$))
$^{13}\text{C-NMR}$ (CDCl_3 , δ ppm):	31.4 (CH_2) 67.4 (d, $\text{C}=\text{CH}$, $^1\text{J}_{\text{C-Rh}} = 13.6$ Hz)

	76.3 (d, C _{1,3} , ¹ J _{C-Rh} = 4.4 Hz)
	92.4 (d, C ₂ , ¹ J _{C-Rh} = 5.2 Hz)
	113.2 (C _{3a,7a})
	119.4 (C _{5,6})
	122.7 (C _{4,7})
¹⁰³ Rh-NMR (CDCl ₃ , δ ppm):	-486
Mass Spectrum (EI, 70eV) m/z:	[M] ⁺ = 326 (100%) [M] ⁺ - COD = 218 (44%)
Analysis Calculated:	C ₁₈ H ₂₆ Rh: C, 62.78; H, 5.58 Found: C, 63.02; H, 6.01

3.8.11 Synthesis of Indenyl-Rhodium(bicyclo[2.2.1]hepta-2,5-diene) **20b** ^[36]

In a 100 mL round flask provided with a nitrogen inlet, indene (0.35 mL, 3.0 mmol) is added in 20 mL of THF. Later, the solution is cooled to -80°C, and *n*-BuLi is added (1.9 mL, 1.6M in hexane, 3.0 mmol), and the whole mixture is allowed to reach room temperature. After one hour at room temperature, the solution is once again cooled to -80°C and **18b** is added (0.69 g, 1.5 mmol). The solution is then allowed to reach room temperature, and the solvent is removed by vacuum, the remaining solid is washed with pentane to filter the insoluble LiCl, thus forming the desired product. Yield: 0.85g (90%)

Melting Point:	130-133°C(dec.)
¹ H-NMR (CDCl ₃ , δ ppm):	0.92 (t, 2H, CH ₂ , ³ J _{H-H} = 1.4 Hz) 2.56 (d.d, 4H, C=CH, ³ J _{H-H} = 1.6 Hz, ² J _{H-Rh} = 2.0 Hz) 3.73 (m, 2H, CH) 4.95 (d, 2H (H _{1,3}), ³ J _{H-H} = 3.0 Hz) 6.02 (d.t, 1H (H ₂), ³ J _{H-H} = 3.0 Hz, ² J _{H-Rh} = 2.2 Hz) 7.02 (m, 2H (H _{4,7})) 7.15 (m, 2H (H _{5,6}))
¹³ C-NMR (CDCl ₃ , δ ppm):	37.47 (d, C=CH, ¹ J _{C-Rh} = 10.4 Hz) 47.41 (d, CH, ¹ J _{C-Rh} = 2.6 Hz) 59.61 (d, CH ₂ , ¹ J _{C-Rh} = 6.7 Hz)

	74.4 (d, C _{1,3} , ¹ J _{C-Rh} = 5.5 Hz)
	91.6 (d, C ₂ , ¹ J _{C-Rh} = 6.0 Hz)
	110.0 (C _{3a,7a} , ¹ J _{C-Rh} = 1.4 Hz)
	120.1 (C _{5,6})
	121.6 (C _{4,7})
¹⁰³ Rh-NMR (CDCl ₃ , δ ppm):	-521
Mass Spectrum (EI, 70eV) m/z:	[M] ⁺ = 309 (100%)
	[M] ⁺ - NBD = 218 (38%)
Analysis Calculated:	C ₁₈ H ₂₆ Rh: C, 62.15; H, 4.56
	Found: C, 63.18; H, 5.56

3.8.12 Synthesis of Indenyl-Rhodium-(biscarbonyl) **20c**

Similar to as described in the literature^[17], in a 50 mL flask fitted with a gas inlet, **20a** (0.60 g, 1.85 mmol) is added in 10 mL of toluene. The gas inlet is opened to allow CO to gently bubble through the solution. In no more than 1 minute, the initially yellow solution turns dark brown, and the bubbling is allowed to proceed for another 2 minutes. After this, the solution is dried under vacuo, and the remaining brown solid corresponds to **20c**, as compared to literature methods. Yield: 0.51 g (97%). A similar reactivity and yield was found while using **20b** (0.57g, 1.85 mmol). Yield: 0.49 (95%).

Melting Point:	110-112°C(dec)
¹ H-NMR (CDCl ₃ , δ ppm):	5.81 (d, 2H, H _{1,3} , ³ J _{H-H} = 2.9 Hz)
	6.10 (d.t, 1H, H ₂ , ³ J _{H-H} = 2.9 Hz, ² J _{H-Rh} = 2.7 Hz)
	7.15 (m, 2H, H _{4,7})
	7.30 (m, 2H, H _{5,6})
¹³ C-NMR (CDCl ₃ , δ ppm):	75.4 (d, C _{1,3} , ¹ J _{C-Rh} = 3.5 Hz)
	97.7 (d, C ₂ , ¹ J _{C-Rh} = 6.1 Hz)
	117.6 (C _{3a,7a} , ¹ J _{C-Rh} = 1.6 Hz)
	118.8 (C _{5,6})
	125.1 (C _{4,7})
	190.1 (CO)

$^{103}\text{Rh-NMR}$ (CDCl_3 , δ ppm):	-1038
FT-IR (KBr):	2038, 1980 cm^{-1} , (ν C=O)
Mass Spectrum (EI, 70eV) m/z:	$[\text{M}]^+ = 274$ (100%) $[\text{M}]^+ - \text{CO} = 246$ (76%) $[\text{M}]^+ - 2\text{CO} = 218$ (24%)
Analysis Calculated:	$\text{C}_{11}\text{H}_7\text{O}_2\text{Rh}$: C, 48.20; H, 2.57; O, 11.68 Found: C, 49.70; H, 2.18; O, 12.32

3.8.13 Synthesis of 1,2,3,4,5-Pentamethylcyclopentadienide-Iron(II)- η^5 -(2,6-diethyl-4,8-dimethyl-s-indacenide) **21a**:

A *n*-BuLi solution (1.3 mL, 1.6M in hexanes, 2.09 mmol) is slowly added to a ligand **8b** (0.5 g, 2.09 mmol) solution in 20 mL of THF at -80°C . The mixture is stirred for two hours at room temperature, yielding the monolithiated ligand. The latter solution is cooled to -80°C and dropwise is added a freshly prepared solution of **15a** (0.6 g, 2.09 mmol). This mixture is allowed to reach room temperature and stirred for two hours. Then, all solvent is removed, and the raw product is washed with pentane and filtered to remove the insoluble Li(acac). Bright red colored crystals unstable in air were obtained. Yield: 0.79g (89%)

Melting Point (sealed capillary):	172-174 $^\circ\text{C}$ (dec)
$^1\text{H-NMR}$ (CDCl_3 , δ ppm):	1.08 (t, 3H, $\text{C}_2\text{-CH}_2\text{-CH}_3$, $^3\text{J}_{\text{H-H}} = 7.4$ Hz) 1.10 (t, 3H, $\text{C}_6\text{-CH}_2\text{-CH}_3$, $^3\text{J}_{\text{H-H}} = 7.4$ Hz) 1.54 (s, 15H, $\text{CH}_3\text{-Cp}$) 2.19 (s, 3H, $\text{CH}_3\text{-C}_8$) 2.22 (q, 2H, $\text{C}_2\text{-CH}_2\text{-CH}_3$, $^3\text{J}_{\text{H-H}} = 7.4$ Hz) 2.27 (q, 2H, $\text{C}_6\text{-CH}_2\text{-CH}_3$, $^3\text{J}_{\text{H-H}} = 7.4$ Hz) 2.32 (s, 3H, $\text{CH}_3\text{-C}_4$) 3.04 (bs, 2H, $\text{C}_7\text{-H}_2$) 4.02 (bs, 2H, $\text{C}_{1,3}\text{-H}$) 6.60 (s, 1H, $\text{C}_5\text{-H}$)
$^{13}\text{C-NMR}$ (C_6D_6 , δ ppm):	9.69 ($\text{CH}_3\text{-Cp}$) 12.70 ($\text{C}_6\text{-CH}_2\text{-CH}_3$)

15.43 (CH_3-C_4)
15.68 (CH_3-C_8)
16.46 ($C_2-CH_2-CH_3$)
22.03 ($C_2-CH_2-CH_3$)
24.81 ($C_6-CH_2-CH_3$)
38.84 (C_7)
62.90, 62.91 ($C_{1,3}$)
77.24 (CH_3-Cp)
88.40 (C_{8a})
90.48 (C_{3a})
92.70 (C_2)
119.60 (C_4)
124.19 (C_5)
125.39 (C_{7a})
135.20 (C_6)
139.36 (C_{4a})
143.52 (C_8)

Mass Spectrum (EI, 70eV) m/z: $[M]^+ = 428$ (100%)
 $[M]^+ - Cp^* = 293$ (26.9%)
 $[Cp^*FeH]^+ = 192$ (44.2%)

Analysis Calculated: $C_{28}H_{36}Fe$: C: 78.53; H: 8.41
Found: C: 78.32; H: 8.56

3.8.14 Synthesis of 1,2,3,4,5-Pentamethylcyclopentadienide-Ruthenium(II)- η^5 -(2,6-diethyl-4,8-dimethyl-*s*-indacenide) **21b**:

A solution of *n*-butyllithium (1.6M in hexane, 2.54 mL, 4.06 mmol) was slowly added to a $-78^\circ C$ cooled solution of the ligand **8b** (0.95g, 4.0 mmol) in 30 mL of THF. The mixture is stirred for two hours at room temperature, yielding the monolithiated anionic ligand. In a second flask with a side exit, 1.08g (1mmol) of **17** is dissolved in 30 mL of THF. This latter solution is dropwise added to the former. This resulting mixture is stirred for 2 hours at room temperature. Then all solvent is removed, and the raw product

is washed with pentane, and filtered to eliminate the insoluble LiCl. A yellow-greenish crystalline solid unstable in air (1.82g, 3.84 mmol) was obtained, with a 97% yield.

Melting Point (sealed capillary): 176-179°C(dec)

¹H-NMR (CDCl₃, δ ppm):

- 1.11 (t, 3H, C₂-CH₂-CH₃, ³J_{H-H} = 7.4 Hz)
- 1.18 (t, 3H, C₆-CH₂-CH₃, ³J_{H-H} = 7.4 Hz)
- 1.59 (s, 15H, CH₃-Cp)
- 2.14 (s, 3H, CH₃-C₈)
- 2.27 (s, 3H, CH₃-C₄)
- 2.37 (q, 2H, C₂-CH₂-CH₃, ³J_{H-H} = 7.4 Hz)
- 2.41 (q, 2H, C₆-CH₂-CH₃, ³J_{H-H} = 7.4 Hz)
- 3.04 (br. s, 2H, C₇-H₂)
- 4.67 (br. s, 2H, C_{1,3}-H)
- 6.24 (s, 1H, C₅-H)

¹³C-NMR (C₆D₆, δ ppm):

- 10.80 (CH₃-Cp)
- 13.13 (C₂-CH₂-CH₃)
- 14.94 (CH₃-C₈)
- 15.18 (C₆-CH₂-CH₃)
- 15.34 (CH₃-C₄)
- 22.59 (C₆-CH₂-CH₃)
- 25.14 (C₂-CH₂-CH₃)
- 39.09 (C₇)
- 66.59 (C₁)
- 66.91 (C₃)
- 82.21 (CH₃-Cp)
- 93.47 (C_{8a})
- 95.06 (C_{3a})
- 96.00 (C₂)
- 119.78 (C₄)
- 123.52 (C₈)
- 124.38 (C₅)
- 134.13 (C_{7a})

138.27 (C_{4a})

148.82 (C₆)

Mass Spectrum (EI, 70eV) m/z: [M]⁺ = 474 (100%)
[M]⁺ - Cp* = 339 (31.0%)
[Cp**RuH*]⁺ = 238 (58.7%)

Analysis Calculated: C₂₈H₃₆Ru: C: 71.00; H: 7.66
Found: C: 71.77; H: 8.02

3.8.15 Synthesis of 1,2,3,4,5-Pentamethylcyclopentadienide-Cobalt(II)-(2,6-diethyl-4,8-dimethyl-*s*-indacenide) **21c**:

A *n*-BuLi solution (1.3 mL, 1.6M in hexanes, 2.09 mmol) is slowly added to a ligand **8b** (0.5 g, 2.09 mmol) solution in 20 mL of THF at -80°C. The mixture is stirred for two hours at room temperature, yielding the monolithiated ligand. The latter solution is cooled to -80°C and dropwise is added a solution of **15b** (0.14 g, 2.09 mmoles) in 30 mL of THF. This mixture is allowed to reach room temperature and stirred for two hours. Then all solvent is removed, and the raw product is washed with pentane and filtered to remove the insoluble Li(acac). A brownish dust unstable in air is obtained. Yield: 0.79g (89%). Given that this is a paramagnetic compound, only Mass spectrometry and elemental analysis were carried out.

Melting Point (sealed capillary): 149-155°C(dec)

Mass Spectrum (EI, 70eV) m/z: [M]⁺ = 431 (32%)
Cp*Co- = 339 (100%)

Analysis Calculated: C₂₈H₃₆Co: C: 77.93; H: 8.41
Found: C: 76.13; H: 9.06

3.8.16 Synthesis of 2,6-diethyl-4,8-dimethyl-*s*-indacenide-Rhodium(I)-(η⁴-1,5-cyclooctadiene) **21d**^[37]

A solution of *n*-BuLi (2.52 mmol, 1.6M in hexanes) is added to a solution of **8b** (0.60 g, 2.52 mmol) in THF (25 mL) at -80°C. The solution is allowed to reach room temperature and stirred for 1.5 hours. Then, the resulting mixture is cooled to -80°C and a solution of **18a** (0.62 g, 1.26 mmol) in THF (20 mL) is added via syringe. The temperature is afterwards raised to room temperature, and the mixture stirred for 2 hours. The solvents are then removed under reduced pressure. To the remaining solid, pentane is added (10 mL) and the insoluble lithium chloride was removed by filtration. The solution is concentrated affording a yellow solid. Yield: 1.1 g (95%)

Melting Point (sealed capillary): 172-179°C

¹H-NMR (C₆D₆, δ ppm):

- 1.08 (t, 3H, C₂-CH₂-CH₃, ³J_{H-H} = 7.5 Hz)
- 1.38 (t, 3H, C₆-CH₂-CH₃, ³J_{H-H} = 7.5 Hz)
- 1.73-1.88 (m, 8H, CH₂, COD)
- 2.21 (s, 3H, CH₃-C₈)
- 2.28 (q, 2H, C₂-CH₂-CH₃, ³J_{H-H} = 7.5 Hz)
- 2.34 (s, 3H, CH₃-C₄)
- 2.59 (q, 2H, C₆-CH₂-CH₃, ³J_{H-H} = 7.5 Hz)
- 2.99 (br. s, 2H, C₇-H₂)
- 4.10 (br. s, 4H, C=CH-COD)
- 4.98 and 5.00 (d, 2H, C_{1,3}-H, ⁴J_{Rh-H} = 1.6 Hz)
- 6.67 (s, 1H, C₅-H)

¹³C-NMR (C₆D₆, δ ppm):

- 13.92 (C₆-CH₂-CH₃)
- 15.32 (CH₃-C₄)
- 15.51 (CH₃-C₈)
- 16.00 (C₂-CH₂-CH₃)
- 23.09 (C₂-CH₂-CH₃)
- 25.00 (C₆-CH₂-CH₃)
- 31.12, 31.67 (CH₂-COD)
- 39.61 (C₇)

66.38 and 66.63 (d, C=CH-COD, $^1J_{C-Rh} = 13.7$ Hz)

75.33 and 75.62 (d, C_{1,3}, $^1J_{C-Rh} = 4.3$ Hz)

110.86 and 113.10 (d, C_{3a,8a}, $^1J_{C-Rh} = 2.5$ Hz)

114.93 (d, C₂, $^1J_{C-Rh} = 5.0$ Hz)

115.37 (C_{4a})

119.56 (C_{7a})

124.84 (C₅)

136.23 (C₈)

139.57 (C₄)

149.12 (C₆)

$^{103}\text{Rh-NMR}$ (C₆D₆, δ ppm): -486

Mass Spectrum (EI, 70eV) m/z: [M]⁺ = 448 (100%)
[M]⁺ - Rh(COD) = 237 (48%)
[Rh(COD)]⁺ = 211 (24%)

Analysis Calculated: C₂₆H₃₃Rh: C: 69.59; H: 7.40
Found: C: 69.64; H: 7.37

3.8.17 Synthesis of 1,2,3,4,5-Pentamethylcyclopentadienide-Cobalt(III)-(2,6-diethyl-4,8-dimethyl-s-indacenide) tetrafluoroborate [21c]⁺[BF₄⁻]:

In a 50 mL round flask, provided with a nitrogen inlet, the cobalt complex **21b** (0.30 g, 0.69 mmol) is mixed with ferrocenium tetrafluoroborate (0.15g, 0.55 mmol). Later, to this flask, 30 mL of THF are added, to allow the solids to dissolve and react with vigorous stirring. After one hour, all THF is evaporated and the remaining solid is washed with 30 mL of pentane, leaving an insoluble brownish product. Yield: 0.26 g (92%, referred to ferrocenium tetrafluoroborate)

Melting Point (sealed capillary): 184-187°C(dec)

$^1\text{H-NMR}$ (CD₃CN, δ ppm): 1.15 (t, 3H, C₂-CH₂-CH₃, $^3J_{H-H} = 6.7$ Hz)
1.26 (t, 3H, C₆-CH₂-CH₃, $^3J_{H-H} = 7.0$ Hz)
1.58 (s, 15H, CH₃-Cp)
2.34 (s, 3H, CH₃-C₈)

2.39 (s, 3H, CH_3-C_4)
2.28 (q, 2H, $C_2-CH_2-CH_3$, $^3J_{H-H} = 6.7$ Hz)
2.52 (q, 2H, $C_6-CH_2-CH_3$, $^3J_{H-H} = 7.0$ Hz)
3.40 (br.s, 2H, C_7-H_2)
5.46 (br.s, 2H, $C_{1,3}-H$)
6.74 (s, 1H, C_5-H)

^{13}C -NMR (CD_3CN , δ ppm):

8.75 (CH_3-Cp)
12.70 ($C_6-CH_2-CH_3$)
15.08 (CH_3-C_4)
15.31 (CH_3-C_8)
15.69 ($C_2-CH_2-CH_3$)
20.43 ($C_2-CH_2-CH_3$)
25.36 ($C_6-CH_2-CH_3$)
40.09 (C_7)
75.11 (C_1)
75.20 (C_3)
95.23 (CH_3-Cp)
106.20 (C_2)
117.45 (C_4)
123.95 (C_{8a})
124.14 (C_{3a})
144.62 (C_{7a})
145.38 (C_5)
148.39 (C_8)
148.54 (C_{4a})
157.90 (C_6)

Mass Spectrum (EI, 70eV) m/z:

$[M]^+ - BF_4^- = 431$ (100%)
 $[M]^+ - (Cp^*Co) - BF_4^- = 339$ (41%)
 $[BF_4]^- = 87$ (16%)

Synthesis of homo- and heterobinuclear complexes

3.8.18 Bis-(1,2,3,4,5-pentamethylcyclopentadienyl-ruthenium(II))- μ -s-indacenediide **22a**:

A solution of *n*-BuLi (3.68 mL, 5.88 mmol) in hexane (1.6 M) is added to a solution of **8b** (0.70 g, 2.94 mmol) in THF (25 mL) at -80°C. The reaction mixture is allowed to reach room temperature and stirred for 1.5 hours, followed by stirring at 50°C for another 2 hours. The solution was cooled to -80°C and **17** (1.60 g, 1.47 mmol) in THF (30 mL) was slowly added via syringe. The mixture was allowed to reach room temperature and stirred for 2 hours. The solvents were evaporated under reduced pressure. To the remaining solid, 15 mL of toluene was added and the insoluble lithium chloride is removed by filtration. (Yield: 1.84 g, 88%).

Melting Point (sealed capillary): 216-217°C(dec)

¹H-NMR (CDCl₃, δ ppm):
1.03 (t, 6H, C_{2,6}-CH₂-CH₃, ³J_{H-H} = 7.4 Hz)
1.52 (s, 30H, CH₃-Cp)
2.25 (q, 4H, C₆-CH₂-CH₃, ³J_{H-H} = 7.4 Hz)
2.38 (s, 6H, CH₃-C_{4,8})
4.93 (bs, 4H, C_{1,3,5,7}-H)

¹³C-NMR (C₆D₆, δ ppm):
11.43 (CH₃-Cp)
15.97 (CH₃-C_{4,8})
15.99 (C_{2,6}-CH₂-CH₃)
17.32 (C_{2,6}-CH₂-CH₃)
68.59 (C_{1,3,5,7})
82.92 (CH₃-Cp)
99.09(C_{3a,4a,7a,8a})
101.26 (C_{2,6})
116.79 (C_{4,8})

Mass Spectrum (EI, 70eV) m/z: [M]⁺ = 710 (100%)
[M]⁺ - Cp*Ru = 473 (51.8%)

Analysis Calculated: C₃₈H₅₀Ru₂: C: 64.38; H: 6.73
Found: C: 64.09; H: 6.58

3.8.19 [(2,6-diethyl-4,8-dimethyl-*s*-indacenediide)-bis-(Rhodium(I)(1,5-cyclooctadiene)) **22b** and **22c**

3.8.19.1 Step by Step

Stepwise synthesis: A solution of *n*-BuLi (0.49 mmol) in hexane (1.6 M) was added to a solution of **8b** (0.22 g, 0.49 mmol) in THF (15 mL) at -80°C. The temperature was raised to room temperature and the mixture was stirred for 1.5 hours. The solution was cooled to -80°C and a solution of **18a** (0.12 g, 0.25 mmol) in THF (10 mL) was added. After stirring for 2 hours, the solvents were removed under reduced pressure. To the remaining solid, 15 mL of toluene was added and the insoluble lithium chloride is removed by filtration. The solution was concentrated giving an orange solid made up of an *anti/syn* isomer mixture in a 1:2 ratio, respectively. (Yield: 0.21 g, 65%).

3.8.19.2 Direct Synthesis

A solution of *n*-BuLi (5.88 mmol) in hexane (1.6 M) was added to a solution of **8b** (0.70 g, 2.94 mmol) in THF (25 mL) at -80°C. The reaction mixture was allowed to reach room temperature and stirred for 1.5 hours, followed by stirring at 50°C for another 2 hours. The solution was cooled to -80°C and **18a** (1.44 g, 2.94 mmol) in THF (30 mL) was slowly added via syringe. The mixture was allowed to reach room temperature and stirred for 2 hours. The solvents were evaporated under reduced pressure. To the remaining solid, 15 mL of toluene was added and the insoluble lithium chloride was removed by filtration. This solution was concentrated, giving an orange solid consisting of an *anti/syn* isomer mixture in a 1:2 ratio (Yield: 1.20 g, 62%). Fractional precipitation using benzene as solvent allowed us to separate these isomers: the *syn* form **22b** precipitates (Yield: 0.72 g, 37% – related to *s*-indacene) giving suitable crystals for X-ray study whereas the *anti* form remains in the benzenic solution (Yield: 0.43 g, 22% related to *s*-indacene).

Syn isomer 22b:

Melting Point (sealed capillary):	208-213°C
¹H-NMR (CDCl ₃ , δ ppm):	1.31 (t, 6H, C _{2,6} -CH ₂ -CH ₃ , ³ J _{H-H} = 7.5 Hz) 1.69-2.10 (m, 16H, CH ₂ , COD) 2.20 (s, 6H, CH ₃ -C _{4,8}) 2.56 (q.d, 4H, C _{2,6} -CH ₂ -CH ₃ , ³ J _{H-H} = 7.5 Hz, ³ J _{H-Rh} = 1.5 Hz) 4.33 (br. s, 8H, C=CH, COD) 4.93 (br. s, 4H, C _{1,3,5,7} -H)
¹³C-NMR (C ₆ D ₆ , δ ppm):	15.08 (CH ₃ -C _{4,8}) 15.22 (C _{2,6} -CH ₂ -CH ₃) 23.78 (C _{2,6} -CH ₂ -CH ₃) 32.19 (CH ₂ -COD) 68.33 (d, C=C, COD, ¹ J _{C-Rh} = 13.0 Hz) 73.69 (d, C _{1,3,5,7} , ¹ J _{C-Rh} = 5.0 Hz) 112.13 (C _{4,8}) 115.92 (d, C _{3a,4a,7a,8a} , ¹ J _{C-Rh} = 1.2 Hz) 117.18 (d, C _{2,6} , ¹ J _{C-Rh} = 6.0 Hz)
¹⁰³Rh-NMR (C ₆ D ₆ , δ ppm):	-261
Mass Spectrum (EI, 70eV) m/z:	[M] ⁺ = 658 (100%) [M] ⁺ - Rh(COD)H = 447 (65.8%)
Analysis Calculated:	C ₃₄ H ₄₄ Rh ₂ : C: 61.98; H: 6.73 Found: C: 62.01; H: 6.69

Anti isomer 22c:

Melting Point (sealed capillary):	196-203°C
¹H-NMR (CDCl ₃ , δ ppm):	1.31 (t, 6H, C _{2,6} -CH ₂ -CH ₃ , ³ J _{H-H} = 7.5 Hz) 1.68-1.78 (m, 16H, CH ₂ , COD) 2.29 (s, 6H, CH ₃ -C _{4,8}) 2.52 (qd, 4H, C _{2,6} -CH ₂ -CH ₃ , ³ J _{H-H} = 7.5 Hz, ³ J _{H-Rh} = 1.4 Hz)

	4.16 (br. s, 8H, C=CH-COD)
	5.00 (br. s, 4H, C _{1,3,5,7} -H)
¹³ C-NMR (C ₆ D ₆ , δ ppm):	15.21 (C _{2,6} -CH ₂ -CH ₃)
	15.59 (CH ₃ -C _{4,8})
	23.55 (C _{2,6} -CH ₂ -CH ₃)
	32.12 (CH ₂ , COD)
	68.56 (d, C=C, COD, ¹ J _{C-Rh} = 13.0 Hz)
	73.75 (d, C _{1,3,5,7} , ¹ J _{C-Rh} = 5.0 Hz)
	110.94 (C _{4,8})
	114.28 (d, C _{3a,4a,7a,8a} , ¹ J _{C-Rh} = 1.6 Hz)
	117.50 (d, C _{2,6} , ¹ J _{C-Rh} = 6.0 Hz)
¹⁰³ Rh-NMR (C ₆ D ₆ , δ ppm):	-334
Mass Spectrum (EI, 70eV) m/z:	[M] ⁺ = 658 (100%)
	[M] ⁺ - Rh(COD)H = 447 (44.4%)
Analysis Calculated:	C ₃₄ H ₄₄ Rh ₂ : C: 61.98; H: 6.73
	Found: C: 62.08; H: 6.72

3.8.20 *anti*-(1,2,3,4,5-Pentamethylcyclopentadienide)-Iron(II)-2,6-diethyl-4,8-dimethyl-*s*-indacendiide-Rhodium(I)-(1,5-cyclooctadiene) **23a**:

A *n*-BuLi solution (1.1 mL, 1.6M in hexanes, 1.7 mmol) is dropwise added to a solution of **21a** (0.7g, 1.63 mmoles) in 30 mL of THF at -80°C. The resulting mixture is vigorously stirred for one hour at room temperature. A solution of **18a** (0.40 g, 0.81 mmoles) in 20 mL of THF is then added to the mixture. All solvent is removed, and the resulting product is washed with pentane and filtered to remove the insoluble LiCl. A black-greenish dust unstable in air (0.89g, 1.39 mmoles) was obtained. Yield: 0.89 g (86%)

Melting Point (sealed capillary):	232-236°C(dec)
¹ H-NMR (CDCl ₃ , δ ppm):	1.03 (t, 3H, C ₂ -CH ₂ -CH ₃ , ³ J _{H-H} = 7.5 Hz)
	1.32 (t, 3H, C ₆ -CH ₂ -CH ₃ , ³ J _{H-H} = 7.5 Hz)
	1.69 (br. s, 8H, CH ₂ , COD)

	1.53 (s, 15H, CH_3 -Cp)
	2.25 (q, 2H, C_2 - CH_2 - CH_3 , $^3J_{H-H} = 7.5$ Hz)
	2.38 (s, 6H, CH_3 - $C_{4,8}$)
	2.53 (qd, 2H, C_6 - CH_2 - CH_3 , $^3J_{H-H} = 7.5$ Hz, $^3J_{H-Rh} = 1.6$ Hz)
	4.32 (s, 4H, C= CH , COD)
	4.20 (s, 2H, $C_{1,3}$ -H)
	5.04 (s, 2H, $C_{5,7}$ -H)
^{13}C -NMR (C_6D_6 , δ ppm):	10.15 (CH_3 -Cp)
	16.24 (CH_3 - $C_{4,8}$)
	14.85(C_6 - CH_2 - CH_3)
	16.55 (C_2 - CH_2 - CH_3)
	22.55 (C_2 - CH_2 - CH_3)
	24.05 (C_6 - CH_2 - CH_3)
	31.88 (CH_2 , COD)
	61.54 ($C_{1,3}$)
	70.60 (d, C=C, COD, $^1J_{C-Rh} = 13.0$ Hz)
	71.81 (d, $C_{5,7}$, $^1J_{C-Rh} = 4.9$ Hz)
	77.01 (CH_3 -Cp)
	92.34 (C_2)
	92.98 ($C_{4,8}$)
	117.62 ($C_{3a,8a}$)
	117.84 (d, $C_{4a,7a}$, $^1J_{C-Rh} = 1.3$ Hz)
	121.03 (d, C_6 , $^1J_{C-Rh} = 6.7$ Hz)
^{103}Rh -NMR (C_6D_6 , δ ppm):	-275
Mass Spectrum (EI, 70eV) m/z:	$[M]^+ = 638$ (62.5%)
	$[M]^+ - Rh(COD)H = 428$ (100.0%)
	$[Rh(COD)]^+ = 211$ (37.5%)
	$[(COD)]^+ = 108$ (10.4%)
Analysis Calculated:	$C_{36}H_{47}FeRh$: C: 67.72; H: 7.42
	Found: C: 67.61; H: 7.56

3.8.21 anti-(1,2,3,4,5-Pentamethylcyclopentadienide)-Ruthenium(II)-2,6-diethyl-4,8-dimethyl-s-indacendiide-Rhodium(I)-(η⁴-1,5-cyclooctadiene) 23b:

Analogue for the procedure in **23a**, using instead a solution of *n*-BuLi (1.6M in hexanes, 1.2 mL, 1.92 mmol), a solution of **21b** (0.85g, 1.79 mmol) in 30 mL of THF, and **18a** (0.44 g, 0.89 mmol) in 20 mL of THF. A black dust very unstable in air was obtained. Yield: 0.92g (75%)

Melting Point (sealed capillary): 235-241°C(dec)

¹H-NMR (C₆D₆, δ ppm):

- 1.11 (t, 3H, C₂-CH₂-CH₃, ³J_{H-H} = 7.5 Hz)
- 1.30 (t, 3H, C₆-CH₂-CH₃, ³J_{H-H} = 7.5 Hz)
- 1.53 (s, 15H, CH₃-Cp)
- 1.77 (s, 8H, CH₂, COD)
- 2.21 (q, 2H, C₂-CH₂-CH₃, ³J_{H-H} = 7.5 Hz)
- 2.27 (s, 6H, CH₃-C_{4,8})
- 2.53 (qd, 2H, C₆-CH₂-CH₃, ³J_{H-H} = 7.5 Hz, ³J_{H-Rh} = 1.6 Hz)
- 4.34 (s, 4H, C=CH, COD)
- 4.74 (s, 2H, C_{1,3}-H)
- 5.00 (s, 2H, C_{5,7}-H)

¹³C-NMR (C₆D₆, δ ppm):

- 10.79 (CH₃-Cp)
- 15.10 (C₆-CH₂-CH₃)
- 15.20 (C₂-CH₂-CH₃)
- 15.29 (CH₃-C_{4,8})
- 22.74 (C₂-CH₂-CH₃)
- 25.25 (C₆-CH₂-CH₃)
- 31.68 (CH₂-COD)
- 65.69 (C_{1,3})
- 70.44 (d, C=C, COD, ¹J_{C-Rh} = 13.1 Hz)
- 71.73 (d, C_{5,7}, ¹J_{C-Rh} = 4.5 Hz)
- 81.71 (CH₃-Cp)

	95.78 (C ₂)
	96.59 (C _{4,8})
	96.62 (C _{3a,8a})
	116.00 (d, C _{4a,7a} , ¹ J _{C-Rh} = 1.4 Hz)
	120.55 (d, C ₆ , ¹ J _{C-Rh} = 6.5 Hz)
¹⁰³ Rh-NMR (C ₆ D ₆ , δ ppm):	-281
Mass Spectrum (EI, 70eV) m/z:	[M] ⁺ = 684 (55.5%)
	[M] ⁺ - Rh(COD)H = 474 (100.0%)
	[Rh(COD)] ⁺ = 211 (44.1%)
	[(COD)] ⁺ = 108 (8.4%)
Analysis Calculated:	C ₃₆ H ₄₇ RuRh: C: 63.24; H: 6.93
	Found: C: 62.91; H: 7.01

3.8.22 *anti*-(1,2,3,4,5-Pentamethylcyclopentadienide)-Cobalt(II)-2,6-diethyl-4,8-dimethyl-*s*-indacendiide-Rhodium(I)-(1,5-cyclooctadiene) **23c**:

Analogue for the procedure in **23a**, using instead a solution of *n*-BuLi (1.6M in hexanes, 1.1 mL, 1.7 mmol), a solution of **21c** (0.71g, 1.64 mmoles) in 30 mL of THF, and **18a** (0.40 g, 0.81 mmoles) in 20 mL of THF. A black dust very unstable in air was obtained. Yield: 0.62g (58.8%)

Melting Point (sealed capillary):	227°C(dec)
Mass Spectrum (EI, 70eV) m/z:	[M] ⁺ = 641 (19%)
	[M] ⁺ - Rh(COD)H = 430 (100%)
	[Rh(COD)] ⁺ = 211 (56%)
Analysis Calculated:	C ₃₆ H ₄₇ CoRh: C: 77.93; H: 8.41
	Found: C: 78.01; H: 8.76

3.8.23 *syn*-(1,2,3,4,5-Pentamethylcyclopentadienide)-Ruthenium(II)-2,6-diethyl-4,8-dimethyl-*s*-indacendiide-Rhodium(I)-(η⁴-1,5-cyclooctadiene) **24a**:

A solution of *n*-BuLi (1.6M in hexane, 1.48 mL, 2.4 mmol) was slowly added to a -78°C cooled solution of the previously prepared compound **21d** (0.95g, 4.0g mmol) in 30 mL of THF. The mixture is stirred for one hour at room temperature, yielding the monolithiated anionic complex. 1.14g (1mmole) of **17** dissolved in 30 mL of THF is then added dropwise. This mixture is stirred for 2 hours at room temperature. Then all solvent is removed, and the raw product is washed with pentane, and filtered to eliminate the insoluble LiCl. A dark orange dust unstable in air (0.45g, 1.12 mmol) was obtained, with a 92% yield. ¹H-NMR analysis reveals the formation of both isomers, 53%-*syn* **24a**: 47%-*anti* **23b**.

Melting Point (sealed capillary): 224-225°C(dec)

¹H-NMR (CDCl₃, δ ppm):

- 1.13 (t, 3H, C₂-CH₂-CH₃, ³J_{H-H} = 7.5 Hz)
- 1.22 (t, 3H, C₆-CH₂-CH₃, ³J_{H-H} = 7.5 Hz)
- 1.73 (s, 8H, CH₂, COD)
- 1.80 (s, 15H, CH₃-Cp)
- 2.19 (q, 2H, C₂-CH₂-CH₃, ³J_{H-H} = 7.5 Hz)
- 2.06 (s, 6H, CH₃-C_{4,8})
- 2.52 (qd, 2H, C₆-CH₂-CH₃, ³J_{H-H} = 7.5 Hz, ³J_{H-Rh} = 1.5 Hz)
- 4.28 (s, 4H, C=CH, COD)
- 4.61 (s, 2H, C_{1,3}-H)
- 4.90 (s, 2H, C_{5,7}-H)

¹³C-NMR (C₆D₆, δ ppm):

- 11.34 (CH₃-Cp)
- 14.73 (CH₃-C_{4,8})
- 14.97(C₆-CH₂-CH₃)
- 15.35 (C₂-CH₂-CH₃)
- 22.76 (C₂-CH₂-CH₃)
- 24.00 (C₆-CH₂-CH₃)
- 31.32 (CH₂-COD)
- 65.97 (C_{1,3})
- 70.77 (d, C=C, COD, ¹J_{C-Rh} = 10.3 Hz)
- 72.71 (d, C_{5,7}, ¹J_{C-Rh} = 5.1 Hz)

	81.55 (CH ₃ -Cp)
	95.83 (C ₂)
	95.71 (C _{4,8})
	97.28 (C _{3a,8a})
	116.48 (d, C _{4a,7a} , ¹ J _{C-Rh} = 1.1 Hz)
	120.41 (d, C ₆ , ¹ J _{C-Rh} = 7.8 Hz)
¹⁰³ Rh-NMR (C ₆ D ₆ , δ ppm):	-245
Mass Spectrum (EI, 70eV) m/z:	[M] ⁺ = 684 (79%)
	[M] ⁺ - Rh(COD)H = 474 (100%)
	[Rh(COD)] ⁺ = 211 (18%)
Analysis Calculated:	C ₃₆ H ₄₇ RuRh: C: 63.24; H: 6.93
	Found: C: 64.08; H: 7.32

3.8.24 anti-(1,2,3,4,5-Pentamethylcyclopentadienide)-Cobalt(III)-2,6-diethyl-4,8-dimethyl-s-indacendiide-Rhodium(I)-(η⁴-1,5-cyclooctadiene) Tetrafluoroborate [23c]⁺[BF₄⁻]:

In a 50 mL round flask, provided with a nitrogen inlet, the cobalt-rhodium complex **23c** (0.30 g, 0.47 mmol) is mixed with ferrocenium tetrafluoroborate (0.10 g, 0.37 mmol). Later, to this flask, 30 mL of THF are added, to allow the solids to dissolve and react with vigorous stirring. After one hour, all THF is evaporated and the remaining solid is washed with 30 mL of hexane, leaving an insoluble black dust. Yield: 0.24 g (88.9%, referred to ferrocenium tetrafluoroborate)

Melting Point (sealed capillary):	171-179°C(dec)
¹ H-NMR (CD ₃ CN, δ ppm):	1.18 (t, 3H, C ₂ -CH ₂ -CH ₃ , ³ J _{H-H} = 7.4 Hz)
	1.39 (t, 3H, C ₆ -CH ₂ -CH ₃ , ³ J _{H-H} = 7.4 Hz)
	1.55 (s, 15H, CH ₃ -Cp)
	1.93 (s, 8H, CH ₂ , COD)
	2.52 (q, 2H, C ₂ -CH ₂ -CH ₃ , ³ J _{H-H} = 7.4 Hz)
	2.32 (s, 6H, CH ₃ -C _{4,8})

	2.69 (q.d, 2H, C ₆ -CH ₂ -CH ₃ , ³ J _{H-H} = 7.4 Hz, ³ J _{H-Rh} = 1.2 Hz)
	4.46 (s, 4H, C=CH, COD)
	5.38 (s, 2H, C _{1,3} -H)
	5.53 (s, 2H, C _{5,7} -H)
¹³ C-NMR (CD ₃ CN, δ ppm):	14.13 (C ₂ -CH ₂ -CH ₃)
	14.28 (C ₆ -CH ₂ -CH ₃)
	14.81 (CH ₃ -C _{4,8})
	15.03 (CH ₃ -Cp)
	19.97 (C ₂ -CH ₂ -CH ₃)
	20.17 (C ₆ -CH ₂ -CH ₃)
	30.30 (CH ₂ -COD)
	69.68 (C _{5,7})
	74.51 (d, C=C, COD, ¹ J _{C-Rh} = 12.8 Hz)
	75.02 (C _{1,3})
	93.01 (CH ₃ -Cp)
	99.75 (C _{4a,7a})
	106.00 (C ₂)
	112.95 (C _{4,8})
	121.54 (C _{3a,8a})
	126.77 (d, C ₆ , ¹ J _{C-Rh} = 5.0 Hz)
¹⁰³ Rh-NMR (C ₆ D ₆ , δ ppm):	-271
Mass Spectrum (EI, 70eV) m/z:	[M] ⁺ - [BF ₄] ⁻ = 641 (22%)
	[M] ⁺ - Rh(COD)H - [BF ₄] ⁻ = 430 (100%)
	[Rh(COD)] ⁺ = 211 (39%)
	[BF ₄] ⁻ = 87 (18%)

References

¹ (a) J. Manriquez, M. Ward, W. Reiff, J. Calabrese, N. Jones, P. Carrol, E. Bunel, J. Miller, *J. Am. Chem. Soc.*, **1995**, *117*, 6182. (b) P. Roussel, D. R. Cary, S. Barlow, J. C. Green, F. Varret, D. O'Hare, *Organometallics* **2000**, *19*, 1071.

² A. Ceccon, S. Santi, L. Orian, A. Bisello, *Coord. Chem. Rev.*, **2004**, *248*, 683.

³ F. Cotton, G. Wilkinson, C. Murillo, M. Bochman, *Advanced Inorganic Chemistry*, Sixth Edition, John Wiley & Sons, Inc., **1999**, 661.

⁴ G. Wilkinson, F. Gordon, A. Stone, E. Abe, *Comprehensive Organometallic Chemistry*, Editors Pergamon Press, New York, **1982**, Vol 5 and 6.

⁵ R. King, P. Treichel, F. Stone, *J. Am. Chem. Soc.*, **1961**, *83*, 3593.

⁶ P. Pauson, *Tetrahedron*, **1985**, *41*, 5885.

⁷ F. G. Bordwell, P. S. Landis, *J. Am. Chem. Soc.*, **1957**, *79*, 1593. b) H. Jenkner, *Chemische Fabrick Kalk* G. M. B. H. Ger. Offen. 2,027,162 (C1. C07c), **1971**, 9.

⁸ a) C. Perthuisot, W. Jones, *J. Am. Chem. Soc.*, **1994**, *116*, 3641. b) W. Porzio, M. Zocchi, *J. Am. Chem. Soc.*, **1978**, *100*, 2048. c) J. O'Connor, C. P. Casey, *Chem. Rev.*, **1987**, *87*, 307

⁹ J. Wild, *J. Org. Chem.*, **1982**, *232*, 233.

¹⁰ H. Amouri, J. Vaissermann, M. N. Rager, Y. Besace, *Inorg. Chem.*, **1999**, *38*, 1211.

¹¹ A. Ceccon, A. Bisello, L. Crociani, A. Gambaro, P. Ganis, F. Manoli, S. Santi, A. Venzo, *J. Organomet. Chem.*, **2000**, *600*, 94.

¹² a) M. Dahrouch, P. Jara, L. Mendez, Y. Portilla, D. Abril, G. Alfonso, I. Chavez, J. M. Manriquez, M. Rivière-Baudet, P. Rivière, A. Castel, J. Rouzaud, H. Gornitzka, *Organometallics* **2001**, *20*, 5591. b)

¹³ A.R. Cutler, P.K. Hanna, J.C. Vites, *Chem.Rev.* **1988**, *88*, 1363

¹⁴ S. Westcott, A. Kakkar, G. Stringer, N. Taylor, T. Marder, *J. of Org. Chem.*, 1990, 394, 777.

¹⁵ C. Bonifaci, A. Ceccon, A. Gambaro, F. Manoli, L. Mantovani, P. Ganis, S. Santi, A. Venzo, *J. Organomet. Chem.*, **1988**, *57*, 97.

¹⁶ J. Ruiz, P. Bentz, B. Mann, C. Spencer, B. Taylor, P. Maitlis, *J. Chem. Soc. Dalton Trans.*, **1987**, 2709.

¹⁷ A. Ceccon, P. Ganis, M. Imhoff, F. Manoli, S. Santi, A. Venzo, *J. Organomet. Chem.*, **1999**, *577*, 167.

¹⁸ J. Pesek, W. Mason, *Inorg. Chem.*, **1983**, *22*, 2958.

¹⁹ A. Bisello, A. Ceccon, A. Gambaro, P. Ganis, F. Manoli, S. Santi, A. Venzo, *J. Organomet. Chem.* **2000**, *593*, 315.

²⁰ (a) C. Creutz, H. Taube, *J. Am. Chem. Soc.*, **1969**, *91*, 3988. (b) C. Creutz, H. Taube, *J. Am. Chem. Soc.*, **1973**, *95*, 1086.

²¹ K. Demadis, C. Hartshorn, T. Meyer, *Chem. Rev.*, **2001**, *101*, 2655.

²² P. Pauson, E. Fischer, R. Jira, M. Rosenblum, M. Whiting, F. Cotton, *J. Organomet. Chem.*, **2001**, *637*, 3.

- ²³ S. Trupia, A. Nafady, W.E. Geiger, *Inorg. Chem.* **2003**, *42*, 5480.
- ²⁴ F. Barriere, N. Camire, W. Geiger, U. Mueller-Westerhoff, R. Sanders, *J. Am. Chem. Soc.*, **2002**, *124*, 7262.
- ²⁵ L. Orian, A. Bisello, S. Santi, A. Ceccon, G. Saielli, *Chem. Eur. J.*, **2004**, *10*, 4029.
- ²⁶ *Handbook of Chemistry and Physics*, **1997-1998**, 78th Edition, Section 9-1.
- ²⁷ J. Manriquez, E. Bunnell, B. Oelckers, E. Roman, C. Vasquez, J. Miller. *Inorg. Synth.*, **1996**, *31*, 267.
- ²⁸ E. Bunel, L. Valle, J. Manriquez, *Organometallics* **1985**, *4*, 1680.
- ²⁹ T. Tilley, R. Grubbs, J. Bercaw, *Organometallics* **1984**, *3*, 274.
- ³⁰ P. Fagan, M. Ward, J. Calabrese, *J. Am. Chem. Soc.*, **1989**, *111*, 1698.
- ³¹ P. Fagan, W. Mahoney, J. Calabrese, I. Williams, *Organometallics*, **1990**, *9*, 1843, and references therein.
- ³² G. Giordano, R. Crabtree. *Inorg. Synth.*, **1990**, *28*, 88.
- ³³ H. Amouri, M. Gruselle, G. Jaouen, *Synth. React. Inorg. Met. Org. Chem.*, **1994** *24*, 401.
- ³⁴ P. Maitlis, K. Moseley, J. Kang, *J. Chem. Soc.*, **1970**, *17*, 2875.
- ³⁵ A. Salzer, C. Taeschler, *Journal of Organomet. Chem.* **1985**, *294*, 261.

³⁶ H. Eshtiagh-Hosseini, J. Nixon, *Journal of the Less-Common Metals*, **1978**, *61*, 107.

³⁷ a) E. Esponda, C. Adams, F. Burgos, I. Chavez, J. M. Manriquez, F. Delpech, A. Castel, H. Gornitzka, M. Rivière-Baudet, P. Rivière, *J. Organomet. Chem.*, **2006**, *691*, 3011 b) A. Bisello, A. Ceccon, A. Gambaro, P. Ganis, F. Manoli, S. Santi, A. Venzo, *Journal of Organomet. Chem.*, **2000**, *593*, 315. c) S. Santi, A. Ceccon, F. Carli, L. Crociani, A. Bisello, M. Tiso, A. Venzo, *Organometallics*, **2002**, *21*, 2676.

Chapter 4: Catalytic Study of Organometallic Rhodium Complexes in Dehydrogenative Silylation of Olefins

Chapter 4

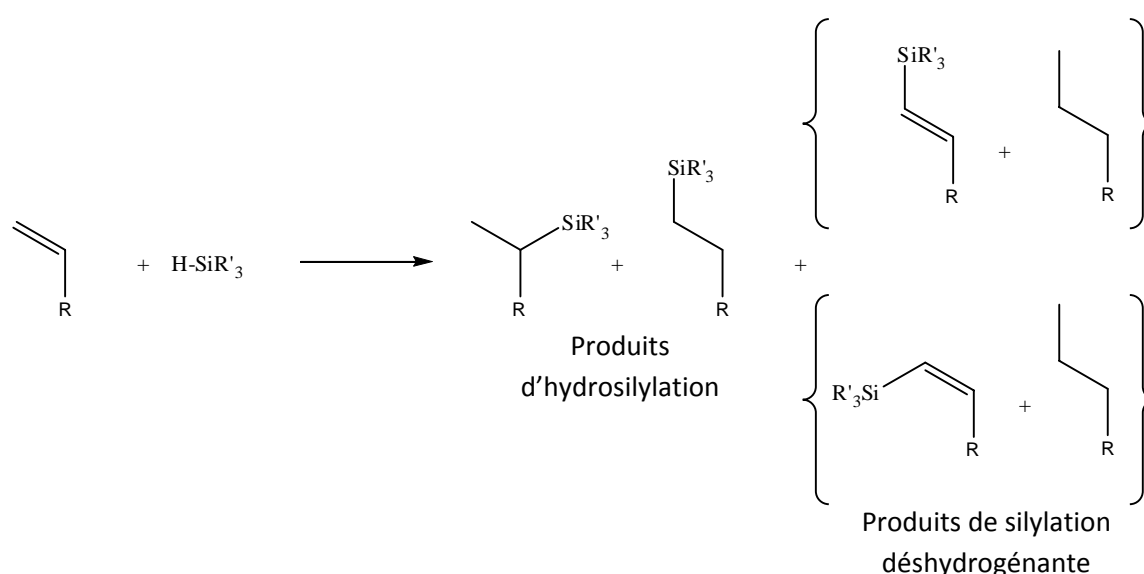
Catalytic Study of Rhodium Organometallic Complexes in Dehydrogenative Silylation of Olefins

Chapter 4: Catalytic Study of Organometallic Rhodium Complexes in Dehydrogenative Silylation of Olefins

Introduction

La réaction de silylation deshydrogénante des oléfines est beaucoup moins connue que la réaction d'hydrosilylation bien que les vinylsilanes présentent un grand intérêt sur le plan industriel (utilisation dans la synthèse de produits naturels, la formation de polycarbosilanes et de polymères).

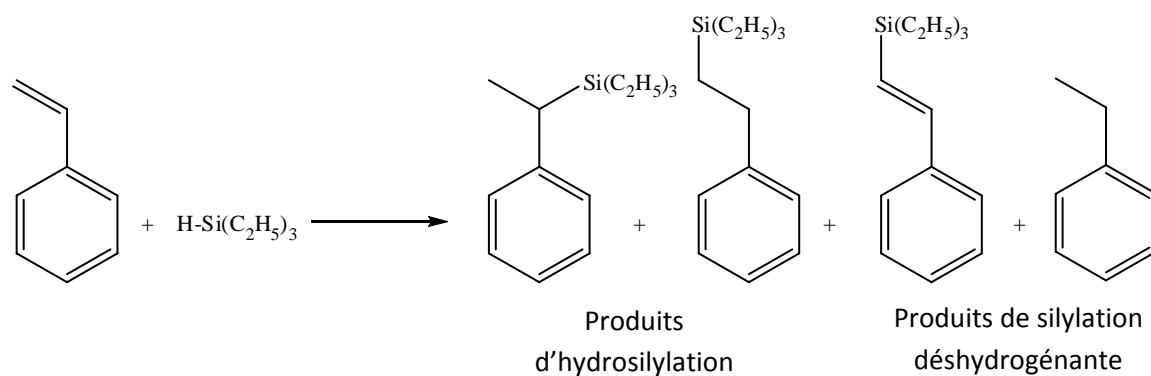
Le principal inconvénient de cette réaction est sa compétition avec la réaction d'hydrosilylation.



Il existe à ce jour quelques catalyseurs spécifiques qui permettent la formation majoritaire de vinylsilanes mais le champ d'investigation reste grand ouvert.

Dans ce chapitre seront décrits les différents tests avec les complexes du rhodium précédemment synthétisés. Nous essayerons également de déterminer l'influence du solvant, de la température, du ligand, des ligands ancillaires et du fragment métallique.

Nous avons choisi d'étudier la réaction de silylation du styrène par le triéthylsilane. Tous les produits formés (produits d'hydrosilylation et produits de silylation deshydrogénante) ont été caractérisés par RMN du proton et par chromatographie en phase gazeuse couplée à la spectrométrie de masse. Les pourcentages relatifs ont été déterminés à partir des chromatogrammes (GC).



Nous avons tout d'abord déterminé les conditions optimales de température, de solvant et le ratio oléfine/silane. Les meilleurs résultats ont été obtenus à 80°C en utilisant le toluène comme solvant et trois équivalents de styrène pour un équivalent de silane.

Plusieurs oléfines ont été testées (éthylène, styrène, 2,4,6-triméthylstyrène, 1-hexène, allylbenzène et le cyclohexène). Les oléfines présentant un atome d'hydrogène en β donnent des réactions secondaires d'isomérisation ce qui diminue considérablement les rendements. Le styrène et le 2,4,6-triméthylstyrène semblent être les deux oléfines les plus adaptées pour ce type de réaction.

En ce qui concerne la nature des silanes, une comparaison entre le triéthylsilane, le triisopropylsilane, le méthyldiphénylsilane et le triéthoxysilane a été effectuée. Les réactions d'hydrosilylation sont fortement favorisées pour le diméthylphénylsilane et le triéthoxysilane. Aucune réaction n'a été obtenue à partir de dihydrosilanes. En fait, seuls les trialkylsilanes ont donné les meilleurs rendements avec cependant une vitesse de réaction plus lente dans le cas du triisopropylsilane vraisemblablement à cause de l'encombrement stérique plus important des substituants.

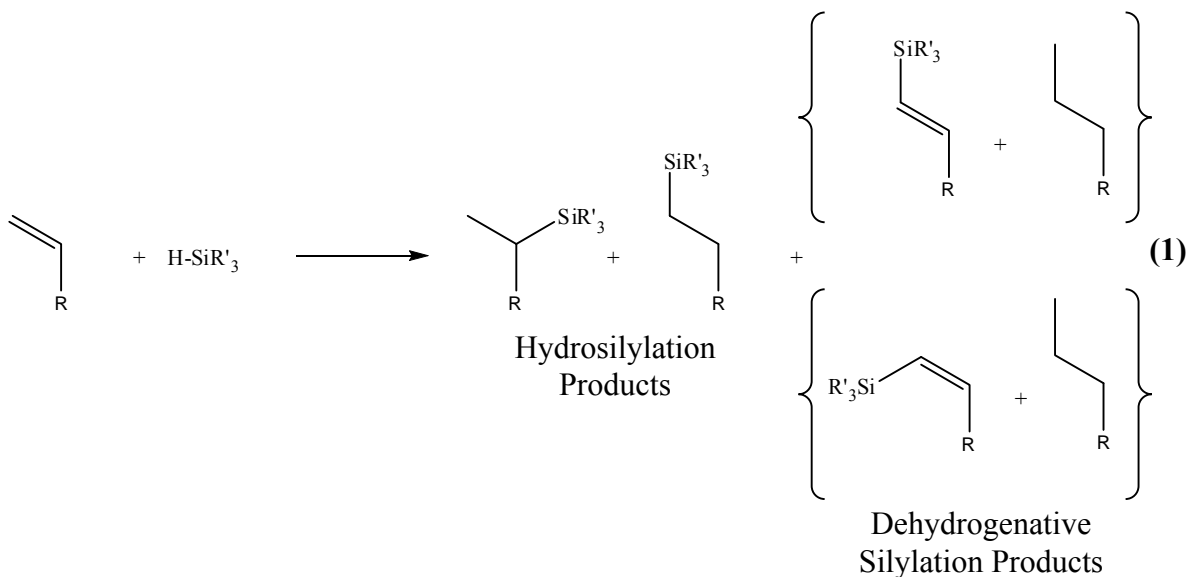
Les complexes du rhodium homo- et hétérobinucléaires se sont révélés les meilleurs catalyseurs pour ce type de réaction comparativement aux mononucléaires. Leur efficacité est tout à fait comparable à celle présentée par le complexe cationique $[\text{Rh}(\text{COD})_2]\text{BF}_4/\text{PPh}_3$ qui est le meilleur catalyseur connu à ce jour pour la silylation deshydrogénante. Nous avons obtenu des rendements en vinylsilanes de 80%. De plus, ils induisent une vitesse de réaction plus grande que celle observée à partir de systèmes catalytiques similaires comme les complexes indényles du rhodium ce qui semble confirmer l'existence d'effet coopératif entre les deux centres métalliques.

4 Introduction

The dehydrogenative silylation reaction of olefins is less documented than hydrosilylation, despite the fact vinylsilanes present multiple applications together with its commercial interest^[1,2,3].

The big value of vinylsilanes lies, amongst others, in the synthesis of natural products^[4], substrates for the formation of polycarbosilanes^[5,6] as well as siloxane polymers or copolymers^[7]. The main inconvenient of the dehydrogenative silylation of olefins is the competition with the hydrosilylation reaction. The first example of a catalytic reaction leading to vinylsilanes took place in 1962, where trialkylsilanes and several olefins were made react with $\text{Fe}(\text{CO})_5$ ^[8], several years before the studies would include other metals in the early 1980s^[9].

As previously described in the first chapter, the products formed can be represented by reaction 1:



Despite the fact there have been articles which have reported catalytic runs at different temperatures, most of these have no comments whatsoever on a plausible explanation of which step (or steps) is (are) most sensitive to heating, or to the influence

Chapter 4: Catalytic Study of Organometallic Rhodium Complexes in Dehydrogenative Silylation of Olefins

on solvent^[10,11]. Other than theoretical studies and their activation energies, to the best of the knowledge of our lab group, temperature and solvent effects are minimally analyzed.

The product abundance strongly depends on the nature of the catalyst and its ligands, the silane and olefin used, etc. In most cases with rhodium catalysts, the formation of a geminal-alkylated hydrosilylation product together with a cis-vinylsilane is detectable only in trace amounts, and very rarely isolated^[12,13].

The olefin, is not only the potential substrate for the formation of an addition product forming hydrosilylation products or a vinylsilane, as it also may have the role of behaving as a hydrogen acceptor for the dihydro-metal intermediate, regenerating the catalytic species. Figure 10 in Chapter 1 revisits the Chalk Harrod and Modified Chalk Harrod Mechanism, where the metallic center undergoing a reductive elimination forming hydrogen as a resulting product, but an olefin (depending on the very nature of the olefin) may react with the MH_2 intermediate, regenerating $[M]$, and forming an alkane.

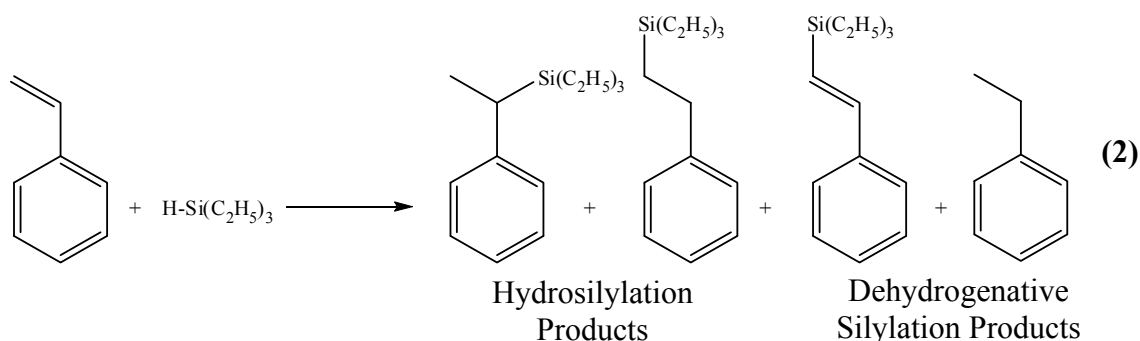
As the formation of a vinylsilane and the alkane is formed in a 1:1 ratio, each selectivity value is listed as a corrected percentile number, discarding the formation of the hydrogenated olefin. Also the products presenting a concentration lower than 1%, are discarded in all result tables.

Here detailed are the results obtained by the previously synthesized and characterized rhodium catalysts, in chapter 3. The main aim of this chapter is to elucidate as much as possible the effects of: solvent, temperature, main ligands, ancillary ligands, and secondary metallic fragment. These factors need to be assessed in order to determine if they have a direct influence on the selectivity of the different formed products, as well as with the reaction rate. All products were characterized in each case by GC-MS and by 1H -NMR, compared to the literature^[14].

4.1 Solvent and Temperature Effect

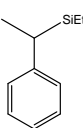
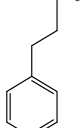
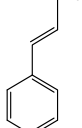
Several experiments were carried out in order to determine the ideal working solvent and temperature. Each run was performed for 100 minutes or until triethylsilane was fully consumed, whichever would happen first. Table 1 summarizes the results of all experiments.

All tests and their results listed in table 1 were performed using complex **23a**, using 100 eqs. of triethylsilane, plus 300 eqs. of styrene, forming the product shown in reaction 2.



Solvent completed 5 mL of the mixture, and each solvent was distilled over sodium and degassed under vacuum and Ar several times before usage. Working Temperatures were 60°C in each case, as well as 80°C and reflux temperatures for toluene and octane. These values were included as an attempt to understand and compare temperature effects.

Table 1: Results of the influence of Solvent and Temperature Effect.

Entry Number	Silane Consumption (%)	Time (mins)	Solvent	Temperature			
1	42.9	100	THF	60	12.6	27.8	59.6
2	16.6	100	Hexane	60	0.5	27.0	72.5
3	20.1	100	Octane	60	0.8	23.1	76.1
4	12.2	100	Toluene	60	3.7	23.6	72.7

Chapter 4: Catalytic Study of Organometallic Rhodium Complexes in Dehydrogenative Silylation of Olefins

5	100.0	80	Toluene	80	1.3	12.9	85.9
6	100.0	100	Octane	80	0.9	18.1	81.0
7	100.0	15	Octane	130 (Reflux)	0.9	22.3	76.8
8	100.0	25	Toluene	120 (Reflux)	0.0	13.0	87.0

Comparing the influence of the solvent at 60°C, a coordinating solvent such as THF resulted in a higher silane consumption, compared to each of the other solvents at the same temperature. This took place against selectivity, highly favoring products of hydrosilylation rather than vinylsilane. A feasible explanation could be that since THF is a nucleophilic solvent, it might coordinate to the metallic center, decreasing its Lewis acid character, hence making it less favorable to abstract the β -hydrogen in the alkyl chain, necessary for the formation of a vinylsilane.

At 60°C, the listed values of silane consumption and product selectivity are virtually identical. Hexane, octane and toluene are non-polar solvents, and their dielectric constants are very low; these similarities are reflected in the minimal differences in the outcome of each catalytic reaction. All other listed solvents probably have no other effect than to keep reagents and intermediates soluble at all times, in addition to delivering thermal energy to all substrates and active species to overcome the activation energy barriers for each relevant step of the catalytic cycle.

Temperatures of 80°C and above are allowed only by toluene and octane, not only making the consumption of silane quantitative, but also greatly increasing the selectivity of vinylsilane formation. Temperatures higher than 80°C reduce the time for complete silane consumption, although this does not increase or alter the selectivity values of any product, with the exception of octane at reflux temperature (130°C). In this last entry of Table 1, a decreased percentile value of vinylsilane may indicate a possible decomposition of the catalysts at temperatures over 120°C.

For the following catalytic reactions, toluene was chosen as solvent. Another test to determine the ideal working temperature was carried out with complexes **22b**, **22c**, **23a** and **23b** using temperatures from 40 to 120°C. Experiments were also tried at 20°C, but in all cases silane consumption was minimal, and there was either no product formation

or simply trace amounts. Figure 3 summarizes in a graph the effect temperature may have with each complex:

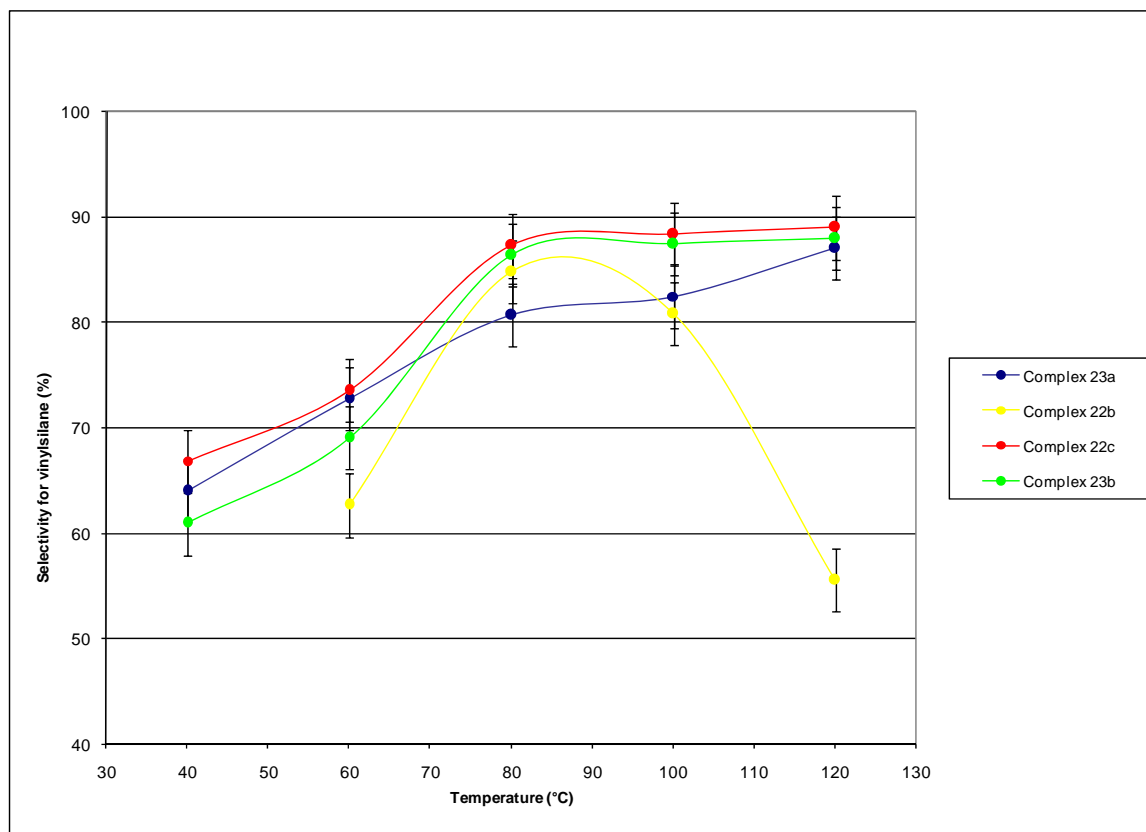


Figure 3: Graph representing the selectivity for the vinylsilane of styrene at different temperatures and for different catalysts.

The above shown graph clearly reveals that at temperatures of 80°C and above, there are only small changes selectivity regardless of the catalyst used, with the exception of Complex **22b**, which decreases the selectivity and the reaction rate of silane consumption at a given time. This may happen due to decomposition of the catalytic species, because of high steric crowding of both $-\text{Rh}(\text{COD})$ moieties which at high temperatures should reduce its effectiveness as a catalyst.

All other catalysts behave similarly, even **19a**, which has a strict pentahapto-ligand (Cp^*), and different only at lower temperatures at which the silane consumption is almost negligible. In conclusion, the ideal temperature for all catalysts is 80°C, and their behavior at other temperatures is comparable.

4.2 Effect of Chemical Substrates

The nature of substrates is critical for the outcome of each experiment. For example, α -olefins may isomerize to internal olefins resulting in silicon isomers, whether in hydrosilylation or in dehydrogenative silylation products. Silanes also have a crucial role in product formation, as it is known that rhodium catalysts have a very low affinity for di- or trihydrosilanes, but react readily with trialkyl(mono hydro)silanes^[15].

In the case of new silylated products, attempts to isolate each one were carried out by distillation at reduced pressure, and a later characterization by NMR and Mass Spectroscopy. Unless specified, most products were identified and compared to literature characterizations^[4].

4.2.1 Effect of Substrate Ratio

In this section, the ideal olefin:silane ratio was determined by using the same test as in Reaction 2, with complex **23b** in each case, and styrene:silane ratios ranging from 10:1 to 1:10.

Figure 4 shows an high completion time (consumption of limiting substrates) with a styrene:triethylsilane ratio of one. Higher ratios dramatically increase reaction rates to almost the same value. Figure 5 shows that both substrates affect product selectivity: the greater the concentration of olefin, the greater the amount of vinylsilane formed.

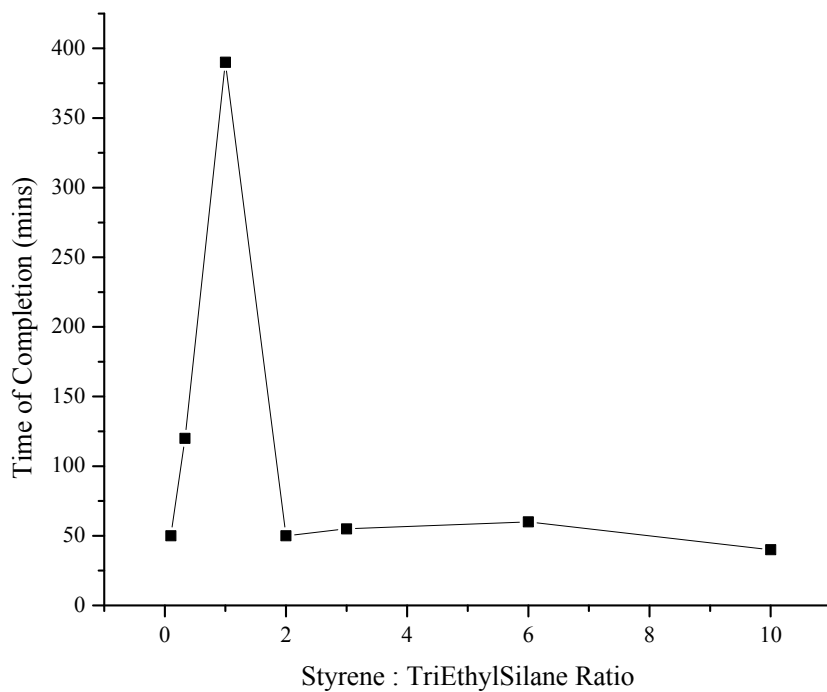


Figure 4: Graph representing the reaction rate depending on the olefin:silane ratio.

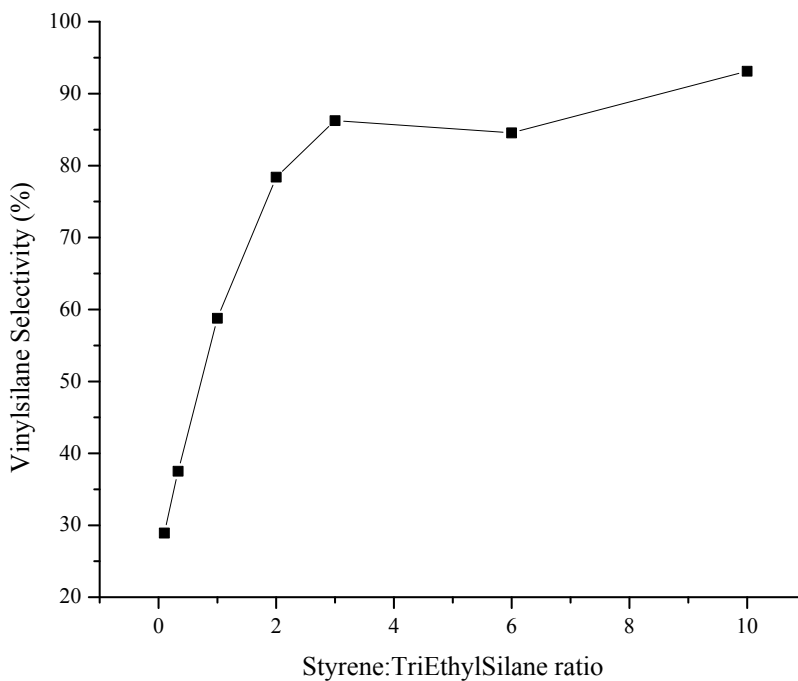
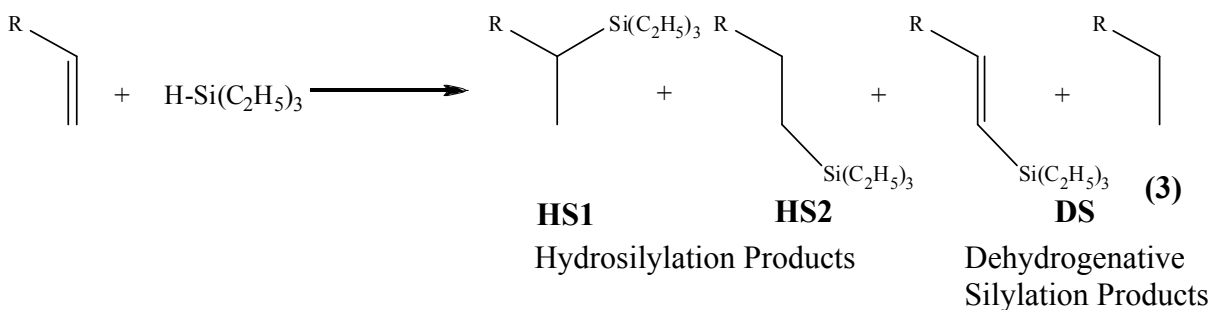


Figure 5: Graph representing the vinylsilane selectivity depending on the substrates ratio.

This tendency could be explained by the effect an olefin may have on the catalytic cycle shown in Figure 2. As previously noted, the olefin also has the role of providing a lower energy path for the reductive elimination of hydrogen by acting as a hydrogen acceptor, boosting the consumption of the intermediate species, thereby yielding the desired vinylsilane. If the olefin is used in a low concentration, the role as a hydrogen acceptor is not carried out, hence the higher concentration of hydrosilylation products. Also, at styrene:silane ratios greater than 3:1, the selectivity does not increase significantly. Therefore, the ideal condition is to use a substrate concentration of 300 equivalents of styrene and together with 100 equivalents of triethylsilane.

4.2.2 Olefin Effect

The nature of the olefin may affect the catalytic cycle depending directly on the nature of the substituent group. Reaction 3 is an attempt to explain the olefin effect, using by varying the nature of the R group.



The products in Reaction 3 are labelled HS1 for the geminal alkylated hydrosilylated product, HS2 for the lineal addition product, and DS for the vinylsilane and completely hydrogenated species.

In each test, 300 equivalents of each chosen olefin together with 100 equivalents of triethylsilane, in toluene at 80°C. In the case of ethylene, 1 bar of this olefin would be used instead. These olefins are diagramed in Figure 6. Four different complexes were

also included, in order to determine a possible greater affinity or reactivity of one particular catalyst for a certain olefin. These catalysts were **23a** and **23b**.

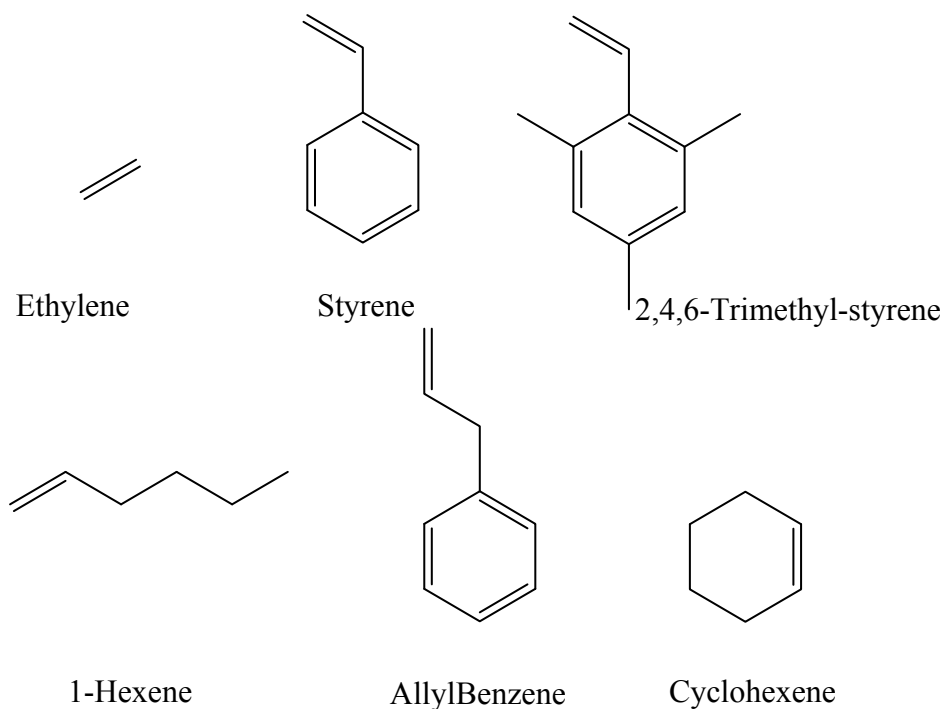


Figure 6: Diagrams of all used olefins.

Table 2: Results using different olefins

Olefin Used	Catalyst	Product Abundancy			Time (mins)	Silane Consumption
		HS1(%)	HS2(%)	DS(%)		
Styrene	23a	1.3	11.1	88.1	60	100%
	23b	0.9	12.8	86.3	55	100%
2,4,6-Trimethylstyrene	23a	0.0	14.1	85.9	420	71%
	23b	0.0	15.0	85.0	420	74%
Ethylene	23a	59.6		40.4	100	100%
	23b	58.2		41.8	100	100%

The above listed results in Table 2 show a fast consumption of triethylsilane for each entry, with similar values for selectivity.

The electron-withdrawing groups, such as phenyl and trimethylphenyl, make a double bond a better hydrogen acceptor, explaining the high vinylsilane selectivity values for styrene and trimethylstyrene. The dramatic difference on the reaction rates could be easily explained by the steric hinderance of the methyl groups in positions 2 and 6 of 2,4,6-Trimethylstyrene, making more difficult the coordination of this olefin, together with delaying the insertion of the olefin whether into the M-H or to the M-Si bonds.

Allylbenzene increases the number of products. In this particular case, not all products were isolated and characterized, due to their large number.

Figure 7 shows how the formation of β -methylstyrenes occurs, and may simultaneously react within the catalytic cycle.

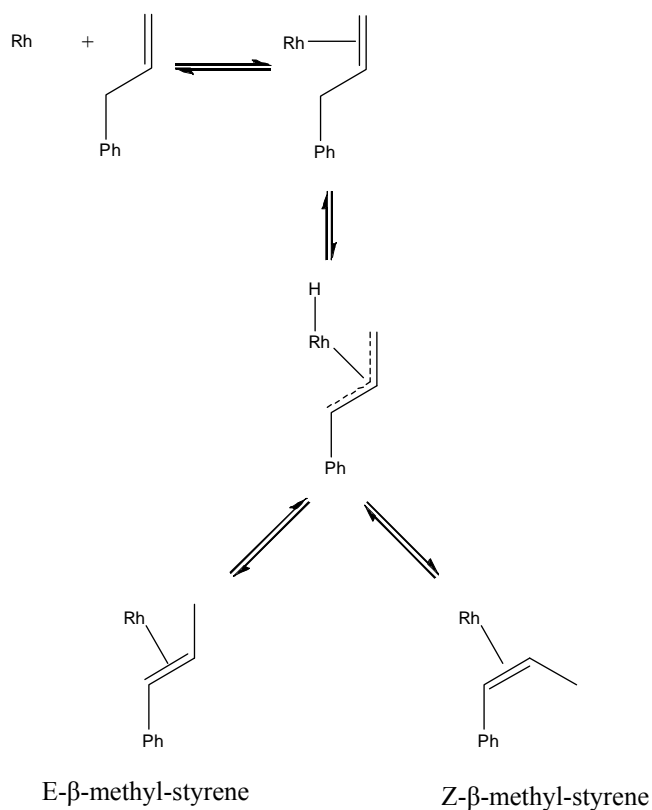


Figure 7: Allylbenzene reacting with rhodium to form its respective isomers.

The formation of these isomers was detected by GC, where the combination of the catalyst in the presence of the olefin in toluene would deliver one extra peak. These

additional peaks were analyzed by mass spectroscopy, and by $^1\text{H-NMR}$, matching the molecular peaks and NMR peaks of both isomers, E- and Z- β -methyl-styrene. Figure 8 graphs the reagent and product abundance after a few hours of reaction^[16].

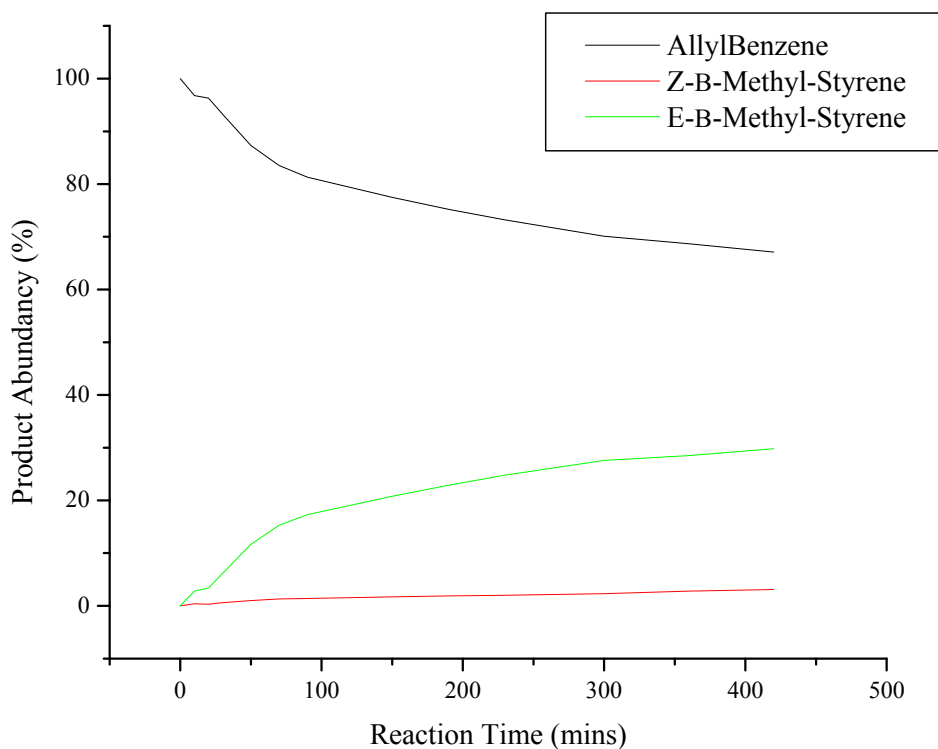


Figure 8: Graph representing the formation of Allylbenzene isomers

Each different olefin, allylbenzene or its isomers, may present many different silylated products, though only two of these of unknown nature were detected. These products were identified only by means of mass spectroscopy, as when attempts to isolate them by means of silica column chromatography or reduced-pressure distillation would only present decomposition products as monitored by $^1\text{H-NMR}$, making it impossible to properly identify them. In table 3, HS and DS stand for hydrosilylation and dehydrogenative silylation products, respectively, only that in this case, there were no means as to distinguish which particular product was formed.

Table 3: Results using AllylBenzene

Complex Used	Product Selectivity (%)				Time (mins)	Silane Consumption
	Z*	E**	HS	DS		
23a	4.7	75.4	6.9	13.0	350	80.5%
23b	4.4	78.0	5.8	11.8	350	81.6%

*: Product Z- β -methyl-styrene

** : Product E- β -methyl-styrene

After 350 minutes, the main product is only the E form of methylstyrene. This may indicate the isomerization reaction has a much lower energy activation barrier which consumes most of allylbenzene forming its isomers, rather than reacting to form the silylated products. After each catalytic run was completed at the given time, almost 80% of allylbenzene had been consumed, thus explaining the high percentage of formation of the E isomer, plus a very low concentration of dehydrogenative silylation products.

Olefins such as 1-hexene and cyclohexene presented no silylated product. In each case, the silane consumption was below the values of 2%, which is clearly within the margins of the experimental error of the GC machine, used to monitor the disappearance of each substrate.

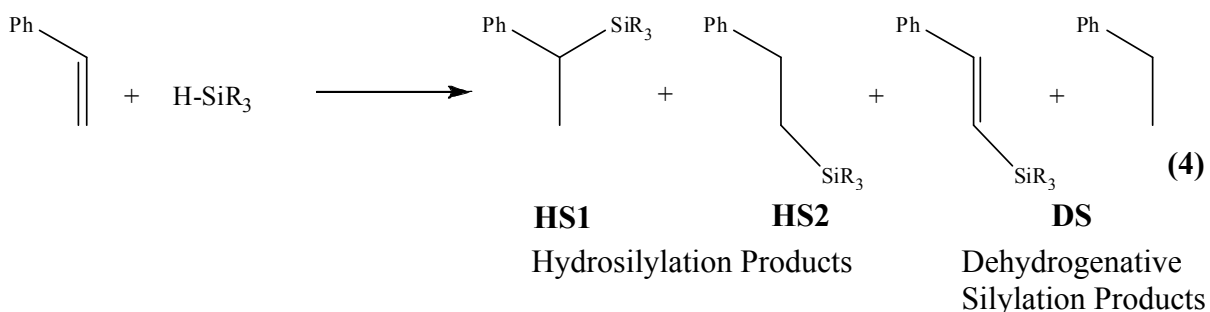
1-Hexene presented several other GC peaks in each chromatogram once started the catalytic run, which a mass spectrum corroborated these were only isomers, surely 2-hexene and 3-hexene. These two olefins were considered for our rhodium complexes as inactive. Hydrosilylation and dehydrogenative silylation of internal olefins is a much more complex procedure, which normally takes place by means of radical reactions, possibly providing a plausible explanation for the lack of reactivity for these olefins.

In general, according to these results, olefin isomerization reactions seemed to occur at much faster rates than the formation of silylated products, drastically restricting the number of adequate substrates that could be used for these Rh catalysts. These results

indicate only olefins without hydrogen atoms in β position together with electron-acceptor groups seem to be suitable, such as styrene and trimethylstyrene.

4.2.3 Silane Effect

Reaction 4 shows the products formed using styrene for olefin, in all catalytic tests using same catalysts as in the previous section. In most cases, product HS1 is undetectable, or in trace amounts which are only detectable by GC-MS, which are discarded in the value of selectivity.



Tables 6 to 9 show the results for all used trialkylsilanes, as those tests with dihydrosilanes, such as diethylsilane and diphenylsilane resulted in a complete lack of activity for all the listed rhodium catalysts.

A comparison between triethylsilane and tri(isopropyl)silane show a marked difference. Changing from a linear to a branched alkyl group boosts the selectivity to a quantitative consumption of the silane forming exclusively the respective dehydrogenative silylation products. There is a much higher reaction time with tri(isopropyl)silane than with triethylsilane, possibly explained by the greater difficulty of inserting an olefin group inside a $\text{Rh-Si}(i\text{-Pr})_3$ bond owning a bulkier group.

Table 4: Results using different silanes:

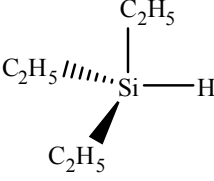
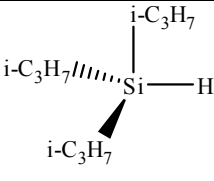
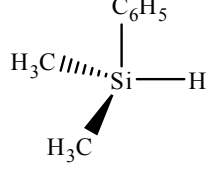
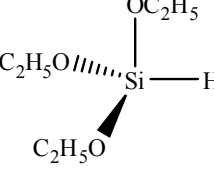
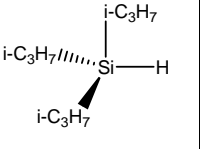
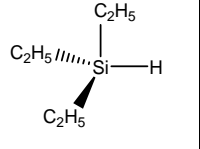
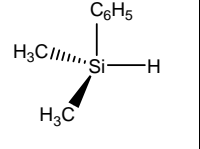
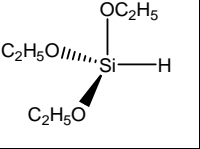
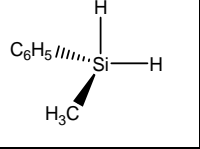
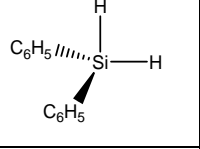
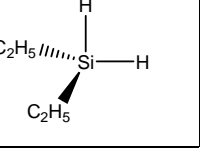
Silane Used	Catalyst	Product Abundance			Time (mins)	Silane Consumption
		HS1(%)	HS2(%)	DS(%)		
	23a	1.3	12.9	85.9	60	100%
	23b	0.9	12.8	86.3	55	100%
	23a	0.0	0.0	100	140	100%
	23b	0.0	0.0	100	150	100%
	23a	0.0	71.2	28.8	55	100%
	23b	0.0	73.8	26.2	60	100%
	23a	0.0	71.8	28.2	250	100%
	23b	0.0	73.4	26.6	250	100%

Table 4 also shows the results for dimethylphenylsilane and triethoxysilane, respectively. These silanes strongly favor hydrosilylation products, together with a very much increased reaction time for triethoxysilane, indicating the lack of reactivity for this substrate.

When a silane has a large electronic density located on the silicon atom, this could form an “overly” stable Rh-Si bond which may decrease the feasibility of inserting the olefin in this bond, favoring the Chalk-Harrod mechanism. This may be the case with dimethylphenylsilane and triethoxysilane. Other failed experiments including different silanes are not listed in tables as results, as in these cases there was no activity

whatsoever from the catalysts. These include substances such as dihydrosilanes (entries 5, 6 and 7 from Table 10).

Table 5: Cone Angle and NMR chemical shift data for ^1H and ^{29}Si for the used silanes.

Silane	Angle ($^\circ$)	$\delta(^1\text{H})$ ppm	$\delta(^{29}\text{Si})$ ppm	Selectivity for DS Products
	160	3.35	12.06	100 %
	132	3.68	0.53	88.1 %
	127	4.53	-17.05	32.5 %
	110	4.29	-58.93	22.0 %
	-	4.44	-35.74	None
	-	5.07	-33.31	None
	-	3.84	-22.72	None

In general, silanes have a strong effect on the selectivity of the formed products. This may happen due to the fact that the rate determining steps in the Chalk-Harrod and Modified Chalk-Harrod mechanisms involve a carbon silicon bond to form and undergo the migratory insertion of the relevant olefin.

According to a thorough theoretical study^[17], the Chalk-Harrod mechanism has for rate determining step the reductive elimination of the Si-C bond. In the case of the Modified Chalk-Harrod mechanism, the rate determining steps are whether the insertion of ethylene into the Rh-Si bond, or oxidative addition of the silane. Therefore, in order to form a larger amount of vinylsilane, a silane should ideally have a fast oxidative addition together with a Rh-Si bond weak enough as to favor the migration of the trialkylsilyl group on the olefin, rather than the migration of the hydrogen group.

These results may be further explained with the data obtained from NMR tools and cone angles from each respective silane. In Table 5, a qualitative correlation between the selectivity value for dehydrogenative silylation products and the NMR chemical shifts for proton and silicon nuclei can be evidenced, indicative that these rhodium catalysts boost their selectivity values when working with silanes with a dipole moment with a negative charge centered on the hydrogen atom and a positive charge on silicon, as in $\text{Si}^{\delta+}-\text{H}^{\delta-}$. The three last entries in table 5 present a dipolar moment of the silicon-hydrogen bond closer to: $\text{Si}^{\delta-}-\text{H}^{\delta+}$, possibly hardening the oxidative addition process on the Rh center. Nevertheless, table 5 also lists some cone angles for some trialkylsilanes (corresponding to each respective phosphine analogue^[18]), revealing both factors, steric and electronic are responsible for the outcome of product selectivity, though steric influence seems to be the most significant factor when determining product selectivity.

Therefore, these catalysts seem capable of presenting very high selectivity values with a fairly limited number of silanes, more specifically, trialkylsilanes. Aryl and Alkoxy groups seem unsuitable, at least for these Rh catalysts.

4.3 Effect of Ligands

The effect ligands present on the outcome of a catalyst is crucial in homogenous catalysis. In this section, ligands shall be studied in two categories. A “main” ligand shall be referred to as the five membered ligand which may (or may not) present a haptotropic shift towards rhodium. These are: Cp*, Indenyl, and Cp*M(s-indacendiide), as seen in Figure 9.

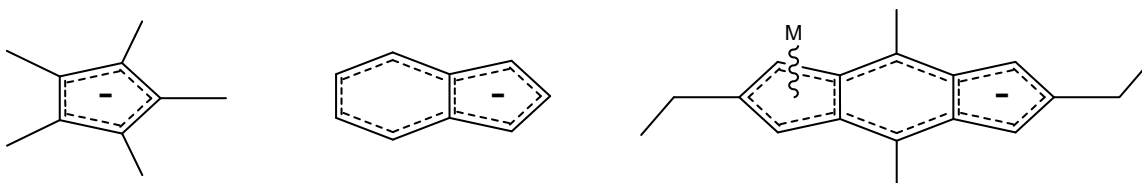


Figure 9: Main ligands used (M: *anti*-Cp*Ru-, *syn*-Cp*Ru-, *anti*-(COD)Rh-, *syn*-(COD)Rh-, *anti*-Cp*Co- and *anti*-Cp*Fe-)

Ancillary ligands are in this case, 1,5-cyclooctadiene (COD), norbornadiene (NBD) and carbon monoxide. These ligands are considered to be “more labile” than the main ligands, and normally, increasing the concentration of one of these ligands in solution may remove another in relatively smooth conditions (intermediate temperatures, low CO pressures, etc.).

4.3.1 Influence of Main Ligand

Several rhodium-based complexes, which differ only by the main ligand, have been tested^[10,19]. Comparison between catalytic results of runs with mono- and binuclear complexes show that in the latter case, the second metallic center created a remarkable effect, the most pronounced consequence being on the activity of the catalyst. Indeed, concentration of Rh was kept constant for all catalytic tests and, this allowed direct assessment of relative activity. Mononuclear complexes presented a reaction time of 450 min (see Table 5), while complete silane consumption is observed within 35 and 180 min, for **22c** and **22b**, respectively. The strong electronic interaction between both metals

channeled through the bridging ligand can be invoked to account for the higher activities of dinuclear complexes. The differences of efficiency between **22c** and **22b**, can be rationalized in terms of steric hindrance due to the proximity of the two Rh(COD) entities in the syn isomer.

The selectivity was also found to depend on the nature (mono- vs. bimetallic) of the catalyst. Indeed, homobinuclear compounds lead to similar product distribution, i.e., 85–88% and 12–15% of dehydrogenative silylation and hydrosilylation products, respectively. In contrast, the selectivity of the reaction in the presence of mononuclear complex **21d** drops to 75%. However, these differences remain weak and hazardous to rationalize. Thus, the difference of activity provides direct evidence for the involvement of cooperative effect between both metal centers during the catalysis. Dehydrogenative silylation and hydrosilylation products result from two competitive catalytic cycles and electronic communication may have stabilized intermediaries, which may have not taken place with mononuclear complexes. Detailed mechanism remain to be clarified and in particular, the precise role of the electronic communication during the reaction. Further exploration in this direction is currently in progress.

Table 6: Catalytic results for styrene and triethylsilane for rhodium complexes

Catalyst	Time (mins)	% of Silane Consumed	Product Selectivity		
			% of HS1:	% of HS2:	% of DS:
21d	600	92.8	10.9	13.9	75.3
22b	180	100	4.2	11.1	84.7
22c	35	100	1.0	11.8	87.2
23a	60	100	1.3	12.9	85.9
23b	55	100	0.9	12.8	86.3
23c	65	100	0.8	12.7	86.5
24a	280	100	0.5	13.8	85.7

Both *syn* isomers (complexes **22b** and **24a**) have higher reaction times compared with the *anti* isomers (complexes **22c**, **23a**, **23b** and **23c**). This difference can be explained due steric hinderance, concealing rhodium with the secondary metallic fragment, hardening the entry of the each analyzed substrates, whether the silane in an oxidative addition plus the coordination of styrene.

The remaining complexes, the *anti* isomers, all have identical behavior, if taken into consideration the fact that complex **22c** has two rhodium centers that may equally react within the catalytic cycle, thus shortening the reaction time. A similar catalytic test with half the concentration of this catalyst (considering equivalents of rhodium instead), required 65 minutes for reaction time. This result may allow us to consider the behavior of all s-indacendiide catalysts similar, if not identical.

If the ^{103}Rh -NMR chemical shifts for **20a**, and all s-indacene related complexes (Chapter 3, Table 9) are taken into consideration, these have similar bonding modes between all complexes to the five membered ring. This can imply that rhodium is not severely affected when changing the secondary metallic group to another, which can explain the catalytic results in Table 6, and their similarities.

Because of this, it is feasible to assume the existence of a cooperative effect in these heterobinuclear complexes in the form of a metallic fragment forcing rhodium to have a greater ring slippage, thus bonding closer to an allylic towards s-indacene, similar to the effect seen in literature^[20,21] and also shown in figure 10. This reaction, due to the information displayed in Chapter 3, is surely favouring a $(\text{M})\eta^5:(\text{Rh})\eta^3$ configuration.

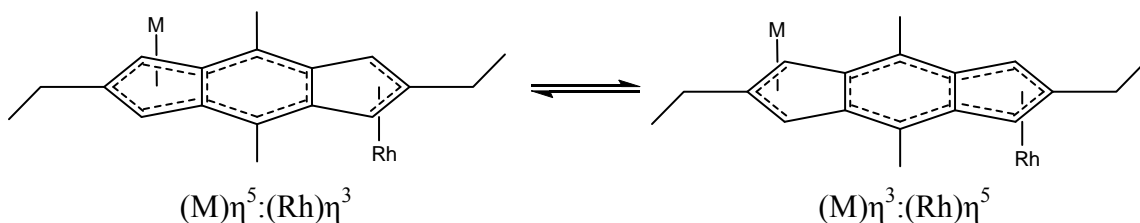


Figure 10: Diagram of the equilibrium between the two possible bonding modes for each metallic fragment.

Table 7: Catalytic results for styrene and triethylsilane for rhodium complexes

Catalyst	Time Taken (mins)	% of Silane Consumed	% of HS1:	% of HS2:	% of DS:
19a	50	100	0.3	18.8	80.9
19b	>600	<2	--	--	--
20a	125	100	1.1	17.4	81.5
20b	120	100	0.4	18.9	80.7
20c	115	100	1.4	16.3	82.3

4.3.2 Influence on Ancillary Ligand

Only three ancillary ligands were studied, being these 1,5-cyclooctadiene (COD), norbornadiene (NBD) and carbon monoxide. The effect these ligands was studied only by simpler Cp*-Rh and indenyl-Rh complexes. Based on the fact ^{103}Rh -NMR presents similar chemical shift values for *s*-indacene and indenyl complexes, the catalytic results could be used for future tests with *s*-indacene rhodium complexes with ancillary ligands other than COD.

The results for the three last entries in table 7 are indicative that the effect of the chosen ancillary ligands is minimal, if any at all. These differences (or high similarities) are clearly indicative that in the case of ligands with flexible coordination modes such as indenyl and *s*-indacene, the ancillary ligand has no effect.

Complexes bearing Cp* which have a radical difference. According to the literature^[2], Cp-Rh moieties have been clearly identified to have a Rh^{V} intermediate species starting from $\text{CpRh}^{\text{I}}(\text{C}_2\text{H}_4)_2$, after undergoing two oxidative additions by a trialkylsilane, after the releasing of the olefinic ligands.

The first two entries of Table 7 are very different, despite the fact that COD and NBD are both dienes. A plausible explanation for this can be elucidated from the proton NMR spectra of complexes **19a** and **19b**, (refer to section 3.3) which show the olefinic protons of both dienes have chemical shift values of 3.99 and 2.56 ppm, respectively. This is clearly indicative that the carbon double bond in complex **19b** is closer to that of a single bond, because of a higher strength and rigidity of the olefin-Rh bond, making NBD behave as an inert ligand in the catalytic systems here described.

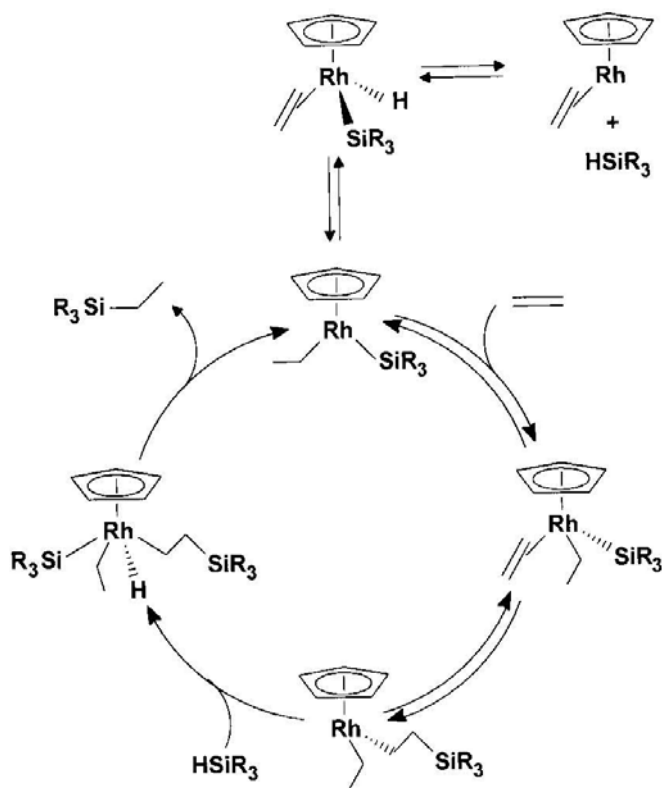


Figure 10: The Duckett Perutz Mechanism^[2]

In the case of complex **19a**, releasing a COD ligand seems far more feasible, and less energy consuming, together with the fact that COD ligand has been reported to be labile^[22] and having different possible coordination modes towards the metallic center^[23], possibly explaining the large difference between complexes **19a** and **19b**. Ligand NBD seems unable to shift from one bonding mode to the other as COD ligand, as NBD is far more rigid.

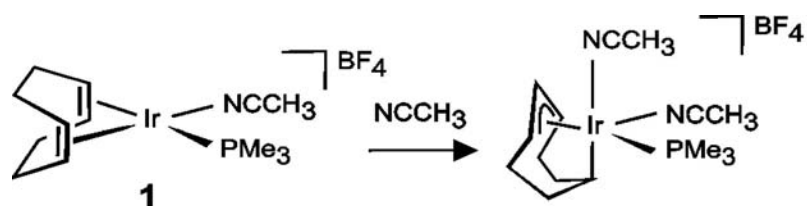


Figure 11: The Versatility of COD ligand, extracted from reference 23.

In general, the effect of the ancillary ligand is dependent on the main ligand, for Cp-like ligands there is a significant importance, whereas in the case of indenyl-like complexes, this seems completely insignificant, suggesting the possibility of two completely different mechanisms for each type of main ligands.

4.4 Conclusions

These studied catalytic systems seem to be applicable to only a few limited substrate systems. Only olefins with electron-acceptor groups seem suitable for these organometallic rhodium complexes, together with only trialkylsilanes. These results prove neutral rhodium complexes are equally effective (if not more) than other cationic species, unlike what has been previously reported^[7]. Also, each previously listed catalyst have turnover values over 2000 in each case, data which have not been reported for simple complexes, also indicative of the presence of a very active catalytic species.

Binuclear complexes showed the presence of a cooperative effect between both metallic centers, which is clearly evidenced when compared with complex **21d**, possibly explained to the different bonding mode Rh has towards indacene once a secondary metallic fragment is bonded to the spacer ligand, regardless of the different behavior these present in ESR and cyclic voltammetry tools.

4.5 Experimental Section

A typical catalytic run consists of a simple round flask with two side exits, attached to a reflux condenser and to an argon inlet, purging several times with the inert gas before use. If the tested catalyst is air or moisture-sensitive, the catalyst would be weighed inside the argon drybox, and later quickly attached to the condenser with a strong Ar flow. After this, the calculated amount of solvent is added via syringe, followed by the respective amount of olefin and silane, while thermally stabilized with an oil bath and controlled via a thermometer, with vigorous stirring. Each sample was collected depending on the reaction rate of each specific case. In most cases, this was done every 5 minutes.

Catalytic tests with ethylene were carried out in a high-pressure Schlenk tube, which was purged with argon and vacuum several times before adding the gaseous olefin. Once this reached 1 bar of pressure, the system was submerged and opened only after 100 mins. Each entry shows a complete triethylsilane consumption, though these time values could be inferior, as collecting samples every 5 or 10 minutes was impossible. Regardless, the same test was carried out and stopped at 40, 60, 80 and 100 minutes, and only at 100 minutes, the consumption of triethylsilane was quantitative.

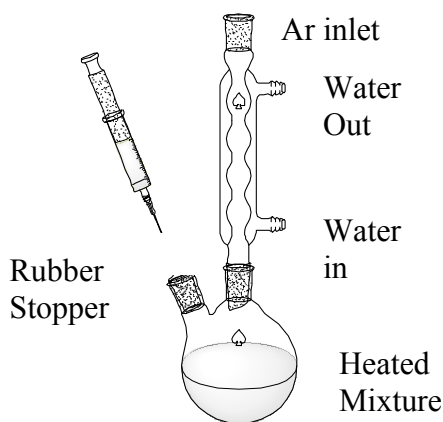
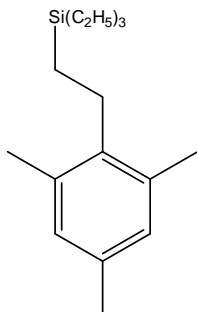


Figure 12: The equipment used in each catalytic run

4.5.1 Characterization silicon products from 2,4,6-trimethylstyrene:

Here, products were purified by a vacuum distillation at 85°C at 0.7 mmHg, forming a mixture of HS2 and DS Products in solution. There were analyzed as a mixture by NMR tools, and further characterized by GC-MS techniques.

Hydrosilylation Product triethyl(2,4,6-trimethylphenethyl)silane:



¹H-NMR (CDCl₃, δ ppm):

- 0.62 (q, 6H, Si-CH₂-CH₃, ³J_{H-H} = 7.1 Hz)
- 0.85 (t, 9H, Si-CH₂-CH₃, ³J_{H-H} = 7.1 Hz)
- 0.98 (t, 2H, Si-CH₂-CH₂-Ph, ³J_{H-H} = 6.7 Hz)
- 2.32 (s, 9H, CH₃-Ph)
- 2.64 (t, 2H, Si-CH₂-CH₂-Ph, ³J_{H-H} = 6.7 Hz)
- 6.89 (s, 2H, Ph-H)

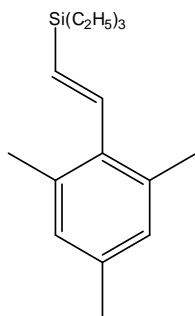
¹³C-NMR (CDCl₃, δ ppm):

- 2.9 (Si-CH₂-CH₃)
- 8.2 (Si-CH₂-CH₃)
- 11.0 (Si-CH₂-CH₂-Ph)
- 20.3 (2,6-CH₃-Ph)
- 21.7 (4-CH₃-Ph)
- 27.2 (Si-CH₂-CH₂-Ph)
- 128.9 (Ph-H)
- 135.2, 135.6 (C_{1,4})
- 140.1 (C_{2,6})

Mass Spectrum (EI, 70eV) m/z:

- [M]⁺ = 262 (100%)
- [M]⁺ - Si(C₂H₅)₃ = 147 (86%)

Dehydrogenative Silylation product (E)-triethyl(2,4,6-trimethylstyryl)silane:



¹ H-NMR (CDCl ₃ , δ ppm):	0.84 (q, 6H, Si-CH ₂ -CH ₃ , ³ J _{H-H} = 7.0 Hz)
	0.92 (t, 9H, Si-CH ₂ -CH ₃ , ³ J _{H-H} = 7.0 Hz)
	2.38 (s, 3H, CH ₃ -C ₄)
	2.52 (s, 6H, CH ₃ -C _{2,6})
	6.12 (d, 1H, Si-CH=CH-Ph, ³ J _{H-H} = 5.6 Hz)
	6.78 (s, 2H, Ph-H)
	6.82 (d, 1H, Si-CH=CH-Ph, ³ J _{H-H} = 5.6 Hz)
¹³ C-NMR (CDCl ₃ , δ ppm):	3.6 (Si-CH ₂ -CH ₃)
	7.8 (Si-CH ₂ -CH ₃)
	20.2 (2,6-CH ₃ -Ph)
	22.3 (4-CH ₃ -Ph)
	89.8 (Si-CH=CH-Ph)
	102.4 (Si-CH=CH-Ph)
	128.7 (Ph-H)
134.2, 134.6, 137.6 (C _{1,2,4,6})	
Mass Spectrum (EI, 70eV) m/z:	[M] ⁺ = 260 (100%)
	[M] ⁺ - Si(C ₂ H ₅) ₃ = 145 (38%)

References

-
- ¹ Y. Horino, M. Luzung, F. Toste, *J. Am. Chem. Soc.*, **2006**, *128*, 11364.
- ² K. Hirano, H. Yorimitsu, K. Oshima, *J. Am. Chem. Soc.*, **2007**, *129*, 6094.
- ³ M. Itoh, K. Iwata, M. Kobayashi, T. Takeuchi, T. Kabeya, *Macromolecules*, **1998**, *31*, 5609.
- ⁴ a) P. Magnus, T. Sakar, S. Djuric, *Comprehensive Organometallic Chemistry*, ed G. Wilkinson, Pergamon press, Oxford, **1982**, *7*, chap. 48, 536. C. Rucker, *Chem. Rev.*, **1995**, *95*, 1009. b) J. Dunoguès, *L'Actualité Chimique*, **1986**, *3*, 11. E. Langkopf, D. Schinzer, *Chem. Rev.*, **1995**, *95*, 1375.
- ⁵ M. Birot, J. Pillot, J. Dunoguès, *J. Chem. Rev.*, **1995**, *95*, 1443.
- ⁶ B. Boury, R. Corriu, D. Peclercq, P. Mutin, J. Planeix, A. Vioux, *Organometallics*, **1991**, *10*, 1457.
- ⁷ a) T. Kendrick, B. Parbhoo, J. While, *The Chemistry of Organic Silicon Compounds*, eds S. Patai and Z. Rappoport, John Wiley & Sons, New York, **1989**, Chap. 21. b) S. Brown, S. Heaton, M. Moore, R. Perutz, G. Wilson, *Organometallics*, **1996**, *15*, 1392.
- ⁸ a) A. Nesmetanov, R. Freilina, E. Chucovskaya, R. Petrova, A. Belyavsky, *Tetrahedron*, **1962**, *17*, 61. b) M. Schroeder, M. Wrighton, *J. Organomet. Chem.*, **1977**, *128*, 345.
- ⁹ a) Y. Zeki, K. Takeshita, K. Kawamoto, S. Murai, N. Sonoda, *Angew. Chem. Int. Ed. Engl.*, **1980**, *19*, 928. b) A. Millan, M. Fernandez, P. Bentz, P. Maitlis, *J. Mol. Cat.*, **1984**, *26*, 89.

- ¹⁰ R. Takeuchi, H. Yasue, *Organometallics*, **1996**, *15*, 2098.
- ¹¹ S. Duckett, R. Perutz, *Organometallics* **1992**, *11*, 90.
- ¹² F. Kakiuchi, K. Nogami, N. Chatani, Y. Seki, S. Murai, *Organometallics* **1993**, *12*, 4748.
- ¹³ A. Onopchenko, E. Sabourin, D. Beach, *Journal of Organometallic Chemistry*, **1984**, *49*, 3389.
- ¹⁴ J. Ruiz, P.O. Bentz, B.E. Mann, C.M. Spencer, B.F. Taylor, P.M. Maitlis, *J. Chem. Soc. Dalton Trans*, **1987**, 2709
- ¹⁵ P. Pawluc, B. Marciniec, I. Kownacki, H. Maciejewski, *Appl. Organometal. Chem.* **2005**, *19*, 49
- ¹⁶ Y. Seki, K. Takeshita, K. Kawamoto, S. Murai, N. Sonoda, *J. Org. Chem.*, **1986**, *51*, 3890.
- ¹⁷ S. Sakaki, M. Sumimoto, M. Fukuhara, M. Sugimoto, H. Fujimoto, S. Matsuzaki, *Organometallics*, **2002**, *21*, 3788
- ¹⁸ S. Zhang, G. Dobson, T. Brown, *J. Am. Chem. Soc.*, **1991**, *113*, 6908.
- ¹⁹ (a) A. Sato, H. Kinoshita, H. Shinokubo, K. Oshima, *Org. Lett.*, **2004**, *6*, 2217. (b) S. Ini, A. Oliver, T. Tilley, R. Bergman, *Organometallics*, **2001**, *20*, 3839. (c) C. Liu, R. Widenhofer, *Organometallics*, **2002**, *21*, 5666. (d) D. Haag, J. Runsink, H. Scharf, *Organometallics*, **1998**, *17*, 398.
- ²⁰ C. Bonifaci, A. Cecon, A. Gambaro, F. Manoli, L. Mantovani, P. Ganis, S. Santi, A. Venzo, *Journal of Organometallic Chemistry* **1998**, 577, 97.

²¹ C. Bonifaci, G. Carta, A. Ceccon, A. Gambaro, S. Santi, *Organometallics* **15**, **1996**, , 1630

²² J. Orsini, W. E. Geiger, *Organometallics* **1999**, *18*, 1854

²³ M. Martín, E. Sola, O. Torres, P. Plou, L. Oro, *Organometallics* **2003**, *22*, 5406

Conclusions

Conclusions

Conclusion

Ces travaux concernent la synthèse de différents complexes organométalliques du rhodium, leur caractérisation par différentes techniques et l'étude de ces composés dans la réaction de silylation déshydrogénante des oléfines.

La première partie est une introduction détaillée sur l'importance de la catalyse dans les technologies actuelles ainsi que l'importance de la conception de nouveaux catalyseurs. Parmi les références citées dans cette introduction, celle de C. Masters qui, dans son livre *Homogeneous Catalysis* définit cette discipline comme un « fine art ». En effet, cette discipline exige un accord subtil entre différents paramètres du métal de transition catalytiquement actif, ajustant sa densité électronique et donc son affinité à chaque substrat, utilisant divers ligands ou l'effet coopératif avec différents fragments organiques ou organométalliques voisins du métal de transition actif pouvant ainsi compenser les besoins électroniques suivant le cycle catalytique.

Le second chapitre décrit la synthèse d'espaceur pontant comme le ligand de type *s*-indacène diversement substitué. Une caractérisation physicochimique approfondie a été réalisée en utilisant les techniques courantes comme la RMN, l'Infra-rouge et la spectrométrie de masse. L'étude par RPE des radicaux anions correspondants a montré une délocalisation électronique sur l'ensemble du ligand, ce qui est particulièrement intéressant pour la suite de ce travail. En effet, les complexes binucléaires ayant ces motifs comme ligands devraient pouvoir présenter une communication électronique entre les deux centres métalliques ce qui induirait différentes propriétés catalytiques.

Le troisième chapitre porte sur la synthèse de complexes du rhodium homo- et hétéro-binucléaires avec le 1,5-dihydro-2,6-diéthyl-4,8-diméthyl-*s*-indacène comme espaceur et leur caractérisation par RMN, spectrométrie de masse. L'étude par RPE de chaque cation radical formé à partir de chaque complexe ainsi que l'étude électrochimique de ces complexes constituent deux techniques de caractérisation particulièrement intéressantes dans le cas de ces complexes. En effet, elles donnent des informations sur le degré de communication électronique entre les deux centres métalliques ce qui a été confirmé par l'étude structurale de

ces complexes par diffraction des rayons X. L'ensemble de ces données montre que la communication est fortement dépendante non seulement du ligand pontant mais aussi des fragments organométalliques. Les complexes hétérobinucléaires semblent présenter un plus faible degré de délocalisation que les complexes homonucléaires.

Dans le quatrième chapitre, sont présentés les résultats obtenus dans différents tests catalytiques de la réaction de silylation déshydrogénante à partir de diverses oléfines et de différents silanes. Les catalyseurs utilisés sont divers catalyseurs connus ainsi que les nouveaux mono-, hétéro- and homobinucléaires complexes synthétisés dans le chapitre précédent.

Chaque complexe du rhodium hétérobi- et homobinucléaire présente effectivement une plus grande vitesse de réaction que des systèmes catalytiques similaires comme les complexes indényles du rhodium ce qui semble confirmer l'effet coopératif.

Bien que l'étude de ces complexes par RPE ainsi que les expériences de voltammétrie cyclique aient montré une plus faible délocalisation électronique dans les complexes hétérobinucléaires, ils se comportent comme des catalyseurs efficaces. Ceci peut s'expliquer par les différents modes de liaison que peut avoir l'atome de rhodium une fois le second fragment métallique fixé à l'espaceur. Cette variation de l'haptacité serait suffisante pour accélérer la vitesse de réaction indépendamment de leurs comportements mis en évidence par RPE et étude électrochimique.

En résumé, ces résultats sont intéressants dans la mesure où ils mettent en évidence un effet coopératif dans des complexes du rhodium hétérobinucléaires utilisant le groupement *s*-indacène comme ligand pontant. Comme nous l'avons indiqué dans le premier chapitre, il n'existe pas de définition précise et unique pour la notion d'effet coopératif. Mais ces résultats montrent qu'il n'y a pas de corrélation entre la mise en évidence d'un transfert monoélectronique et l'efficacité d'un centre catalytique en présence d'un second fragment métallique. Dans le cadre de cette étude, il semble que l'effet coopératif correspond plutôt un réarrangement électronique qui convient mieux aux besoins de l'ensemble des centres métalliques.

Conclusions

This project details the synthesis of different organometallic rhodium complexes and their characterization by means of different tools, including a study of these new products as catalysts in the dehydrogenative silylation of olefins.

The first part of this project is an introductory chapter, being a collection of recent and not so recent relevant articles, about the importance of catalysis in nowadays technology, as well as the importance of the design of catalysis. Within the references of this chapter, Christopher Masters in his book “Homogeneous Catalysis” defines this discipline as “a fine art”. This discipline requires a fine tuning of the behavior of each transition metal catalyst, adjusting its electronic density thus its affinity for any relevant substrate, using modified ligands, or cooperative effects with different organic or organometallic moieties neighboring the catalytic center that could compensate for electronic needs throughout the catalytic cycle.

The second chapter displays a complete characterization of the chosen spacer molecule, such as substituted *s*-indacene ligand in different positions, revealing by means of common spectroscopic tools such as NMR, FT-IR as well as mass spectrometry, the successful characterization of these ligands, but also their effective electronic distribution throughout the whole molecule in the case of generated radical species characterized by ESR. This is evidently a promising result, as a binuclear complex derived from these spacer molecules with one metal owning catalytic properties could present electronic communication that would result in different catalytic properties.

The third chapter refers to the synthesis of homo- and heterobinuclear rhodium complexes using 1,5-dihydro-2,6-diethyl-4,8-dimethyl-*s*-indacene, and their respective characterization using NMR, mass spectrometry, amongst other means. The most important characterization tools used were ESR of each respective cation radical formed from each complex, together with cyclic voltammetry. These tools combined, provided information which was later supported by X-ray structures of a few binuclear complexes about the degree of communication the two metallic centers would have. This resulted in the fact that electronic communication is strongly dependant not only on the spacer

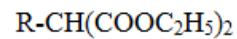
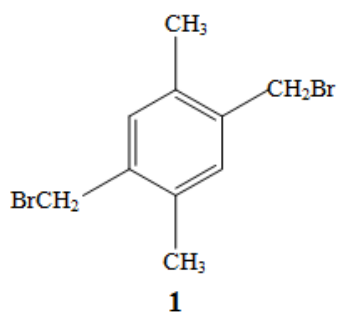
Conclusions

ligand, but also on the metallic fragments. Heterobinuclear complexes turned out to have a decreased degree of delocalization, while homobinuclear products presented a much greater degree of delocalization.

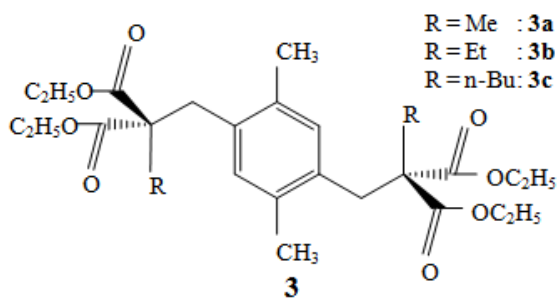
The fourth chapter presents the results obtained for several catalytic tests in the dehydrogenative silylation, using different olefins and silanes. The catalysts used were already reported catalysts, together with those novel mono-, heterobi-, and homobinuclear complexes synthesized in the previous chapter. Each heterobi- and homobinuclear rhodium catalyst, effectively does present a greater reaction rate when compared to a similar system, such as indenyl rhodium complexes, evidencing a cooperative effect. Despite the fact that ESR and cyclic voltammetry tools indicate a lower electronic delocalization for heterobinuclear complexes, these do effectively behave very efficiently as catalysts, which possibly indicates the different bonding mode Rh has towards indacene once a secondary metallic fragment is bonded to the spacer ligand is sufficient to boost the reaction rate, regardless of the different behavior these present in ESR and cyclic voltammetry tools.

Finally, these results have an academic interest, where the cooperative effect of heterobinuclear rhodium complexes using s-indacene with has been evidenced, regardless if tools such as ESR and cyclic voltammetry indicates otherwise. As indicated in the introductory chapter, there is no single definition for cooperative effect, but these results certainly do evidence there is no correlation on how effective an electronic transfer happens and the effectiveness on how a catalytic center behaves in the presence of a secondary metallic fragment. In the case of this project, a cooperative effect is an electronic rearrangement which suits best the needs of both metallic centers.

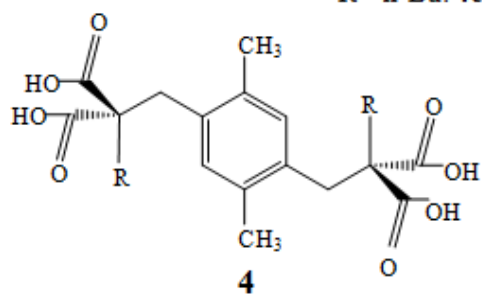
Compound Number Summary:



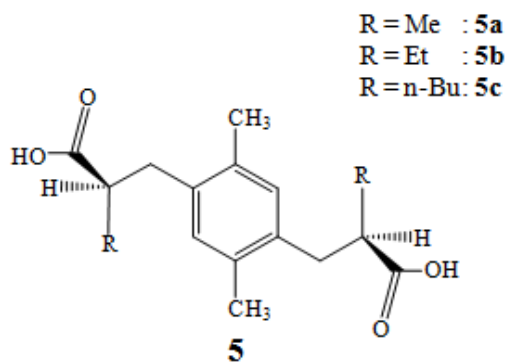
2 R = Me : 2a
 R = Et : 2b
 R = n-Bu: 2c



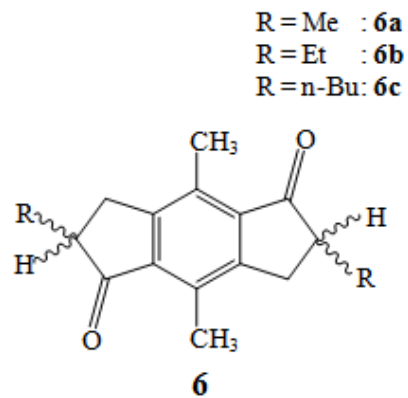
R = Me : 3a
 R = Et : 3b
 R = n-Bu: 3c



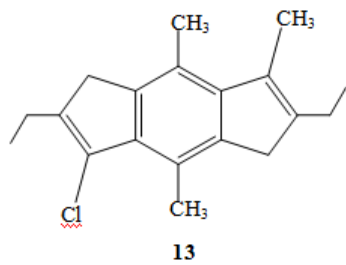
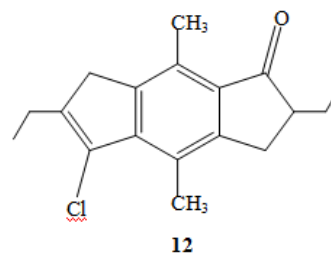
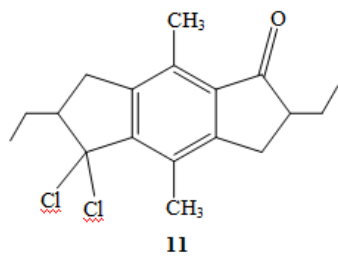
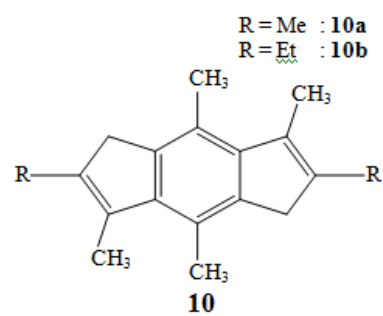
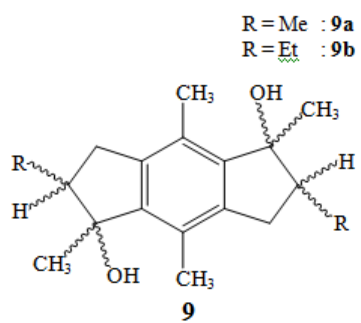
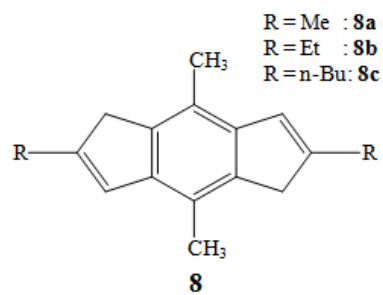
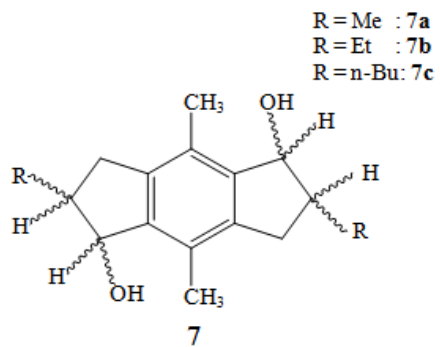
R = Me : 4a
 R = Et : 4b
 R = n-Bu: 4c



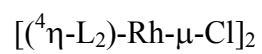
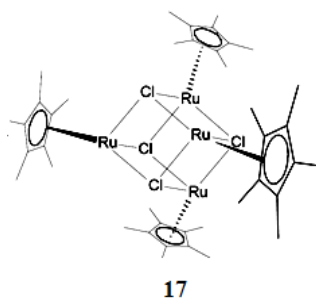
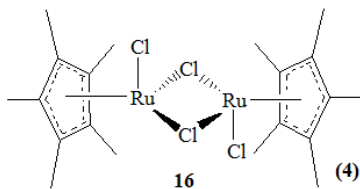
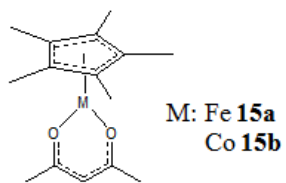
R = Me : 5a
 R = Et : 5b
 R = n-Bu: 5c



R = Me : 6a
 R = Et : 6b
 R = n-Bu: 6c

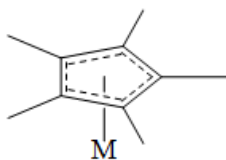


M(acac)₂
 M: Fe 14a
 Co 14b



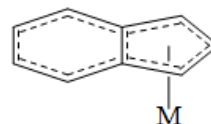
18a: $\text{L}_2 = 1,5\text{-cyclooctadiene}$

18b: $\text{L}_2 = \text{norbornadiene}$



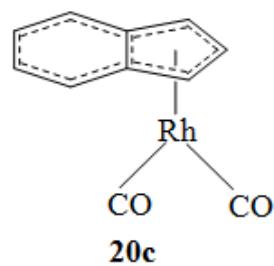
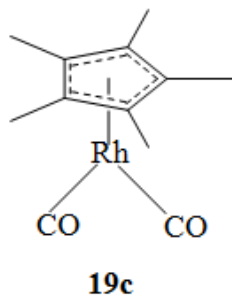
19a: M = Rh-(η^4 -1,5-cyclooctadiene)

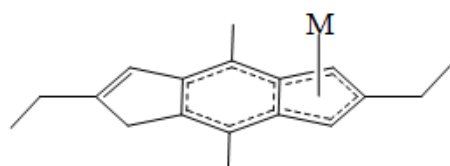
19b: M = Rh-(η^4 -Norbornadiene)



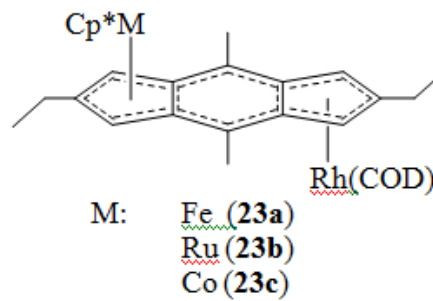
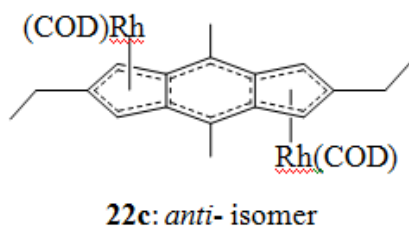
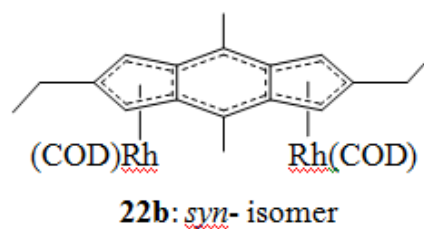
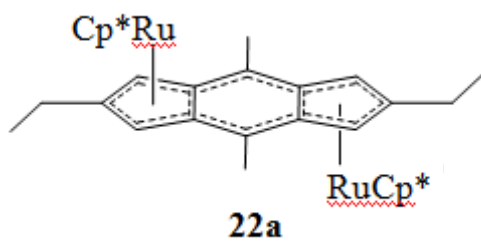
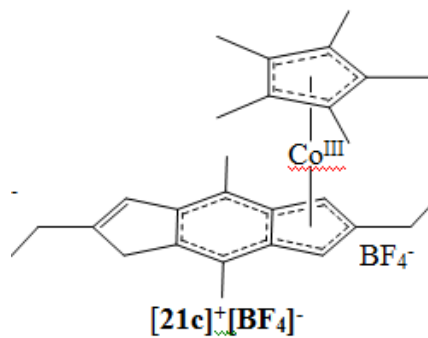
20a: M = Rh-(η^4 -1,5-cyclooctadiene)

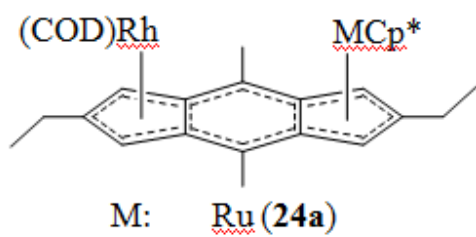
20b: M = Rh-(η^4 -Norbornadiene)





- 21a:** M = Cp*Fe-
21b: M = Cp*Ru-
21c: M = Cp*Co-
21d: M = (COD)Rh-





UNIVERSITE PAUL SABATIER
Thèse d'Université, spécialité Chimie Moléculaire
Soutenance prévue le 29 novembre 2007
ADAMS Christopher

Synthèse, caractérisation et étude de l'activité catalytique de complexes organo métalliques du rhodium dans la réaction de silylation deshydrogénante des oléfines

Ce travail concerne l'étude de nouveaux complexes homo- et hétéro-bimétalliques du rhodium comportant le motif *s*-indacène comme groupement pontant dans le but de les utiliser comme catalyseurs dans des réactions de silylation deshydrogénante d'oléfines. Après un bref rappel sur l'importance de la catalyse et de la mise au point de nouveaux catalyseurs, le deuxième chapitre décrit un procédé général de synthèse de ligands de type *s*-indacène polysubstitués. Une étude physicochimique complète (RMN du ^1H , ^{13}C , spectrométrie de masse) de ces nouveaux ligands a été réalisée. Ces motifs donnent également des radicaux anions après oxydation des dérivés dilithiés correspondants. L'étude par RPE a permis de mettre en évidence une bonne délocalisation de l'électron célibataire sur ces systèmes tricycliques. La synthèse de divers complexes monométalliques et homo- et hétéro-bimétalliques est ensuite développée ainsi que leurs caractéristiques physicochimiques. L'étude par RPE des cations radicaux correspondants et des expériences de voltampérométrie cyclique montrent que la délocalisation électronique dépend non seulement du ligand pontant mais aussi de la nature du fragment métallique. De plus, les complexes hétérobinucléaires présentent un plus faible degré de délocalisation que leurs analogues homobinucléaires. L'étude des propriétés catalytiques de ces complexes a été également réalisée dans le dernier chapitre dans le cas des réactions de silylation d'oléfines (deshydrogénation couplante). Une comparaison a été établie entre des catalyseurs connus (complexes indényles du rhodium) et les nouveaux complexes mono-, hétéro- and homobinucléaires. Chaque complexe du rhodium hétérobi- et homobinucléaire présente effectivement une plus grande vitesse de réaction que celle des systèmes catalytiques similaires.

Mots clés : *s*-indacène, RPE, complexes du rhodium, catalyse, silylation

Synthesis, characterization and catalytic study of organometallic rhodium complexes in the dehydrogenative silylation of olefins

This work concerns the synthesis of new homo- and heterobinuclear organometallic rhodium complexes using *s*-indacene as a bridging ligand, together with the determination of their efficiency in the catalytic system of the dehydrogenative silylation of olefins. After a short introduction about the importance of catalysis, the second chapter describes an extensive synthetic procedure to produce poly-substituted-1,5-dihydro-*s*-indacenes, and their characterization by NMR (^1H , ^{13}C , mass spectrometry) and EPR spectra of their anion radical. The synthesis of different mononuclear, homo- and heterobinuclear complexes are then described, and characterized by classical tools (NMR, mass spectrometry) and also ESR reactions and cyclic voltammetry experiments. The behavior the catalysts previously synthesized in catalysis, more particularly in the Dehydrogenative Silylation of olefins have also been described.

Keywords: *s*-indacene, ESR, Rhodium complexes, catalysis, dehydrogenative silylation

Laboratoire d'Hétérochimie Fondamentale et Appliquée UMR-CNRS 5069, Université Paul Sabatier, Bat 2R1118 -route de Narbonne - 31062 Toulouse cédex 9
Departamento de Inorganica, Facultad de Química, Pontificia Universidad Católica de Chile - Casilla 306 - Santiago